PROPERTIES OF HYBRID FIBER REINFORCED CONCRETE FOR IMPACT LOADING

A Thesis Submitted to
the Graduate School of Engineering and Sciences of
İzmir Institute of Technology
in Partial Fulfillment of the Requirements for the Degree of

DOCTOR OF PHILOSOPHY

in Civil Engineering

by
Mohammad Musa ALAMI

July 2021
İZMİR

ACKNOWLEDGMENTS

I would like to express my endless gratitude to my supervisor Assist. Prof. Dr. Selçuk SAATCI and co-supervisor Assoc. Prof. Dr. Tahir Kemal ERDEM for helping me in so many ways, for their patience and guidance throughout the preparation of this thesis. I am deeply grateful to ministry of higher education of Afghanistan to grand me this opportunity to complete my doctor of philosophy degree.

I would like to thank the Scientific and Technical Research Council of Turkey (TÜBİTAK) for their financial support [Project number: 115M296] and Cengiz Kızılırmak for his help during the impact loading tests in Dokuz Eylül University. Also I would like to thank ÇimSa ready-mix concrete plant in Mersin to countenance us to test the real size barriers by pendulum test setup. Moreover, I would like to thank the Materials Research Center at İzmir Institute of Technology for obtaining the chemical composition of materials by XRF method.

I would like to express my special thanks to the jury members; Assoc. Prof. Dr. Engin AKTAŞ, Prof. Dr. Burak FELEKOĞLU, Prof. Dr. Mustafa ŞAHMARAN, Assist.Prof. Süleyman Bahadır KESKİN for their attendance at my thesis defense presentation and valuable suggestions to the thesis.

Finally, I would like to express my special thanks to my family for their endless love and patient throughout my life and especially my wife who made me to overcome all the difficulties with her encouragement, support and love. This thesis dedicated to them.

ABSTRACT

PROPERTIES OF HYBRID FIBER REINFORCED CONCRETE FOR IMPACT LOADING

Concrete is a brittle material and does not have significant energy absorption capacity before its fracture. Adding fibers to a concrete mix increases its ductility. Recently, there is significant development in the concrete technology to produce a concrete that can exhibit deflection hardening and show high energy absorption capacity.

In this thesis, two kinds of cement based composites with high energy absorption capacity were studied: 1. Engineered Cementitious Composites (ECC). This material can exhibit deflection hardening under bending and it is produced only with synthetic fibers and fine aggregate, 2. Hybrid Fiber Reinforced Concrete (HyFRC). This material can exhibit deflection hardening under bending. It was produced with fine and coarse aggregates and hybrid fibers (both steel and synthetic fibers).

The experimental program of this study consists of two main stages. The first stage is to design these composites and test their basic properties in fresh and hardened states, such as compressive strength, flexural behavior, freezing-thawing resistance, chloride ion permeability and sorptivity. In the second stage, dynamic tests (drop tests on small size specimens and pendulum impact tests on real size new generation road concrete barriers with a selected HyFRC mixture) were carried out to determine their energy absorption capacities.

Based on the ECC results, fly ash/cement ratio of 1.2 and 20% perlite replacement of sand were selected for HyFRC mixtures. According to the mechanical behavior and durability test results of HyFRC, ST3,0.75_P0.25_D16 mixture (steel fiber type= ST3, steel fiber volume=0.75%, PVA volume=0.25%, D_{max}=16mm) was found to have the best performance, and accordingly, this composite was selected for the real-size barrier pendulum test. The same mixture without fibers was also tested under pendulum test as control normal concrete since the present road barriers in the market do not employ fibers. As a result of this study, the HyFRC barrier was found to perform higher impact resistance.

ÖZET

DARBE YÜKLEMESİ İÇİN HİBRİT FİBER DONATILI BETONUN ÖZELLİKLERİ

Beton kırılmadan önce fazla enerji emme kapasitesi olmayan, gevrek bir malzemedir. Betona fiber eklenmesi, sünekliği arttırmaktadır. Son yıllarda, eğilme altında pekleşme ve yüksek enerji emme kapasitesi gösteren beton üretilmesiyle, beton teknolojisinde önemli gelişmeler yaşanmıştır.

Bu tezde, yüksek enerji emme kapasitesine sahip 2 çeşit çimento esaslı kompozit çalışılmıştır: 1. Tasarlanmış Çimento Esaslı Kompozit (ECC). Bu malzeme eğilme altında pekleşme gösterebilmekte ve sadece ince agrega ve sentetik fiberlerle üretilmektedir. 2. Hibrit Fiber Takviyeli Beton (HyFRC). Bu malzeme eğilme altında pekleşme gösterebilmekte olup iri ve ince agrega ile beraber hibrit (sentetik ve çelik) fiberlerle üretilmektedir.

Deneysel program iki ana aşamadan oluşmaktadır. İlkinde bahsi geçen kompozitler tasarlanıp, taze ve sertleşmiş haldeki temel özellikleri (basınç dayanımı, eğilme davranışı, donma-çözülme direnci, klor iyonu geçirimliliği ve kılcal su emme) belirlenmiştir. İkinci aşamada, karışımların enerji emme kapasitelerini belirlemek için dinamik testler (küçük numuneler için düşme testi, seçilen bir HyFRC karışımı ile üretilmiş gerçek boyutlarda yeni nesil yol bariyeri için sarkaç testleri) gerçekleştirilmiştir.

ECC sonuçları baz alınarak, HyFRC betonlarında, uçucu kül/çimento oranı 1.2 ve kumun perlitle ikame oranı %20 olarak seçilmiştir. HyFRC'nin mekanik ve dayanıklılık test sonuçlarına göre, ST3, 0.75_P0.25_D16 karışımı (çelik fiber tipi ST3 ve miktarı %0.75, PVA lif miktarı %0.25, agrega Dmaks değeri 16 mm olan karışım) en iyi performansı göstermiş ve dolayısı ile bu kompozit gerçek boyutlu bariyerin sarkaç testleri için kullanılmıştır. Sarkaç testlerinde ayrıca, mevcut bariyerler fibersiz olarak üretildiği için, bu kompozitin fibersiz hali de kontrol betonu olarak kullanılmıştır. Sonuç olarak, HyFRC bariyerinin daha yüksek darbe dayanımına sahip olduğu bulunmuştur.

TABLE OF CONTENTS

LIST OF FIGURES viii

LIST OF TABLES xiii

LIST OF ABBREVIATIONS xv

CHAPTER 1. INTRODUCTION 1

1.1. Objective 1

1.2. Scope 1

CHAPTER 2. GENERAL INFORMATION 2

2.1. Fiber Reinforced Concrete 2

2.1.1. Mechanism of Fiber Reinforcement 4

2.1.2. Workability of Fiber Reinforced Concrete 6

2.1.3. Types of Fiber Reinforced Concrete 6

2.2. Concrete Road Barriers 7

CHAPTER 3. LITERATURE REVIEW 11

3.1. Engineered Cementitious Composites (ECC) 11

3.1.1 Compressive Strength 14

3.1.2. Flexural Performance 17

3.1.3. Impact Loading 21

3.1.4. Durability 23

3.2. Hybrid Fiber Reinforced Concrete (HyFRC) 28

3.2.1. Workability 31

3.2.2. Compressive Strength 33

3.2.3. Flexural Performance 37

3.2.4. Impact loading 42

3.2.5. Durability 46

CHAPTER 4. EXPERIMENTAL STUDY 53

4.1. Materials 53

4.1.1. Cement 53

4.1.2. Fly Ash 54
4.1.3. Aggregates 55
4.1.4. Superplasticizer 58
4.1.5. Polyvinyl Alcohol (PVA) Fiber 58
4.1.6. Steel Fibers 59
4.2. Mixture Types and Proportions 60
4.2.1. ECC Proportions 60
4.2.2. HyFRC Proportions 61
4.2.3. Normal Concrete (NC) Proportions 63
4.2.4. Steel Fiber Reinforced Concrete (SFRC) Proportions 63
4.3. Mixing Procedure, Casting, and Curing 63
4.3.1. Mixing Procedure 63
4.3.2. Specimen Casting and Curing 66
4.4. Testing Methods 67
4.4.1. Slump and Slump Flow Test 67
4.4.2. Compressive Strength Test 68
4.4.3. Four-Point Bending Test 69
4.4.4. Impact Loading Test 71
4.4.5. Rapid Chloride Permeability Test (RCPT) 75
4.4.6. Freezing and Thawing Test 76
4.4.7. Sorptivity Test 76
4.4.8. Pendulum Test for Real-Size Barriers 77

CHAPTER 5. RESULTS AND DISCUSSIONS 79
5.1. Engineered Cementitious Composite (ECC) 79
5.1.1. Compressive Strength 79
5.1.2. Static Bending Test 80
5.1.3. Dynamic Bending Test 84
5.1.4. Comparison of Dynamic and Static Bending Results 86
5.1.5. Rapid Chloride Permeability Test (RCPT) 88
5.1.6. Freezing and Thawing Test (F-T) 89
5.1.7. Sorptivity Test 91
5.2. Hybrid Fiber Reinforced Concrete (HyFRC) 93
5.2.1. Consistency and Superplasticizer Requirement 93

5.2.2. Compressive Strength 97
5.2.3. Static Bending Test 100
5.2.4. Dynamic Bending Test 109
5.2.5. Comparison of Static and Dynamic Bending Tests Results 114
5.2.6. Freezing and Thawing (F-T) Test 119
5.2.7. Rapid Chloride Permeability Test (RCPT) 123
5.2.8. Sorptivity Test 125
5.2.9. Pendulum Test for Real-Size Barriers 126

CHAPTER 6. CONCLUSIONS 131
6.1. Engineered Cementitious Composite (ECC) 131
6.2. Hybrid Fiber Reinforced Concrete (HyFRC) 132
6.3. Recommendations 133

REFERENCES 135

APPENDIX A 140
ECC Static Bending Test Load-Deflection Curves at 7, 28, and 90 Days Age 140
APPENDIX B 147
ECC Dynamic Bending Test Load-Deflection Curves at 90 Days Age 147
APPENDIX C 150
All HyFRC Static Bending Test Load-Deflection Curves at 28 Days Age 150
APPENDIX E 163
Five Selected HyFRC Static Bending Test Load-Deflection Curves at 7 Days Age 163
APPENDIX F 166
Five Selected HyFRC Static Bending Test Load-Deflection Curves at 90 Days Age 166
APPENDIX G 168
Normal Concrete 7, 28, and 90 days Static Bending Test Load-Deflection Curves 168
APPENDIX H 169
SFRC 7, 28, and 90 days Static Bending Test Load-Deflection Curves 169
APPENDIX I 170
Selected Mixtures Dynamic Bending Test Load-Deflection Curves at 28 days 170
APPENDIX J 173
Selected Mixtures Static Bending Test Load-Deflection Curves, specemen size (60 x 10 x 10 cm) at 28 days 173

LIST OF FIGURES

Figure **Page**

Figure 2.1. Types of fibers……....2
Figure 2.2. Shapes of steel fibers……...3
Figure 2.3. Schematic behavior of fibers bridging across a crack…….4
Figure 2.4. Load-deflection behavior of plain and fiber reinforced concrete……....5
Figure 2.5. Effect of short and long fibers on the fiber reinforced concrete…….5
Figure 2.6. Steel road barriers accident……8
Figure 2.7. Concrete road barriers cross section……...9
Figure 3.1. Tensile stress–strain curve and crack width development of ECC……...12
Figure 3.2. ECC under bending loads……..12
Figure 3.3 Compressive strength of ECCs……..15
Figure 3.4. Fly ash effects on ECC compressive strength……...16
Figure 3.5. EPA effects on ECC compressive strength……...17
Figure 3.6. Fracture toughness test results for ECC……18
Figure 3.7. Bending performance of ECC……...19
Figure 3.8. Flexural performance of ECC……...19
Figure 3.9. Fly ash effects on ECC flexural strength……..20
Figure 3.10. Flexural stress-deflection curves of ECC……...20
Figure 3.11. Specimens after testing……...21
Figure 3.12. Load–displacement relationships of (a) ECC and concrete beams, and (b) R/ECC and R/C beams in single impact experiment ...……...22
Figure 3.13. Impact energy of ECC mixtures……..23
Figure 3.14. Water absorption of ECC……24
Figure 3.15. Chloride ion penetration of ECC…….24
Figure 3.16. Charge passed ECC specimens before and after 30 days water curing…..25
Figure 3.17. Sorptivity rest results for different ECC mixtures before self-healing, (a) for M1, (b) for M2, and (c) for M3…….26
Figure 3.18. Relative pulse velocity and mass loss changes as a function of number of freezing and thawing cycles…… ……27
Figure 3.19. Specimens surface appearance after freeze–thaw cycles……27
Figure 3.20. Cracking behavior in deflection hardening of HyFRC……...28
Figure 3.21. Flexural behavior of five mixtures……..29

Figure 3.22. Flexural behavior of single fiber and hybrid fiber proportion at the same total volume fraction……30
Figure 3.23. Relative slump of FRC tested……31
Figure 3.24. Tests stability and deformability of HFR-SCC……...32
Figure 3.25. Slump flow behavior of SC-HyFRC……...33
Figure 3.26. Effect of fiber and fly ash content on HyFRC……34
Figure 3.27. Effect of hybrid fiber on compressive strength……..35
Figure 3.28. Compressive strength results……..36
Figure 3.29. Load-deflection curves of HyFRC……38
Figure 3.30. Effect of fly ash content on HyFRC……...38
Figure 3.31. Load-deflection curve of FRC under three-point bending test……...40
Figure 3.32. Load-deflection curves……42
Figure 3.33. Failure impact energy graph……43
Figure 3.34. Different types and shaped of fibers……...44
Figure 3.35. Impact resistance for initial crack……...44
Figure 3.36. (a) RC and (b) UHPFRCC slabs after impact loading by ‘‘Solid Round’’ projectiles 12.7 mm……....46
Figure 3.37. Early and ultimate water absorption of different fiber-reinforced concretes: (a) polypropylene fiber-reinforced specimens, (b) steel fiber-reinforced (b) specimens, and (c) hybrid fiber-reinforced specimens…….....47
Figure 3.38. Sorptivity test results……..48
Figure 3.39. Load-deflection curves (a) PVA and steel FRC (b) effect of MC addition and aggregate content on PVA FRC……49
Figure 3.40. Freeze-thaw resistance of 2SHCC (a) mass loss (b) relative dynamic modulus of elasticity……50
Figure 3.41. Chloride ion penetration test results with various latex and fibers contents ……51
Figure 4.1. Micrograph of the portland cement particles……54
Figure 4.2. Micrograph of fly ash particles……54
Figure 4.3. Gradation curve for the Aggregates……..55
Figure 4.4. Fine and coarse aggregates combination curve……56
Figure 4.5. Micrograph of the quartz particles……56
Figure 4.6. Photo of the perlite particles……57
Figure 4.7. Micrograph of the perlite particles……57

Figure 4.8. Photograph of the PVA fibers……...59
Figure 4.9. 20-liter capacity mixer for ECC production……..64
Figure 4.10. Rotating drum mixer with 100-L capacity……..65
Figure 4.11. Measuring of the slump flow of concrete……...68
Figure 4.12. ECC compressive strength by universal testing machine……...69
Figure 4.13. Concrete compressive strength testing machine……69
Figure 4.14. ECC mixtures flexural testing……70
Figure 4.15. 600 x 150 x 150 mm prismatic specimens for flexural testing……...71
Figure 4.16. 600 x 100 x 100 mm prismatic specimens for flexural testing……...71
Figure 4.17. Impact loading test……..72
Figure 4.18. ECC impact loading test…….....73
Figure 4.19. HyFRC impact loading test……74
Figure 4.20. Impact loading test specimen……..……74
Figure 4.21. Rapid chloride permeability test……75
Figure 4.22. Schematic diagram of the sorptivity test……76
Figure 4.23. Concrete road barriers cross section (units are centimeters)……...77
Figure 4.24. Pendulum test method for real size concrete barriers……78
Figure 4.25. Concrete barriers connected pins for pendulum test.....…..…….78
Figure 5.1. ECC compressive strength graphs……80
Figure 5.2. Static bending curves for ECC at 7 days……...81
Figure 5.3. Static bending curves for ECC at 28 days……81
Figure 5.4. Static bending curves for ECC at 90 days……81
Figure 5.5. ECC flexural strength graphs……...…82
Figure 5.6. ECC toughness graphs……..……84
Figure 5.7. Dynamic bending curves for ECC at 90 days……...85
Figure 5.8. Dynamic bending results graphs for ECC at 90 days……...…86
Figure 5.9. Static and dynamic bending graphs for ECC at 90 days……...87
Figure 5.10. Static and dynamic flexural comparing graphs for ECC……87
Figure 5.11. Static and dynamic toughness comparing graphs for ECC……88
Figure 5.12. RCPT test results for ECC at 90 days……89
Figure 5.13. F-T test weight gain graphs for ECC at 90 days……91
Figure 5.14. Effect of fly ash content on sorptivity on ECC at 90 days age…….....92

Figure 5.15. Effect of perlite content on sorptivity on ECC at 90 days age……92
Figure 5.16. Sorptivity test graphs for all ECC at 90 days age……...93
Figure 5.17. Effect of D_{max} on Superplasticizer demand for HyFRC and NC……95
Figure 5.18. Effect of D_{max} on slump flow values of HyFRC and NC……95
Figure 5.19. Effect of PVA and steel fiber amount on Superplasticizer demand for HyFRC…….96
Figure 5.20. Effect of PVA and steel fiber amount on slump flow of HyFRC……...96
Figure 5.21. Effect of D_{max} on compressive strength of HyFRC and NC……...98
Figure 5.22. Effect of PVA and steel fiber content on compressive strength of HyFRC...98
Figure 5.23. 7, 28 and 90-day compressive strength of selected mixtures……....100
Figure 5.24. Static bending curves for selected HyFRC at 7 days……....101
Figure 5.25. Static bending curves for selected HyFRC at 28 days……...101
Figure 5.26. Static bending curves for selected HyFRC at 90 days……...102
Figure 5.27. Effect of D_{max} on static flexural strength of HyFRC and NC……....103
Figure 5.28. Effect of D_{max} on static flexural toughness of HyFRC and NC……104
Figure 5.29. Effect of PVA content on static bending flexural strength of HyFRC.....105
Figure 5.30. Effect of PVA content on static bending toughness of HyFRC……105
Figure 5.31. 7, 28 and 90 days static bending flexural strength of selected mixtures...107
Figure 5.31. 7, 28 and 90 days static bending toughness of selected mixtures…….107
Figure 5.32. Static bending curves for NC, HyFRC, SFRC, Per20% at 7 days……108
Figure 5.33. Static bending curves for NC, HyFRC, SFRC, Per20% at 28 days…..…108
Figure 5.34. Static bending curves for NC, HyFRC, SFRC, Per20% at 90 days……..109
Figure 5.35. Dynamic bending curves for selected HyFRC, SFRC, Per20% at 28 days……..……...……110
Figure 5.36. Dynamic flexural strength values for selected mixtures at 28 days…….112
Figure 5.37. Dynamic toughness values for selected mixtures at 28 days……....113
Figure 5.38. Dynamic bending curves for HyFRC, SFRC, and Per20% at 28 days….113
Figure 5.39. Static bending curves for HyFRC, SFRC, and Per20% at 28 days……...114
Figure 5.40. Comparing static and dynamic bending tests load-deflection curves…...117
Figure 5.41. Comparison of static and dynamic flexural strengths……..…118
Figure 5.42. Comparison of static and dynamic flexural toughness……118
Figure 5.43. F-T test specimens weight loss percentage……...…120

Figure 5.44. F-T test specimens UPV loss percentage……..121
Figure 5.45. All tested specimens after 300 freeze-thaw cycles……...…122
Figure 5.46. RCPT test results for selected mixtures……124
Figure 5.47. Sorptivity test result graphs of selected specimens……...126
Figure 5.48. Capillary water absorption values after 72 hours……..126
Figure 5.49. Normal concrete and HyFRC barriers after impact test……...….127
Figure 5.50. Impact mass acceleration change…….....128
Figure 5.51. Concrete specimens acceleration change……..128
Figure 5.52. Dynamic balance diagram of concrete barriers…….129
Figure 5.53. Difference between impact force and specimen inertia force……...…130

LIST OF TABLES

Table **Page**

Table 3.1 Typical mix design by weight for ECC-45……...……...13
Table 3.2 Different types of fly ashes %.....……15
Table 3.3 Compressive strength results of ECC ……..……16
Table 3.4 Load and energy capacity of composites.....…...22
Table 3.5 Mixture proportions of HyFRC ……..……29
Table 3.6. Compressive strength results ……..……...36
Table 3.7. Fiber proportions ……...41
Table 3.8. Number of blows ……..……..45
Table 4.1. Chemical composition of portland cement, fly ash and quartz……..53
Table 4.2. Specific gravity and absorption capacity of the aggregates……...55
Table 4.3. Properties of the superplasticizer……....58
Table 4.4. Geometric and mechanical properties of PVA fibers…….59
Table 4.5. Geometric and mechanical properties of steel fibers…….59
Table 4.6. ECC mixture proportions……...60
Table 4.7. HyFRC mixture proportions (by weight) (binder content = 600 kg/m^3)…...61
Table 4.8. HyFRC mixtures……62
Table 4.9. Mixing sequence for ECC mixtures……..64
Table 4.10. Mixing sequence for HyFRC mixtures……65
Table 4.11. Mixing sequence for Normal Concrete mixture……...66
Table 4.12. Mixing sequence for SFRC mixtures……...66
Table 4.13. Chloride Ion Penetrability Based on Charge Passed……75
Table 5.1. ECC compressive strength results…….79
Table 5.2. ECC static bending flexural strength results…….82
Table 5.3. ECC static bending toughness results……83
Table 5.4. ECC dynamic flexural and toughness results……85
Table 5.5. ECC dynamic and static bending test results at 90 days……86
Table 5.6. ASTM C 1202 Charge Passed Classification…….88
Table 5.7. RCPT test results for ECC at 90 days……88
Table 5.8. F-T test results for ECC at 90 days……89
Table 5.9. Sorptivity test results for ECC at 90 days……..91

Table 5.10. Slump-flow test results and superplasticizer demand for HyFRC and normal Concrete……..……...94
Table 5.11. HyFRC and normal concrete compressive strength…….97
Table 5.12. 7, 28 and 90-day compressive strength of selected mixtures……...99
Table 5.13. HyFRC static bending flexural strength and toughness……102
Table 5.14. 7, 28 and 90-day flexure strength and toughness of selected mixtures…..106
Table 5.15. Dynamic flexural strength and toughness values of selected mixtures at 28 days…….……111
Table 5.16. Static and dynamic flexure strength and toughness of selected mixtures..115
Table 5.17. Dynamic increase factors of selected mixtures……..115
Table 5.18. Weight and ultrasonic pulse velocity (UPV) loss after 300 cycles…….....119
Table 5.19. ASTM C 1202 Charge Passed Classification…….123
Table 5.20. RCPT test results of selected mixtures……...123
Table 5.21. Sorptivity test results of selected mixtures…….125

LIST OF ABBREVIATIONS

HyFRC:	Hybrid Fiber Reinforced Concrete
ECC:	Engineered Cementitious Composites
SFRC:	Steel Fiber Reinforced Concrete
NC:	Normal Concrete
RC:	Reinforced Concrete
FRC:	Fiber Reinforced Concrete
CPC:	Compact Reinforced Composite
RPC:	Reactive Powder Concrete
SIFCON:	Slurry Infiltrated Fibered Concrete
HES-ECC:	High-early-strength Engineered Cementitious Composites
LW-ECC:	Lightweight Engineered Cementitious Composites
SH-ECC:	Self-Healing Engineered Cementitious Composites
HFR-SCC:	Hybrid Fiber Reinforced Self-Compacting Concrete
SCC:	Self-Consolidating Concrete
SC-HyFRC:	Self-Consolidating Hybrid Fiber Reinforced Concrete
SHCC:	Strain-Hardening Cement-Based Composites
UHPFRCC:	Ultra-High Performance Fiber Reinforced Cementitious Composites
2SHCC:	Sustainable Strain-Hardening Cement Composite
PFRC:	Polypropylene Fiber Reinforced Concrete
GFRC:	Glass Fiber Reinforced Concrete
PC:	Plain Concrete
RCPT:	Rapid Chloride Permeability Test
UPV:	Ultrasonic Pulse Velocity
DIF:	Dynamic Increase Factor
F-T:	Freezing and Thawing Test
D_{max}:	the Maximum Aggregate Size
FA/C:	Fly Ash to Cement Ratio
RS:	River Sand
ST:	Steel Fiber
ST1:	Steel Fiber Type 1
ST2:	Steel Fiber Type 2

ST3:	Steel Fiber Type 1
FA/PC:	Fly Ash to Portland Cement Ratio
A/B:	Aggregate to Binder Ratio
W/B:	Water to Binder Ratio
PVA:	Polyvinyl Alcohol
SMA:	Shape Memory Alloy Fibers
PE:	Polyethylene Fibers
CAI:	Compression after Impact
I-TAI:	Indirect-Tension after Impact Test
PP:	Polypropylene Fiber
MC:	Methyl Cellulose
PET:	Polyethylene Terephthalate
MSF:	Macro Synthetic Fiber
SEM:	Scanning Electron Microscope

CHAPTER 1

INTRODUCTION

1.1. Objective

There are three major purposes of this project:

1) To develop high energy absorption capacity cement based composites
2) To obtain suitable steel fiber/PVA combination that exhibits flexural hardening under bending
3) To investigate the possibility of producing new generation concrete road barriers with these composites

1.2. Scope

Based on the literature review, four types of mixtures were designed for this study:

1) Normal (or conventional) concrete
2) Steel Fiber Reinforced Concrete (SFRC)
3) Engineered Cementitious Composites (ECC)
4) Hybrid Fiber Reinforced Concrete (HyFRC)

The experimental program of this study consists of two main stages. The first stage is to design the mixtures and test their basic properties in fresh and hardened states. The second stage consists of the dynamic tests for small specimens and real size road barriers.

CHAPTER 2

GENERAL INFORMATION

2.1. Fiber Reinforced Concrete

Concrete containing a hydraulic cement, water, aggregate, and discontinuous discrete fibers is called fiber reinforced concrete. It may also contain pozzolans and other admixtures (Mehta and Monteiro, 2007). Concrete is brittle under tensile loading but mechanical properties can be improved by using short discrete fibers, which prevent and control initiation and propagation of cracks.

Fibers are produced from various materials with different shapes. Fibers can be steel, organic polymers, carbon, glass, asbestos, and cellulose as shown in Figure 2.1. Figure 2.2 shows the various shapes of steel fibers.

Figure 2.1. Types of fibers

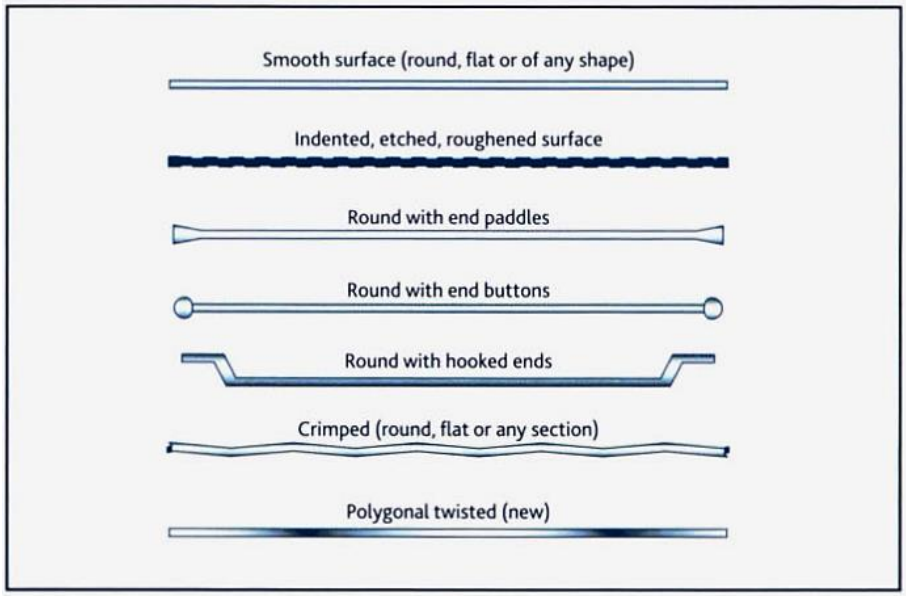

Figure 2.2. Shapes of steel fibers

(Source: Technical Report, 2007)

Steel fibers are the mostly used fibers in concrete with fiber content less than 2%. The types of fibers and its volume fraction has a marked effect on the properties of fiber reinforced concrete. The classification of fiber reinforced composites as a function of their fiber volume fraction is given bellow (Mehta and Monteiro, 2007):

Low volume fraction (<1%). The fibers are used to reduce shrinkage cracking. These fibers are used in slabs and pavements that have large surface leading to high shrinkage.

Moderate volume fraction (1-2%). This amount of fibers increases the tensile strength, fracture toughness, and impact resistance. It is used in structures that require energy absorption capability, improved capacity against delamination, spalling, and fatigue.

High volume fraction (>2%). The fibers used to enhance the strain-hardening of the composites and it is called as high-performance fiber reinforced composites. Recently, even better composites were developed and are referred as ultra- high-performance fiber reinforced composites.

2.1.1. Mechanism of Fiber Reinforcement

Tensile strength of plain concrete is low and it fails suddenly due to propagation of microcracks under applied stress. The principal role of the fibers is to bridge across the cracks that developed in the matrix, when the strain of the composite has reached the ultimate strain capacity of the matrix. Fibers transfer the load to the matrix and cause multiple cracking, this continues until the fibers fail or debonding and increases the fracture toughness (work for fracture). Fibers obstruct the microcrack propagation and delay the onset of tension cracks. As a result, tensile strength increases. Figure 2.3 shows the schematic behavior of fibers bridging around the crack in fiber reinforced concrete.

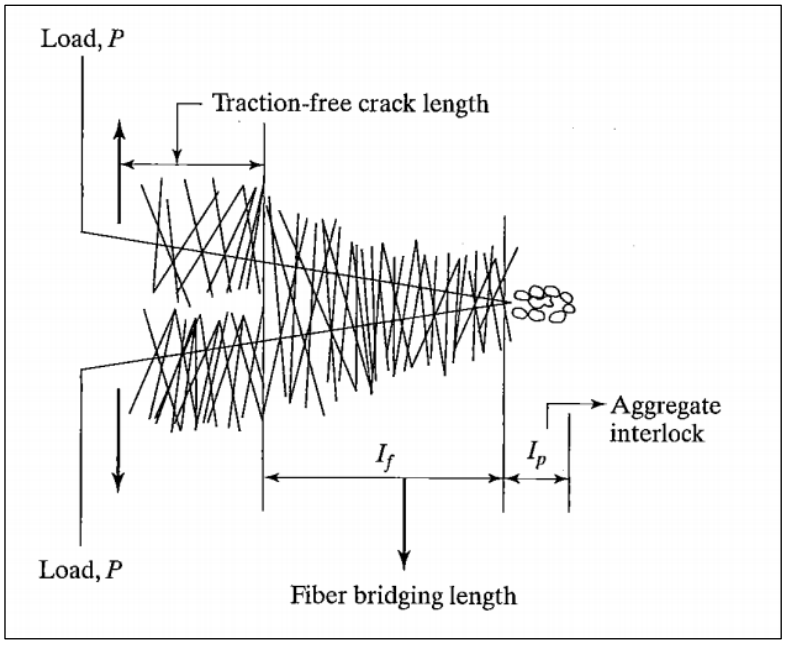

Figure 2.3. Schematic behavior of fibers bridging across a crack
(Source: Elfgren et al., 1989)

Typical load-deflection curves for unreinforced and fiber reinforced concrete are shown in Figure 2.4. Unreinforced plain concrete fails suddenly once the deflection corresponding to ultimate flexural strength exceed; however, fiber reinforced concrete continues to sustain loads even at deflection that excess fracture deflection of plain concrete.

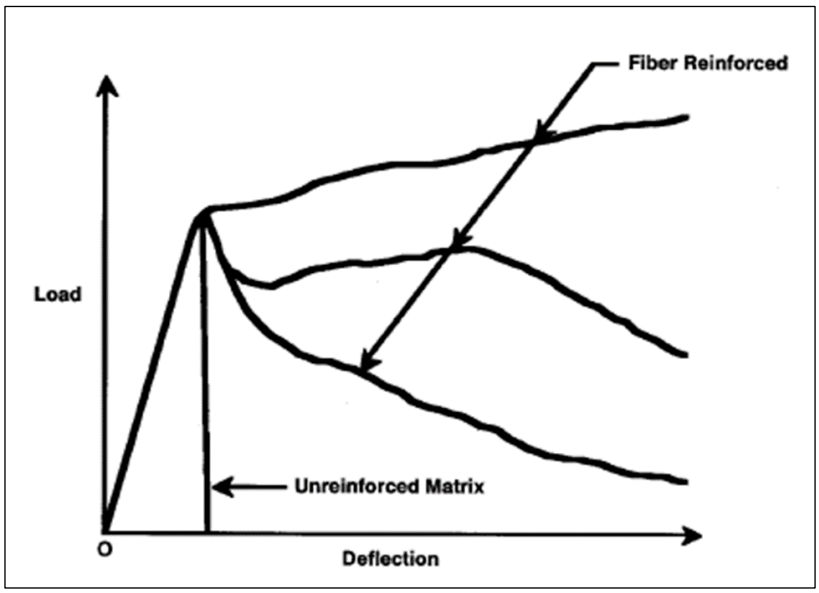

Figure 2.4. Load-deflection behavior of plain and fiber reinforced concrete (Source: ACI 544.1R-2002).

The mechanical behavior of fiber reinforced concrete depends not only on the properties of fibers and matrix, but also on the bonding between them. The bond between fiber and matrix has to be optimized. If weak, they could slip out and would not show bridging. On the other hand; if very strong, fibers break before they dissipate energy in sliding out.

Figure 2.5 shows the effect of short and long fibers on the fiber reinforced concrete. Short fibers are using to bridge the microcracks and long fibers for bridging the marcrocracks (Mehta and Monteiro, 2007).

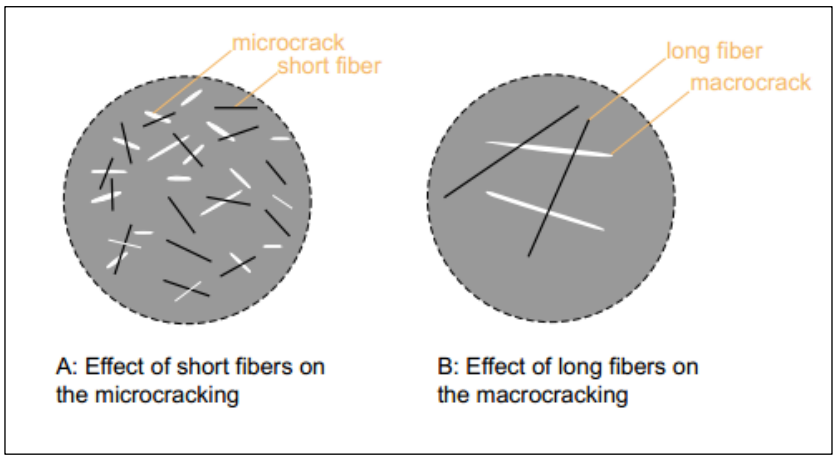

Figure 2.5. Effect of short and long fibers on the fiber reinforced concrete (Source: Mehta and Monteiro, 2007)

2.1.2. Workability of Fiber Reinforced Concrete

The addition of any type of fibers to plain concrete reduces the workability. Regardless of the fibers, the reduction of workability is proportional to the volume concentration of the fibers in the concrete. To increase the workability the fibers can have low aspect ratio (length-to-diameter ratio) and low concentration; and air-entrainment, superplasticizer, and higher volume of paste can be used.

The slump cone test is not a good method to measure the workability of fiber reinforced concrete. Addition of 1.5% of steel or glass fiber by volume to a concrete could reduce the slump from 200 mm to 25 mm (Mehta and Monteiro, 2007). Fibers generally tend to stiffen a concrete mix, and make it seem harsh when static. Under vibration the stiffening effect of the fibers tends to disappear (Mindess et al., 2003). Therefore, the Ve-Be test is considered more suitable for evaluating the workability of fiber reinforced concrete mixtures.

2.1.3. Types of Fiber Reinforced Concrete

Although steel fibers are the most widely used fibers, also there is a new generation of high performance fiber reinforced composites. The mechanical properties such as strength, toughness, and durability are significantly improved in these composites. The following types have already demonstrated (Mehta and Monteiro, 2007).

- **Compact Reinforced Composites (CPC):** It was created by Elfgren et al. (1989) in Denmark by using metal fibers, 6 mm long and 0.15 mm in diameter, and volume fractions 5-10%. High frequency vibration is required to sufficient compaction. CRC is used when very high mechanical properties required.
- **Reactive Powder Concrete (RPC):** It was found in 1990's in France. It is a cement based composite with high strength and high durability by optimizing the mix proportions. Following materials are used: cement, water, silica fume, quartz sand, and short steel fibers with 13 mm long and 0.15 mm in diameter.
- **Slurry Infiltrated Fibered Concrete (SIFCON)**: This type is obtained by placing the fibers in a formwork and then infiltrating a high fuidity mortar slurry

to coat the fibers. SIFCON shows a very ductile response and it is used for repairing of slabs and pavemenrts.

- **Engineered Cementitious Composites (ECC)**: It has ultra-high tensile strain capacity. The tensile capacity of ECC is 3-7%, while the tensile strain capacity of conventional concrete is about 0.01%. Polyvynilalchol (PVA) fibers are used which are coated with special material to optimize the bonding between fiber and matrix.
- **Hybrid Fiber Reinfoced Concrete (HyFRC)**: It is the combination of conventional concrete matrix with a mixture of more than one type of fibers. This composite may contain fibers of different materials, sizes, aspect fractions, and shapes.

This research includes three different types of concrete mixtures: normal concrete (C30/37), Engineered Cementitious Composites (ECC), and Hybrid Fiber Reinforced Concrete (HyFRC). The mechanical and durability properties of these concretes were investigated. The next chapter includes a brief literature review about these types of fiber reinforced concretes and their behaviors.

2.2. Concrete Road Barriers

Considering the number of vehicles on the roads and world traffic, it is observed that a large number of traffic accidents occur and there are loss of life and property. Moreover, the number of traffic accidents generally increases every year. Between in 2013-2014, almost 9 million traffic accidents occurred in Turkey, almost 43000 people died and 2 million people were injured (Security General Directorate, 2015). The accidents those occur as the result of exiting the vehicles from the road are 1/5 of all accidents that happed in highways. (Gözen, 2008).

Use of barriers on the roads is the common method that reduces the loss of life and property by preventing the exiting of the vehicles from the road and the crossing to opposite traffic direction. The road barriers are placed on the roadside (on shoulder and/or central refuge) to ensure the traffic safety. It is a very effective system to prevent the escaping and flying of vehicles from the road. It is also an effective technique to stop the crossing of vehicles to the other traffic direction. Therefore, road barriers are

designed to reduce internal impact intensity of vehicle and to slow down and stop the vehicle securely.

In Turkey, most of the road barriers are made from steel. Steel road barriers cannot prevent heavy vehicles, and at some accidents, they cause injuries and deaths by entering into the vehicle as shown in Figure 3.6. There are many news in the national media of Turkey related to these type of accidents (Turkish Ready Mixed Concrete Association, 2015). Therefore, the steel road barriers are gradually replaced by concrete road barriers in Europe, America, and Turkey. On these bases, this study focused on concrete road barriers to investigate their properties. The importance of this topic can be verified by the fact that, Turkish Cement Manufacturers' Association arranged recently a workshop entitled as "International Concrete Road Barriers and Road Safety".

Figure 2.6. Steel road barriers accident

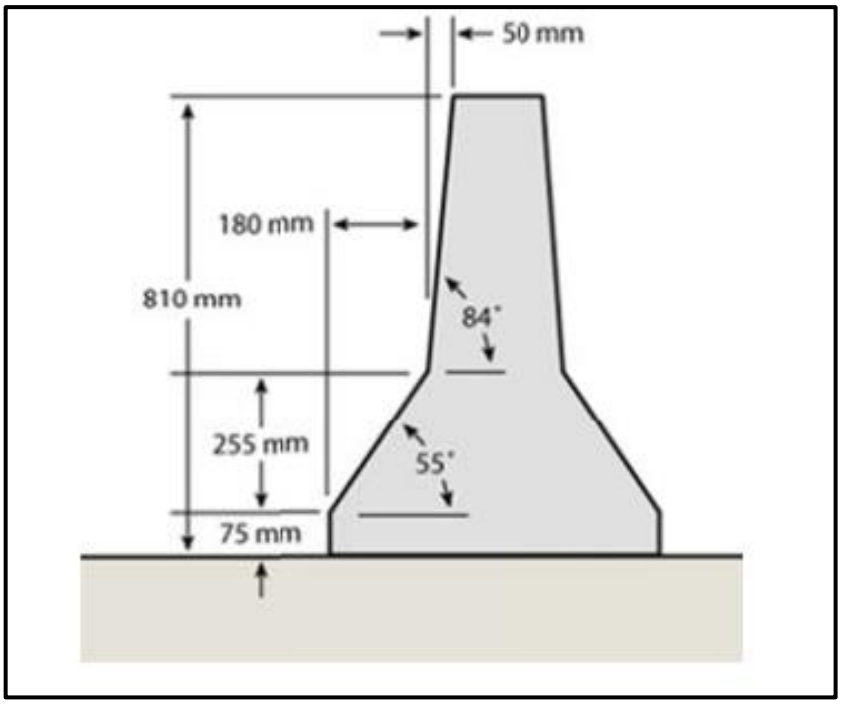

Figure 2.7. Concrete road barriers cross section

Concrete road barriers can be casted in place or prefabricated as precast concrete. Precast road barriers became common in recent years with the purpose of reducing surface roughness and increasing the manufacturing precision. New Jersey type (shown in Figure 3.7) is common in Turkey among other types. The concrete road barriers were applied in 1988 in Istanbul between Mavievler-Bostancı at 3-km location. According to data of Istanbul Security Directorate. The traffic accidents are decreased 48 percent under favor of concrete road barriers during that certain time. According to statistics, after the application of concrete road barriers, the number of traffic accidents on Eskişehir road reduced 8 percent (Gözen, 2008). Wide knowledge about the concrete road barriers can be gained from Yeğinobalı (2011). The advantages of concrete road barriers can be listed as follows:

- Procuring of materials is easy and local production
- Easy production of precast or cast-in-place of concrete
- Service life can be 40-50 years (compared to steel road barriers, they are economic at long period of time)
- The hitting vehicle's wheels staying on road barrier surface, not changing direction and slowing down, and also minimizing the damage.
- After a traffic accident, the other accident can be stopped securely at same location. (Repairing is necessary for steel road barrier.)

- When they prevent to tumble and prevent to cross the other direction, surrounding trees, lighting poles and installation damages are prevented as well.
- They are portable and can be moved to desired location.
- They have multipurpose usage (sound insulation for environment, screening of other direction traffic, and etc.)
- Can be produced with different shapes and colors

Despite all these advantages there are also some disadvantages of concrete road barriers, as listed below:

- Energy absorption capacity of concrete is low.
- Precaution is required about de-icing salt corrosion and snow accumulation.
- Concrete road barriers are heavy. (Precast usage is more difficult than steel road barriers.)

One of the aims of this study is to overcome these disadvantages. The energy absorption capacity of concrete is low. The best solution is to produce the new generation of concrete with high energy absorption capacity cement based composites. The durability of such composites is expected to be higher. Moreover, this study will employ lightweight aggregates to reduce the weight of the barriers.

CHAPTER 3

LITERATURE REVIEW

Cement based materials like concrete do not have high strain capacity. In order to prevent brittle behavior of concrete, fiber reinforced concrete is produced, but normal type of fiber reinforced concrete may not have high deformation property especially under tensile load. At the present time, high performance cement based composites show higher deformation under tensile load. In recent years, two types of them come into prominence. The first type is Engineered Cementitious Composites (ECC) and the second type is Hybrid Fiber Reinforced Concrete (HyFRC)

3.1. Engineered Cementitious Composites (ECC)

Engineered Cementitious Composites (ECC) is a new class of High Performance Fiber Reinforced Cementitious Composites (HPFRCC) micro-mechanically designed to achieve high damage tolerance under severe loading and high durability under normal service conditions. Unlike ordinary concrete, ECC has very high tensile strain capacity in the range of 3-5% which can be considered as a ductile material (Şahmaran and Li, 2009). It shows a strain capacity 300–500 times greater than normal concrete as shown in Figure 3.1. ECC beam bends similar to a ductile metal plate under bending loads as shown in Figure 3.2.

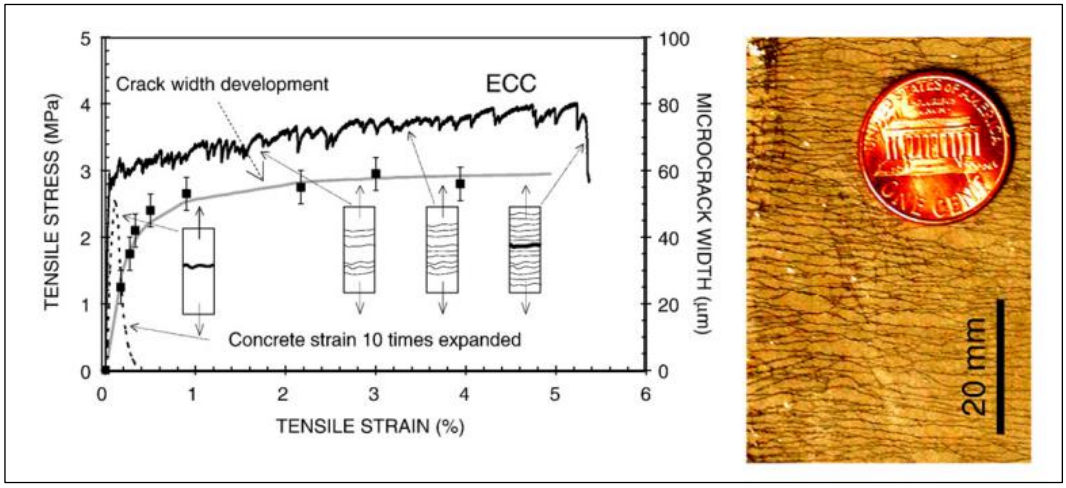

Figure 3.1. Tensile stress–strain curve and crack width development of ECC (Source: Şahmaran and Li, 2009).

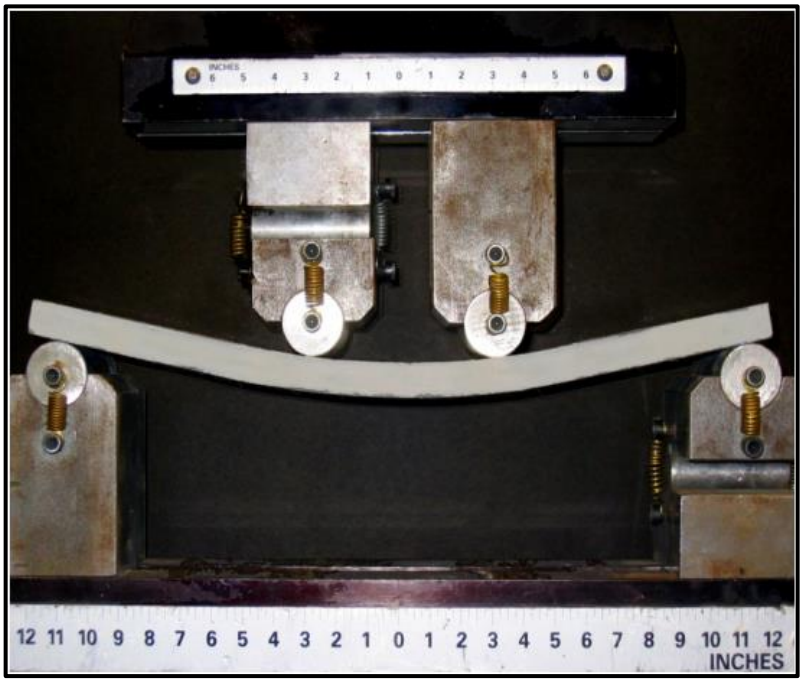

Figure 3.2. ECC under bending loads (Source: Yang and Li, 2010)

The main reason of high ductility of ECC is the flexural hardening which occurs after the formation of the first crack due its micromechanics design (Şahmaran and Li, 2009). During loading, the first cracks have widths up to average of 60 μm. When loading is continued, the number of cracks increase instead of the width of first crack as shown in Figure 3.1. After the formation of first crack the material deforms in this way, at the same time load is increased until the material reaches its ultimate strength. Even

at the maximum deformation, average crack width remains constant at the level of 60 µm. This behavior is gained with the control of fiber and matrix interface interaction and micromechanics design. For instance, chemical bonding between fiber and matrix interface should be low and after rupture of the bond the friction between fiber and matrix should be sufficient (Li 1998, Wang and Li 2007, Li et al. 1995, Li et al. 2002).

The ingredients of ECC are cement, sand, fiber, water, and some mineral and chemical admixtures. Coarse aggregate is not used because it affects homogenous and ductile behavior of ECC. The non-ionic polymer with steric action such as Polyvynilalcohol (PVA) coated with a special material is used to optimize the bonding between fiber and matrix. It can be cast as normal method or extrusion by using of optimum amount of superplasticizer to reduce the water content and enhance the workability of ECC. The PVA is used about 2% or less by volume with the diameter of 50 µm (Schneider, 1991). The typical mix design for ECC (ECC-M45) with self-consolidating casting are given in Table 3.1.

Table 3.1 Typical mix design by weight for ECC-45 (Source: Li, 2007)

Cement	**Water**	**Sand**	**Fly Ash**	**HRWR**	**Fiber (Vol. %)**
1.00	0.56	0.80	1.20	0.012	2.00

The range of tensile strength and ductility of ECC can be adjusted depending on the demands of a particular structure. It is a very good repair composite especially for pavements, slabs, and bridge decks and it is also used to retrofit structures that resist seismic loads. Li et al. (2007) summarized the types and their applications as bellow.

- Self-consolidating ECC (e.g., ECC M45 and its variants) is designed for large-scale, on-site construction applications.
- High-early-strength ECC (HES-ECC) is designed for applications that require rapid strength gain, such as transportation infrastructure that must be quickly reopened to the public.
- Lightweight ECC (LW-ECC) is designed for applications where the dead load of structural members must be minimized.
- Green ECC (G-ECC) is designed to maximize material greenness and infrastructure sustainability.

- Self-healing ECC (SH-ECC) emphasizes the functionality of recovering transport and mechanical properties after experiencing damage.

The overall advantages of ECC are flexural hardening, self-control of cracks, high tensile strain capacity, high tensile strength, high durability, and self-healing ability of cracks.

3.1.1 Compressive Strength

In structural design the most common and important parameter of concrete is its compressive strength. It means that material with higher strength is expected to have higher structural strength. This concept is correct only of the material strength property governs the failure, however, if tensile fracture failure occurs, a high strength material does not necessarily mean higher structural strength. Reasonably, a high toughness and ductile material like ECC, can lead to higher structural strength (Li, 2003). Compressive strength of ECC are similar as normal to high-strength concrete which is between 25 to 95 MPa (Li, 2007).

Zhu et al. (2014) studied the effects of various types of mineral admixtures (fly ash, slag, and silica fume) on compressive strength of ECC. This research found that the compressive strength becomes weak as the content of single mineral admixture increase, especially for ECC with high volume of fly ash.

Ma et al. 2016 examined the influence of fly ash types on mechanical properties of ECC. Five types of fly ash were used in this study and chemical properties of these fly ashes are given in Table 2.2. The compressive strengths of ECCs with different fly ashes are shown in Figure 3.3. Results in this study indicate that CaO content has the main role in compressive strength of ECC, the mixture E with high CaO content shows the highest compressive strength and the mixture A with low CaO content shows the lowest compressive strength.

Table 3.2 Different types of fly ashes % (Source: Ma et al. 2016)

Fly ash No.	SiO_2	Al_2O_3	Fe_2O_3	CaO	Loss on ignition
A	54.3	36	2.6	1.7	1.5
B	50.5	17.8	7.4	4.3	2.4
C	56.2	31.4	3.9	2.8	2.1
D	47.5	24.9	5.7	4.2	2.2
E	54.2	22.6	7.2	8.6	1.4

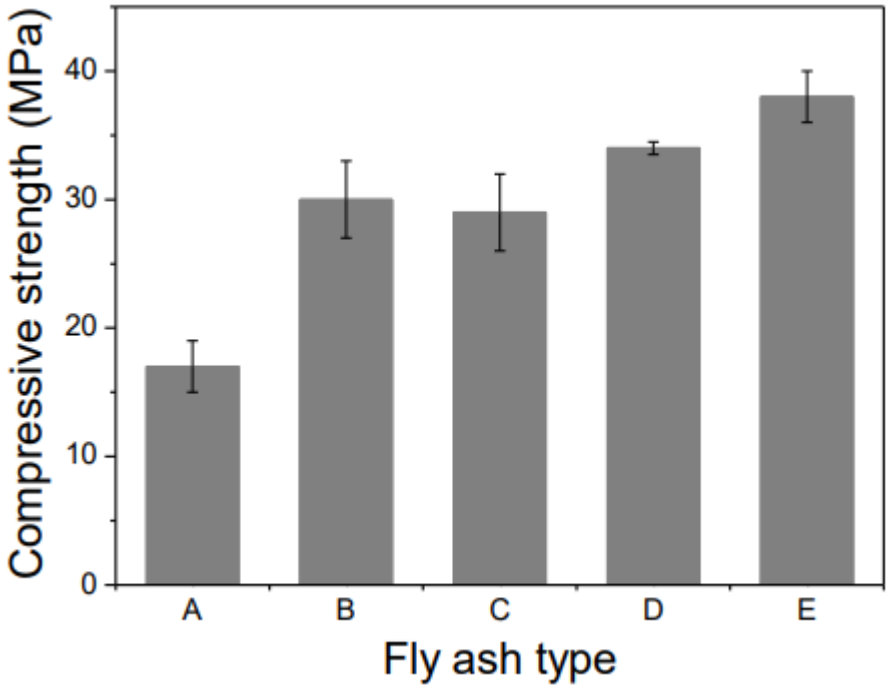

Figure 3.3 Compressive strength of ECCs
(Source: Ma et al. 2016)

Ammasi and Ragul (2018) investigated the fly ash content effect on the strength of ECC. In this research, five mixtures with replacing cement content with Class F fly ash in the range of 40%, 60%, 80%, and 100% were studied. The compressive strength results are shown in Figure 3.4. Results show that the compressive strength is decreasing as the fly ash content increases.

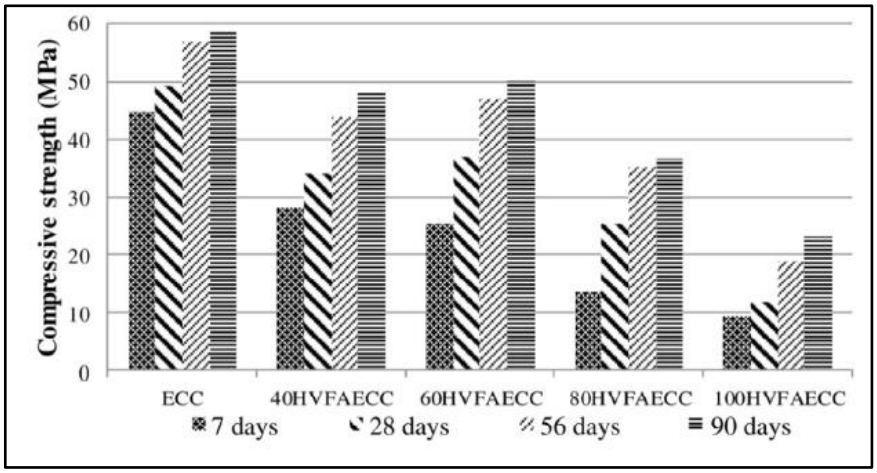

Figure 3.4. Fly ash effects on ECC compressive strength
(Source: Ammasi and Ragul, 2018)

Keskin et al. (2013) investigated the effect of presoaked expanded perlite aggregate on the mechanical properties of ECC. In this study, expanded perlite aggregate was soaked in water for 24 hours, then replaced 10, 20, and 30% of the fine aggregate of ECC mixtures. Results show that presoaked lightweight aggregate significantly decreases the compressive strength of ECC Table 3.3. However, when the compressive strength development is concerned, the increase in compressive strength of tested mixtures between 28 and 90 days were 19.9, 15.2, 20.6, and 23.4% for ECC-0, ECC-10, ECC-20, and ECC-30 respectively. The ECC-30 mixture displayed the highest increase due to internal curing of the mixture in 90 days age.

Table 3.3 Compressive strength results of ECC (Source: Keskin et al. 2013)

Mechanical Property	ECC-0		ECC-10		ECC-20		ECC-30	
	28 days	90 days	28 days	90 days	28 days	90 days	28 days	90 days
Compressive Strength (MPa)	60.8	72.9	53.6	61.8	48.6	58.7	39.8	49.1

Jedidi et al. (2015) searched the effect of expanded perlite aggregate dosage on properties of lightweight concrete. Expanded perlite was used 15, 30, 45, 60, and 80% by volume of sand. These mixtures contained high amount of expanded perlite with the unit weights varied between 560 and 1510 kg/m^3. Figure 3.5 shows the compressive strength results of this study, indicating that the compressive strength values decrease with an increase in expanded perlite aggregate content from 0% to 80%.

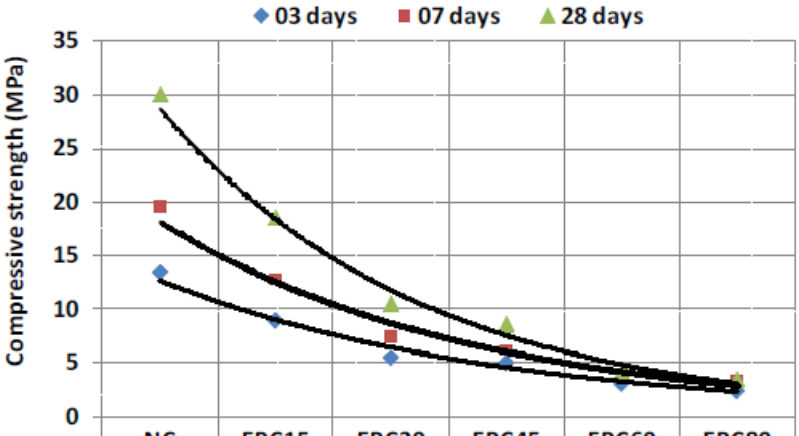

	NC	EPC15	EPC30	EPC45	EPC60	EPC80
03 days	13,5	9	5,5	5	3,1	2,4
07 days	19,5	12,7	7,5	6,2	3,8	3,2
28 days	30	18,5	10,5	8,6	4,2	3,4

Figure 3.5. EPA effects on ECC compressive strength
(Source: Jedidi et al. 2015)

Barnat-Hunek et al. (2018) studied the effect of perlite aggregate content on microstructure-mechanical properties of hybrid fiber-reinforced self-compacting lightweight concrete. In this study, washed quartz sand was replaced with perlite by 5% and 15%. It was seen that the compressive strength decreases as perlite content increases. Compressive strength at 28 days was 74.63 and 68.32 MPa for 5% and 15% replacements, respectively.

3.1.2. Flexural Performance

The flexural reaction of ECC reflects its tensile ductility (Wang and Li, 2007). “Under bending, multiple microcracking forms at the base of the beam, allowing it to undergo a large curvature development, a phenomenon that has resulted in the popular name of bendable concrete.” (Li, 2007). “The fully bridged flat crack with limited width allows load transfer from the bridging fibers back into the matrix to activate additional flaw sites into new microcracks.” (Yang and Li, 2014). With this mechanism a flexural strength of 10 to 15 MPa is easily achievable and is escorted by a significant deflection-hardening regime (Li, 2007).

Turk and Nehdi (2018) studied the effects of limestone powder and high-volume fly ash on mechanical properties of ECC. Nine ECC mixtures were prepared by replacing 0%, 50%, and 100% of silica sand with limestone powder on mass based with the FA/C ratio 1.2, 2.2, and 3.2. Fracture toughness results of this study is given in Figure 3.6. The fracture toughness and flexural strength of all ECC mixtures decreased at all testing ages when the FA/C ratio increased from 1.2 to 3.2 due to reduction of cement content.

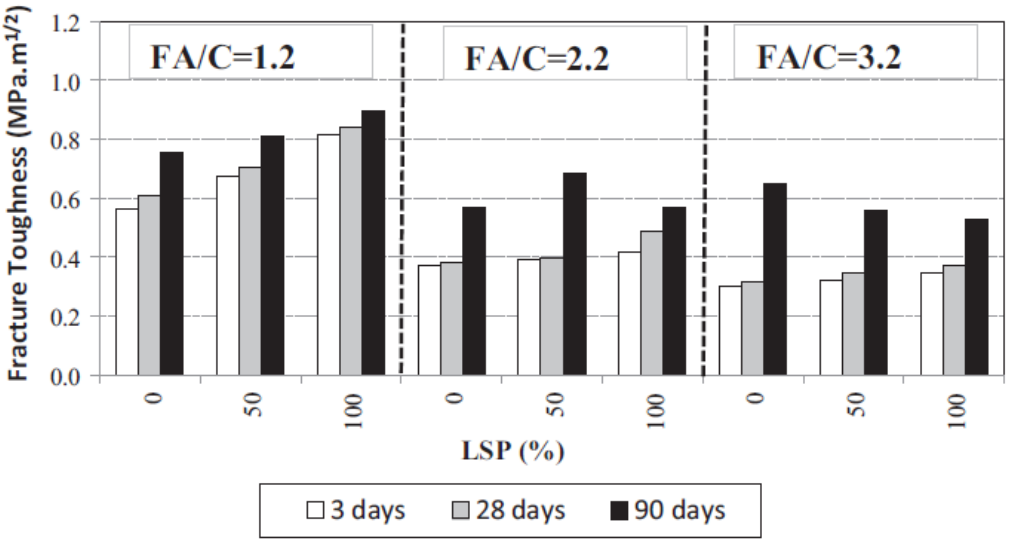

Figure 3.6. Fracture toughness test results for ECC

(Source: Turk and Nehdi, 2018)

Zhang et al. (2014) investigated mechanical properties of ECC with different volumes of fly ash. In this study fly ash to cement ratios were 1.2, 2.2, and 4 with mixtures names M1, M2, and M3 respectively. The specimen dimensions for bending test was 400 x 70 x 16 mm. The four-point test was performed on longer span and thinner depth which shows larger bending capacity as 10 to 20 mm as shown in Figure 3.7. The flexural performance of these specimens are given in Figure 3.8. Results show that flexural strength decreases when fly ash content increases, however, increasing fly ash content makes ECC more ductile.

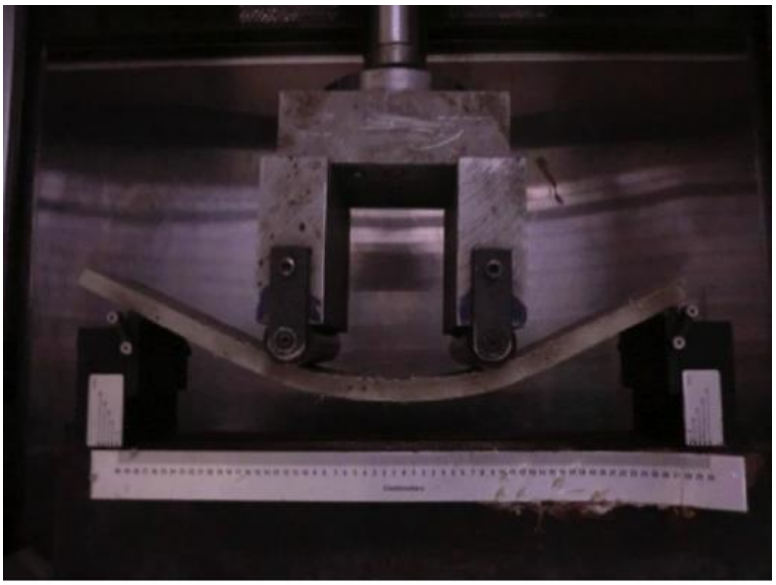

Figure 3.7. Bending performance of ECC

(Source: Zhang et al. 2014)

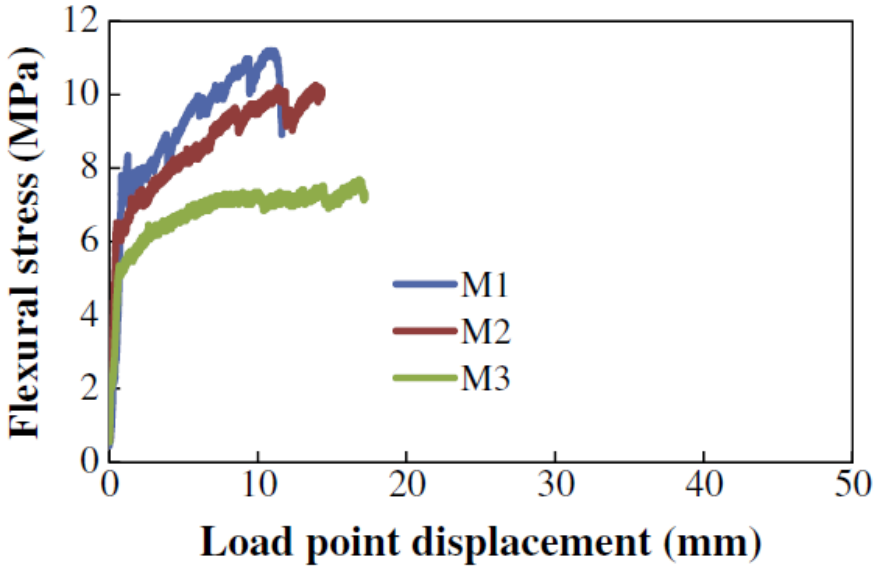

Figure 3.8. Flexural performance of ECC

(Source: Zhang et al. 2014)

Ammasi and Ragul (2018) investigated the fly ash content effect on the flexural strength of ECC. Fly ash content was 40%, 60%, 80%, and 100% by replacing cement content. Results show that flexural strength decreases when the fly ash content increases as shown in Figure 3.9.

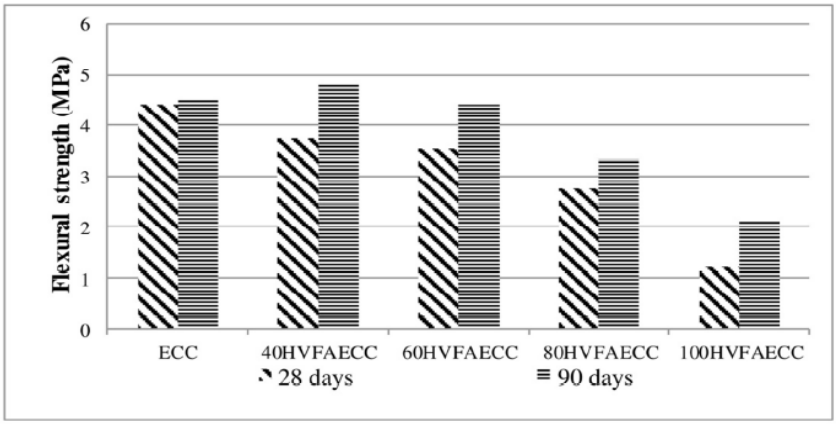

Figure 2: Flexural Strength (MPa)

Figure 3.9. Fly ash effects on ECC flexural strength

(Source: Ammasi and Ragul, 2018)

Keskin et al. (2013) investigated the effect of presoaked expanded perlite aggregate on the mechanical properties of ECC. In this study, expanded perlite aggregate was soaked in water for 24 hours, then replaced 10, 20, and 30% of the fine aggregate of ECC mixtures. Figure 3.10 presents typical flexural stress-deflection curves for each ECC mixture at age of 28 days. There is a significant decrease of flexural strength as the amount of presoaked perlite replacement increases, which can be attributed to large aggregate sizes and the low strength of expanded perlite. The fracture toughness also decreased as the amount of presoaked perlite increased.

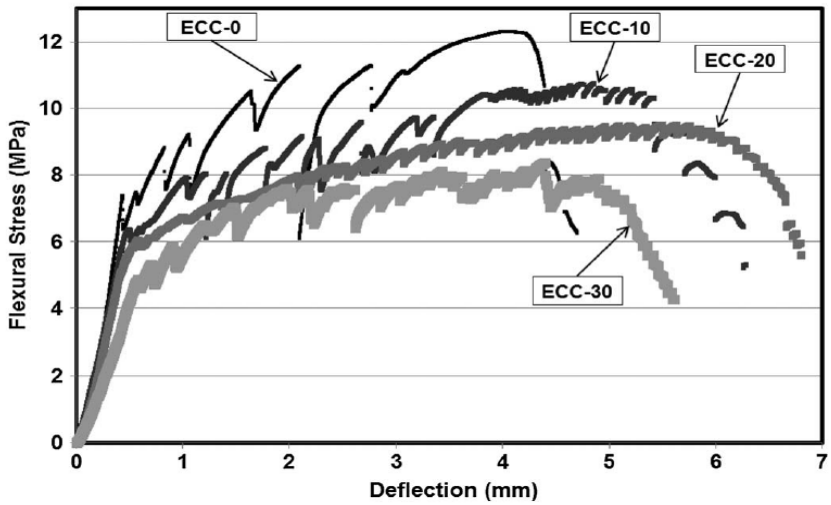

Figure 3.10. Flexural stress-deflection curves of ECC

(Source: Keskin et al. 2013)

3.1.3. Impact Loading

ECC is a unique high performance fiber reinforced concrete which exhibites high ductility and damage tolerance under tensile and shear loading (Yang and Li, 2012).

Zhang et al. (2007) studied the performance of hybrid-fiber ECC blast/shelter panels subjected to drop weight impact load. Drop weight test was conducted on full-scale hybrid-fiber ECC blast/shelter panels (2 m x 1 m x 0.05-0.1 m). Control specimens normal reinforced concrete (RC) for the impact tests were full-scale (2 m x 1 m x 0.1 m) prototypes of commercially available concrete blast or shelter doors with a nominal compressive strength of 40 MPa. The FRC followed a recommended (ACI 1996) typical mix containing 1% steel fibers to represent conventional FRC performance. For the hybrid-fiber ECC specimens, the same mix containing 0.5% steel and 1.5% polyethylene fibers (by volume). ECC panel specimens of different thicknesses (50, 75, and 100 mm) as ECC50, ECC75, ECC100 as well as normal RC and steel FRC panels of thickness 100 mm. All panels were reinforced orthogonally with 8 mm diameter mild steel bars spaced at 150 mm center to center. All mixtures specimens after testing are shown in Figure 3.11. In this figure the number of impacts to perforation are shown in the brackets. The tests on ECC100 were aborted after the tenth impact in view of the very minor damage exhibited, indicative of many more impacts required to achieve perforation. The ECC75 and ECC50 specimens also performed better than the FRC and RC specimens even though they had lower tackiness.

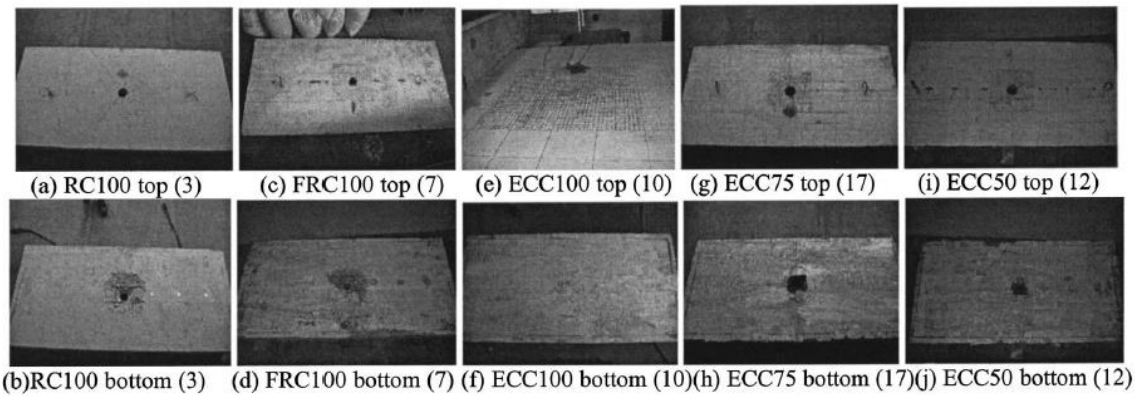

Figure 3.11. Specimens after testing

(Source: Zhang et al. 2007)

Yang and Li (2012) studied tailoring of ECC for impact resistance. Low speed drop weight tower test was carried out on ECC beams. ECC beams having dimensions 305 × 76 × 51 mm with and without a single steel bar reinforcement were tested under three-point-bending drop weight impacts. The 5 mm diameter smooth steel bar was placed close to the bottom side with a clear cover of 18mm. The reinforcing ratio was 0.5%. A control specimen using reinforced concrete (fc′=40 MPa) was also tested. The load-deflection curves of these beams are shown in Figure 12. Table 3.4 shows the load and energy capacities of the four beams. Results indicates that load and energy capacity of ECC and R/ECC mixtures significantly increased when compared with normal concrete and R/C mixtures.

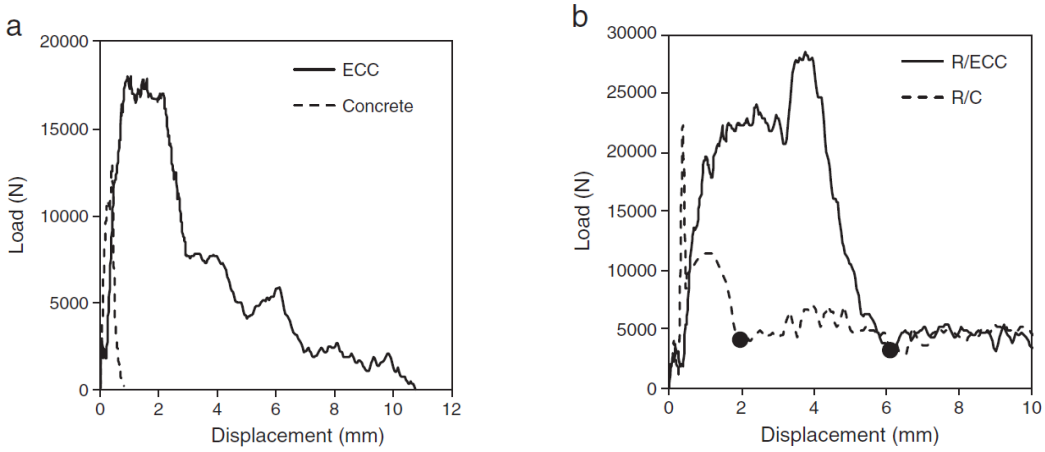

Figure 3.12. Load–displacement relationships of (a) ECC and concrete beams, and (b) R/ECC and R/C beams in single impact experiment.
(Source: Yang and Li, 2012)

Table 3.4 Load and energy capacity of composites (Source: Yang and Li, 2012)

	Concrete	R/C	Improvement due to reinforcement	ECC	R/ECC	Improvement due to reinforcement
Load capacity (kN)	13	22	9	18	29	11
Energy capacity (N-m)	4	17	13	69	102	33

Ali et al. (2017) investigated impact loading behavior of Hybrid-ECC. Drop weight impact test was conducted according ACI-544 guidelines at 90 days age. One ECC mixture without fiber, one control ECC mixture, and three ECC mixtures with

additional shape memory alloy (SMA) fibers 0.5%, 1%, and 1.5% by volume fraction were tested. Figure 3.13 shows the energy absorption capacities of these mixtures. Results illustrate that the ECC mixture without fiber (ECC0-0) failed after only one hit by the drop weight and split into multiple trashes, which reflects its brittle behavior under impact loading. ECC2-0 carried impact loading up to failure about 13 and 39 times higher than ECC0-0 which reflect the beneficial effect of including PVA fibers in ECC. The SMA fiber addition significantly improved the impact resistance of ECC specimens as 1423%, 1687%, and 1628% for ECC2-0.5, ECC2-1, and ECC2-1.5 respectively.

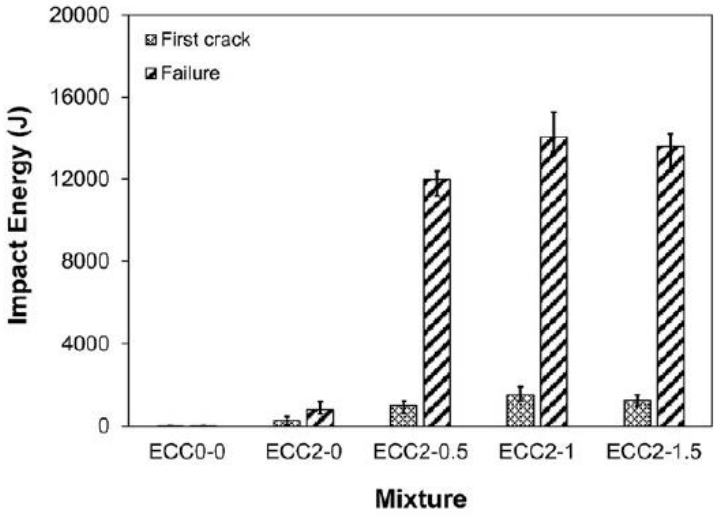

Figure 3.13. Impact energy of ECC mixtures
(Source: Ali et al. 2017)

3.1.4. Durability

ECC is designed to achieve high damage tolerance under severe loading and high durability under normal service conditions (Sahmaran and Li, 2009). ECC composite is highly durable under accelerated weathering, freezing and thawing cycles with or without de-icing salts, alkali-silicate reaction, and chloride immersion (Li et al. 2007).

Ammasi and Ragul (2018) investigated the fly ash content effect on the durability of ECC. Fly ash content was 40%, 60%, 80%, and 100% by replacing cement content. To determine the durability properties, water absorption and rapid chloride ion permeability tests were performed in this study. Figure 3.14 and Figure 3.15 show that

the water absorption and chloride ion penetration of ECC without fly ash were higher than ECC with fly ash. The water absorption demand and chloride ion penetration of ECC with fly ash decreased as the percentage of fly ash increased. The lesser water absorption and chloride ion penetration were due to the dense matrix created by the pozzolanic action of fly ash as the curing increased.

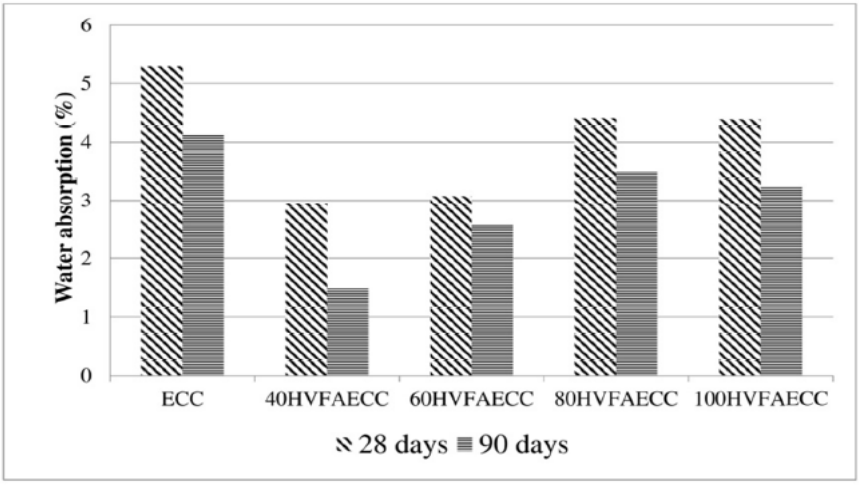

Figure 3.14. Water absorption of ECC
(Source: Ammasi and Ragul, 2018)

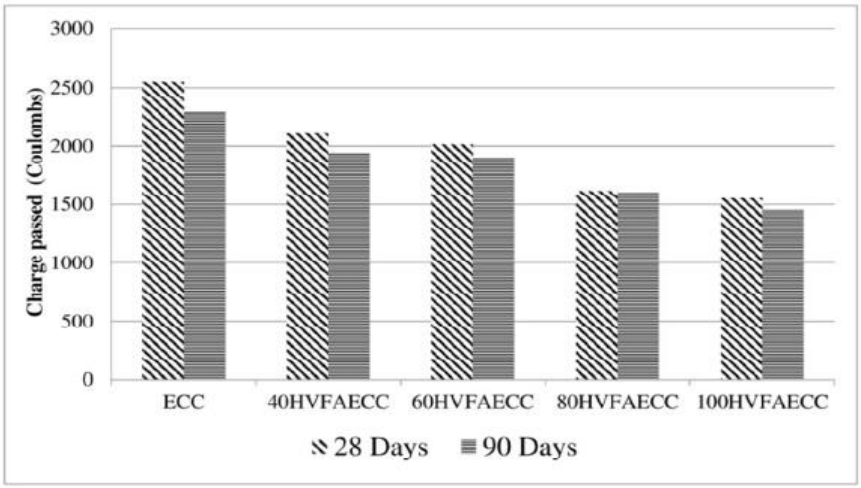

Figure 3.15. Chloride ion penetration of ECC
(Source:Ammasi and Ragul, 2018)

Sahmaran and Li 2009 studied durability properties of micro-cracked ECC containing high volume fly ash. In this study, mixtures contained two different amounts of fly ash as a replacement of cement (55 and 70% by weight of total cementitious

material). Salt ponding, rapid chloride permeability and sorptivity tests were performed on virgin and micro-cracked specimens after 28 days. Results show that micro-cracks made by mechanical pre-loading increase the chloride transport and the sorptivity values of ECC. In this study chloride ion penetration and sorptivity increased as the fly ash content increases from 55 to 70% in virgin and micro-cracked specimens. The reason was explained as follows: Normally, it is accepted that increasing fly ash content is an effective means for reducing the coefficient of chloride diffusion due both its chloride binding effect and pore refinement. However, these benefits are usually manifested at later ages.

Zhang et al. (2014) investigated durability behavior of ECC with different volumes of fly ash. In this study, rapid chloride penetration test (RCPT) and sorptivity test were applied on ECC with fly ash to cement ratios of 1.2, 2.2, and 4 with mixture names as M1, M2, and M3, respectively. As Figure 3.16 shows, the charge passed increases as fly ash content increases for the virgin specimens. Cracks provide an extra lane for the charge to pass through, leading to a larger charge passed from cracked specimens compared with that from the virgin ones. Figure 3.17 shows sorptivity test results, and as seen, the sorptivity of ECC increases as the fly ash content increases since higher fly ash content makes the matrix more porous. The existence of crack after loading increases the water absorption capacity of ECC because micro-cracks act as capillary pipe absorbing and storing water in the crack, thus increasing the absorbed water weight.

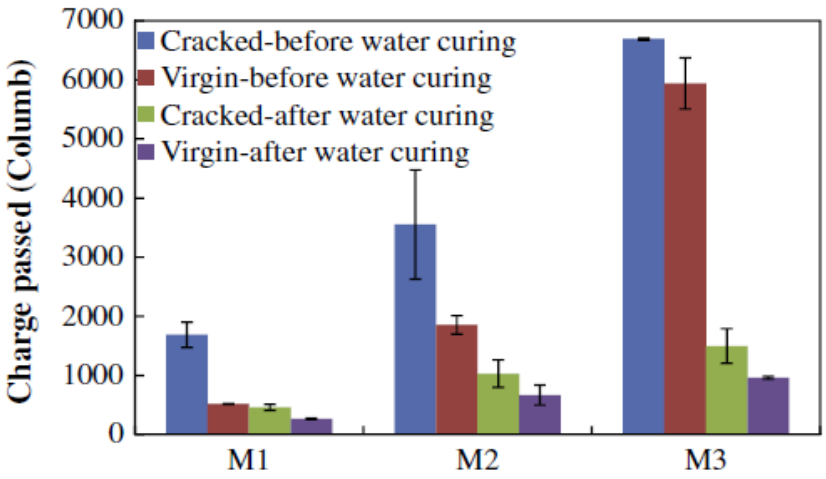

Figure 3.16. Charge passed ECC specimens before and after 30 days water curing (Source: Zhang et al. 2014)

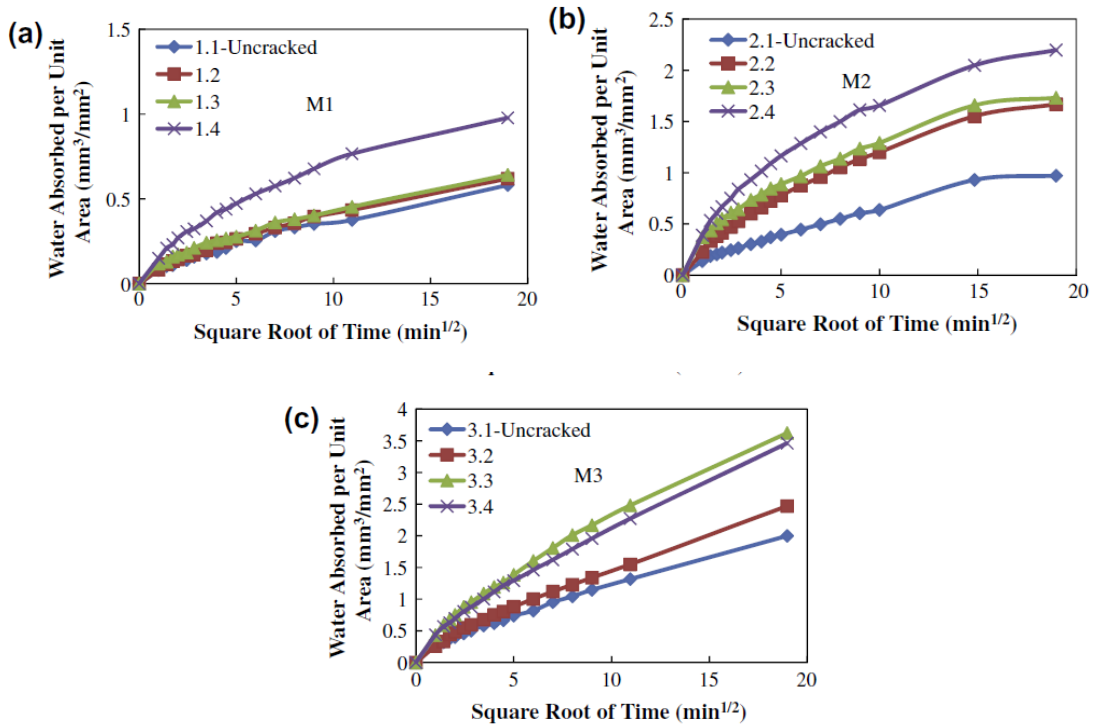

Figure 3.17. Sorptivity rest results for different ECC mixtures before self-healing, (a) for M1, (b) for M2, and (c) for M3

(Source: Zhang et al. 2014)

Sahmaran et al. (2012) searched frost resistance and microstructure of ECC. In this study, ECC mixtures with two different fly ash to cement ratios (1.2 and 2.2 by weight) as ECC1 and ECC2 are prepared. The same mixtures without PVA fiber were also investigated to compare the behavior of ECC and its matrix. All mixtures were exposed to the freeze and thaw cycles up to 300 cycles according ASTM C666. Figure 3.18 shows relative pulse velocity and mass loss changes as a function of number of freezing and thawing cycles. Control ECC mixtures without fiber rapidly failed in freezing and thawing cycles as ECC1 matrix after 210 cycles and ECC2 matrix after 60 cycles. Both ECC mixtures showed excellent performance when exposed to freezing and thawing cycles, even after 300 cycles. The addition of PVA fiber to ECC matrixes improved the freeze–thaw resistance considerably. Results also indicate that freeze-thaw resistance of ECC decreases as fly ash content increases. ECC specimens exhibited some surface scaling at the end of the freeze-thaw cycles. Surface scaling of ECC1 was less than ECC2 as seen in Figure 3.19.

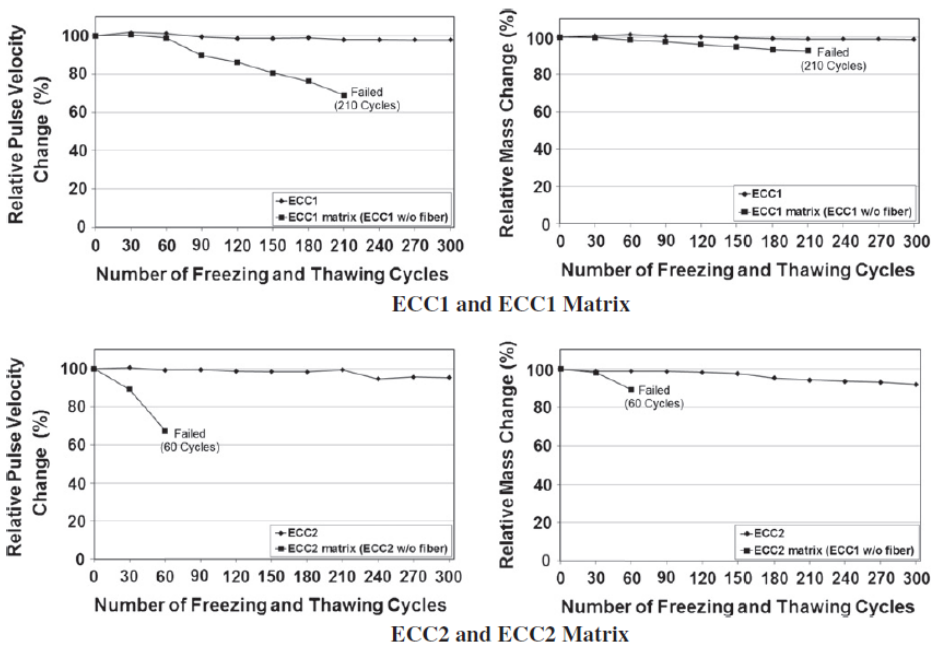

Figure 3.18. Relative pulse velocity and mass loss changes as a function of number of freezing and thawing cycles

(Source: Sahmaran et al. 2012)

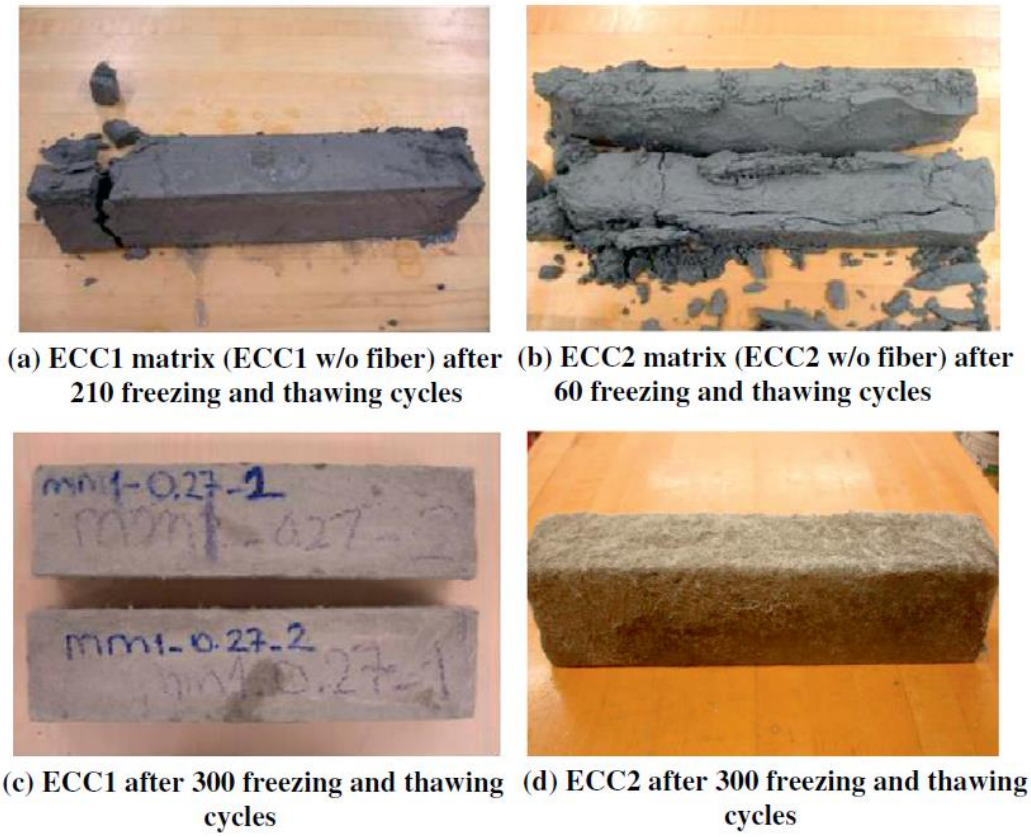

Figure 3.19. Specimens surface appearance after freeze–thaw cycles

(Source: Sahmaran et al. 2012)

3.2. Hybrid Fiber Reinforced Concrete (HyFRC)

Hybrid fiber-reinforced concrete (HyFRC) contains two or more types of fibers with different materials, length, and aspect ratio. These composites are produced with fine and coarse aggregates and hybrid fibers. It is cheaper and more workable compared to ECC due to the lower cost of steel fiber than PVA, lower cost of coarse aggregate than fine aggregate and less amount of fibers in total. HyFRC exhibits deflection hardening under bending loads.

Deflection hardening mechanism under bending is explained by Blunt and Ostertag (2009a) as follows: Microcracks first occur under bending for unnotched specimens over a diffuse area. The formation of diffuse system can promote material impermeability by delaying crack coalescence and interconnectivity. It is also the mechanism of ductility enhancement of a material. Use of hybrid fibers can provide this type of mechanism of cracking to material. As shown in Figure 3.20 the small spacing of microfibers provides a source of immediate crack flanking. As stresses increase in the cracked region, the primary mechanism of crack growth resistance is smoothly transferred to the larger fibers which provide the primary source in the fiber bridging zone after crack coalescence and localization.

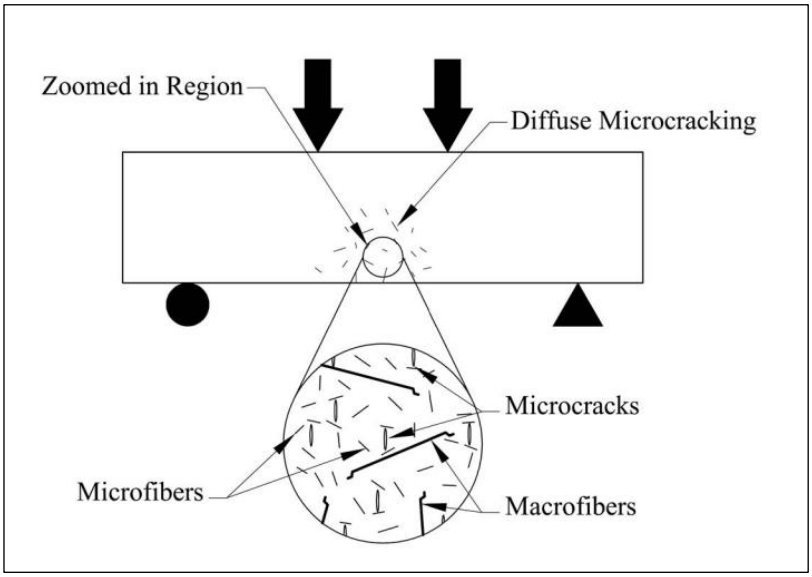

Figure 3.20. Cracking behavior in deflection hardening of HyFRC

(Source: Blunt and Ostertag, 2009a)

For the hybird fiber composites that exhibit flexural hardening under bending, adjusting the maximum aggregate size (D_{max}), finding proper amount and size of fiber combination is critical for workability and mechanical properties. These parameters are investigated by Blunt and Ostertag (2009b). Various mixture combinations were used in this study; the D_{max} of aggregate, PVA fiber volume fraction, steel fiber parameters (sizes, aspect ratios, and volume fractions) are given in Table 3.5. The results of four-point bending test for these mixtures are shown in Figure 3.21 and Figure 3.22.

Table 3.5 Mixture proportions of HyFRC (Source: Blunt and Ostertag, 2009b)

Mixtures	Dmax of aggregate, mm	PVA volume fraction, %	Steel Fiber					
			Steel Fiber 1			Steel Fiber 2		
			Length, mm	Aspect ratio	Volume Fraction, %	Length	Aspect ratio	Volume Fraction, %
F1	25	–	–	—	—	60	65	0.7
F2	25	0.3	–	—	—	60	65	0.7
F3	25	0.3	–	—	—	60	80	0.7
F4	9.5	0.2	30	55	0.5	60	80	0.5
F5	9.5	0.2	30	55	0.5	60	80	0.8

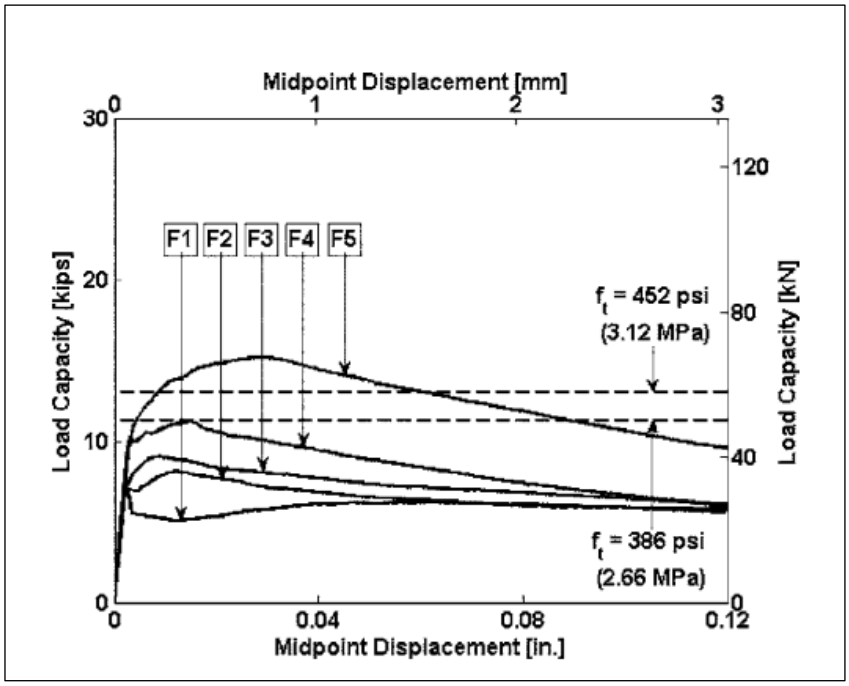

Figure 3.21. Flexural behavior of five mixtures
(Source: Blunt and Ostertag, 2009b)

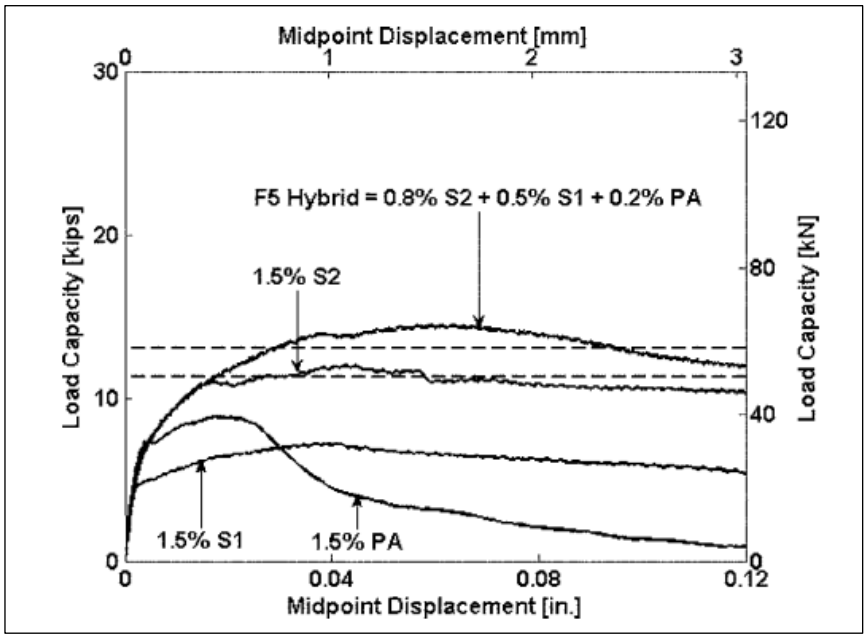

Figure 3.22. Flexural behavior of single fiber and hybrid fiber proportion at the same total volume fraction

(Source: Blunt and Ostertag, 2009b)

As seen in the Figure 3.21, these mixtures show different behaviors. F5 mixture has the best performance according the criteria that indicated by researchers as drawn with the as dashed line. F5 mixture shows the best ductility among the other mixtures and it has the highest energy absorption capacity.

Flexural performance of hybrid fiber and single fiber composites are shown in Figure 3.22. The total amount of fiber is adjusted constant at 1.5% for all mixtures. Here, PA states for PVA fiber, S1 states for steel fiber with 30 mm length and aspect ratio of 55, and S2 states for steel fiber with 60 mm length and aspect ratio of 80. It shows that proper combination of hybrid fibers has better performance. Important point from this comparison is that ECC also contains single fiber, therefore it conforms the importance of comparing ECC and HyFRC in this research.

As it is a relatively new composite and there are many unknowns which have not been studied in literature yet, this study which includes producing a low cost deflection hardening composite with less amount of fibers that shows a deflection hardening behavior is very important. One application of hybrid fiber reinforced concrete which will be also investigated in this study is concrete road barriers.

3.2.1. Workability

The addition of any type of fibers to plain concrete reduces the workability. Reduction of workability is proportional to many other parameters such as maximum aggregate size, fiber volume, fiber type, and fiber aspect ratio. To increase the workability, the fibers can have low concentration, air-entraining admixture and superplasticizer can be used, and paste volume can be increased. The combination of hybrid fiber reinforced concrete and self-consolidating concrete together can provide a way to produce a concrete with superior properties in fresh and hardened states (Sahmaran et al. 2005).

Yang (2011) studied the workability of concrete reinforced with hybrid or monolithic steel and polyvinyl alcohol fibers. In this study, all mixtures were classified into three groups. The first and second group was tested to determine the effect of length and volume fraction of monolithic polyvinyl alcohol (PVA) and steel (ST) fiber on the workability and mechanical properties of concrete. The third group was designed to examine the hybridization of different lengths and types of fibers using PVA and ST fibers. The slump of each fresh concrete mixture was measured immediately after the completion of mixing. Results show that the initial slump of steel fiber reinforced concrete (SFRC) was generally lower than PVA fiber reinforced concrete and concrete without fiber (Figure 3.23). This trend was also perceived in hybrid fiber reinforced concrete. This may be attributed to the fact that the increase in volume fraction and length of fiber leads to a fiber-balling effect, which decreases the workability of concrete.

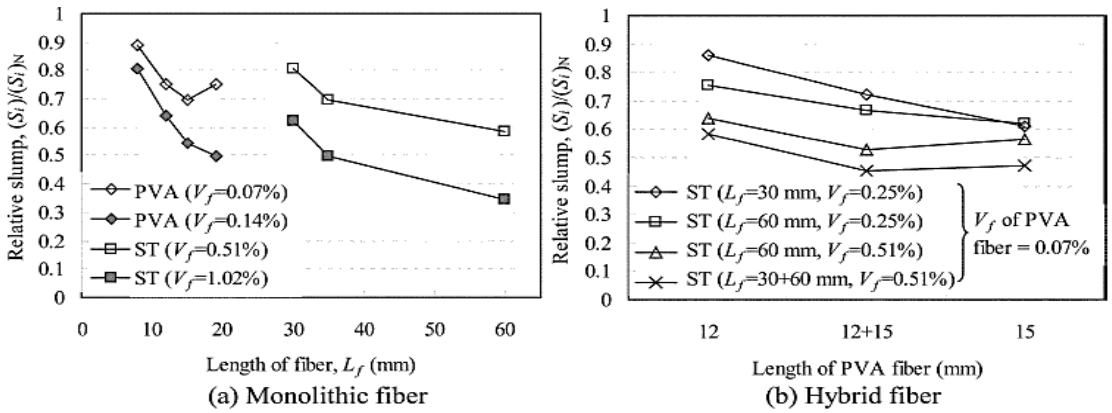

Figure 3.23. Relative slump of FRC tested

(Source: Yang, 2011)

Sahmaran et al. (2005) investigated the workability of hybrid fiber reinforced self-compacting concrete (HFR-SCC). In this two cylindrical steel fiber types, one with hooked ends (Dramix ZP 305) and one straight type (Dramix OL 6/16), were used. Three workability test methods were applied on these mixtures as slump flow, J-ring, and V-funnel tests. Results show that as the volume fraction of OL 6/16 fibers increased, t500 and V-funnel time decreased (Figure 3.24). On the other hand, the slump flow (D) and J-ring test results were not affected from fiber inclusion. It is also stated in this study that the OL 6/16 fibers which are smaller than ZP 305 fibers, have less potential to prevent the movement of aggregates. In addition, OL 6/16 fibers are coated with brass and have very smooth surfaces, which reduce the energy loss during the movement of particles. Oppositely, ZP 305 fibers have hooked ends, and relatively larger dimensions thus cause blocking of particles during flow.

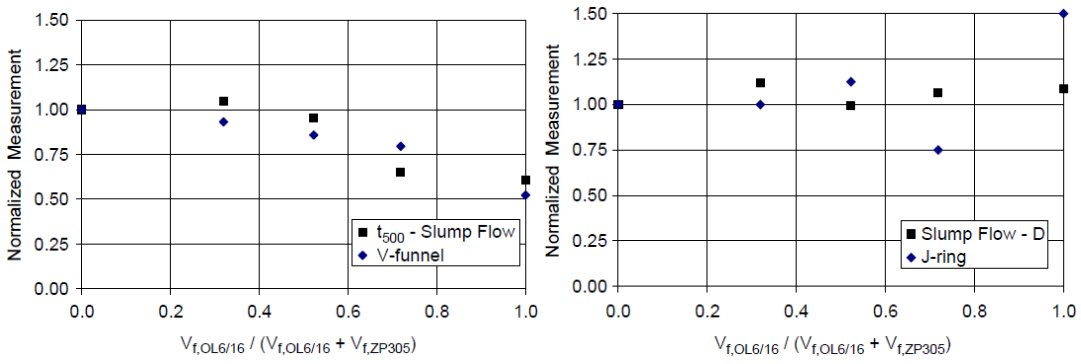

Figure 3.24. Tests stability and deformability of HFR-SCC
(Source: Sahmaran et al. 2005)

Jen et al. (2016) studied workability of self-consolidating hybrid fiber reinforced concrete. Three types of composites were investigated in this study as self-consolidating concrete (SCC), hybrid fiber reinforced concrete (HyFRC), and self-consolidating hybrid fiber reinforced concrete (SC-HyFRC). Steel and PVA fibers were used. Figure 3.24 provides a summary on how the different parameters investigated in this study influenced the workability and the flow diameter of tested composites. The addition of PVA microfibers and steel fibers decrease the workability and the flow diameter of the SC-HyFRC. Increasing the fine to coarse aggregate ratio and optimizing the chemical admixture additions provided effective ways to enhance the flow diameter of the SC-HyFRC composite as schematically shown in Figure 3.25.

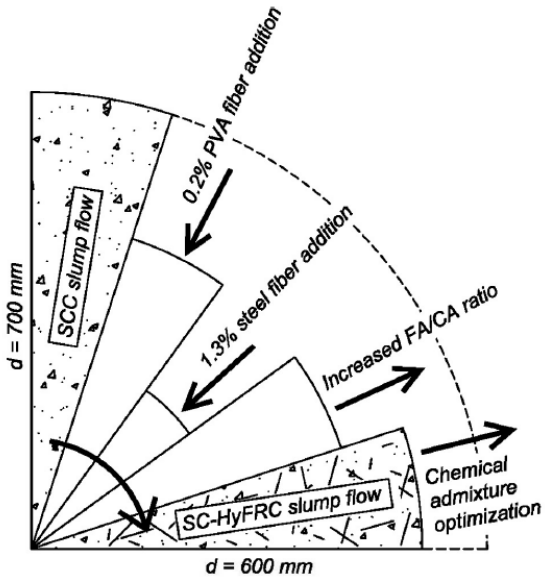

Figure 3.25. Slump flow behavior of SC-HyFRC

(Source: Jen et al. 2016)

3.2.2. Compressive Strength

Sharma et al. (2009) investigated the mechanical properties of hybrid steel and lead fibers. The results showed that combination of steel fibers and flexible lead fibers remarkably increased the mechanical properties of fiber reinforced concrete. The hybrid fiber reinforced concrete possesses excellent flexural toughness, compressive and tensile strength comparable to that of steel fiber reinforced concrete.

Banyhussan et al. (2016) studied the effect of aggregate and fly ash content on compressive strength of deflection-hardening hybrid fiber reinforced concrete. Three different fibers were used at the maximum of 2% of volume in single or hybrid systems as polyvinyl-alcohol (P), hooked-end steel (S), and nylon (N) fibers. The fly ash to Portland cement ratios (FA/PC) were 0.20, 0.45, and 0.70 by weight, and aggregate to binder ratios (A/B) were 1.0, 1.5, and 2.0 by weight. The mixtures were labeled such that the ingredients were identifiable from their IDs. For example, in the case of the label P0.5S1N0.5_0.20_1.0, polyvinyl-alcohol (P), hooked-end steel (S) and nylon (N) fibers represent 0.5%, 1.0% and 0.5% of total mixture volume, respectively. For the same mixture, 0.20 and 1.0 stand for FA/PC ratio and A/B ratio, respectively.

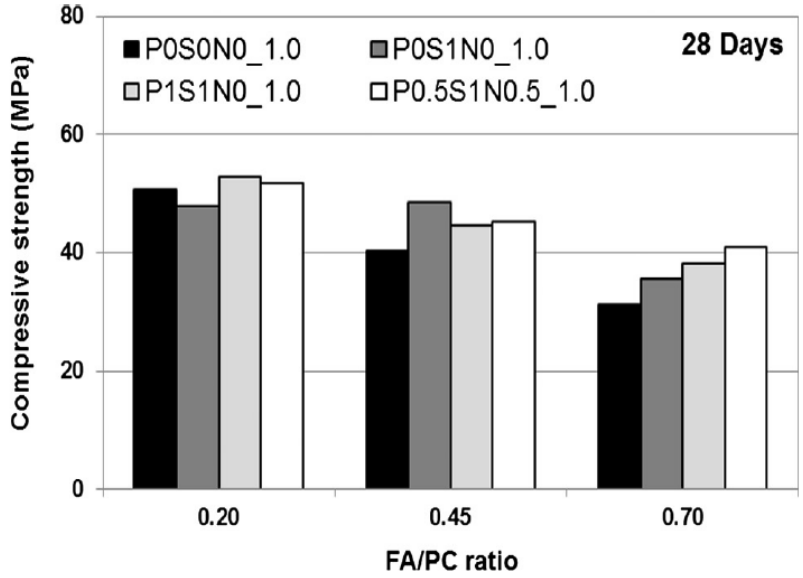

Figure 3.26. Effect of fiber and fly ash content on HyFRC
(Source: Banyhussan et al. 2016)

Effects of fiber use on the compressive strength results at a constant A/B ratio (1.0) and different FA/PC ratios are shown in Figure 3.25. Results showed that compressive strength improved after reinforcing the fibreless control mixtures with only 1% of hooked-end steel fiber due to the ability of fibers to delay crack formation. It is also found that the hybridization of fibers increased the compressive strength of concrete which almost seen in with FA/PC ratio of 0.70. Increased FA/PC ratios caused relatively low compressive strength as seen in Figure 3.26.

Wang et al. (2017) studied the effect of high strain rate on compressive behavior of strain-hardening cementitious composites in comparison to the ordinary fiber-reinforced concrete. Four different mixtures were tested: the two strain-hardening cement-based composites (SHCCs) were SHCC-ST+PE which contains 0.5% steel fiber and 1.5% polyethylene (PE) fibers, and SHCC-PVA is only reinforced with 2% polyvinyl-alcohol (PVA) fibers. The two FRHSCs have different water/cement ratios in order to achieve different level of strength, and both mixtures were reinforced with 0.5% of steel fibers by volume of the concrete. Two cylinders with different dimensions of D100 x 200 mm and D77 x 154 mm were used to determine compressive strength. Figure 3.27, which illustrates the results of this study, shows that the compressive strength significantly increased with hybridization of fibers in the mixtures.

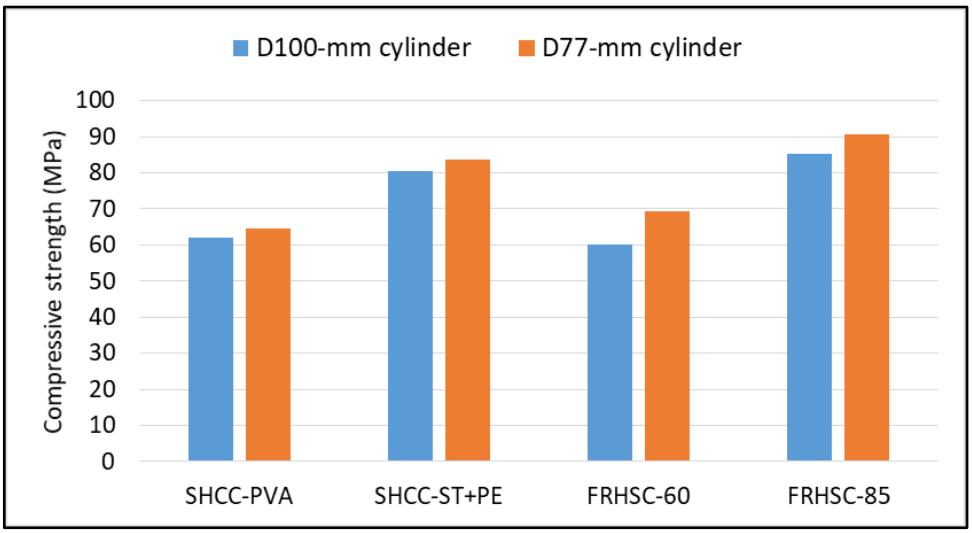

Figure 3.27. Effect of hybrid fiber on compressive strength
(Source: Wang et al. 2017)

Vibhuti et al. (2013) investigated the mechanical properties of hybrid fiber reinforced concrete for pavements. Steel fibers of 1% and polypropylene fibers of 0.036% were used individually or together to form hybrid fiber reinforced concrete. Four types of concrete used in this study were plain concrete (PC), polypropylene fiber reinforced concrete (PFRC), steel fiber reinforced concrete (SFRC) and hybrid fiber reinforced concrete (HFRC). Compressive strength tests were carried out by casting 150 x 150 x 150 mm cubes. Table 3.6 shows compressive strength results at 14 and 28 days. The compressive strength of concrete mixtures increased by 7.29% and 10.85% for PFRC, 11.75% and 13.58% for SFRC, and 14.30% and 17.11% for HFRC at 14 and 28 days, respectively. The results also indicated that hybridization of fibers improved the compressive strength marginally as compared to single fiber addition.

Table 3.6. Compressive strength results (Source: Vibhuti et al. 2013)

Compositions	Curing Days	Compression Strength (MPa)		Flexural Strength (MPa)	
		Obtianed	Increase %	Obtianed	Increase %
PC	14	40.08	0.00	3.95	0.00
	28	43.60	0.00	4.35	0.00
PFRC	14	43.00	7.29	4.20	6.33
	28	48.33	10.85	4.76	9.43
SFRC	14	44.79	11.75	4.35	10.13
	28	49.52	13.58	5.13	17.93
HFRC	14	45.81	14.30	4.80	21.52
	28	51.06	17.11	5.84	34.25

Caggiano et al. (2020) studied the compressive strength of hybrid steel/polypropylene fiber reinforced concrete. Five mixtures (plus a reference plain concrete) were produced with same total volume of fibers (0.75% of volume fraction) but different fractions of polypropylene and steel fibers. Mixtures were labeled with steel fibers (S) and polypropylene (P). For example, the mixture HySP-FRC-0.55-0.20 illustrates 0.55% volume fraction of steel fiber and 0.20% volume fraction of polypropylene fibers. Results show that compressive strength increased when adding fiber to composite (Figure 3.28). In this study, there was some decrease in compressive strength of hybrid steel/polypropylene fiber reinforced concrete with respect to steel fiber reinforced concrete.

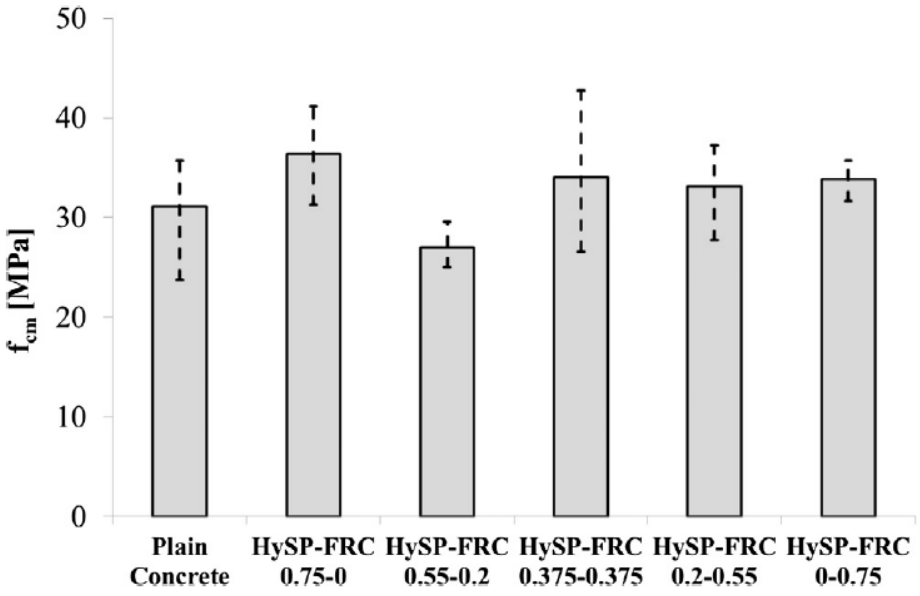

Figure 3.28. Compressive strength results
(Source: Caggiano et al. 2020)

3.2.3. Flexural Performance

Plain concrete has high compressive strength but poor tensile strength and low flexural strength due to its brittle characteristic. Addition of fibers as reinforcement in concrete may not change its compressive strength and modulus of elasticity but some of the main mechanical properties such as fracture toughness, ductility and crack-width control are improved (Monteiro et al. 2018).

Ahmed et al. (2007) investigated the flexural strength of hybrid fiber reinforced cement based composites containing high volume fly ash. The total volume fraction of the steel and/or PVA fibers was kept constant at 2.5% as (Steel 2.5%, Steel 1.5% + PVA 1%, Steel 1% + PVA 1.5%, Steel 0.5% + PVA 2%, and PVA 2.5%). Effects of increase in fly ash content as replacement of cement of 50%, 60%, and 70% on the flexural response of hybrid steel–PVA composites were also evaluated. Figure 3.28 shows the load-deflection curves of the mixtures tested in this study. The composite with 2.5% steel (ST) fibers shows high flexural strength but low deflection capacity due to its high modulus. On the other hand, the composites with 2.5% PVA fibers show lower flexural strength but higher deflection capacity than that of steel fiber composites due to their low stiffness. Flexural stresses versus mid-span deflection curves of hybrid fiber composites are found to lay between those of steel and PVA fiber composites (Figure 3.29). The flexural strength in hybrid fiber composites is found to be higher than that of the composite with PVA fibers alone, while the deflection capacity is found to be higher than that of the composite with steel fibers alone. In this case, the steel fibers maintain their ability to increase the flexural strength of the composite due to their high stiffness and PVA fibers maintain their ability to increase the deflection capacity of the composite due to their low stiffness. Figure 3.30 shows that the flexural strength of hybrid fiber composites decreased as the fly ash content increased.

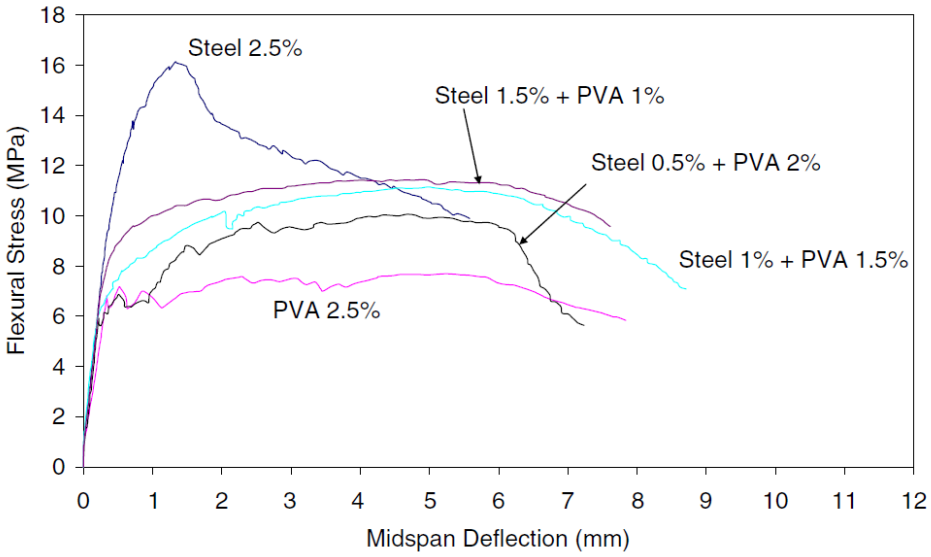

Figure 3.29. Load-deflection curves of HyFRC

(Source: Ahmed et al. 2007)

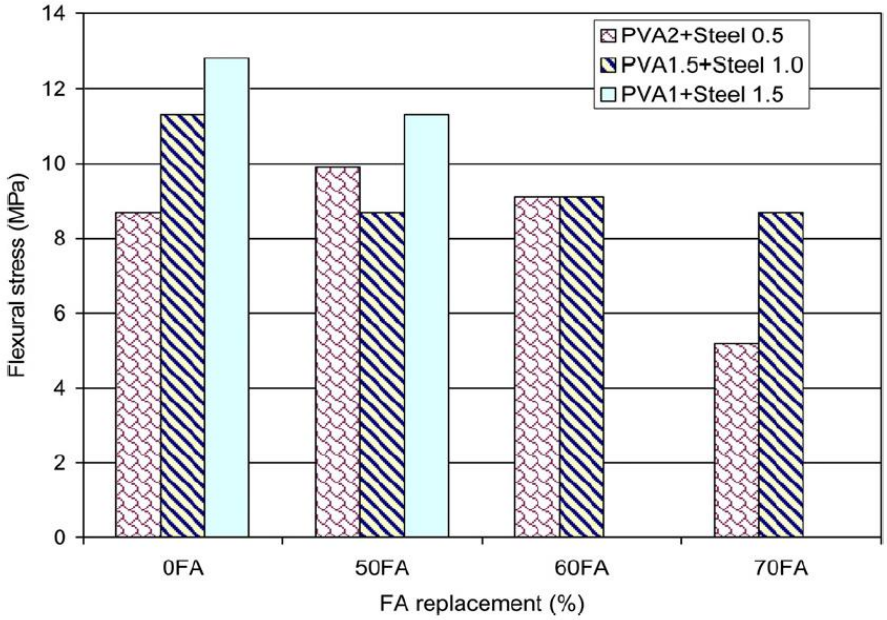

Figure 3.30. Effect of fly ash content on HyFRC

(Source: Ahmed et al. 2007)

Yang (2011) studied the load-displacement behavior of concrete reinforced with hybrid or monolithic steel and polyvinyl alcohol fibers. In this study, all mixtures were classified into three groups. The first and second groups were tested to determine the effect of length and volume fraction of monolithic polyvinyl alcohol (PVA) and steel (ST) fibers on the mechanical properties of concrete. The third group was designed to

examine the hybridization of different lengths and types of fibers using PVA and ST fibers. The load-displacement relationship of the concrete was measured using prismatic beams with dimensions of 75 x 75 x 450 mm under a symmetrical center-point top-loading system. The load-deflection curves under three-point bending is shown for different specimens in Figure 3.31. In this study, load-deflection was not provided in the figure for fiberless concrete and monolithic PVA FRC specimens due to their strong brittle failure characteristics. The load-deflection curve of concrete reinforced with monolithic steel FRC fiber of a 30 mm and 35 mm length was very similar. The flexural strength and deflection hardening area after peak load were significantly improved with increasing steel fiber length to 60 mm and increasing the volume fraction of steel fibers as shown in Figure 3.31(a). This indicates that the increase of fiber length and volume plays a strong role in enhancing the flexural strength and energy absorption capacity of monolithic steel FRC. The load-deflection characteristics of hybrid PVA-ST FRC was significantly improved with increasing the length of steel fiber as the shown in Figure 3.31(b). For the hybrid FRCs with a 0.25% steel fiber volume fraction, the load capacity sharply dropped with the development of initial flexural cracks by approximately 50% of the peak load and then remained constant. On the other hand, hybrid PVA-ST FRC with a 0.51% steel fiber-volume fraction did not show a sharp decrease of load capacity immediately after peak load as shown in Figure 3.31(c).

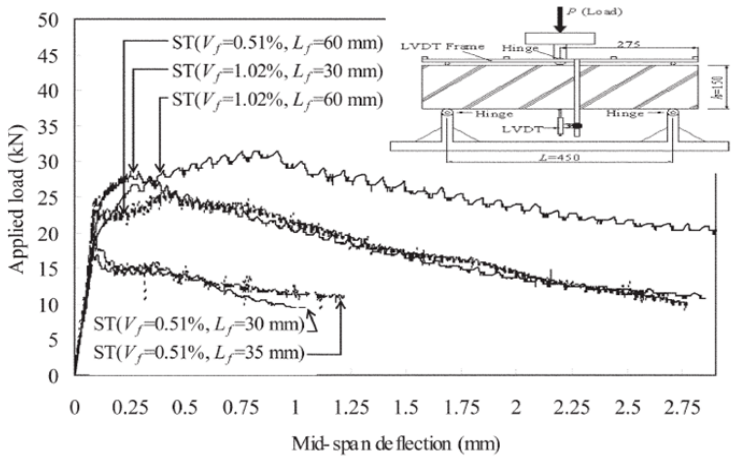

(a) Monolithic ST fiber

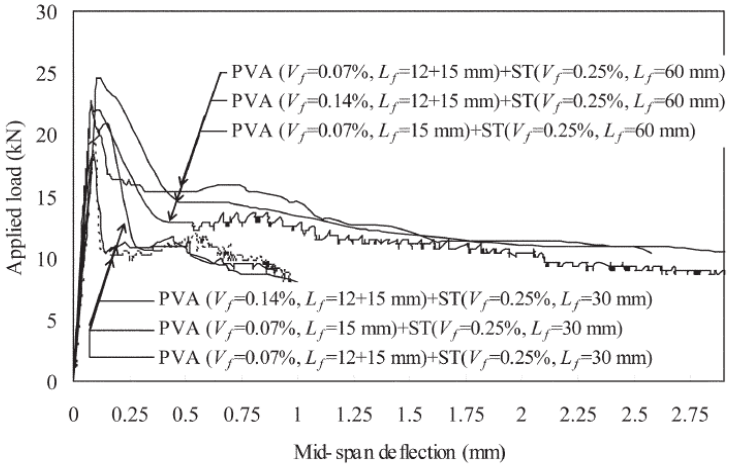

(b) Hybrid PVA-ST fibers (V_f of ST fiber=0.25%)

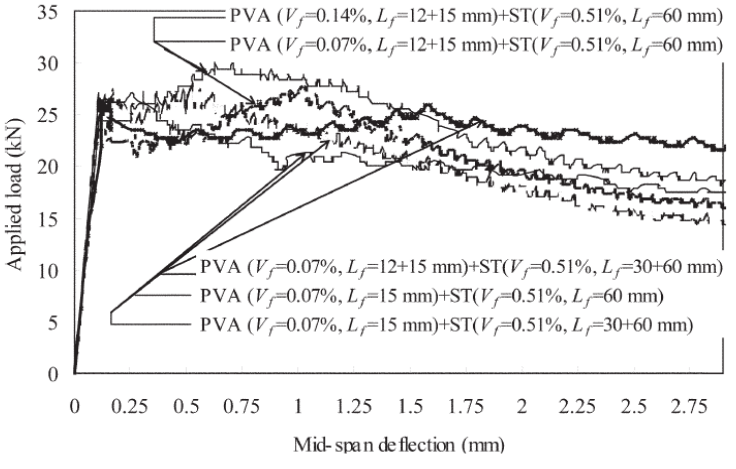

(c) Hybrid PVA-ST fibers (V_f of ST fiber=0.51%)

Figure 3.31. Load-deflection curve of FRC under three-point bending test (Source: Yang, 2011)

Vibhuti et al. (2013) also investigated the flexural strength of hybrid fiber reinforced concrete for pavements. The mixture proportions were explained in the previous section. Table 3.7 shows flexural strength results at 14 and 28 days. The compressive strength of concrete mixtures was increased by 6.33% and 9.43% for PFRC, 10.13% and 17.93% for SFRC, and 21.52% and 34.25% for HFRC at 14 and 28 days, respectively. The results showed that hybridization of fibers improved the flexural strength significantly as compared to single fiber addition.

Blunt and Ostertag (2009) investigated the performance-based approach for the design of a deflection hardening hybrid fiber-reinforced concrete. Four-point flexure test was carried out according to ASTM C1609 standard on 152 x 152 x 608 mm prismatic specimens with a clear span of 456 mm. Table 3.6 shows fiber proportions of the mixtures, and their corresponding flexural performance are provided in Figure 3.32. Use of a small amount of PVA fibers increased the composite flexural strength (compare Mix A to Mix B). An increase in the aspect ratio of the S2 type fiber raised the flexural strength further (compare Mix B to Mix C). Use of a smaller aggregate size and combination of two sizes of steel fibers increased the flexural performance significantly (Mix D and Mix E).

Table 3.7. Fiber proportions (Source: Blunt and Ostertag, 2009)

Trial				
Batch	Maximum aggregate size (mm)	Fiber volume fraction (%)		
		PVA	S1	S2[a]
A	25.4	—	—	0.7
B	25.4	0.3	—	0.7
C	25.4	0.3	—	0.7
D	9.5	0.2	0.5	0.5
E	9.5	0.2	0.5	0.8

[a]Aspect ratio (length/diameter) of fiber for Mixes A and B=65, aspect ratio for Mixes C, D, and E=80 at constant fiber length.

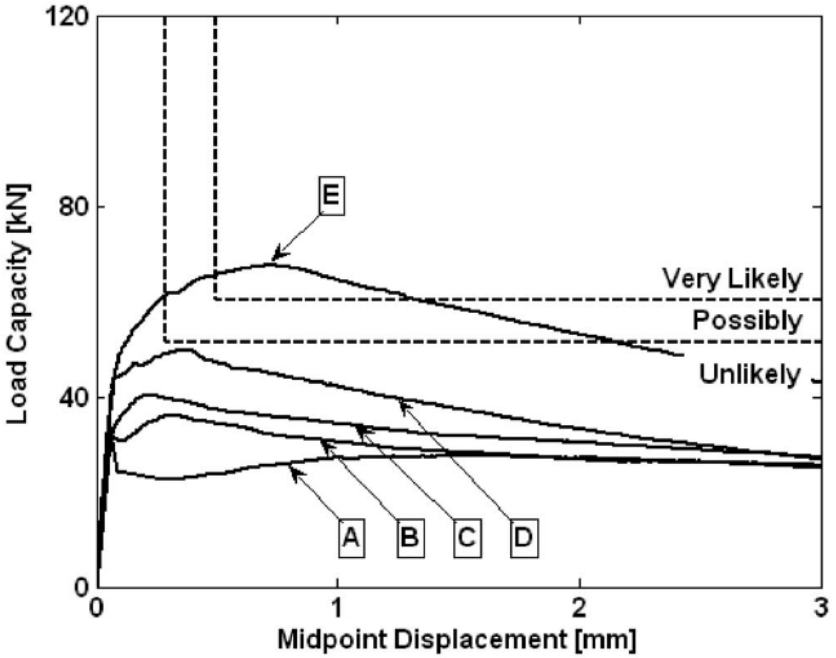

Figure 3.32. Load-deflection curves
(Source: Blunt and Ostertag, 2009)

3.2.4. Impact loading

Concrete structures may be exposed to loading within short time periods such as earthquakes, impacts and explosion during their service lives. Concrete structures must be designed to resist dynamic loads by improving the energy absorption capacity of the material by adding fibers. Fibers have the potential to increase the bond of the Portland cement paste and the concrete matrix and improve the mechanical properties (Al-Masoodi et al. 2016).

Mohammadi et al. (2009) studied the impact resistance of steel fiber reinforced composites containing steel fibers of mixed aspect ratio. Three different volume fractions (1.0%, 1.5% and 2.0%) of mixed steel fibers were used with 0.6 x 2.0 x 25 mm and 0.6 x 2.0 x 50 mm sizes in different proportions. Beam specimens with 100 x 100 x 500 mm dimensions were tested under impact loading. The drop weight type impact tests were conducted on the test specimens, and the number of blows of the hammer required to make first visible crack and ultimate failure of the specimen were recorded. Figure 3.33 shows failure energy capacity of the tested mixtures of this study. Graphs show that the impact resistance of the concrete mixtures increased with the increase in volume fraction of fibers from 1% to 2%. The highest impact resistance is given by the

concrete containing 100% 50 mm + 0% 25 mm long fibers followed by concrete 65% 50 mm + 35% 25 mm long fibers, 50% 50 mm + 50% 25 mm long fibers, 35% 50 mm + 65% 25mm long fibers, and 0% 50 mm + 100% mm long fibers. It means that by decreasing the long fibers' volume fraction and increasing short fibers' volume fraction, the impact resistance of the concrete decreased. Because of the small length of the fibers, they had less bond resistance and were pulled out of the matrix.

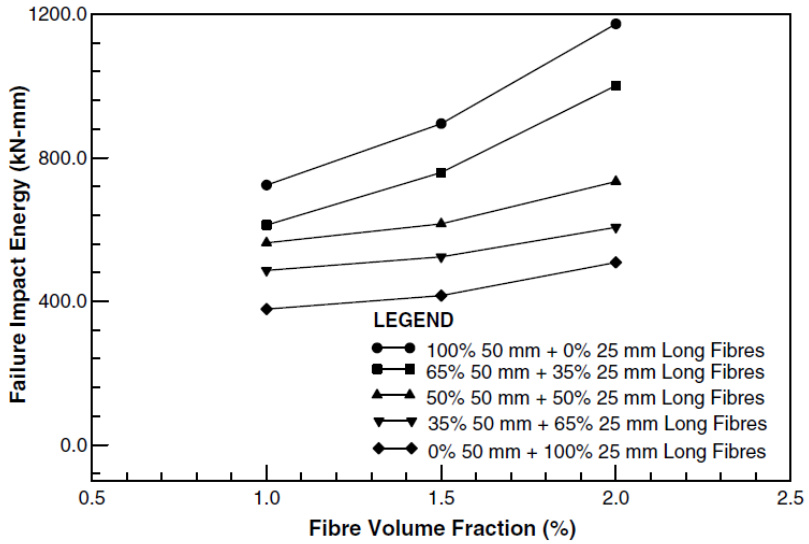

Figure 3.33. Failure impact energy graph

(Source: Mohammadi et al. 2009)

Al-Masoodi et al. (2016) studied the dynamic properties of concrete with different types and shapes of fibrous reinforcement. In this research, three different shapes of steel fibers (Hook Ended Steel Fiber (HKSF-35 mm), Proposed Steel Fiber I (γ-shape) (PSFI-35 mm) and Proposed Steel Fiber II (W-shape) (PSFII-35 mm)) and two types of Polypropylene Fiber (PPI and PPII) were used as shown in Figure 3.34. The newly modified W-shape steel fiber has the greatest influence on concrete static and dynamic properties. PP fiber slightly reduced the concrete mechanical properties, but improved the dynamic properties by 15% when compared to plain concrete (PC).

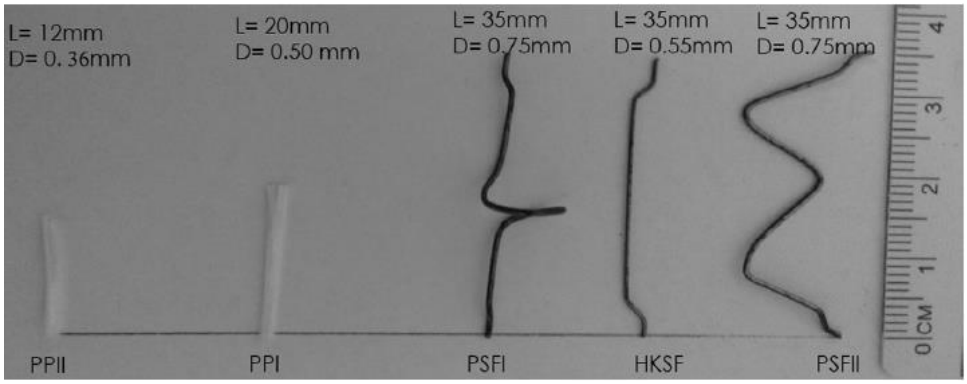

Figure 3.34. Different types and shaped of fibers

(Source: Al-Masoodi et al. 2016)

Naraganti et al. (2019) studied the impact resistance of hybrid fiber reinforced concrete containing sisal fibers. In this study, three types of fibers were used as sisal, polypropylene (PP), and steel fibers. Apart from Mono-fiber reinforced concrete (mono-FRC), resistance of hybrid fiber reinforced concrete (HyFRC) containing steel-Polypropylene (S-PP) and Steel-Sisal (S-Si) fibers to impact loading was also evaluated. Drop-weight test was applied according to ACI 544. Impact resistance improved with the increase in fiber dosage. Hybrid combination of steel-PP fibers exhibited superior performance as compared to steel-sisal fiber combination and Mono-FRC as seen in Figure 3.35. SPFRC improved the impact resistance by 15 times at volume fraction of 1.50%. This improved performance is the result of the synergy between steel and PP fibers.

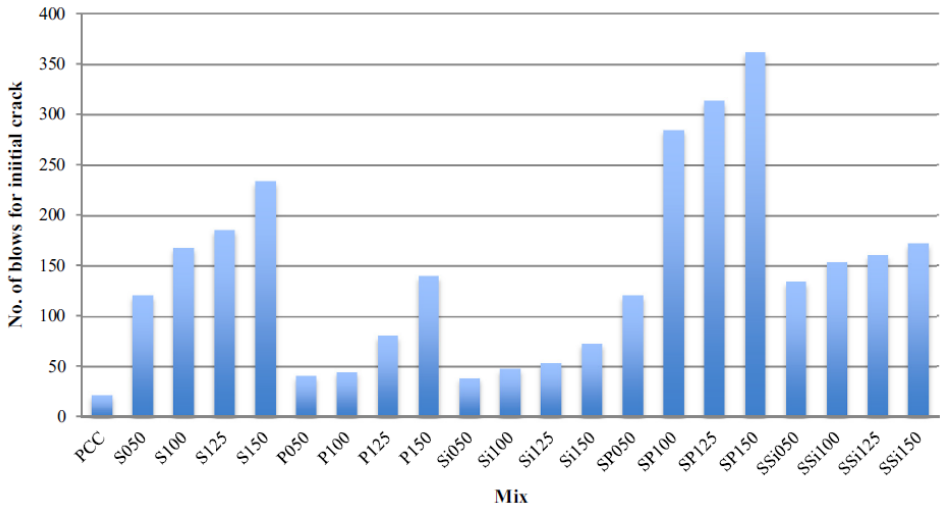

Figure 3.35. Impact resistance for initial crack

(Source: Naraganti et al. 2019)

Dawod et al. (2006) investigated the damage assessment of impacted hybrid fiber reinforced concrete (HyFRC). In this study, drop-weight impact test was applied on HyFRC under compression or flexural impact. The assessment of low velocity impact damage in concrete is achieved by matching the visible damage with the results obtained from compression after impact (CAI) test or indirect-tension after impact (I-TAI) test. Galvanized steel fiber and alkaline resistant glass fiber were used. Table 3.8 shows the number of blows till occurrence of initial crack and complete failure in flexural impact. The results showed that HyFRC experienced high resistance to micro-cracks coalescence at first crack and macro-crack growth at complete failure.

Table 3.8. Number of blows (Source: Dawod et al. 2006)

Mixtures	**PC**	**GFRC**	**SFRC**	**HyFRC**
Fiber Content		0.8% Glass	0.8% Steel	0.4% Glass + 0.4% Steel
No of blows to first crack, Height = 90 cm	*	5	3	9
No of blows to failure, Height = 90 cm	2	6	7	14
No of blows to first crack, Height = 60 cm	*	12	8	14
No of blows to failure, Height = 60 cm	5	13	14	20

Nicolaides et al. (2015) studied the impact and blast load resistance of ultra-high performance fiber reinforced cementitious composites (UHPFRCC). Four slab specimens with 1000 x 1000 x 50 mm dimensions were produced with two UHPFRCC and two reinforced concrete (RC). Two types of steel fibers (6 mm length and 0.16 mm diameter; and 13 mm length and 0.16 mm diameter) were used in UHPFRCC by total volume of 6%. The impact resistance of UHPFRCCs was experimentally verified in a series of firing shots, performed at field. Figure 3.36 shows the damage of RC and UHPFRCC slabs after firing shots of solid round projectile. The damage on UHPFRCC slabs was considerably lower, comparing to the corresponding damage of RC slabs. As shown in Figure 3.36(b), 5 out of 15 projectiles did not damage to penetrate the UHPFRCC slabs.

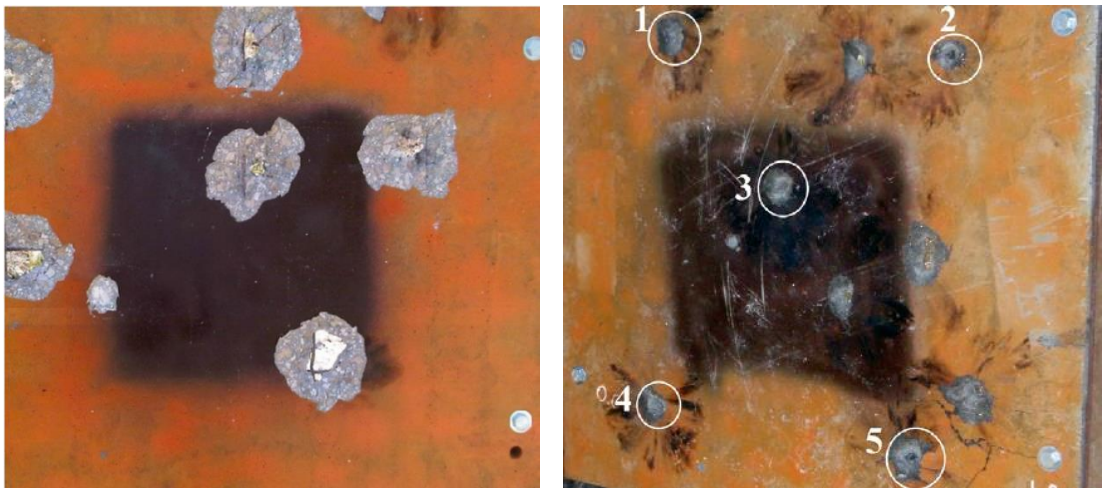

(a) (b)

Figure 3.36. (a) RC and (b) UHPFRCC slabs after impact loading by ‘‘Solid Round’’ projectiles 12.7 mm

(Source: Nicolaides et al. 2018)

3.2.5. Durability

The main disadvantages of conventional concrete are relatively low tensile strength and poor resistance to crack opening and propagation. The crack opening increases water penetration to concrete which reduce concrete durability. Development of new types of concretes improved many properties such as flexural strength, toughness, and durability. Durability does not have a single quantitative measurement, there are several methods to evaluate durability such as water absorption, depth of water penetration, water permeability, chloride permeability, sodium sulphate permeability, magnesium sulphate permeability, sorptivity, carbonation resistance, subjecting concrete specimens to wet-dry cycles and freeze-thaw cycles (Yehia et al. 2016).

Afroughsbet and Ozbakkaloglu (2015) studied the durability properties of high-strength concrete containing steel and polypropylene fibers. In this study, hooked-end steel fibers with a 60-mm length were used at four different fiber volume fractions of 0.25%, 0.50%, 0.75%, and 1.0%. Polypropylene fibers with a 12-mm length were used by 0.15%, 0.30%, and 0.45%. Some mixtures were produced with the combination of steel and polypropylene fibers at a total fiber volume fraction of 1.0% by volume of the concrete. All the fiber-reinforced concretes contained 10% silica fume as a cement replacement. Water absorption of concrete mixtures were examined to evaluate the durability. Figure 3.37 shows early and ultimate water absorption of different fiber-

reinforced concretes. Combined use of silica fume with steel or polypropylene fibers in concrete results in a significant decrease in the water absorption of concrete. The combined use of fibers and silica fume lead to mixes with lower water absorption compared to those seen in mixes containing only silica fume. Among all fiber-reinforced concretes, the mixture with 0.3% PP and 0.7% steel fibers has been found to exhibit the lowest water absorption.

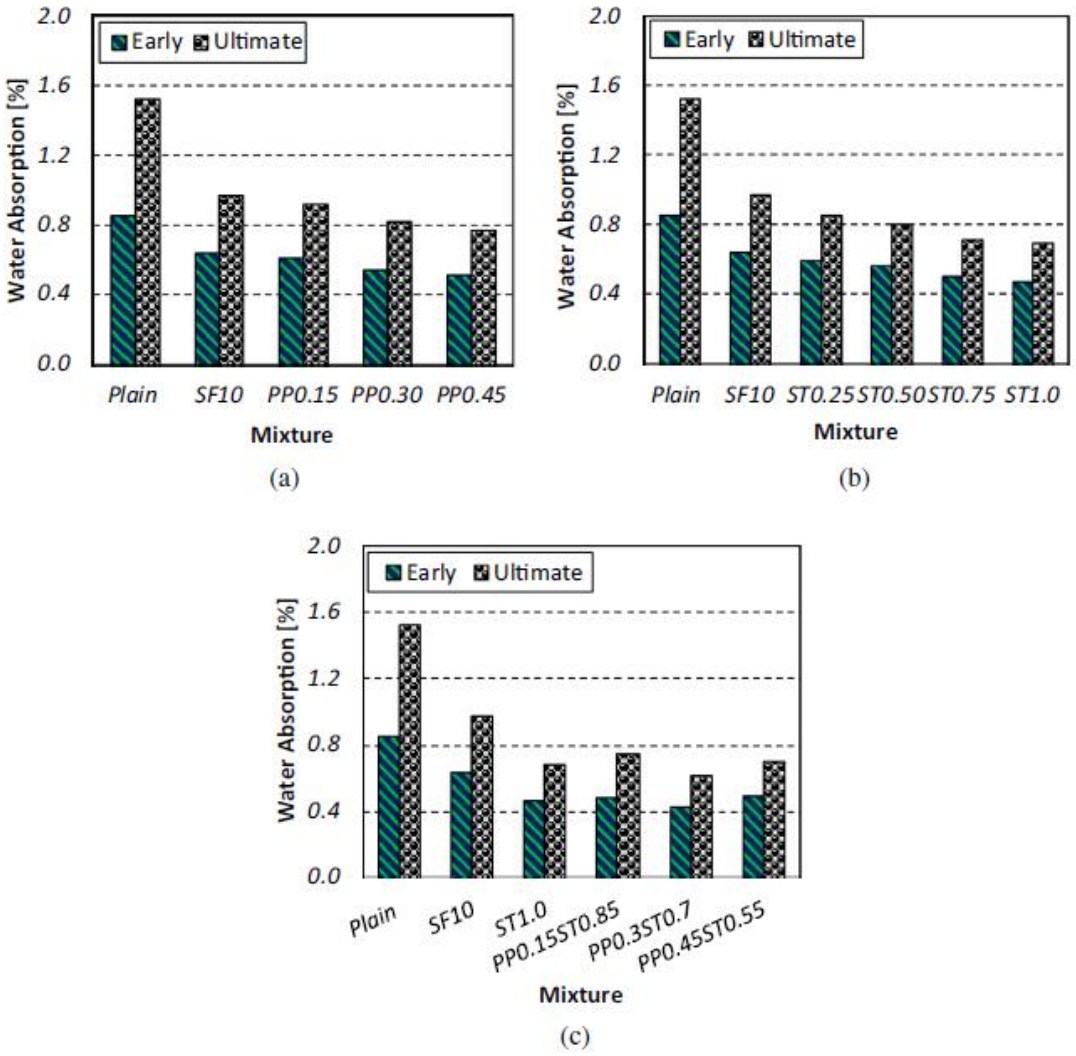

Figure 3.37. Early and ultimate water absorption of different fiber-reinforced concretes: (a) polypropylene fiber-reinforced specimens, (b) steel fiber-reinforced specimens, and (c) hybrid fiber-reinforced specimens

(Source: Afroughsbet and Ozbakkaloglu, 2015)

Jirobe et al. (2015) studied the strength and durability properties of hybrid fiber reinforced concrete. In this study, 50% crimped steel fiber and 50% polypropylene fiber

were used with total fiber volume of 0.5%, 1%, and 1.5%. Figure 3.38, which shows the sorptivity test results, indicates that conventional concrete and HyFRC with 0.5% fiber have the same sorptivity values. After that, sorptivity values increased by increasing fibers content to 1% and 1.5%.

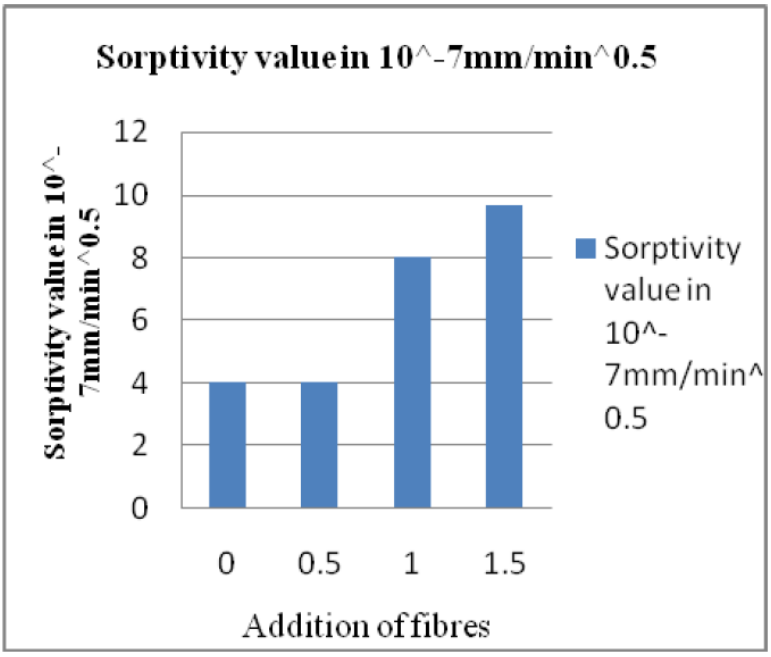

Figure 3.38. Sorptivity test results

(Source: Jirobe et al. 2015)

Shao et al. (2011) investigated the durability performance of flexural hardening fiber reinforced concrete. Five mixtures of fiber reinforced concrete were investigated as (1) plain concrete, (2) PVA fiber concrete, (3) steel fiber concrete, (4) PVA fiber concrete methyl cellulose (MC), and (5) PVA mortar. Methyl cellulose was added to batch #4 to enhance the bond between PVA fibers and concrete matrix for better flexural hardening response. Freeze and thaw test was applied according to ASTM C666. Six samples with dimensions of (25mm x 75mm x 350mm) were cast for each mixture. Load-deflection curves were determined before and after 200 freezing and thawing cycles (Figure 3.39). PVA fiber concrete and PVA fiber mortar experienced a loss in flexural strength and toughness after freezing and thawing cycles. It was likely that the toughness reduction in PVA fiber concrete and mortar was related to the deterioration of the bond by freeze-thaw cycles. By using the methyl cellulose, the reduction was less pronounced due to enhanced bonding.

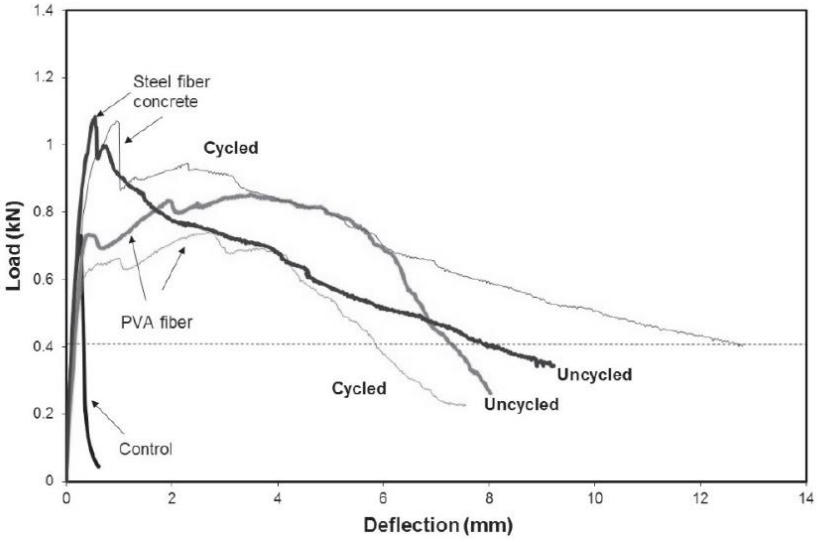

(a)

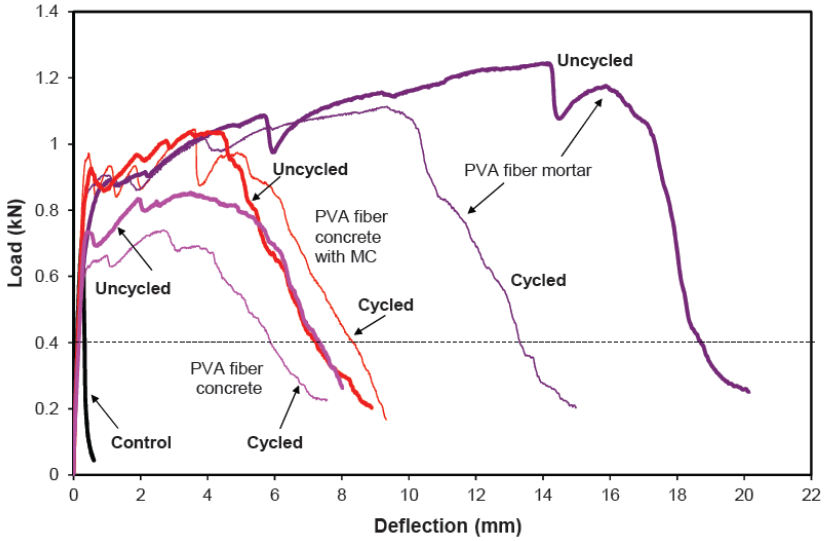

(b)

Figure 3.39. Load-deflection curves (a) PVA and steel FRC (b) effect of MC addition and aggregate content on PVA FRC

(Source: Shao et al. 2011)

Jang et al. (2014) studied the freeze-thaw cycling on sustainable strain-hardening cement composite (2SHCC) and normal SHCC. The combination of polyvinyl alcohol (PVA) and polyethylene terephthalate (PET) fibers was used in this study. Freeze-thaw testing was conducted according to ASTM C 666 Procedure. The dynamic modulus of elasticity and weight for the mixtures were measured at every 30 cycles of freezing and thawing until a total of 300 cycles. Figure 3.40 shows mass loss relative dynamic modulus of elasticity of 2SHCC and SHCC. The variation in the both

values over the entire duration of freezing and thawing cycles provided a good indication of the deterioration of cement composites. Also both strain-hardening cement composites with raw or recycled components survived more than 300 freezing-thawing cycles, and mass loss remained nearly constant and decreased only 1%.

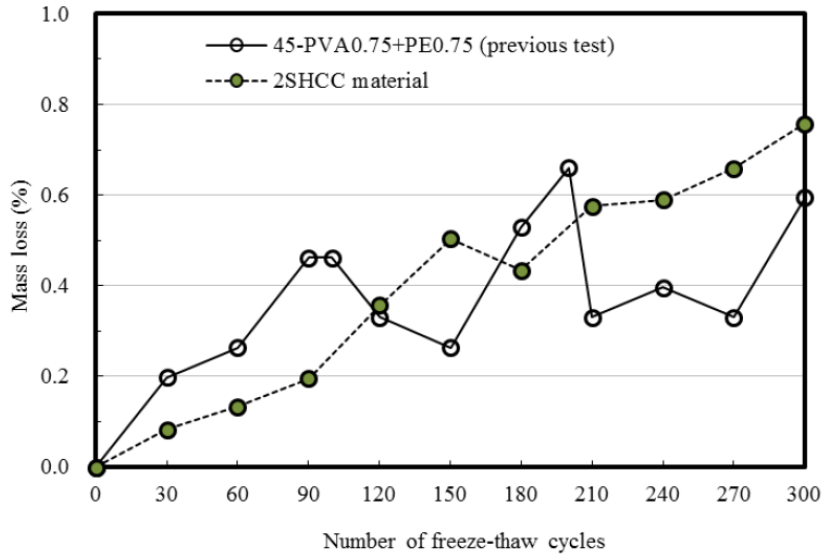

(a)

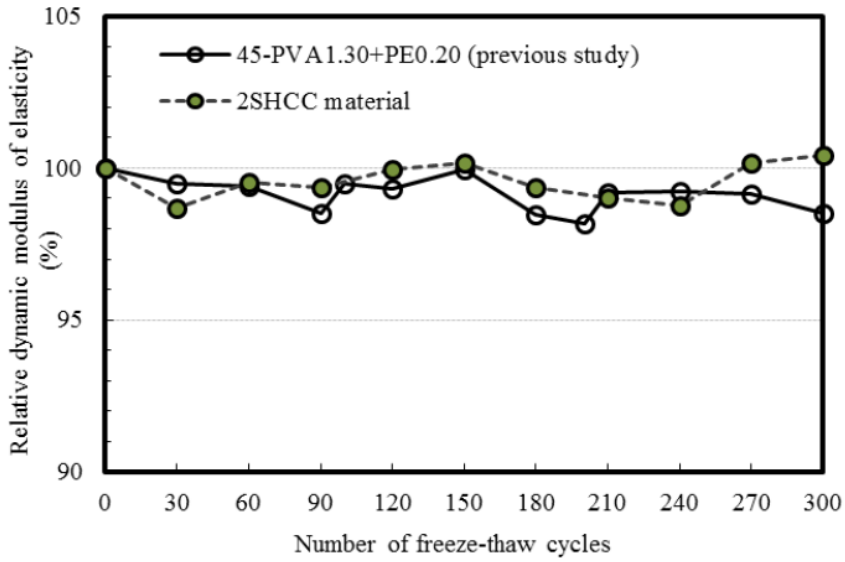

(b)

Figure 3.40. Freeze-thaw resistance of 2SHCC (a) mass loss (b) relative dynamic modulus of elasticity

(Source: Jang et al. 2014)

Kim and Park (2013) investigated durability of hybrid fiber reinforced concrete containing styrene butadiene latex. Two types of synthetic fibers were used as polyvinyl alcohol fiber/macro synthetic fiber (PVA/MSF) and polypropylene fiber (PP)/MSF. Styrene butadiene latex was added at 0%, 5%, 10%, and 15% of the cement weight. Styrene butadiene latex improves the fluidity of concrete. Chloride ion penetration test was performed according to the ASTM C1202 standard with specimen size (150 mm x 50mm) after curing for 28 days. Figure 3.41, which shows the chloride ion penetration test results, indicate that the chloride penetration rate decreased with increasing amount of latex. This is attributed to the latex filling the voids within the HyFRC and forming a thick film, which led to a reduction in the penetration rate. The HyFRC containing the hydrophilic PVA fiber had a lower penetration rate than the HyFRC incorporating the hydrophobic PP fiber. This was attributed to stronger hydrogen-bonding between the hydrophilic PVA fiber and the matrix, which reduced the amount of micro-voids between the fiber and the matrix.

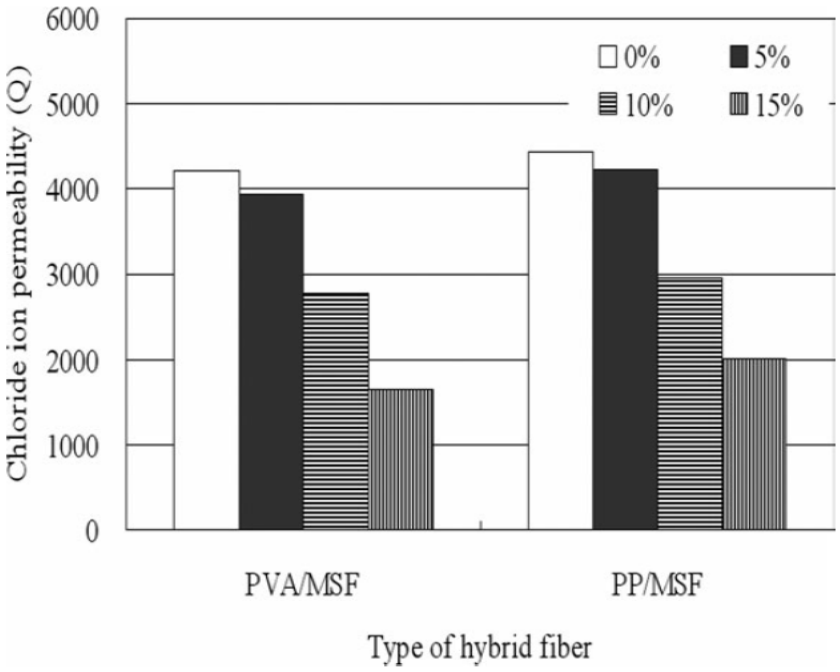

Figure 3.41. Chloride ion penetration test results with various latex and fibers contents (Source: Kim and Park, 2013)

Thendral and Hemapriya (2018) studied the rapid chloride penetration test of hybrid fiber reinforced concrete. Two types of fibers were used as hooked end steel and polypropylenes fibers. Three types of concrete were tested as normal concrete, steel

fiber reinforced concrete (SFRC) with volume of fraction of (0.5%, 1%, 1.5%, and 2%), and hybrid fiber reinforced concrete (HyFRC) with volume fraction of 1% (0.8SF0.2PP, 0.7SF0.3PP, 0.6SF0.4PP, and 0.5SF0.5PP). Chloride ion penetration test was carried out on selected mixtures according to the ASTM C1202 standard with specimen size (100 mm x 50mm) after curing for 28 days. The cumulative charge passed from normal concrete, SFRC, and HyFRC were 1109, 768, and 492 coulombs, respectively. The hybrid fiber reinforced concrete showed higher resistance to permeability.

CHAPTER 4

EXPERIMENTAL STUDY

4.1. Materials

Materials which were used in this experimental program are explained below.

4.1.1. Cement

CEM I 42.5 R Portland cement (PC), conforming to TS EN 197-1: 2012, with specific gravity of 3.06 and Blaine fineness of 325 m^2/kg was used in all mixtures of this investigation. The chemical composition, presented in Table 4.1, was obtained by XRF method in the Materials Research Center at İzmir Institute of Technology. Figure 4.1 shows a micrograph of the portland cement particles. The photo was taken by the scanning electron microscope (SEM) at the same center.

Table 4.1. Chemical composition of portland cement, fly ash and quartz

	Portland Cement	Fly Ash	Quartz
SiO_2 (%)	5.727	52.280	98.670
Al_2O_3 (%)	7.850	27.060	0.634
Fe_2O_3 (%)	2.184	8.623	0.123
CaO (%)	68.970	3.296	0.212
MgO (%)	3.455	3.728	0.270
SO_3 (%)	1.920	0.261	0.005
K_2O (%)	0.528	2.260	0.001
Na_2O (%)	8.500	0.110	0.110
Loss on ignition (%)	1.65	0.85	-
SiO_2+ Al_2O_3+ Fe_2O_3 (%)	-	87.963	-
Pozzolanic Activity İndex, 7 Days (%)	-	77	-
Pozzolanic Activity İndex, 28 Days (%)	-	85	-

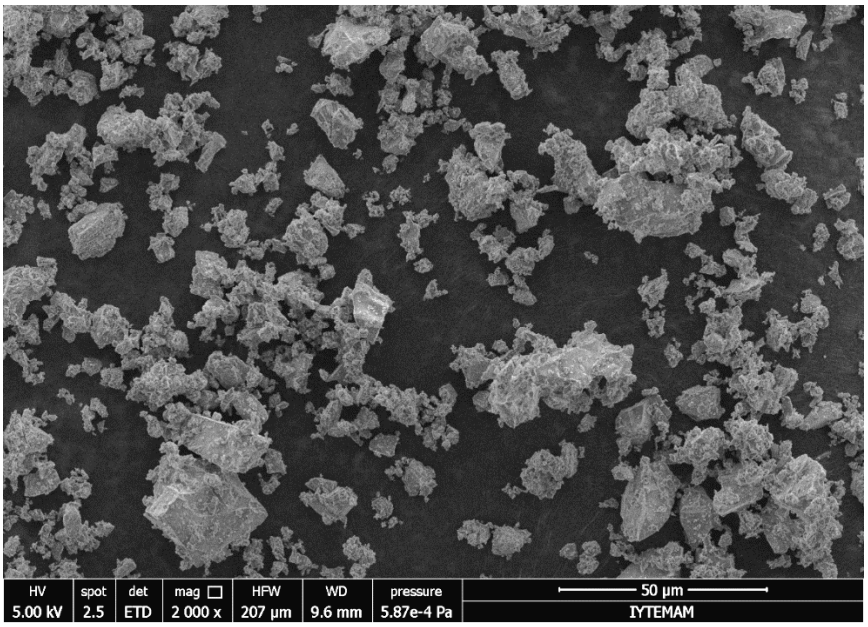

Figure 4.1. Micrograph of the portland cement particles

4.1.2. Fly Ash

Class-F fly ash, according to ASTM C 618, with a specific gravity of 2.61 and Blaine fineness of 290 m^2/kg was used during this study. The oxide composition, obtained by XRF method in the Materials Research Center of İzmir Institute of Technology, of fly ash are given in Table 4.1. A SEM image of the fly ash particles is shown in Figure 4.2.

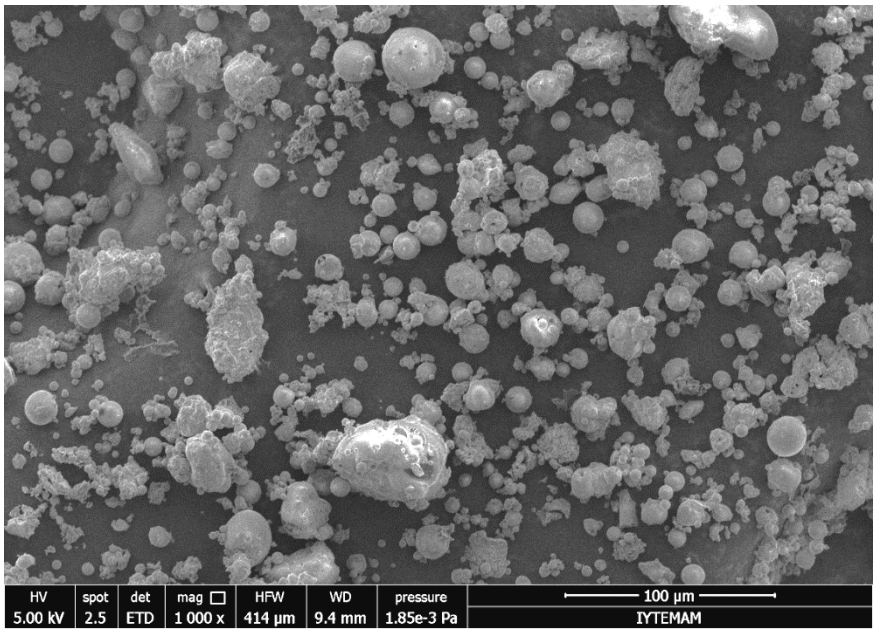

Figure 4.2. Micrograph of fly ash particles

4.1.3. Aggregates

Crushed limestone coarse aggregate with 16 mm D_{max} and river sand as fine aggregate were used for this research. The gradation curve for aggregates is shown in Figure 4.3. The Fuller equation [$P = \left(\frac{d}{D}\right)^n$ where, P = passing %, d = aggregate size being considered, D = maximum aggregate size, and n = 0.5] was used to find a good grading combination for coarse and fine aggregates as shown in Figure 4.4. Trials yielded that a good combination was obtained when 48% fine and 52% coarse aggregate are mixed. For some mixtures in the study, coarse aggregate was sieved through the 8 mm opening sieve to have Dmax = 8 mm,. Specific gravity and absorption capacity of coarse and fine aggregates are given in Table 4.2.

Table 4.2. Specific gravity and absorption capacity of the aggregates

	Fine aggregate	Coarse aggregate	Quartz
Specific gravity	2.58	2.56	2.55
Absorption capacity (%)	2.67	1.37	0.97

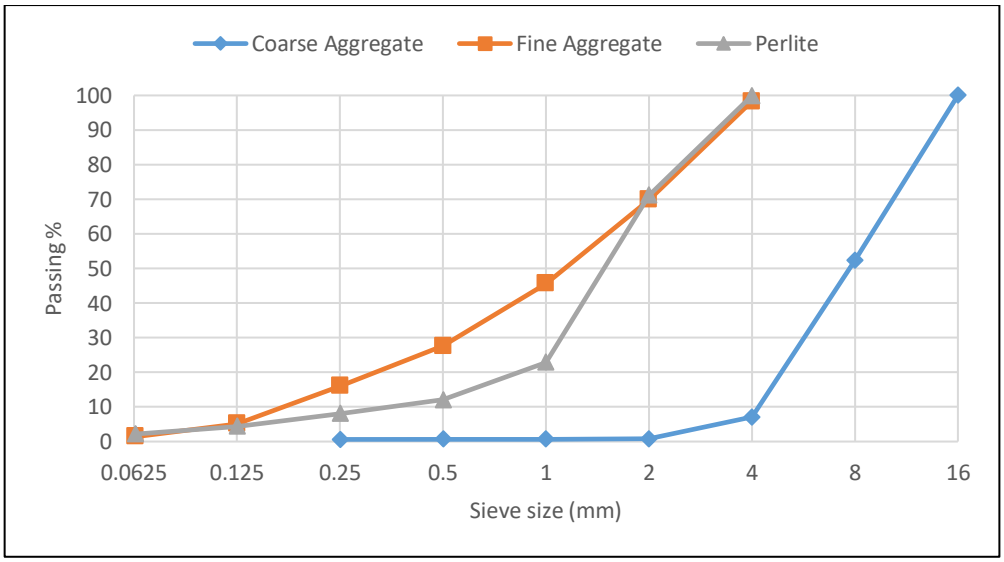

Figure 4.3. Gradation curve for the Aggregates

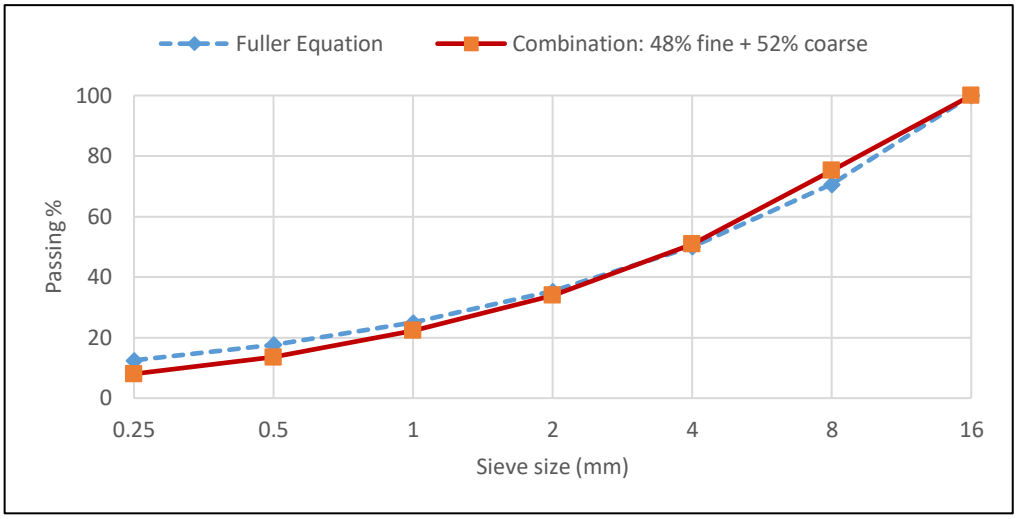

Figure 4.4. Fine and coarse aggregates combination curve

In the production of ECC mixtures, quartz sand with 0.5 mm D_{max} was used. The chemical composition of the quartz sand is given in Table 4.1. Basic physical properties of the quartz are presented in Table 4.2. Figure 4.5 shows a SEM image of the quartz particles.

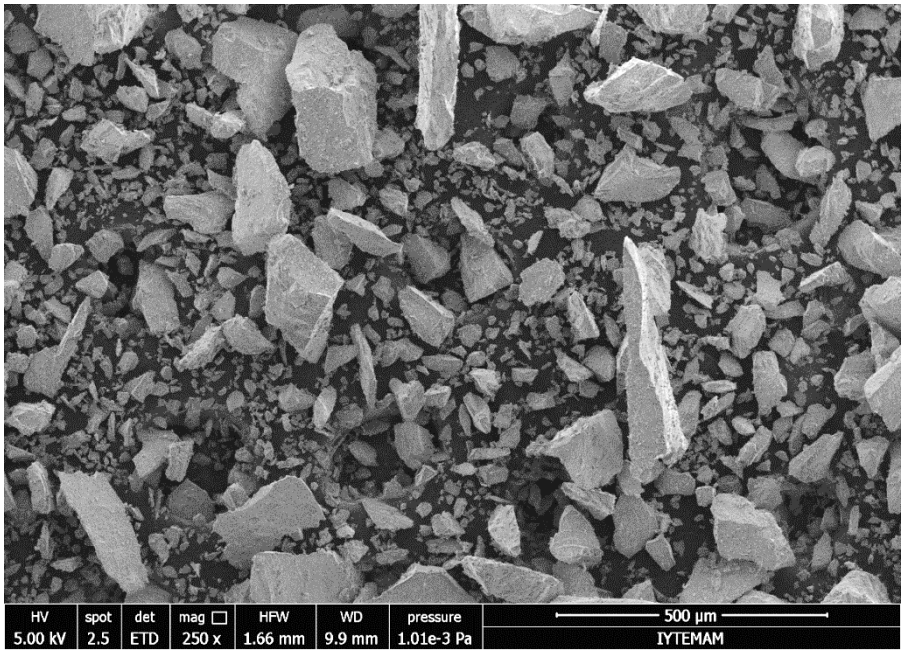

Figure 4.5. Micrograph of the quartz particles

Expanded perlite aggregate with 4 mm Dmax was also used in both ECC and HyFRC mixtures. The gradation curve for perlite aggregate is shown in Figure 4.3. The quasi-spherical shape of the perlite is shown in Figure 4.6. Figure 4.7 shows micrograph of the perlite particles.

Figure 4.6. Photo of the perlite particles

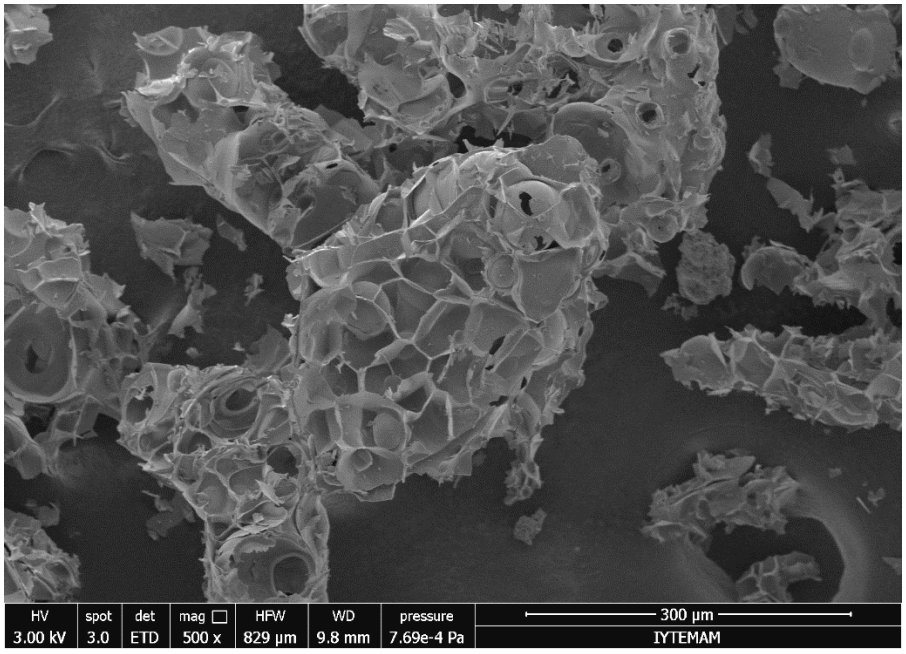

Figure 4.7. Micrograph of the perlite particles

4.1.4. Superplasticizer

The water to cement ratio of ECC is quite low and HyFRC has low workability, therefore, superplasticizer was used to obtained sufficient workability. Commercially available polycarboxylate based superplasticizer (MGlenium SKY 608) was used in this research. The admixture is classified as type F according to ASTM C 494/ C 494M 38. The properties of the abovementioned superplasticizer obtained from the manufacturer are given in Table 4.3.

Table 4.3. Properties of the superplasticizer

Type	Polycarboxylic-based
Color	Opaque
Density	1.063-1.103 kg / liter
Chlorine content	< 0.1 %
Alkali content	< 3 %
Recommended dosage	About 1% of cement content

4.1.5. Polyvinyl Alcohol (PVA) Fiber

Polyvinyl alcohol (PVA) fiber, shown in Figure 4.8, was used in ECC mixtures based on the standard M45 ECC mixture in the literature (Li 2007). Low amount of PVA fibers were also used in HyFRC mixtures based on the literature review to obtain a low price mixture with high performance. The geometric and mechanical properties of the PVA fibers are given in Table 4.4.

Figure 4.8. Photograph of the PVA fibers

Table 4.4. Geometric and mechanical properties of PVA fibers

Fiber Type	Length (mm)	Diameter (μm)	Specific Gravity	Nominal Strength (MPa)	Apparent Strength (MPa)	Strain (%)	Young Modulus (GPa)
PVA	8	40	1.3	1610	1092	6	42.8

4.1.6. Steel Fibers

Three types of hooked-end Bekaert brand and Dramix generation steel fibers were used in this study. The geometric and mechanical properties of the steel fibers are given in Table 4.5.

Table 4.5. Geometric and mechanical properties of steel fibers

Fiber Type	**Aspect Ratio**	**Length (mm)**	**Diameter (mm)**	**Tensile Strength (MPa)**	**Geometry**
40/30 3D	40	30	0.75	1225	
65/60 3D	65	60	0.90	1160	
65/60 5D	65	60	0.90	2300	

4.2. Mixture Types and Proportions

Based on the aim of this research and the literature review, four types of mixtures were designed for this study. These mixture types are:

- Engineered Cementitious Composites (ECC),
- Hybrid Fiber Reinforced Concrete (HyFRC),
- Normal Concrete (NA), and
- Steel Fiber Reinforced Concrete (SFRC).

In this section the mixture proportions and mixing procedure for these mixtures are explained.

4.2.1. ECC Proportions

Standard M45 ECC (Li 2007) mixtures with various fly ash ratios (1.2, 1.7, and 2.2) were prepared. ECC mixtures were labeled according to FA/PC ratio as FA1.2, FA1.7, and FA2.2. Based on the results, the mixture with best performance, which is FA1.2, was reproduced by replacing 10%, 20% or 30% (by weight) of the quartz sand with presoaked expanded perlite. Such mixtures were labeled as FA1.2_P10, FA1.2_20, and FA1.2_30. The proportions of the ECC mixtures are in Table 4.6.

Table 4.6. ECC mixture proportions

Mixtures	**PC**	**W/B**	**A/B**	**FA/PC**	**PVA by volume, %**	**Perlite aggregate, replacing quartz, %**	**Superplasticizer**
FA1.2	1	0.27	0.36	1.2	2	-	As per need
FA1.7	1	0.27	0.36	1.7	2	-	As per need
FA2.2	1	0.27	0.36	2.2	2	-	As per need
FA1.2_P10	1	0.27	0.36	1.2	2	10	As per need
FA1.2_P20	1	0.27	0.36	1.2	2	20	As per need
FA1.2_P30	1	0.27	0.36	1.2	2	30	As per need

4.2.2. HyFRC Proportions

This type is hybrid reinforced concrete (HyFRC). The HyFRC mixtures were designed to have a binder content of 600 kg/m3. The proportions for HyFRC mixture type are given in Table 4.8. For each HyFRC type given in Table 4.7, three types of steel fibers (ST1, ST2, or ST3), and two coarse aggregate types (with 8 mm and 16 mm D_{max}) were used. Therefore, it makes the total number of the HyFRC mixtures thirty-six as shown in Table 4.8. Additionally, presoaked expanded perlite was also used in one of the mixtures by replacing 20% (by weight) of the sand.

Table 4.7. HyFRC mixture proportions (by weight) (binder content = 600 kg/m^3)

Mix	PC	FA/PC	Water/Binder	RS	CA	Steel fiber (Vol%)	PVA (Vol%)
1	1	1.2	0.40	2.3	2.5	0.50	0.25
2	1	1.2	0.40	2.3	2.5	0.50	0.50
3	1	1.2	0.40	2.3	2.5	0.75	0.25
4	1	1.2	0.40	2.3	2.5	0.75	0.50
5	1	1.2	0.40	2.3	2.5	1.25	0.25
6	1	1.2	0.40	2.3	2.5	1.25	0.50

Table 4.8. HyFRC mixtures

Steel Fiber Type	Steel Fiber Volume(%)	PVA Fiber Volume (%)	Dmax (mm)
Bekaert 40/30 3D	0.50	0.25	8
		0.50	
	0.75	0.25	
		0.50	
	1.25	0.25	
		0.50	
Bekaert 65/60 3D	0.50	0.25	
		0.50	
	0.75	0.25	
		0.50	
	1.25	0.25	
		0.50	
Bekaert 65/60 5D	0.50	0.25	
		0.50	
	0.75	0.25	
		0.50	
	1.25	0.25	
		0.50	
Bekaert 40/30 3D	0.50	0.25	16
		0.50	
	0.75	0.25	
		0.50	
	1.25	0.25	
		0.50	
Bekaert 65/60 3D	0.50	0.25	
		0.50	
	0.75	0.25	
		0.50	
	1.25	0.25	
		0.50	
Bekaert 65/60 5D	0.50	0.25	
		0.50	
	0.75	0.25	
		0.50	
	1.25	0.25	
		0.50	

The HyFRC mixtures were labeled to show steel fiber type, steel fiber content, PVA content, and D_{max}, respectively. For example, ST2,1.25_P0.25_D8 mixture identifies that steel fiber type is ST2, steel fiber content is 1.25%, PVA amount is 0.25%, and D_{max} of aggregate is 8mm. In the case of 20% perlite replacement, the mixture was named as ST2,0.75_P0.25_Per20%_D16.

4.2.3. Normal Concrete (NC) Proportions

One Normal Concrete (NC) without any fibers was also prepared with the same proportions as HyFRC. It is plain concrete with ~30 MPa compressive strength. This is the control mixture for making comparison with other mixtures.

4.2.4. Steel Fiber Reinforced Concrete (SFRC) Proportions

Depending on the results of the HyFRC mixtures, one mixture of HyFRC with best performance is produced without PVA. SFRC mixture was produced with the same proportions as HyFRC except PVA fiber.

4.3. Mixing Procedure, Casting, and Curing

All of the mixtures were mixed, cast and cured in the Materials of Construction Laboratory of Civil Engineering Department at Izmir Institute of Technology. All of the procedures explained below were performed in the same manner as much as possible for all of the mixtures to eliminate the effects of variations on the results.

4.3.1. Mixing Procedure

Hobart type mixture with 20-liter capacity mixer was used for ECC mixtures as shown in Figure 4.9. The mixing order and time for ECC mixture is given in Table 4.9.

Figure 4.9. 20-liter capacity mixer for ECC production

Table 4.9. Mixing sequence for ECC mixtures

Step	Description	Mixer Speed (grade)	Mixing Duration (minute)
1	Introducing the cement, fly ash and quartz sand into the mixer and cover the mixer upper part with plastic sheet to eliminate dusting and loss of material	1	1
2	Introducing 2/3 of water into the mixer	2	1.5
3	Adding the superplasticizer diluted in 1/3 remaining amount of water	3	2
4	Opening the cover of the mixer and adding the PVA fibers	1	1
5	Final mixing	1	2.5

Rotating drum mixer with 100-L capacity, shown in Figure 4.10, was used for HyFRC, Normal Concrete, and SFRC. The mixing details for HyFRC, NC and SFRC are presented in Table 4.10, Table 4.11 and Table 4.12, respectively.

Figure 4.10. Rotating drum mixer with 100-L capacity

Table 4.10. Mixing sequence for HyFRC mixtures

Step	Description	Mixing Duration (minutes)
1	Introducing the sand into the mixer	1
2	Moisture correction for aggregates	-
3	Adding coarse aggregates to the mixer	1
4	Introducing 2/3 of the water (adding the presoaked perlite in this step if any)	1
5	Introducing the portland cement and fly ash	2
6	Adding the superplasticizer diluted in 1/3 remaining amount of water	4
7	Adding the steel fibers	2
8	Adding the PVA fibers	1
9	Final mixing	4

Table 4.11. Mixing sequence for Normal Concrete mixture

Step	Description	Mixing Duration (minutes)
1	Introducing the sand into the mixer	1
2	Moisture correction for aggregates	-
3	Adding coarse aggregates to the mixer	1
4	Introducing 2/3 of the water (adding the presoaked perlite in this step if any)	1
5	Introducing the portland cement and fly ash	2
6	Adding the superplasticizer diluted in 1/3 remaining amount of water	5

Table 4.12. Mixing sequence for SFRC mixtures

Step	Description	Mixing Duration (minutes)
1	Introducing the sand into the mixer	1
2	Moisture correction for aggregates	-
3	Adding coarse aggregates to the mixer	1
4	Introducing 2/3 of the water (adding the presoaked perlite in this step if any)	1
5	Introducing the portland cement and fly ash	2
6	Adding the superplasticizer diluted in 1/3 remaining amount of water	4
7	Adding steel fibers	1
8	Final mixing	4

4.3.2. Specimen Casting and Curing

ECC mixtures were cast without any vibration and just finished by a trowel. Almost all HyFRC, SFRC, and NC mixtures were self-consolidating and no mechanical vibration was required. However, manual vibration such as formwork shaking by hand was required for the mixtures with higher amounts of PVA and steel fibers.

ECC mixtures with molds stored in isolated plastic sheets for 7 days as moisture curing, then the specimens were removed from molds and dry-cured in laboratory condition until the day of testing (7days, 28days, or 90days).

After casting the HyFRC, SFRC, and NC specimens, they were covered with isolated plastic sheets for 48 hours before demolding. Then they were stored in isolated plastic bags for 7 days as moisture curing and dry-cured at laboratory conditions until the day of testing (7days, 28days, or 90days).

4.4. Testing Methods

Slump (ASTM C143), slump flow test (ASTM C1611), compressive strength (ASTM C109 and C39), four-point bending test (ASTM C1609), freeze-thaw cycles test (ASTM C666), rapid chloride ions permeability test (ASTM C1202), sorptivity (ASTM C1585), impact loading test on small size specimens, and real size barrier impact loading test were made on fresh and hardened states of all four types of mixtures of this study. The tests used in the experimental program of this study are explained below:

4.4.1. Slump and Slump Flow Test

Slump test was made according to ASTM C 143 (Standard Test Method for Slump of Hydraulic-Cement Concrete). This test was applied on hybrid fiber reinforced and normal concrete types. Fibers in fresh concrete reduce workability, therefore, the superplasticizer was added to the concrete to achieve sufficient workability. By adding the superplasticizers, the HyFRC and normal concrete mixtures got almost self-consolidating behavior. Thus, the slump flow test was also made according to ASTM C 1611 (Standard Test Method for Slump Flow of Self-Consolidating Concrete).

A sample of freshly mixed concrete is placed in a slump cone mold without any tamping and vibration. Then the mold is raised and the concrete is allowed to spread. After spreading the concrete, for the less flowable mixtures the normal slump is measured and for the highly flowable mixtures the two diameters of the spread are measured in orthogonal directions as shown in Figure 4.11. The slump flow is calculated as the average of the two diameters as shown below:

$$\text{Slump flow} = \frac{(d_1 + d_2)}{2}$$

Where d_1 is the maximum diameter and d_2 is the diameter perpendicular to d_1.

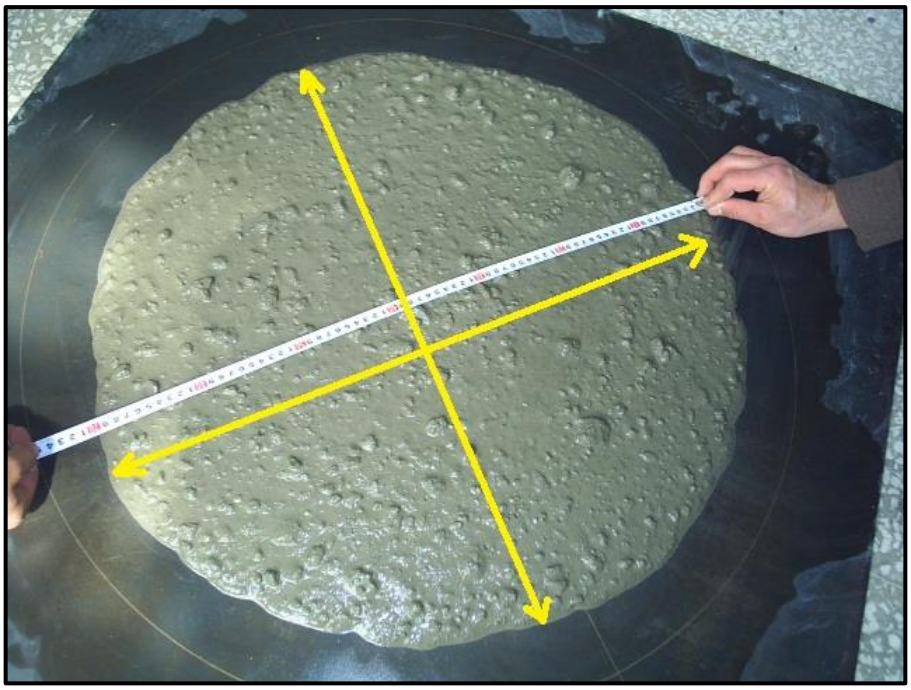

Figure 4.11. Measuring of the slump flow of concrete

4.4.2. Compressive Strength Test

ECC mixture specimens' compressive strength were tested according to ASTM C 109 (Standard Test Method for Compressive Strength of Hydraulic Cement Mortars (Using 2-in. or 50 mm Cube Specimens)). HyFRC and normal concrete mixtures were tested according to TS EN 206-1, (Concrete-Complementary British Standard to BS EN 206-1) and ASTM C 39 (Standard Test Method for Compressive Strength of Cylindrical Concrete Specimens).

Three 50-mm cubes were cast for each mixture of ECC for 7, 28, 90 days. The compressive strength test was carried out by universal testing machine with 250-kN capacity at the stroke rate of 0.51 mm/min as seen in Figure 4.12. Three 150-mm cubes were cast for each mixture of HyFRC, NC and SFRC, and they were tested by 2000-kN capacity compressive machine at the stroke rate of 2.3 mm/min as shown in Figure 4.13.

Figure 4.12. ECC compressive strength by universal testing machine

Figure 4.13. Concrete compressive strength testing machine

4.4.3. Four-Point Bending Test

Static bending test was applied on according to JSCE-SF4 (Method of Tests for Flexural Strength and Flexural Toughness of Steel Fiber Reinforced Concrete) and ASTM C 1609 (Standard Test Method for Flexural Performance of Fiber-Reinforced

Concrete (Using Beam with Third-Point Loading)). This test evaluates the flexural strength and flexural toughness of fiber reinforced concrete. This test method is used for composites with single or combination of fibers of same or different materials that are not longer than 60 mm. The tests were performed by the universal testing machine with 250-kN capacity.

Three specimens with dimensions (360 x 75 x 50 mm) were cast for each ECC mixture for testing at 7, 28, and 90 days. Then these specimens were tested under three-point bending test in (L/3 = 100 mm) at the stroke rate of 0.3 mm/min as seen in Figure 4.14.

For the HyFRC and NC mixtures, three 600 x 150 x 150 mm prismatic specimens were tested under three-point bending in (L/3 = 150 mm) at 28 days (Figure 4.15). The stroke rate was 0.1 mm/min before peak point and 0.25 mm/min was after peak piont. Some selected mixtures were tested at 7 and 90 days as well.

Dynamic bending tests that will be explained in the next section used specimens with 600 x 100 x 100 mm dimensions and they had 30 mm notch at the middle. To compare the static and dynamic bending results, same type of specimens were also cast for some mixtures and tested as explained above (Figure 4.16).

The mid-span deflections for the specimens were recorded during the test by a video-extensometer.

Figure 4.14. ECC mixtures flexural testing

Figure 4.15. 600 x 150 x 150 mm prismatic specimens for flexural testing

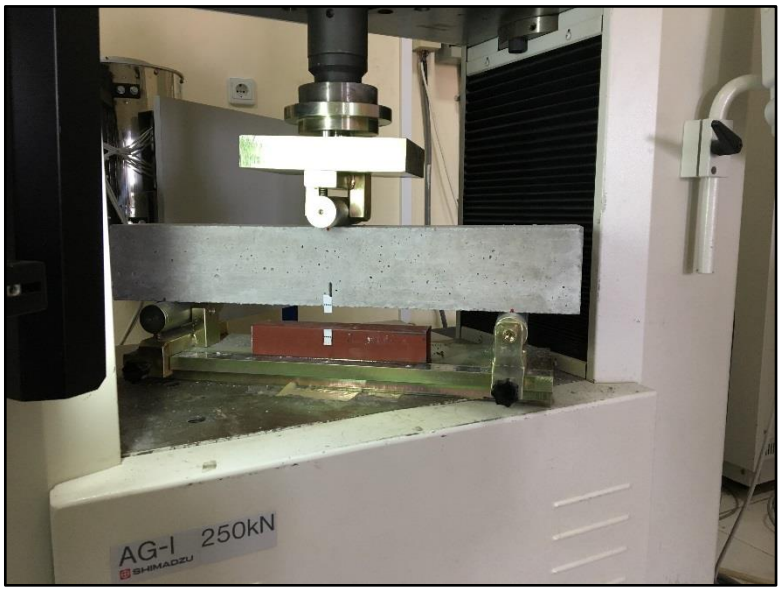

Figure 4.16. 600 x 100 x 100 mm prismatic specimens for flexural testing

4.4.4. Impact Loading Test

Impact loading tests were made by a drop-weight test machine in Dokuz Eylül University (Figure 4.17). Drop-weight test is an instrumented machine allowing the free-fall of a cylindrical hammer with changeable weight from an adjustable height onto the mid-span of the specimen (Yardımcı et al. 2017). Two piezoelectric load cells were attached to the supports for obtaining the reaction forces vs. time history. The sum of the reaction forces is considered as the true bending force in strength, toughness and

fracture energy calculations (Banthia et al. 1989, Dancygier et al. 2012). Mid-span deflection vs. time history was obtained by a noncontact laser displacement sensor which is placed under the notched specimen. This system provides complete load-deflection curves of the beam samples subjected to low-velocity flexural impact loading.

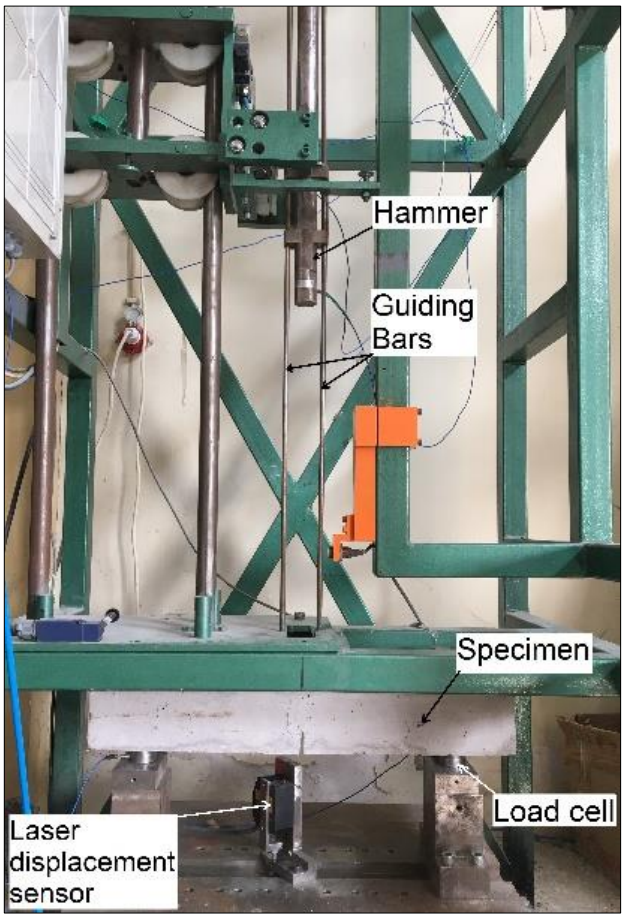

Figure 4.17. Impact loading test

For each ECC mixture, three specimens with 360 x 75 x 50 mm dimensions were tested under impact loading (Figure 4.18). Span length was 250 mm, hammer height was 600 mm and hammer weight was 4.26 kg. For the HyFRC specimens, 600 x 100 x 100 mm specimens with 30 mm notch depth were used (Figure 4.19). Span length was 450 mm and the height of the same hammer was adjusted to 2000 mm. The drop of the hammer provided a hammer tip velocity of 6.264 m/s.

A small cylindrical steel was used in the middle and top of specimen where the hammer hits in order to distribute the load equally as seen in Figure 4.20.

Figure 4.18. ECC impact loading test

Figure 4.19. HyFRC impact loading test

Figure 4.20. Impact loading test specimen

4.4.5. Rapid Chloride Permeability Test (RCPT)

Rapid chloride permeability test (RCPT) was carried out for all ECC, selected HyFRC, one SFRC, and one normal concrete according to ASTM C 1202 (Standard Test Method for Electrical Indication of Concrete's Ability to Resist Chloride Ion Penetration). This test determines the electrical conductance of concrete by rapid indication of its resistance to the penetration of chloride ions. Three cylindrical specimens of 50 mm thick and 100 mm in diameter were tested for 6 hours as seen in Figure 4.21. These specimens were obtained by cutting slices from 100x200 mm cylindrical specimens. A voltage of 60V DC continued across the circular sides of the specimens during the test. One side was immersed in a 3.0% salt (NaCl) solution and the other in a 0.3 M sodium hydroxide (NaOH) solution. Table 4.13 shows chloride ion penetrability based on charge passed.

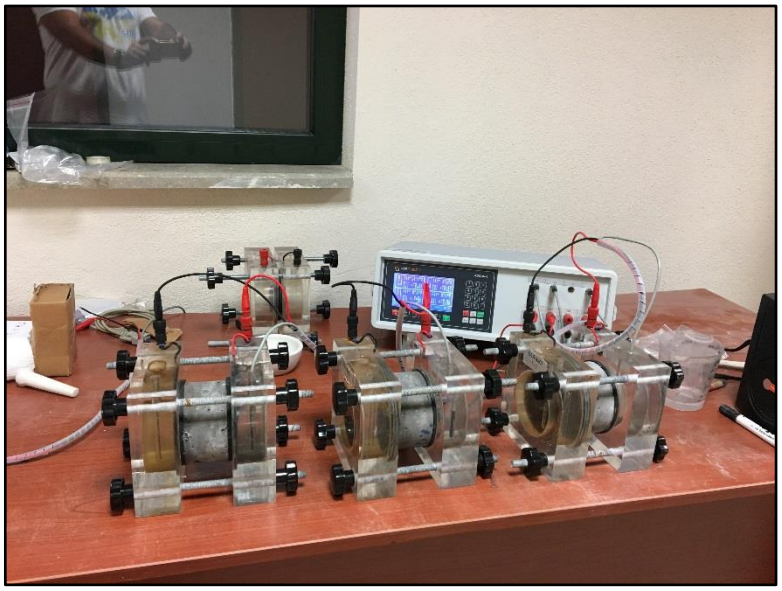

Figure 4.21. Rapid chloride permeability test

Table 4.13. Chloride Ion Penetrability Based on Charge Passed

Charge Passed (Coulombs)	Chloride Ion Penetrability
>4,000	High
2,000-4,000	Moderate
1,000-2,000	Low
100-1,000	Very Low
<100	Negligible

4.4.6. Freezing and Thawing Test

Freezing and thawing tests were performed for all ECC, selected HyFRC, one SFRC, and one NC according to ASTM C 666 (Standard Test Method for Resistance of Concrete to Rapid Freezing and Thawing). This test evaluates the resistance of concrete to rapidly repeated cycles of freezing and thawing in an incubator in the laboratory. Three 280x100x100 mm prismatic specimens were cast for HyFRC and NC mixtures while three 220x75x75 mm prismatic specimens were tested for each ECC mixture. Weight and ultrasonic pulse velocity UPV losses after 300 cycles were evaluated.

4.4.7. Sorptivity Test

Sorptivity tests were carried out for all ECC, and selected HyFRC, SFRC, and NC according to ASTM C 1585 (Standard Test Method for Measurement of Rate of Absorption of Water by Hydraulic-Cement Concrete). This test is used to determine the water absorption capacity of concrete by measuring the increasing in the mass of the specimen when only one surface of it is exposed to water. In this test the absorption of water is a function of time, and the mechanism of the absorption is capillary pressure. Three cylindrical specimens of 50 mm thick by 100 mm in diameter were prepared for this test as seen in Figure 4.22. These specimens were obtained by cutting slices from 100x200 mm cylindrical specimens.

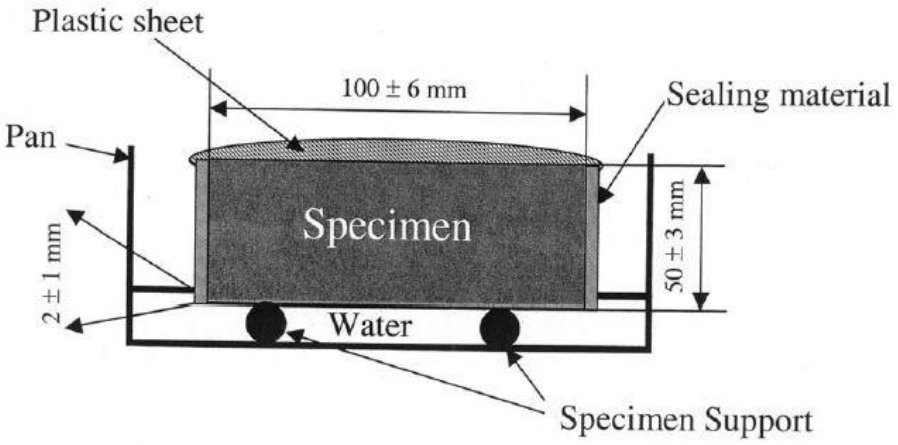

Figure 4.22. Schematic diagram of the sorptivity test
(Source: ASTM C 1585)

4.4.8. Pendulum Test for Real-Size Barriers

Impact tests were also carried out on the real size concrete barriers. For these tests, the standard New Jersey road barriers were prepared with two meter length and cross section parameters shown in Figure 4.23. One road barrier was produced with NC as control specimen, and one road barrier was produced with one selected HyFRC. The selection was based on the best energy absorption capacity found from mechanical and impact tests of small size specimens.

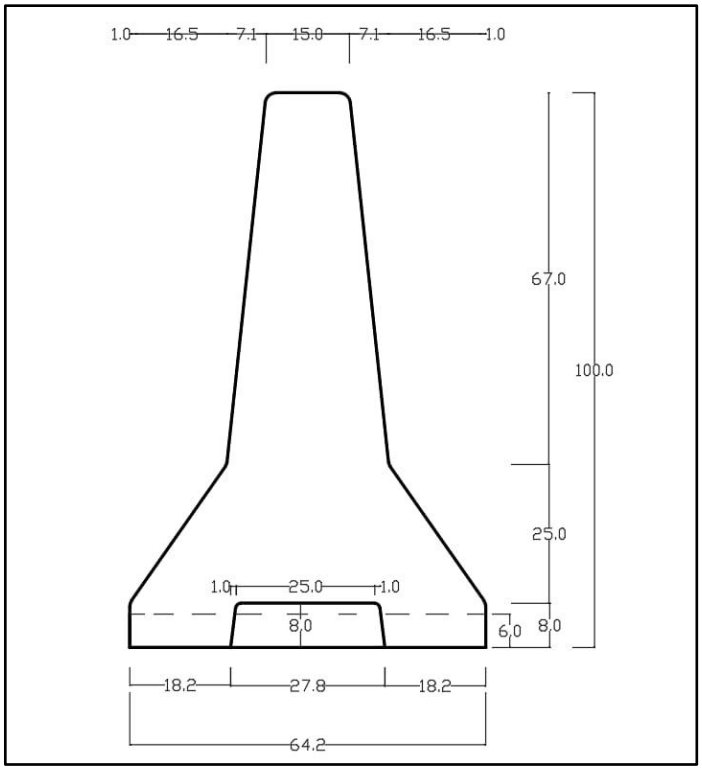

Figure 4.23. Concrete road barriers cross section (units are centimeters)

In this method, the impact load was applied by using a pendulum system (Figure 4.24) which is placed in ÇimSa ready-mix concrete plant in Mersin as. Impact mass weight is about 1000 kilograms made from concrete and steel plates which remain rigid compared to concrete barrier. The center of the impact mass was raised by 1.15 m and it was released by cutting the rope holding the impact mass. Then the impact mass hit the barrier at a speed of 4.75 m/s.

The tested barrier is placed in the middle of two barriers with equal dimensions and connected by pins to prevent the sliding on the ground as seen in Figure 4.25. This

system consists of three barriers which is not connected to any other point, therefore, this system simulated the boundary conditions in real practice.

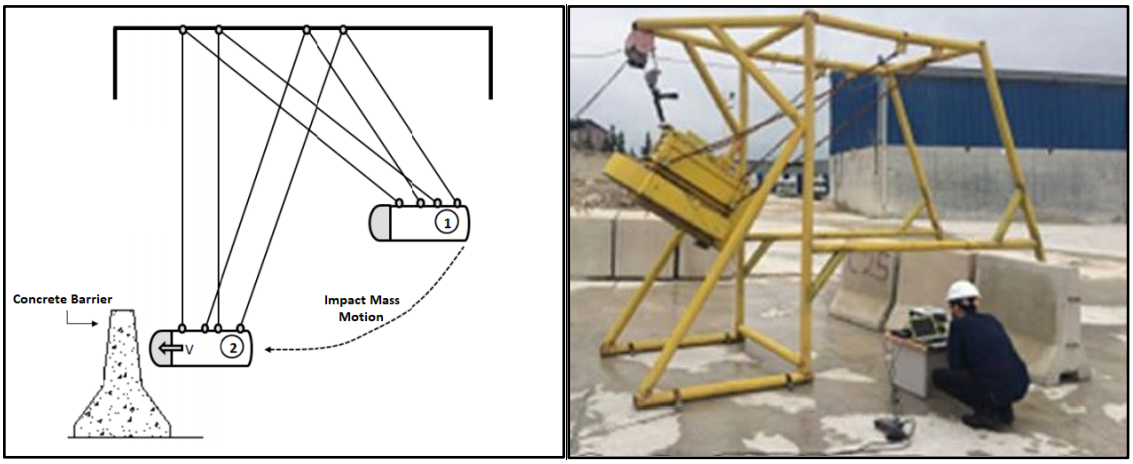

Figure 4.24. Pendulum test method for real size concrete barriers

Figure 4.25. Concrete barriers connected pins for pendulum test

CHAPTER 5

RESULTS AND DISCUSSIONS

5.1. Engineered Cementitious Composite (ECC)

In this section, compressive strength, static bending, impact bending, rapid chloride ions permeability, freeze-thaw cycles, and sorptivity tests of ECC mixtures will be discussed

5.1.1. Compressive Strength

Table 5.1 shows compressive strength values for all ECC mixtures at 7, 28, and 90 days.

Table 5.1. ECC compressive strength results

Mixtures	Compressive strength (**MPa**)		
	7 days	**28 days**	**90 days**
FA1.2	30.2	57.1	69.2
FA1.7	25.88	52.16	64.51
FA2.2	16.1	49.6	63.8
FA1.2_P10	29.15	48.5	62.12
FA1.2_P20	19.27	40.31	56
FA1.2_P30	16.74	31.15	40.52

Compressive strength results are shown in Figure 5.1. Aging effect show that the compressive strength increases as time increase, after mixing cement based materials hydration process takes place and it gives concrete its strength within time. Cement based materials develop strength with continued hydration. Strength gaining rate is faster at the begging and the rate gets reduced with age (Shetty 2006).

Figure 5. 1 indicates that the compressive strength decreases as the FA/PC increases especially at early ages. This can be explained by the relatively lower portland cement contents which can slow down the rate of strength gain.

The results for the ECC mixtures with saturated perlite show that the compressive strength decreases when the perlite content increases because quartz sand

is replaced with expanded perlite which has significantly lower compressive strength. Moreover, according as Keskin et al. (2013), large aggregate size and lower strength of expanded perlite act as stress concentrator that reduced the compressive strength.

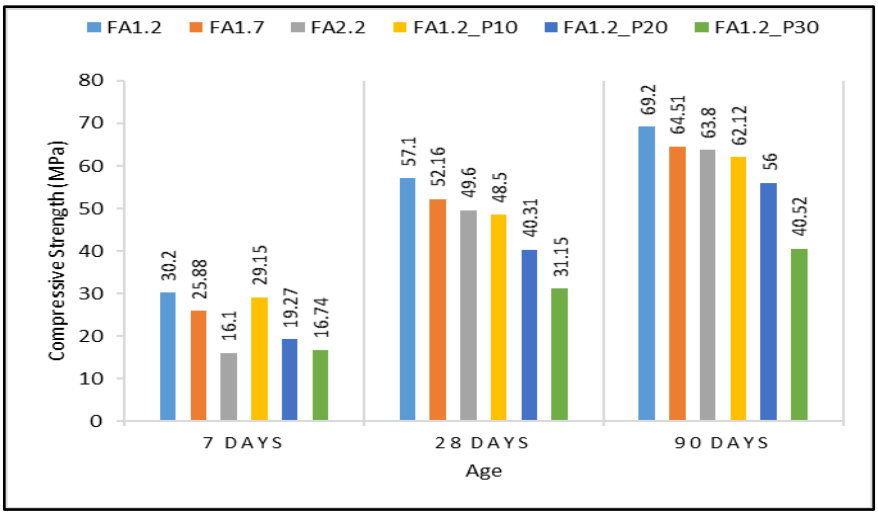

Figure 5.1. ECC compressive strength graphs

5.1.2. Static Bending Test

Static bending load-deflection curves for all ECC mixture are given APPENDIX A. As seen in figures, three line graphs belonging to three specimens are drawn for each mixture. The typical load-deflection curves which demonstrate the almost average curve of three specimens are shown in Figures 5.2-5.4. These curves were used to calculate the flexural strength and toughness. The ultimate flexural strength is calculated from the ultimate load of these graphs as:

$$f_{max} = \frac{P_{max}\ x\ L}{bd^2}$$

Where, f_{max}= ultimate flexural strength (MPa), P_{max}= peak load (N), L= the span length (mm), b = width of the specimen (mm), d = depth of the specimen (mm). Then the average strength value of three specimens were calculated. The toughness is calculated as the average area under the three curves until 3 mm deflection by Euler's method.

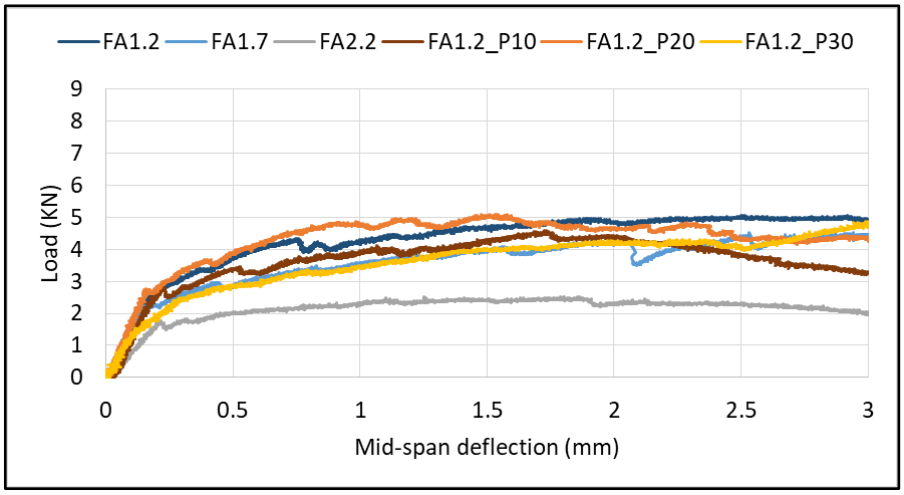

Figure 5.2. Static bending curves for ECC at 7 days

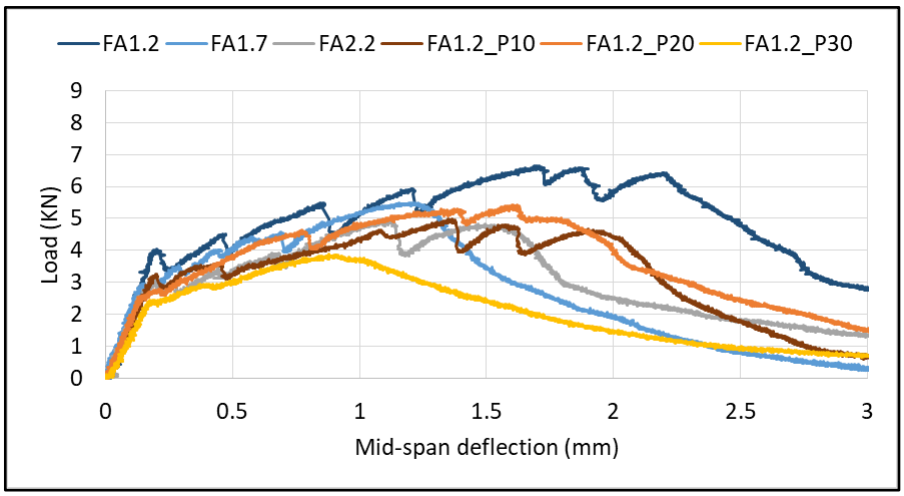

Figure 5.3. Static bending curves for ECC at 28 days

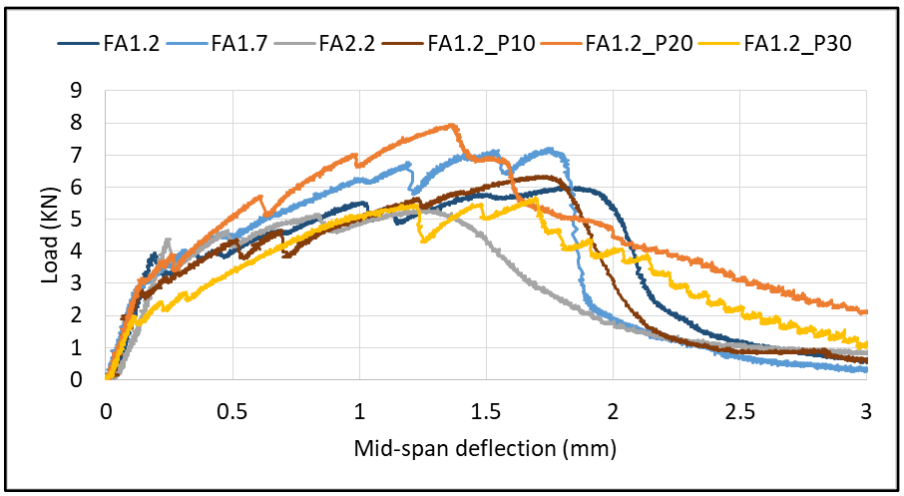

Figure 5.4. Static bending curves for ECC at 90 days

Static bending flexural strength values from static bending test for all ECC mixtures at 7, 28, and 90 days are given in Table 5.2.

Table 5.2. ECC static bending flexural strength results

Mixtures	Flexural strength (**MPa**)		
	7 days	**28 days**	**90 days**
FA1.2	7.5	10.08	10.4
FA1.7	6.63	9.33	9.43
FA2.2	4.4	7.9	8.4
FA1.2_P10	6.73	9.5	11.07
FA1.2_P20	8.11	9.07	11.5
FA1.2_P30	7.16	5.77	9.3

Figure 5.5 shows that the static bending flexural strength increases as time passes. The increase in strength from 28 days to 90 days is less for the mixtures without expanded perlite when compared to perlite incorporated mixtures. There is significant increasing of static bending flexural strength and compressive strength in mixtures with perlite content, due to the continuing pozzolanic reaction with the internal curing that provided by presoaked perlite (Keskin et al. 2012).

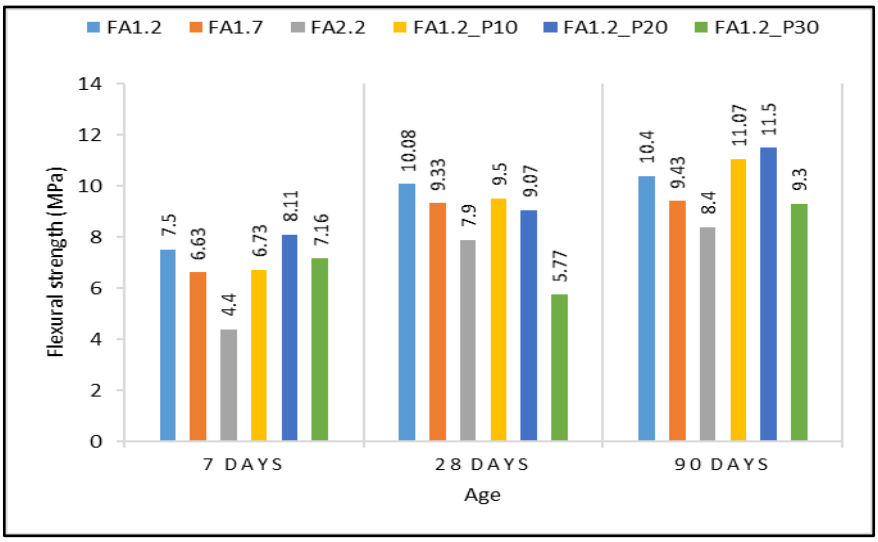

Figure 5.5. ECC flexural strength graphs

Results show that the static bending flexural strengths decrease as the FA/PC increases as was the case for compressive strength. This is also due to relatively lower PC contents which can slow down the rate of strength gain. Moreover, more fibers are

pulled out instead of rupture and achieve the maximum bridging stress that fibers can reach (Wang et al. 2019).

Similar to compressive strength test results, ECC mixtures with saturated perlite show less flexural strength when perlite content increases. Again, this can be explained by the lower compressive strength, larger aggregate size, and stress concentrator effect of expanded perlite (Keskin et al. 2013).

Static bending toughness values for all ECC mixtures at 7, 28, and 90 days are given in Table 5.3.

Table 5.3. ECC static bending toughness results

Mixtures	Toughness (**Joule**)		
	7 days	**28 days**	**90 days**
FA1.2	11.8	12.81	9.2
FA1.7	9.65	8.2	8.5
FA2.2	6.9	8.2	8.7
FA1.2_P10	9.71	9.55	11.29
FA1.2_P20	12.35	10.97	12.97
FA1.2_P30	10.41	6.31	11.04

The effect of age on toughness was not clear from Table 5.3. Some of the mixtures showed higher toughness and some of them showed less toughness at different ages. Therefore, a general trend could not be observed.

Results show that for all ages, static bending toughness decreases as the FA/PC increases from 1.2 to 1.7 since lower amount of PC resulted in less brittle matrix. Except 7 days, the results were similar for FA/PC ratios of 1.7 and 2.2. At 7 days, the pozzolanic reactions of FA are not significant and the matrix is less brittle. After 28 days, the amount of FA and age did not make a significant change in the toughness.

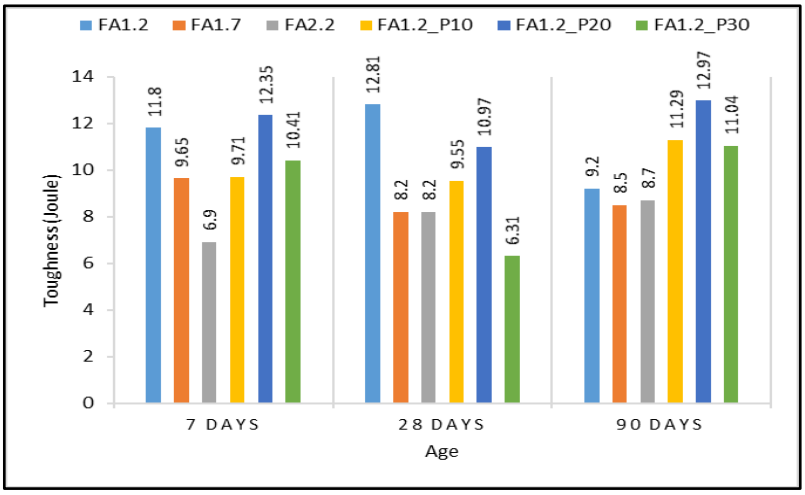

Figure 5.6. ECC toughness graphs

For the perlite incorporated mixtures, 20% replacement of perlite exhibited the highest toughness Perlite can act as flaws to increase the toughness.

5.1.3. Dynamic Bending Test

Dynamic bending test were applied only on 90-day ECC specimens. Dynamic bending load-deflection curves for all ECC mixtures are given in APPENDIX B. As seen in those figures, three line graphs are drawn for the three specimens belonging to each mixture. The typical load-deflection curves which demonstrate the average curve of three specimens are shown in Figure 5.7. Flexural strength and toughness were calculated by using these curves. The dynamic flexural strength is calculated from the ultimate load of these graphs as:

$$f_{max} = \frac{3\ x\ P_{max}\ x\ L}{2bd^2}$$

Where, f_{max}= ultimate flexural strength (MPa), P_{max}= peak load (N), L= the span (mm), b = width of the specimen (mm), d= depth of the specimen (mm). Then the average values of three specimens is considered for analysis. The toughness is calculated as the average area under the three curves until 3 mm deflection by Euler's method.

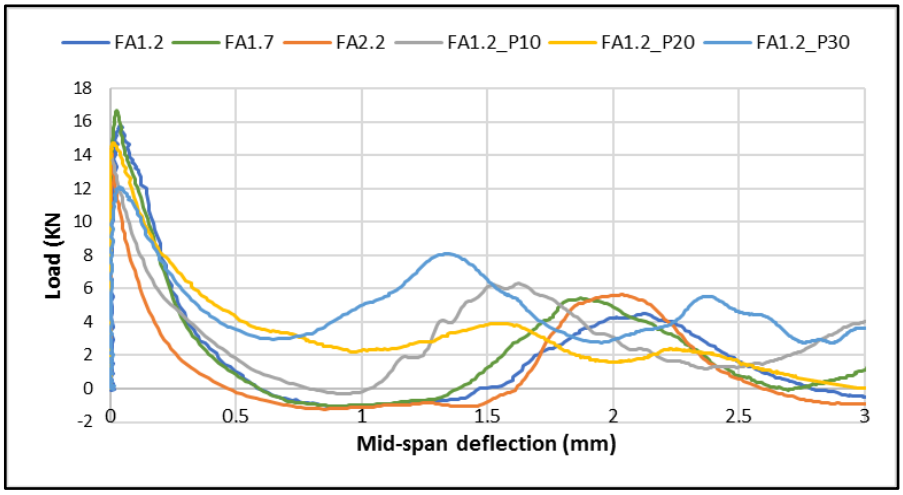

Figure 5.7. Dynamic bending curves for ECC at 90 days

Dynamic flexural strength and toughness values for all ECC mixtures at 90 days are given in Table 5.4.

Table 5.4. ECC dynamic flexural and toughness results

Mixtures	Flexural strength (MPa)	Toughness (Joule)
FA1.2	32.38	6.1
FA1.7	31.99	6.72
FA2.2	30.94	7.39
FA1.2_P10	26.7	8.58
FA1.2_P20	28.72	11.65
FA1.2_P30	26.02	13.58

Similar to static flexural strength values, the results show that the dynamic flexural strength decreases as fly ash content increases as seen in Figure 5.8. This is due to relatively lower PC contents which can slow down the rate of strength gain. In addition more fibers are pulled out instead of rupture and achieve the maximum bridging stress that fibers can reach. The dynamic flexural strength slightly decreased when expanded perlite is used due to lower strength of expanded perlite when compared to quartz. There is no significant difference in dynamic bending flexural strength for mixtures with expanded perlite but the flexural strength is slightly higher for 20% perlite replacement.

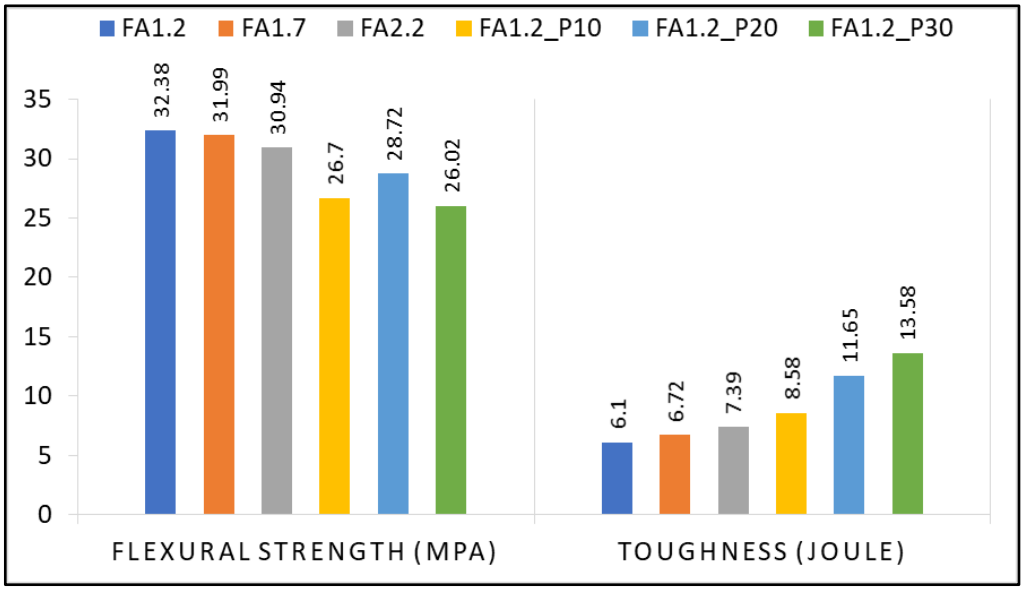

Figure 5.8. Dynamic bending results graphs for ECC at 90 days

Dynamic bending toughness values for all ECC mixtures at 90 days are given in Table 5.4. Contrary to the static bending test, results show that dynamic bending toughness increases as the fly ash content increase.

Results point out the significant increase in dynamic bending toughness with an increase in expanded perlite content.

5.1.4. Comparison of Dynamic and Static Bending Results

Table 5.5. ECC dynamic and static bending test results at 90 days

Mixures	Flexural strength (MPa)		Toughness (Joule)	
	Static Loading	Impact Loading	Static Loading	Impact Loading
FA1.2	10.4	32.38	9.2	6.1
FA1.7	9.43	31.99	8.5	6.72
FA2.2	8.4	30.94	8.7	7.39
FA1.2_P10	11.07	26.7	11.29	8.58
FA1.2_P20	11.5	28.72	12.97	11.65
FA1.2_P30	9.3	26.02	11.04	13.58

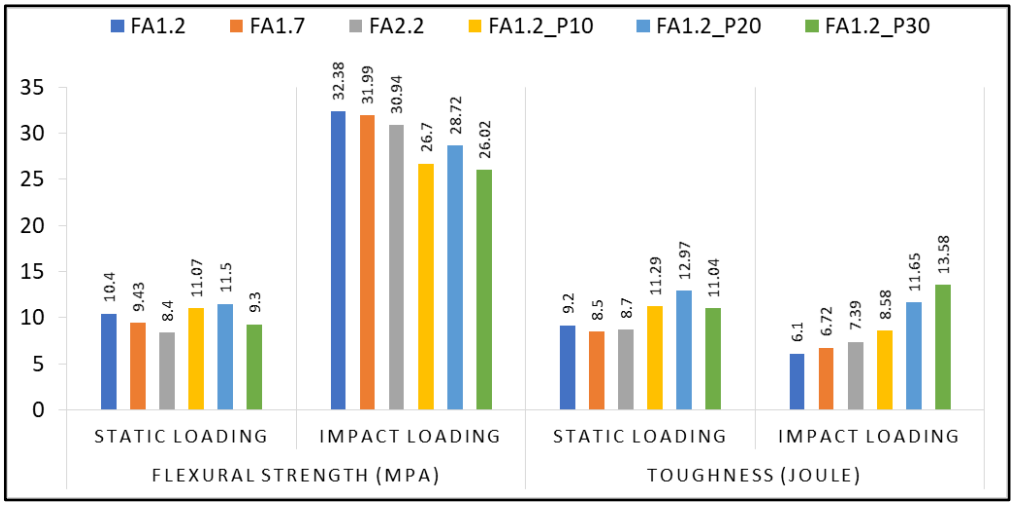

Figure 5.9. Static and dynamic bending graphs for ECC at 90 days

The dynamic increase factor (DIF) can be calculated in this study because the static and dynamic tests were performed on the ECC specimens with the same dimensions, the spam length, and the same loading point. Figure 5.10 compares dynamic and static flexural strength. Dynamic increase factor (ratio of dynamic to static flexural strength) for FA1.2, FA1.7, FA2.2, FA1.2_P10, FA1.2_P20, and FA1.2_P30 mixtures are 2.49, 2.71, 2.85, 1.93, 1.99 and 2.24, respectively. Results show that the static bending flexural strengths decrease as the FA/PC increases and ECC mixtures with saturated perlite show less flexural strength when perlite content increases. Opposing to the static bending test, results show that dynamic bending toughness increases as the fly ash content increase and significant increase in dynamic bending toughness with an increase in expanded perlite content.

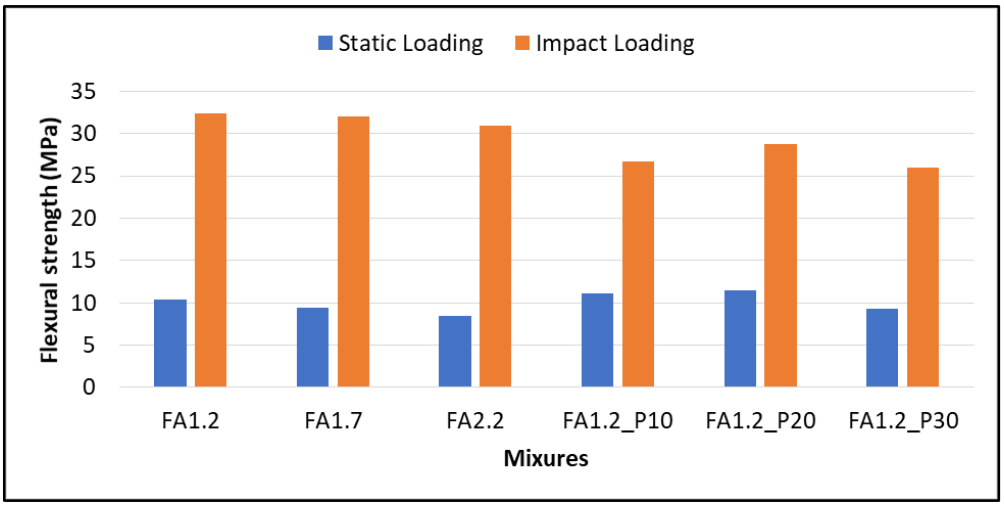

Figure 5.10. Static and dynamic flexural comparing graphs for ECC

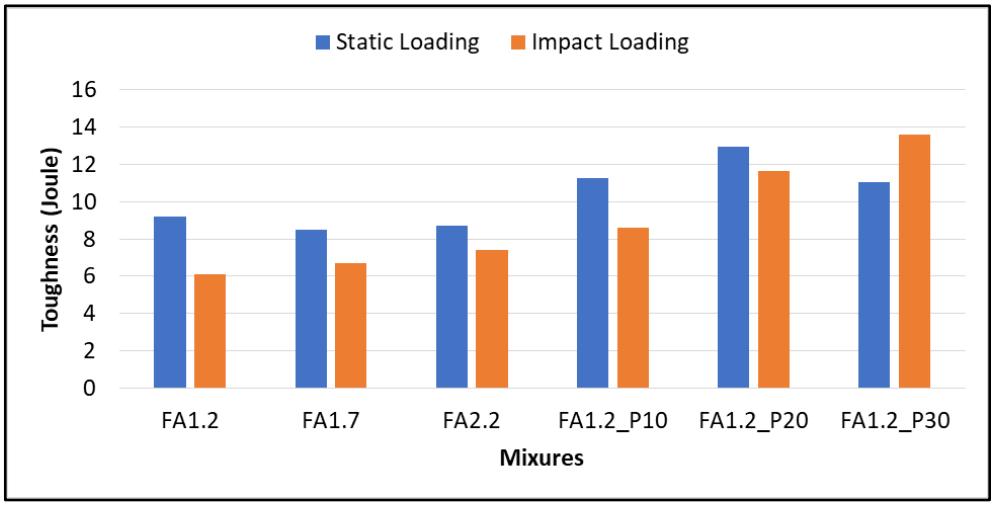

Figure 5.11. Static and dynamic toughness comparing graphs for ECC

5.1.5. Rapid Chloride Permeability Test (RCPT)

Rapid Chloride Permeability Test (RCPT) classification according ASTM C 1202 and tests results for all ECC mixtures at 90 days are given in Table 5.6 and Table 5.7, respectively.

Table 5.6. ASTM C 1202 Charge Passed Classification

Charge Passed (Coulombs)	Chloride Ion Penetrability
>4,000	High
2,000-4,000	Moderate
1,000-2,000	Low
100-1,000	Very Low
<100	Negligible

Table 5.7. RCPT test results for ECC at 90 days

Mixture IDs	FA1.2	FA1.7	FA2.2	FA1.2_10	FA1.2_20	FA1.2_30
RCPT Values (Coulombs)	57.66	144.66	193.33	90.66	105.33	185

Figure 5.12 shows RCPT test results. It can be observed that the charge passed increase as fly ash content increases. This can be explained by the fact that higher fly ash content makes ECC more porous and therefore provides more aisles for charge to pass through as stated by Zhang et al. (2014). Results also specified that passing of

charge increases as perlite content increases because the lightweight perlite aggregate is a porous material which provide more pores for passing the charges. Results also indicate that the FA1.2 mixture which has the lowest fly ash content and no perlite devours the highest permeability resistance.

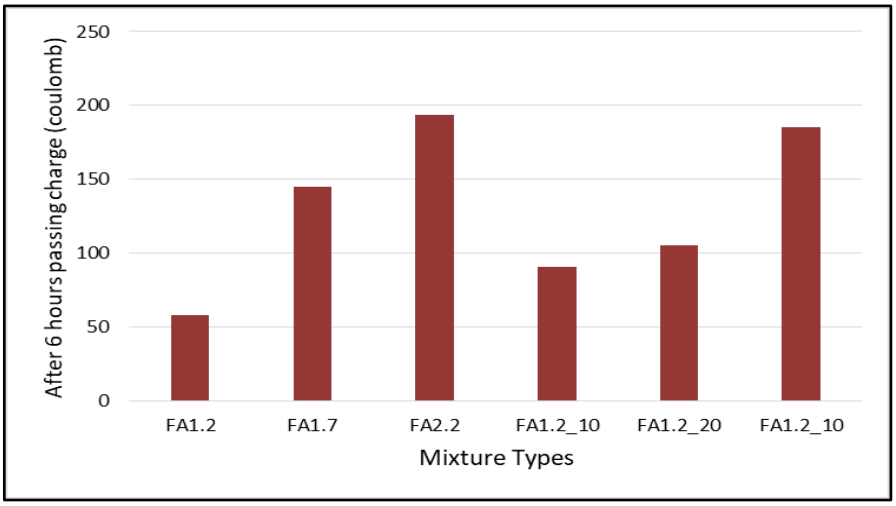

Figure 5.12. RCPT test results for ECC at 90 days

5.1.6. Freezing and Thawing Test (F-T)

Freezing and thawing test (F-T) values for all ECC mixtures at 90 days are given in Table 5.8. Two parameters are obtained from F-T test as weight loss and ultrasonic pulse velocity (UPV) loss after 300 cycles. In the testing time of ECC specimens, it was noticed that the UPV setup was not reliable, therefore, only the weight loss parameters are discussed.

Table 5.8. F-T test results for ECC at 90 days

Mixture IDs	Initial weight (gr)	Saturated Weight after (1 day)	Weight after 300 Cycles (61 days)	Weight Gain After 300 Cycles (%)
FA1.2	2692.9	2692.85	2706.05	0.49
FA1.7	2649.7	2649.85	2663.2	0.5
FA2.2	2591	2591.05	2611.05	0.77
FA1.2_10	2630.9	2630.85	2643.75	0.49
FA1.2_20	2513.3	2513.35	2532	0.74
FA1.2_30	2495.25	2495.75	2519.3	0.95

Generally, concrete weight decreases after freeze and thaw cycles but in this study all ECC mixtures seemed to gained weight. This was probably due to the unsaturated state of the specimens at the beginning of the tests, which may originate from the low permeability and very dense structure of ECC. According to the standard, specimens are saturated for 24 hours before testing but here it seems that all ECC specimens were not saturated in 24 hours and absorbed water until the end of testing. Table 5.8 shows that the absorption capacity (weight gain %) of all ECC specimens are less 1% within 60 days which means that ECC is dense and homogenous composite. In addition, visual inspection of the specimens did not imply weight loss since there was not surface scaling for any of the ECC composite.

Figure 5.13 shows that there is small increment of weight gain as fly ash content ratio increase from 1.2 to 1.7 but there is large increment of weight gain as fly ash content increase from 1.7 to 2.2. As known, fly ash reacts with lime (CaOH) coming from cement hydration reactions to produce additional calcium silicate hydrate (C-S-H) binder. The higher weight gain of the 2.2 FA/PC mixtures may be due to the fact that there is not enough lime in the mixture to react with high amount of fly ash. Accordingly, some part of the fly ash can stay free and absorb water.

Figure 5.13 also shows that increasing perlite content into ECC increased the weight of the specimens during the freeze and thawing test due to its higher water absorption capacity. All specimens were stored in isolated plastic bags for 7 days for moisture curing and then dry cured at laboratory conditions until the testing age (90 days). Therefore, the specimens were partially dry. Before freeze and thaw cycles all the specimens were put in water for 24 hours to be saturated. The results indicate that mixture with perlite content was not fully saturated in 24 hours so these mixtures absorbed water until the end of freeze and thaw test, resulting in an increase in the weights.

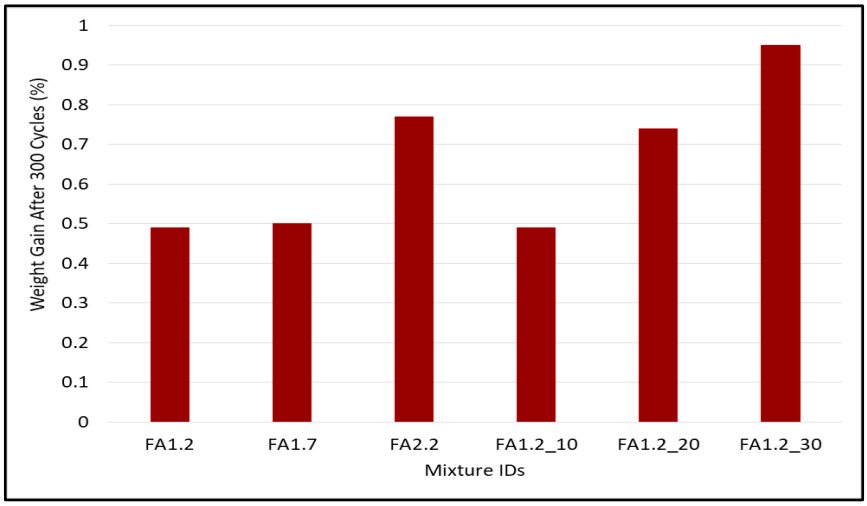

Figure 5.13. F-T test weight gain graphs for ECC at 90 days

5.1.7. Sorptivity Test

Sorptivity test or capillary water absorption values for all ECC mixtures at 90 days are given in Table 5.9.

Table 5.9. Sorptivity test results for ECC at 90 days

Time		Capillary Water Absorption (%)					
Seconds	**Hours**	**FA1.2**	**FA1.7**	**FA2.2**	**FA1.2_P10**	**FA1.2_P20**	**FA1.2_30**
60	0.02	0.10	0.07	0.15	0.13	0.20	0.19
300	0.08	0.22	0.16	0.34	0.27	0.41	0.45
600	0.17	0.26	0.24	0.40	0.37	0.50	0.53
1200	0.33	0.34	0.37	0.54	0.45	0.64	0.68
1800	0.50	0.39	0.44	0.62	0.53	0.73	0.79
3600	1	0.46	0.55	0.75	0.62	0.86	0.93
7200	2	0.53	0.64	0.88	0.70	0.98	1.09
10800	3	0.57	0.71	0.98	0.76	1.06	1.20
14400	4	0.60	0.76	1.06	0.80	1.11	1.27
18000	5	0.63	0.81	1.12	0.83	1.17	1.34
21600	6	0.66	0.84	1.17	0.86	1.20	1.38
86400	24	0.85	1.18	1.68	1.08	1.54	1.87
172800	48	1.00	1.43	2.08	1.24	1.77	2.22
259200	72	1.08	1.56	2.25	1.32	1.90	2.40

Figure 5.14 shows sorptivity test results of ECC with various contents of fly ash. Results show that capillary water absorption capacity increases as fly ash content increases. The reason is that there is not enough lime (C-S-H) in the concrete to react with high amount of fly ash, therefore, some of fly ash can stay free and absorb water.

Figure 5.15 illustrates that the capillary water absorption capacity increases as expanded perlite content increases due to its porous structure that has relatively higher water absorption capacity. Results also point out that the mixture (FA1.2) which contains lowest fly ash and no perlite shows the lowest sorptivity as shown in Figure 5.16.

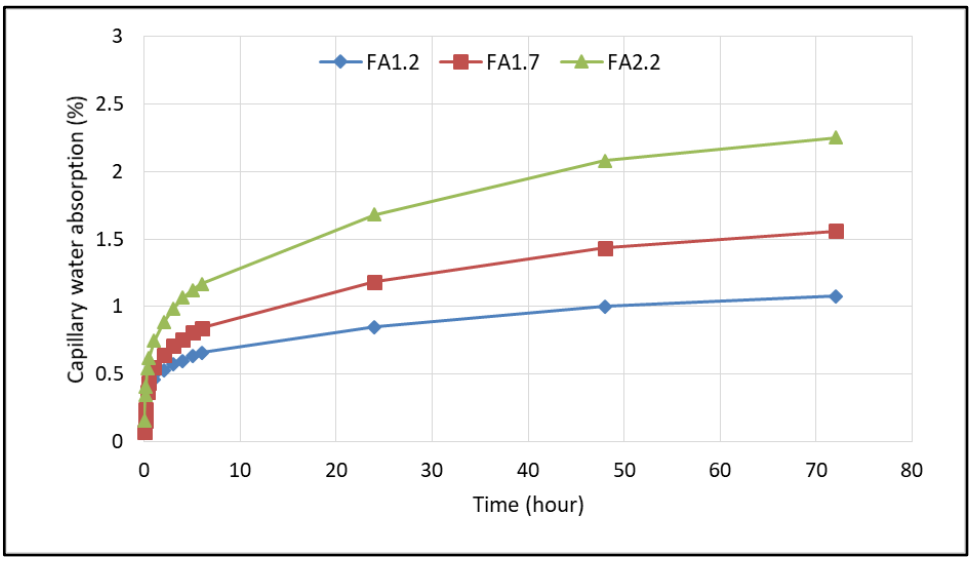

Figure 5.14. Effect of fly ash content on sorptivity on ECC at 90 days age

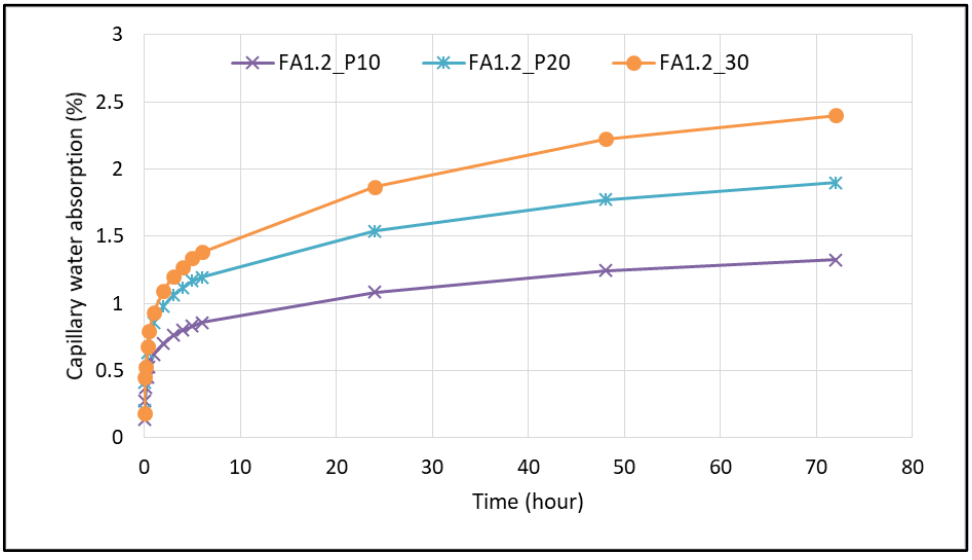

Figure 5.15. Effect of perlite content on sorptivity on ECC at 90 days age

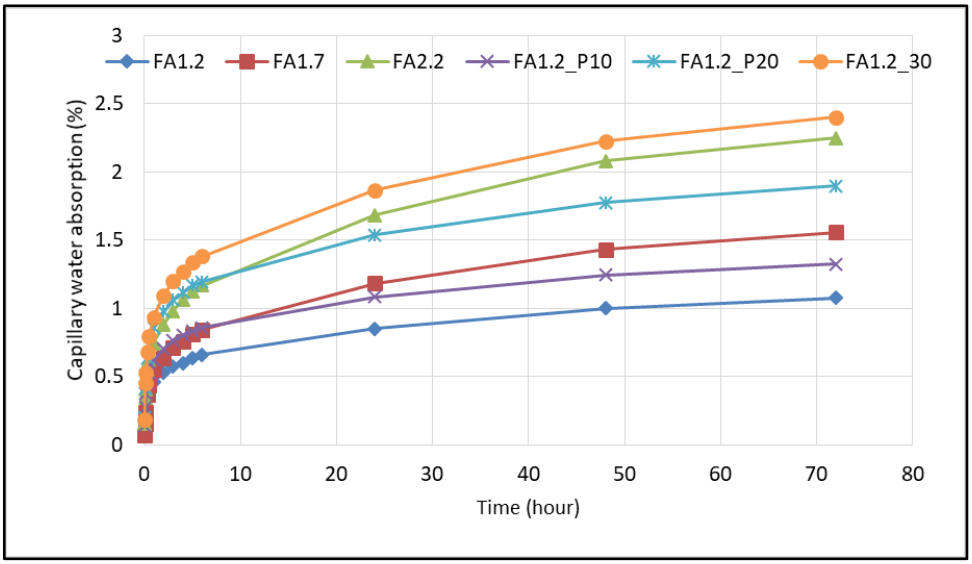

Figure 5.16. Sorptivity test graphs for all ECC at 90 days age

5.2. Hybrid Fiber Reinforced Concrete (HyFRC)

In this section, the test results of all HyFRC mixtures, a mixture of steel fiber reinforced concrete, and one mixture of normal concrete (NC) are discussed. These tests include consistency, compressive strength, static bending, dynamic bending, rapid chloride ion permeability, freeze-thaw, and sorptivity tests.

5.2.1. Consistency and Superplasticizer Requirement

Slump-flow test values and superplasticizer demand for the HyFRC mixtures and the normal concrete at 28 days are given in Table 5.10.

Table 5.10. Slump-flow test results and superplasticizer demand for HyFRC and normal Concrete

Mix. No	Mix. IDs	Slump flow (cm)	SP demand (gr)	**Mix. No**	Mix. IDs	Slump flow (cm)	SP demand (gr/55Lt)
1	ST1,0.50_P0.25_D8	35.5	77	**20**	ST1,0.50_P0.25_D16	40.25	72
2	ST2,0.50_P0.25_D8	34.5	80	**21**	ST2,0.50_P0.25_D16	40.75	82
3	ST3,0.50_P0.25_D8	32.5	86	**22**	ST3,0.50_P0.25_D16	42.75	91
4	ST1,0.50_P0.50_D8	22.5	122	**23**	ST1,0.50_P0.50_D16	40.5	117
5	ST2,0.50_P0.50_D8	21	142	**24**	ST2,0.50_P0.50_D16	36.5	132
6	ST3,0.50_P0.50_D8	23	152	**25**	ST3,0.50_P0.50_D16	30	147
7	ST1,0.75_P0.25_D8	36.5	88	**26**	ST1,0.75_P0.25_D16	39.5	82
8	ST2,0.75_P0.25_D8	29.5	100	**27**	ST2,0.75_P0.25_D16	41	92
9	ST3,0.75_P0.25_D8	31.5	104	**28**	ST3,0.75_P0.25_D16	40	97
10	ST1,0.75_P0.50_D8	25	137	**29**	ST1,0.75_P0.50_D16	31	132
11	ST2,0.75_P0.50_D8	22	147	**30**	ST2,0.75_P0.50_D16	30	140
12	ST3,0.75_P0.50_D8	22	152	**31**	ST3,0.75_P0.50_D16	28.5	144
13	ST1,1.25_P0.25_D8	26.5	97	**32**	ST1,1.25_P0.25_D16	40.5	92
14	ST2,1.25_P0.25_D8	21	102	**33**	ST2,1.25_P0.25_D16	32	97
15	ST3,1.25_P0.25_D8	24.5	102	**34**	ST3,1.25_P0.25_D16	24.5	97
16	ST1,1.25_P0.50_D8	21	142	**35**	ST1,1.25_P0.50_D16	35	137
17	ST2,1.25_P0.50_D8	21	147	**36**	ST2,1.25_P0.50_D16	21.5	142
18	ST3,1.25_P0.50_D8	21	152	**37**	ST3,1.25_P0.50_D16	20.5	147
19	Normal Concrete	38	19	**38**	ST3,0.75_P0.25_Per20%_D16	45	0

Superplasticizer was used to achieve sufficient workability for casting the composites. Superplasticizer contents were not kept constant in the mixtures and special attention was paid to obtain uniform distribution of fibers and sufficient workability. Sufficient workability was decided to need no mechanical vibration for casting and to have homogeneous concrete ingredients. However, manual vibration such as formwork shaking by hand was necessary for the mixtures with higher amounts of PVA and steel fibers. After several trials, the maximum slump-flow diameter is decided to be 40+5 cm to ensure homogeneity of all mixtures.

Figures 5.17-20 show the effect of D_{max} and PVA content on the superplasticizer demand and slump flow values of HyFRC and NC. Results show as the D_{max} decreases from 16mm to 8mm superplasticizer demand increases because with finer particles the total surface area of aggregate increases and this requires more water to cover the surface as shown in Figure 5.17. Also the slump-flow values decrease as D_{max} decreases because the finer particles make the concrete more cohesive and reduce the flowability as shown on Figure 5.19.

Results illustrate that the superplasticizer demand significantly increased with adding the fibers, demand of superplasticizer for normal concrete is 19 gr/55Lt and it is

varying from 72-152 gr/55Lt for HyFRC as shown in Figure 5.17. The reason might be explained by the fact that fibers addition increases the surface area and paste requirement to cover the ingredients. Another reason is the increases in the internal friction in the concrete. The lower consistency of the fiber reinforced concretes is noted also by [Tabatabaeian et al. (2017), Barnat-Hunek et al. (2018)]

Adding saturated perlite aggregate reduced the superplasticizer requirement to zero because perlite, which replaces angular quartz particles, has spherical shape and enhance the consistency. Therefore, the mixture with perlite shows the highest slump-flow diameter of 45 cm as shown in Figure 5.18.

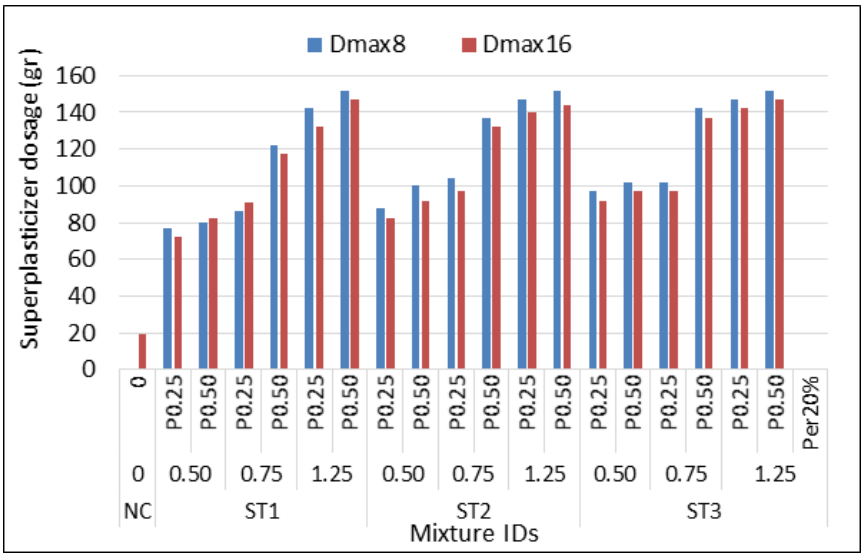

Figure 5.17. Effect of D_{max} on Superplasticizer demand for HyFRC and NC

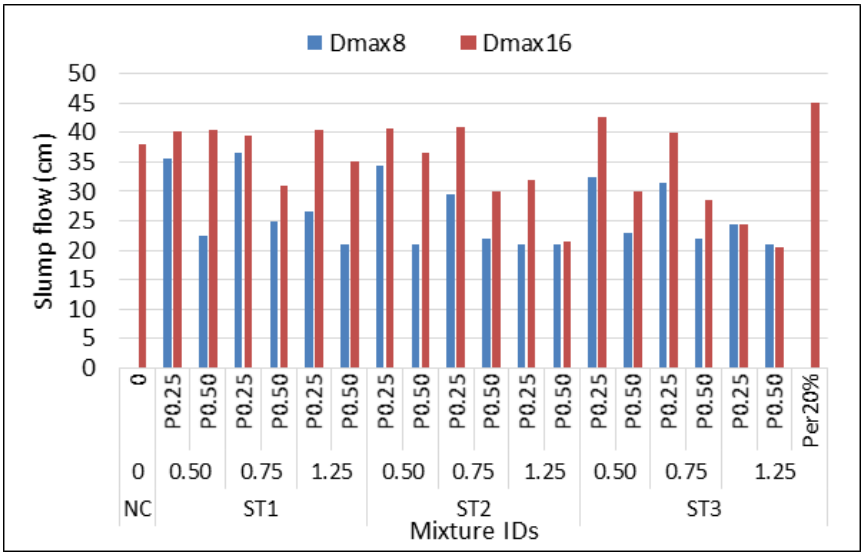

Figure 5.18. Effect of D_{max} on slump flow values of HyFRC and NC

As Figure 5.19 indicates, superplasticizer demand increases as the PVA and steel fiber volume fraction increase, which means that increasing the fiber content decreases the consistency of the concretes. Figure 5.20 shows that the slump-flow diameter decreases as PVA and steel fiber content increase. It is also observed that the superplasticizer demand increases and slump-flow diameter decreases by increasing the length of steel fibers. This may be attributed to the fact that the increase of volume of fraction and length of fiber leads a fiber-balling effect which decrease the workability of concrete (Yang, 2011). The other reason might be explained by the presence of fibers that prevent cement paste from flowing which decrease the workability of the concrete (Tabatabaeian et al. 2017).

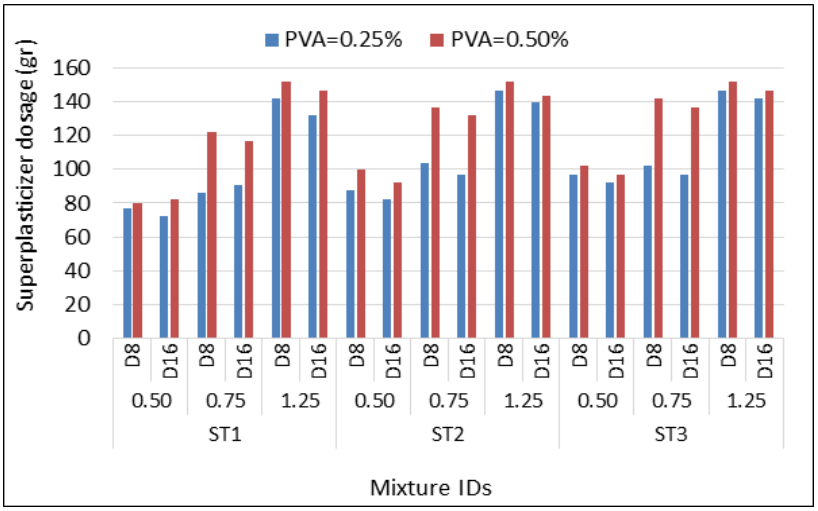

Figure 5.19. Effect of PVA and steel fiber amount on Superplasticizer demand for HyFRC

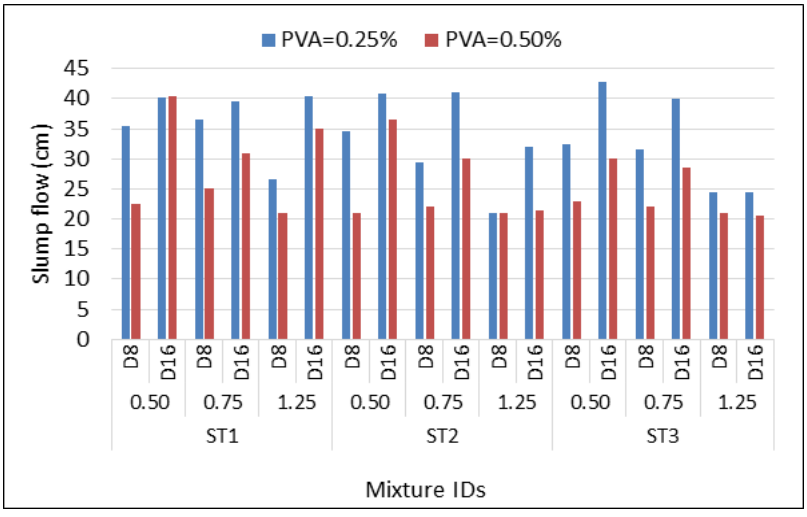

Figure 5.20. Effect of PVA and steel fiber amount on slump flow of HyFRC

5.2.2. Compressive Strength

Table 5.11 and Figure 5.21 show the compressive strength values for 37 HyFRC and one normal concrete mixtures at 28 days.

Table 5.11. HyFRC and normal concrete compressive strength

Mix. No	Mix. IDs	Compressive Strength (Mpa)	Mix. No	Mix. IDs	Compressive Strength (Mpa)
1	ST1,0.50_P0.25_D8	34.91	**20**	ST2,0.50_P0.25_D16	37.26
2	ST2,0.50_P0.25_D8	36.6	**21**	ST3,0.50_P0.25_D16	38.35
3	ST3,0.50_P0.25_D8	35.43	**22**	ST1,0.50_P0.50_D16	38.63
4	ST1,0.50_P0.50_D8	35.47	**23**	ST2,0.50_P0.50_D16	37.04
5	ST2,0.50_P0.50_D8	37.04	**24**	ST3,0.50_P0.50_D16	39.32
6	ST3,0.50_P0.50_D8	35.94	**25**	ST1,0.75_P0.25_D16	36.56
7	ST1,0.75_P0.25_D8	34.96	**26**	ST2,0.75_P0.25_D16	38.05
8	ST2,0.75_P0.25_D8	35.56	**27**	ST3,0.75_P0.25_D16	39.9
9	ST3,0.75_P0.25_D8	35.93	**28**	ST1,0.75_P0.50_D16	37.23
10	ST1,0.75_P0.50_D8	36.82	**29**	ST2,0.75_P0.50_D16	36.15
11	ST2,0.75_P0.50_D8	38.37	**30**	ST3,0.75_P0.50_D16	39.3
12	ST3,0.75_P0.50_D8	36.39	**31**	ST1,1.25_P0.25_D16	37.34
13	ST1,1.25_P0.25_D8	36.21	**32**	ST2,1.25_P0.25_D16	38.23
14	ST2,1.25_P0.25_D8	36.27	**33**	ST3,1.25_P0.25_D16	36.35
15	ST3,1.25_P0.25_D8	37.03	**34**	ST1,1.25_P0.50_D16	40.04
16	ST1,1.25_P0.50_D8	37.65	**35**	ST2,1.25_P0.50_D16	39.75
17	ST2,1.25_P0.50_D8	39.54	**36**	ST3,1.25_P0.50_D16	38.99
18	ST3,1.25_P0.50_D8	39.47	**37**	ST3,0.75_P0.25_Per20%_D16	17.31
19	ST1,0.50_P0.25_D16	36.33	**38**	Normal Concrete	31.18

Figure 5.21 shows that compressive strength of normal concrete is around 30 MPa and the HyFRC compressive strengths ranged between 34 MPa and 40 MPa. Compressive strength of HyFRC was higher than normal concrete due to the ability of fibers to delay and bridge crack formation that enhance the compressive strength of concrete (Şahmaran and Yaman 2007).

Compressive strength generally increased when aggregate D_{max} increased from 8mm to 16mm as seen in Figure 5.21. These observations can be explained by the fact that larger aggregate size shows more tortuous crack path, providing a rougher fracture surface, and cracks prefer to propagate along the weaker interfacial zone or larger pores in the matrix under loading as the crack reaches an aggregate particle where it is forced to propagate either through the aggregate or travel around the aggregate-mortar interface which increase the mechanical behavior of the matrix (Banyhussan et al. 2016).

Figure 5.22 illustrates the effect of PVA and steel fiber volume fraction on compressive strength. Results show that compressive strength values increase as PVA and steel fiber content increase. Fibers are capable of transferring larger tensile stresses from a cracked matrix to the fibers and can enhance the compressive strength (Choi et al. 2005).

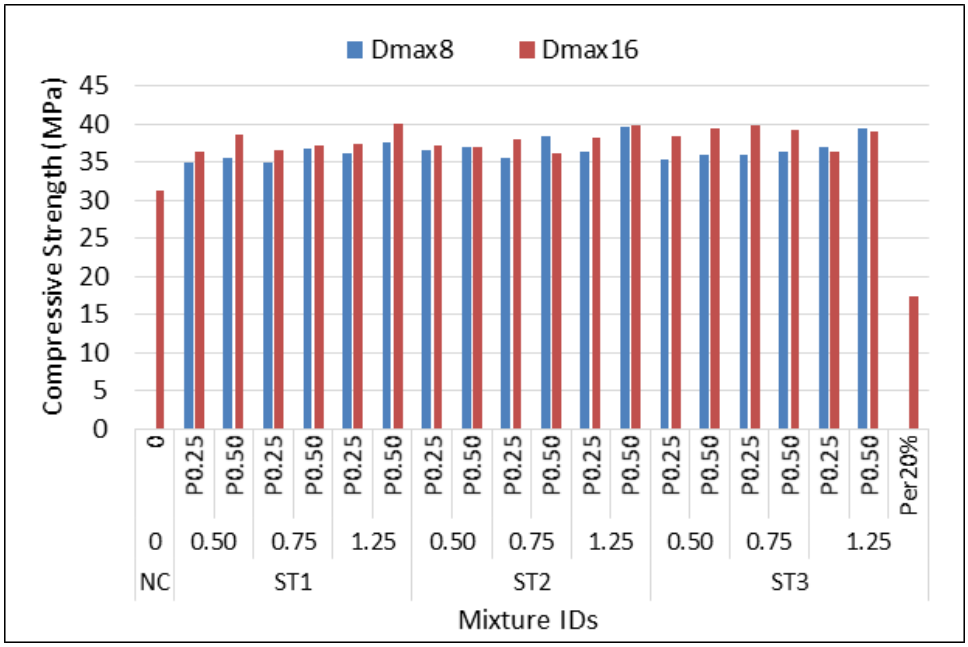

Figure 5.21. Effect of D_{max} on compressive strength of HyFRC and NC

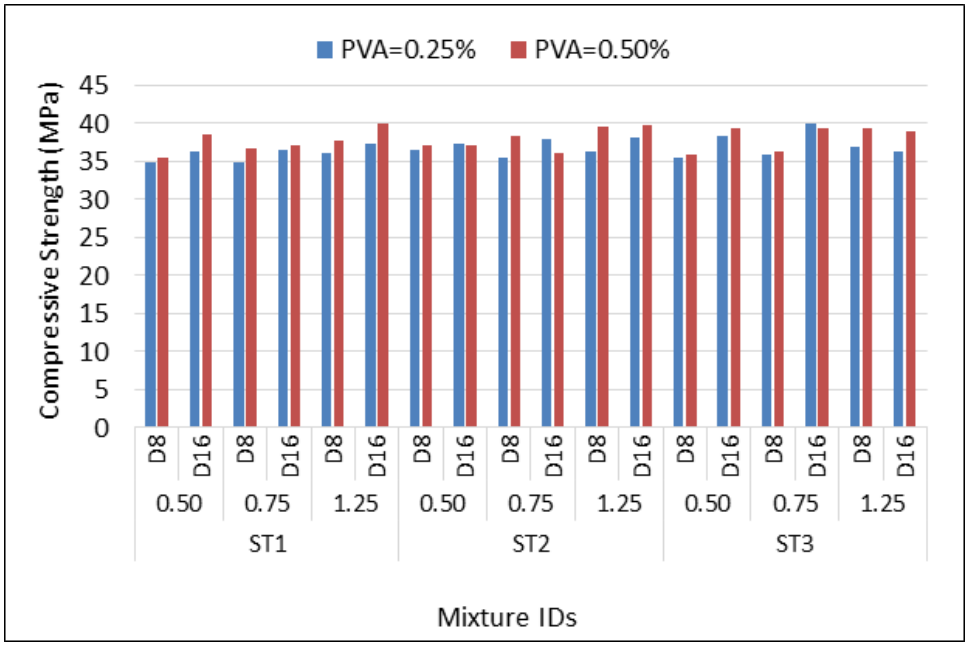

Figure 5.22. Effect of PVA and steel fiber content on compressive strength of HyFRC

After first stage of testing for HyFRC, the ST3,0.75_P0.25_D16 mixture, which exhibited the highest flexural strength and toughness, was selected for further tests (the related results and Discussions will be presented in Section5.2.3). To identify the effect of each parameter (steel fiber type, PVA usage, D_{max} and perlite usage), ST3,0.75_P0.25_D16 mixture was taken as reference and several mixtures were prepared by varying only one parameter at a time as shown in Table 5.12. The mixture without PVA became a SFRC. Table 5.12 shows compressive strength results for five selected HyFRC mixtures without perlite, a HyFRC with perlite, a SFRC mixture, and a normal concrete at 7, 28, 90 days.

Table 5.12. 7, 28 and 90-day compressive strength of selected mixtures

Mixtures	Compressive strength (**MPa**)		
	7 days	**28 days**	**90 days**
Normal Concrete	17.99	31.18	39.10
ST1,0.75_P0.25_D16	20.75	36.56	41.87
ST2,0.75_P0.25_D16	18.51	38.05	40.58
ST3,0.75_P0.25_D16	21.45	39.90	43.25
ST2,1.25_P0.25_D16	18.42	38.23	42.84
ST2,1.25_P0.25_D8	22.65	36.27	45.70
ST3,0.75_P0_D16 (SFRC)	19.80	35.10	39.30
ST3,0.75_P0.25_Per20%_D16	10.16	17.31	21.98

Figure 5.23 shows aging effect of selected mixtures. There were stable increment in the compressive strength values for all selected mixtures with continued ages. It is attributed to the influence of ongoing hydration densifying the matrix of concrete (Banyhussan et al. 2016). The mixture with 20% perlite aggregate replacement caused a significant decrease in compressive strength as compared with HyFRC mixtures without perlite. There were more than 50% decrease in compressive strength values due to perlite incorporation to selected HyFRC at all ages. It is because of the large aggregate size and lower strength of expanded perlite (Keskin et al. 2013). There were 8%, 13%, and 10% decrease in compressive strength values for SFRC mixture at 7, 28, and 90 days respectively. It was found out that addition of PVA fiber increased compressive strength of concrete.

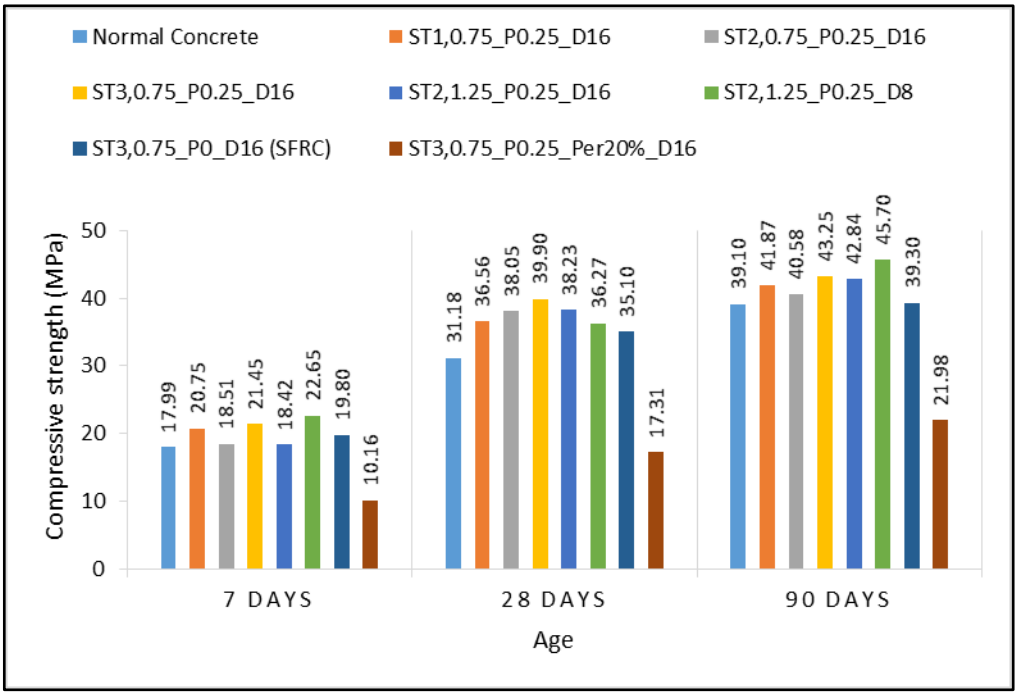

Figure 5.23. 7, 28 and 90-day compressive strength of selected mixtures

5.2.3. Static Bending Test

Two types of bending tests were applied on HyFRC which are static bending test and dynamic bending test as explained in detail in Chapter 4. Static bending test was carried out on all HyFRC mixtures but dynamic bending test was applied on some selected mixtures.

Four-point bending test were applied as static bending on all HyFRC mixtures at 28 days age. Static bending test load-deflection curves for all HyFRC mixtures at 28 days are given APPENDIX C. As seen in those figures, three line graphs are drawn for each mixture which indicate three tested specimens. Two parameters were measured from this test as flexural strength and toughness. The ultimate flexural strength is calculated from the ultimate load of these graphs as:

$$f_{max} = \frac{P_{max}\ x\ L}{bd^2}$$

Where, f_{max}= ultimate flexural strength (MPa), P_{max}= peak load (N), L= the span (mm), b = width of the specimen (mm), d= depth of the specimen (mm). Then the average values of three specimens is considered for the discussions. The toughness is

calculated as the average area under the three curves until 3 mm deflection by Euler's method. The typical load-deflection curves which demonstrate almost the average curve of three specimens for a normal concrete, a steel fiber reinforced concrete, and six selected HyFRC mixtures at 7, 28, 90 days are shown in Figures 5.24-26.

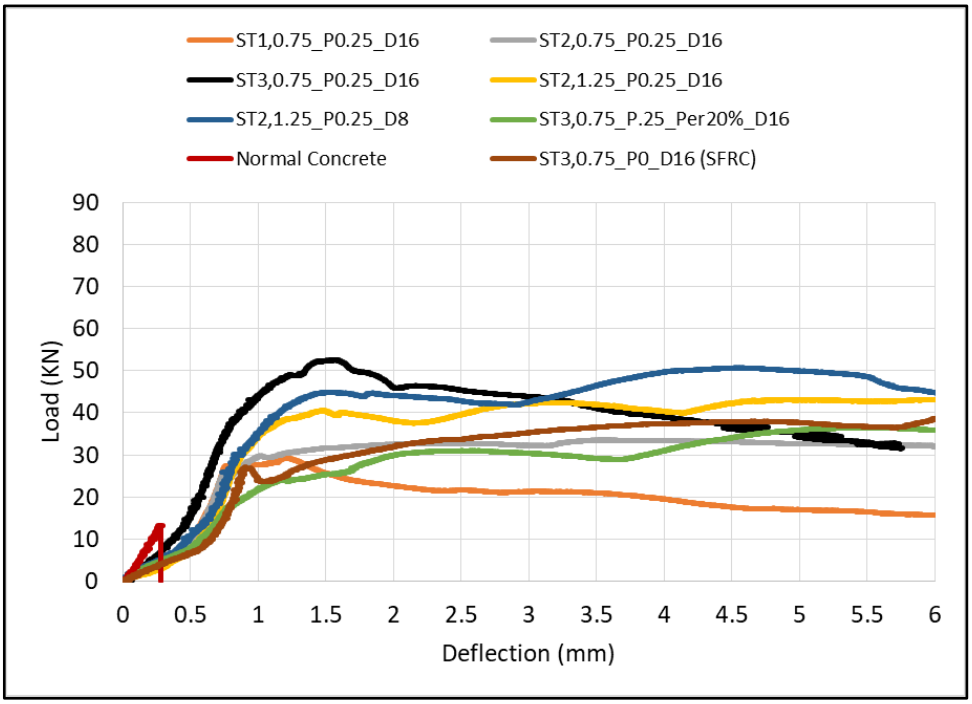

Figure 5.24. Static bending curves for selected HyFRC at 7 days

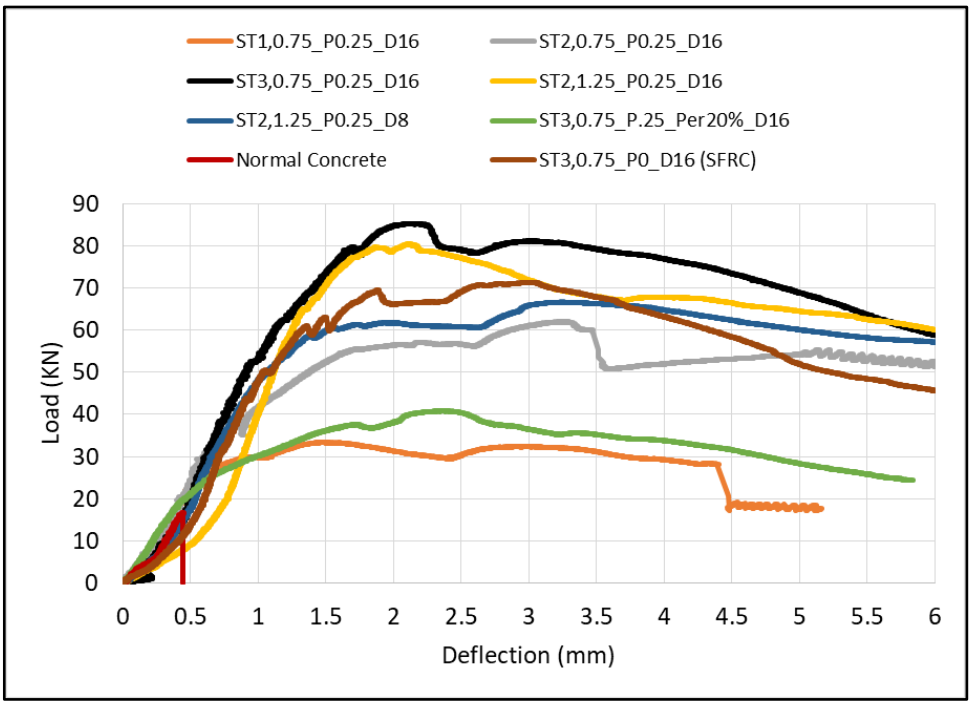

Figure 5.25. Static bending curves for selected HyFRC at 28 days

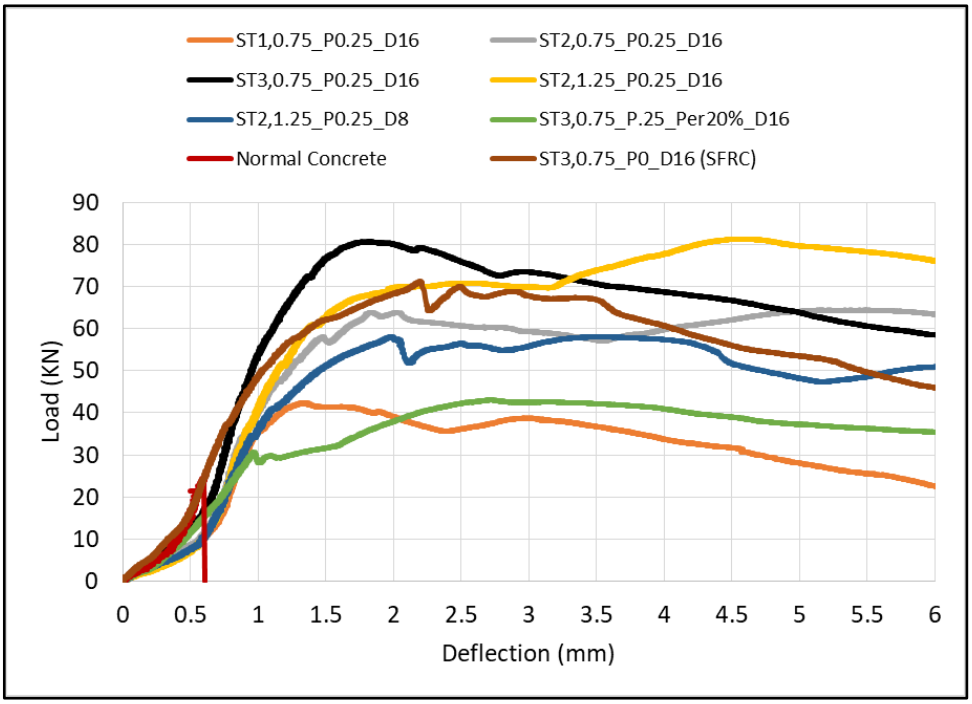

Figure 5.26. Static bending curves for selected HyFRC at 90 days

Table 5.13 shows flexural strength values for 37 HyFRC and one normal concrete mixtures at 28 days.

Table 5.13. HyFRC static bending flexural strength and toughness

Mix. No	Mix. IDs	Flexural Strength (Mpa)	Toughness (Kn.mm)Joule	Mix. No	Mix. IDs	Flexural Strength (MPa)	Toughness (Kn.mm)Joule
1	ST1,0.50_P0.25_D8	4.06	70.69	**20**	ST2,0.50_P0.25_D16	5.78	96.96
2	ST2,0.50_P0.25_D8	6.38	105.84	**21**	ST3,0.50_P0.25_D16	6.1	97.9
3	ST3,0.50_P0.25_D8	6.44	104.15	**22**	ST1,0.50_P0.50_D16	4.76	67.54
4	ST1,0.50_P0.50_D8	4.46	68.48	**23**	ST2,0.50_P0.50_D16	6.07	98.94
5	ST2,0.50_P0.50_D8	5.31	86.13	**24**	ST3,0.50_P0.50_D16	7.34	118.75
6	ST3,0.50_P0.50_D8	6.61	102.41	**25**	ST1,0.75_P0.25_D16	4.75	86.09
7	ST1,0.75_P0.25_D8	4.35	77.6	**26**	ST2,0.75_P0.25_D16	8.21	128.32
8	ST2,0.75_P0.25_D8	6.95	120.61	**27**	ST3,0.75_P0.25_D16	11.1	170.16
9	ST3,0.75_P0.25_D8	8.93	146.02	**28**	ST1,0.75_P0.50_D16	5.82	88.72
10	ST1,0.75_P0.50_D8	6.19	96.79	**29**	ST2,0.75_P0.50_D16	7.88	131.69
11	ST2,0.75_P0.50_D8	7.44	119.52	**30**	ST3,0.75_P0.50_D16	7.87	132.69
12	ST3,0.75_P0.50_D8	7.74	115.83	**31**	ST1,1.25_P0.25_D16	6.05	101.15
13	ST1,1.25_P0.25_D8	5.7	89.17	**32**	ST2,1.25_P0.25_D16	9.96	151.61
14	ST2,1.25_P0.25_D8	8.67	137.26	**33**	ST3,1.25_P0.25_D16	10.04	168.9
15	ST3,1.25_P0.25_D8	8.81	141.24	**34**	ST1,1.25_P0.50_D16	7.11	103.26
16	ST1,1.25_P0.50_D8	5.7	89.16	**35**	ST2,1.25_P0.50_D16	8.44	129.95
17	ST2,1.25_P0.50_D8	7.77	125.15	**36**	ST3,1.25_P0.50_D16	9.82	158.35
18	ST3,1.25_P0.50_D8	7.91	122.32	**37**	ST3,0.75_P0.25_Per20%_D16	5.88	93.36
19	ST1,0.50_P0.25_D16	4.31	77.98	**38**	Normal Concrete	2.09	2.58

Static bending flexural strength and toughness generally increased when aggregate Dmax increased from 8mm to 16mm (Figures 5. 27-28). These observations

can be explained by the fact that larger aggregate size shows more tortuous crack path, providing a rougher fracture surface, and cracks prefer to propagate along the weaker interfacial zone or larger pores in the matrix under loading as the crack reaches an aggregate particle where it is forced to propagate either through the aggregate or travel around the aggregate-mortar interface which increase the mechanical behavior of the matrix (Banyhussan et al. 2016).

Use of fiber hybridization resulted a significant increase of 194 up to 531% in the maximum flexural strength and 2617 up to 6595% in toughness when compares to normal plain concrete as seen in Figures 5. 27-28 due to the ability of fibers to delay and bridge crack formation that enhances the flexural behavior of concrete (Şahmaran and Yaman 2007). Hay and Ostertag (2015) stated that "A hybrid fiber-reinforced composite consisting of steel macrofibers and polyvinyl alcohol (PVA) microfibers results in a composite with a higher propensity for multiple cracking under tension" which enhance the mechanical properties of the concrete.

The mixture with 20% perlite aggregate replacement caused a significant decrease in static flexural strength of 47%, and toughness of 45% as compared with HyFRC mixtures without perlite (Figures 5. 27-28) because of the lower strength of expanded perlite and the greater local water-to-cement ratio in interfacial transition zone (Li et al. 2021).

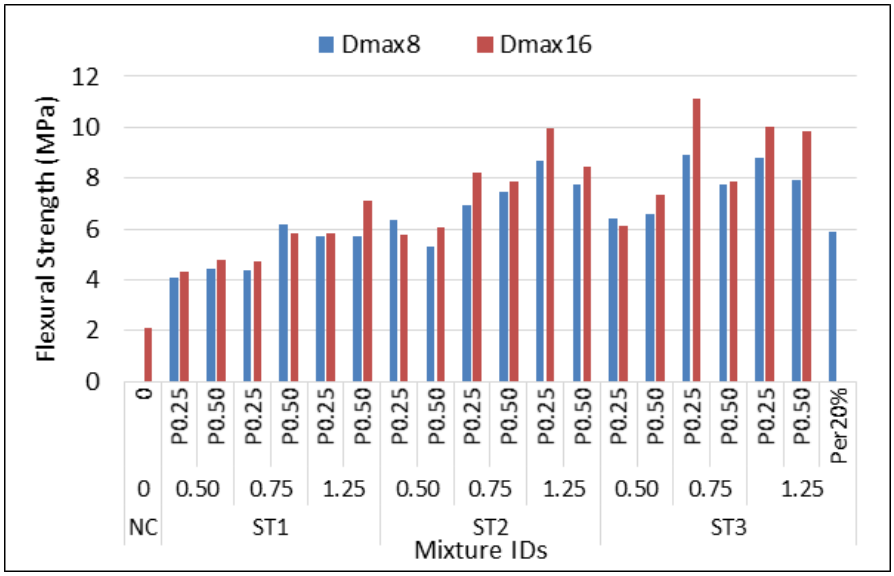

Figure 5.27. Effect of D_{max} on static flexural strength of HyFRC and NC

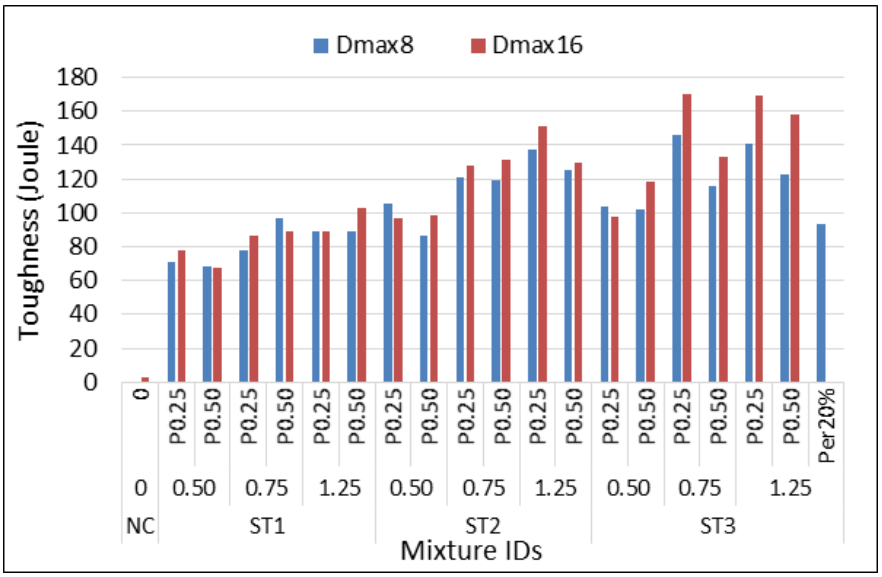

Figure 5.28. Effect of D_{max} on static flexural toughness of HyFRC and NC

Static flexural strength and toughness of HyFRC mixtures generally decreased when the PVA content increased from 0.25% to 0.50% (Figure 5.29 - 5.30). This was probably due to the significant decrease in workability of the mixture and high demand of superplasticizer which can cause bleeding and balling of fibers. On the other hand, an increasing trend was observed in flexural strength and toughness with an increase in steel fiber content. The effects of steel fiber content and type are also shown in Figures 5.29 and 5.30. The mixtures with ST2 and ST3 had considerably higher flexural strength and toughness when compared to the mixtures with ST1 probably due to the longer length and higher aspect ratio of both ST2 and ST3 providing greater interfacial bond strength by larger contact area between the fiber and matrix (Yang 2011). The length and aspect ratio of ST2 and ST3 were the same but ST3 results were higher than those of ST2 due an extra hook in ST3 type (5D) which was not present in ST2 type (3D). Moreover, tensile strength of ST3 type fiber was significantly higher than ST1 and ST2 (Tensile strength of ST1, ST2 and ST3 are 1225 MPa, 1160 MPa and 2300 MPa, respectively.)

.

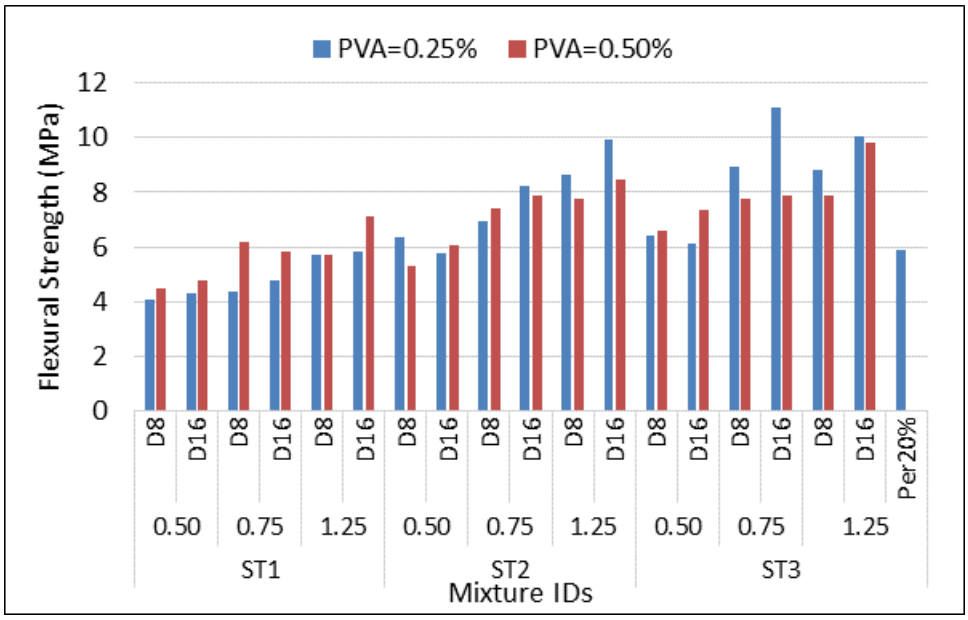

Figure 5.29. Effect of PVA content on static bending flexural strength of HyFRC

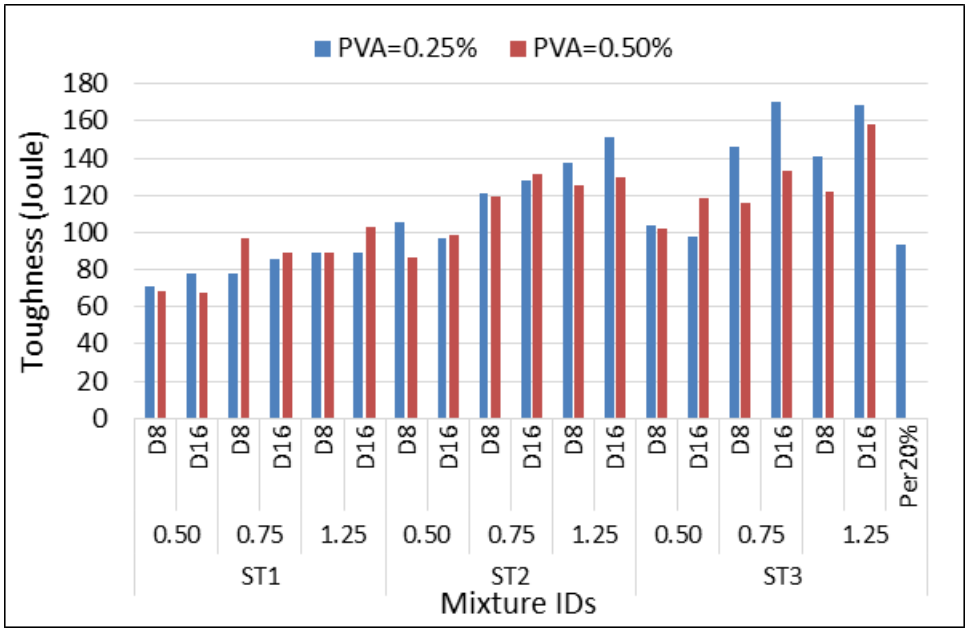

Figure 5.30. Effect of PVA content on static bending toughness of HyFRC

As explained in the previous section, ST3,0.75_P0.25_D16 mixture was selected as reference and several mixtures were produced by changing the mix-design parameters to identify their effects. Table 5.14 shows static flexural strength and toughness values for five selected HyFRC, a normal plain concrete, a mixture with perlite content, and one steel fiber reinforced concrete (SFRC) mixtures at 7, 28, and 90 days.

Table 5.14. 7, 28 and 90-day flexure strength and toughness of selected mixtures

Mixtures	Flexural strength (**MPa**)			Toughness (**Joule**)		
	7 days	**28 days**	**90 days**	**7 days**	**28 days**	**90 days**
Normal Concrete	2.09	2.88	2.75	2.58	4.32	4.47
ST1,0.75_P0.25_D16	3.67	4.75	5.97	58.55	86.09	94.05
ST2,0.75_P0.25_D16	4.53	8.21	9.15	74.96	128.32	135.13
ST3,0.75_P0.25_D16	6.11	11.10	10.66	97.90	170.16	165.92
ST2,1.25_P0.25_D16	5.81	9.96	10.11	91.74	151.61	148.75
ST2,1.25_P0.25_D8	6.48	8.67	7.64	102.42	137.26	118.87
ST3,0.75_P0_D16 (SFRC)	6.32	9.11	10.08	80.14	134.70	141.48
ST3,0.75_P0.25_Per20%_D16	4.31	5.88	4.97	59.13	93.36	86.77

Figure 5.31-32 shows aging effect of five selected HyFRC mixtures, a plain concrete, a mixture with perlite concrete, and an SFRC mixture. There were significant increment in the static bending flexural strength and toughness values from 7 days age to 28 days age for all selected mixtures due to ongoing hydration that densify the matrix of the concretes (Banyhussan et al. 2016). There were small or no increment in the flexural strength and toughness values from 28 days age to 90 days due to dry curing. Recall that all specimens were stored in isolated plastic bags for 7 days followed by dry curing at laboratory condition.

The mixture with 20% perlite aggregate replacement caused a significant decrease in static flexural strength (29%, 47%, and 53% decrement at 7, 28, and 90 days respectively) and toughness (40%, 45%, and 48% decrement at 7, 28, and 90 days respectively) as compared with same HyFRC mixture without perlite at all ages.

The SFRC mixture has not caused significant decrement in static bending flexural at 7 days age but 18%, and 5% decrement was caused at 28, and 90 days age respectively. Also there were 18%, 21%, and 15% decrement in static bending toughness at 7, 28, 90 days. It was found that addition of PVA fiber increases static flexural strength and toughness of HyFRC. Figures 5.32-34 show the typical load-deflection curves for a normal plain concrete, the selected HyFRC (ST3,0.75_P0.25_D16), the same HyFRC mixture without PVA as SFRC, and the same HyFRC mixture with perlite at 7, 28, and 90 days.

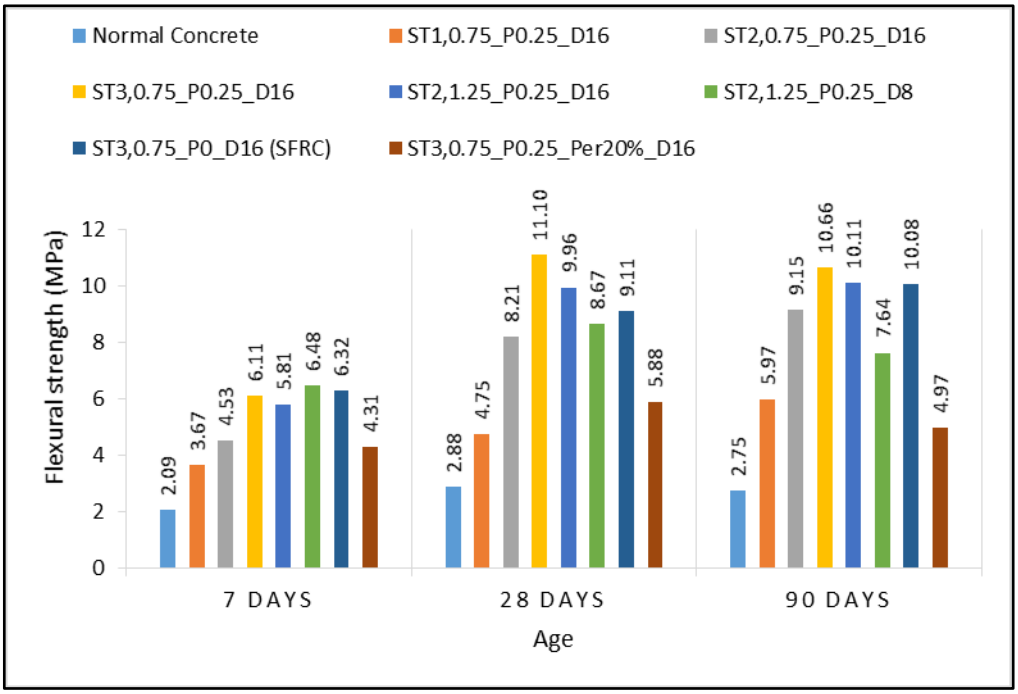

Figure 5.31. 7, 28 and 90 days static bending flexural strength of selected mixtures

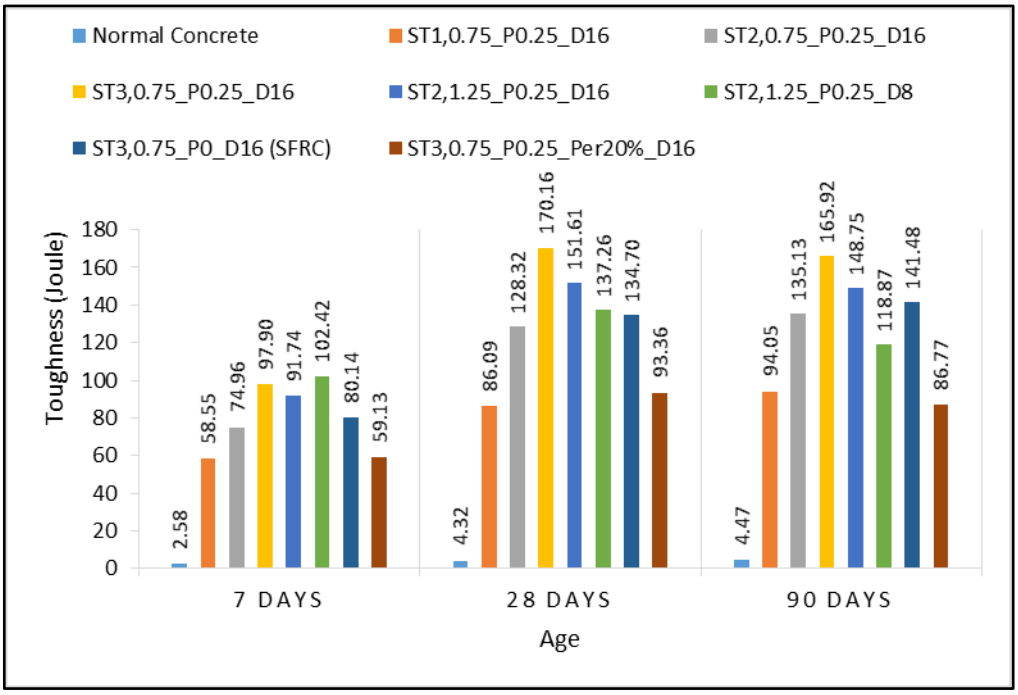

Figure 5.31. 7, 28 and 90 days static bending toughness of selected mixtures

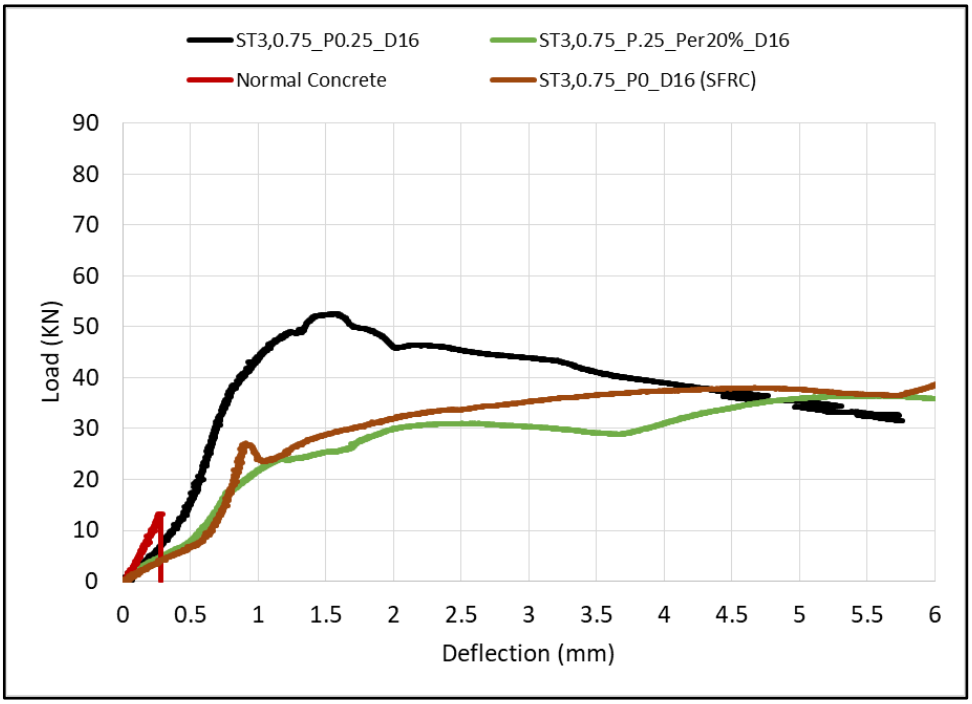

Figure 5.32. Static bending curves for NC, HyFRC, SFRC, Per20% at 7 days

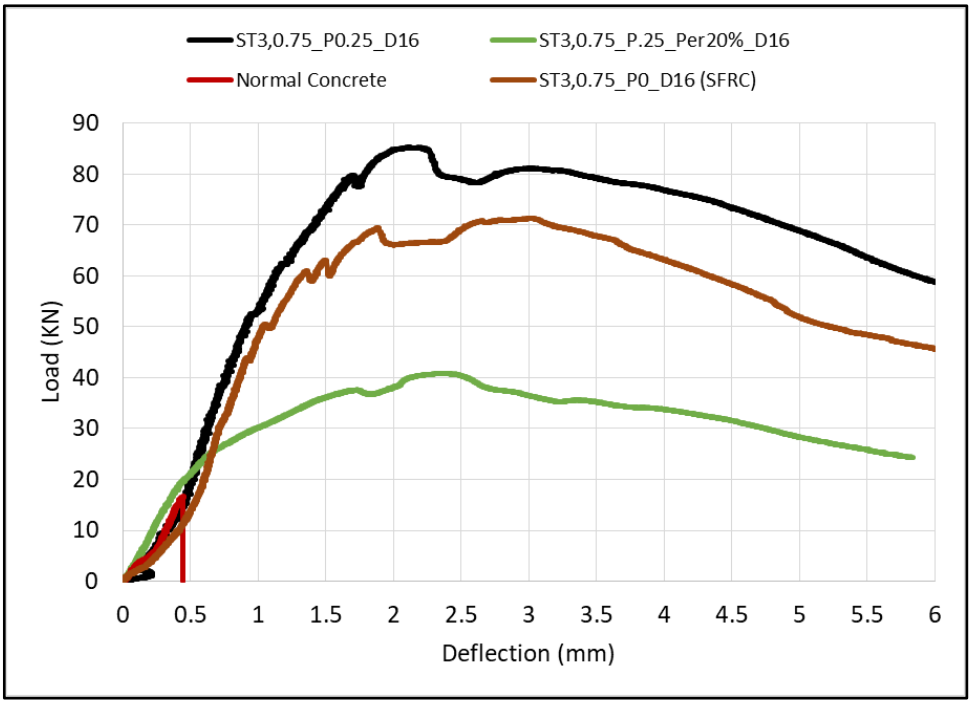

Figure 5.33. Static bending curves for NC, HyFRC, SFRC, Per20% at 28 days

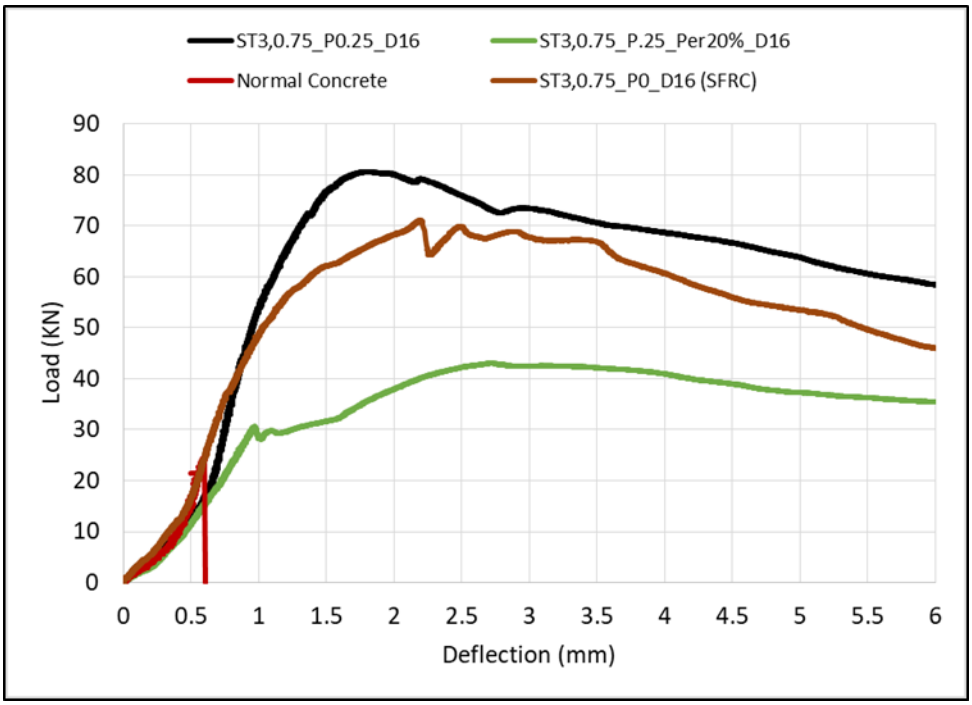

Figure 5.34. Static bending curves for NC, HyFRC, SFRC, Per20% at 90 days

5.2.4. Dynamic Bending Test

Impact loading test was made by a drop-weight test machine as discussed in Chapter 4. This test was applied as dynamic bending test on the selected HyFRC mixtures at 28 days age. Dynamic bending test load-deflection curves for five selected HyFRC mixtures, a HyFRC mixture with perlite, and a SFRC mixture at 28 days are given in APPENDIX J. As seen in those figures, three line graphs belonging to each of the three specimens are drawn for each mixture. The ultimate flexural strength is calculated from the ultimate load of these graphs as:

$$f_{max} = \frac{3\ x\ P_{max}\ x\ L}{2bd^2}$$

Where, f_{max}= ultimate flexural strength (MPa), P_{max}= peak load (N), L= the span (mm), b = width of the specimen (mm), d= depth of the specimen (mm). Then the average values of three specimens is calculated. The toughness is calculated as the average area under the three curves until 3 mm deflection by Euler's method. The typical load-deflection curves which show almost the average curve of three specimens

for a steel fiber reinforced concrete, and five selected HyFRC mixtures, and a HyFRC with perlite content at 28 days are shown in Figures 5.35.

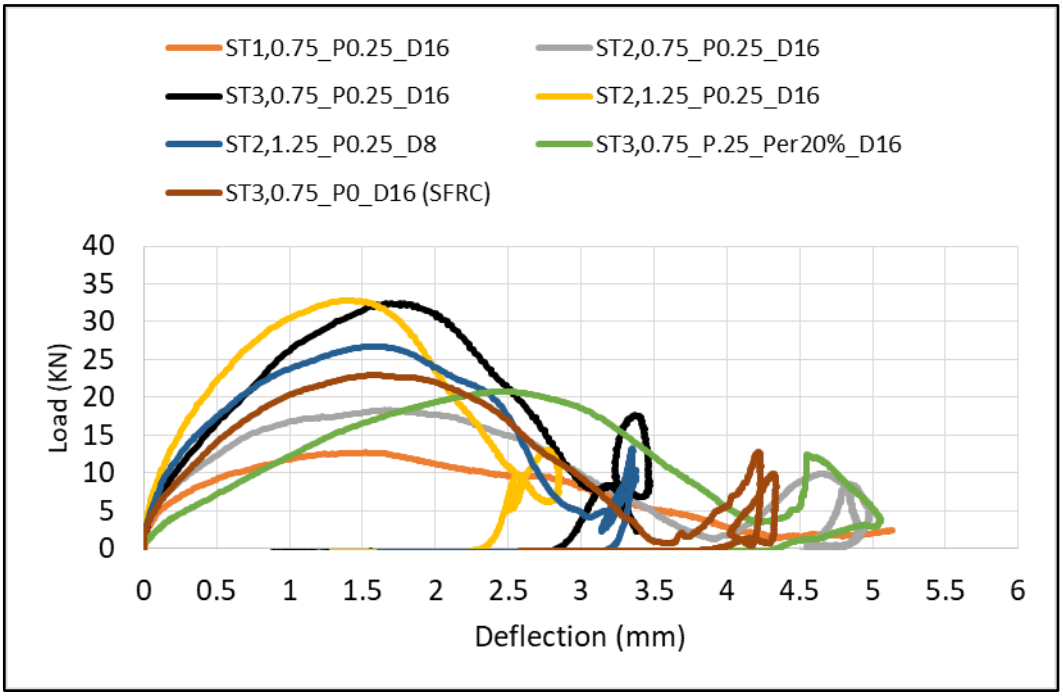

Figure 5.35. Dynamic bending curves for selected HyFRC, SFRC, Per20% at 28 days

The ST3,0.75_P0.25_D16 mixture, which exhibited the highest static flexural strength and toughness, was selected for the investigation under low-velocity impact loading. To see the effect of steel fiber types for impact loading, the same mixture with three types of steel fibers were selected. The same mixture without PVA content as steel fiber reinforced concrete and with perlite content also tested under impact loading. To see the effect of steel fiber content and D_{max}, two more mixtures were also selected as (ST2,1.25_P0.25_D16 and ST2,1.25_P0.25_D8). Totally, seven mixtures were tested under impact loading. Table 5.15 shows dynamic bending flexural strength and toughness values for these seven mixtures at 28 days.

Table 5.15. Dynamic flexural strength and toughness values of selected mixtures at 28 days

Mixture IDs	Flexural strength (MPa)	Toughness (Joule)
ST1,0.75_P0.25_D16	18.30	31.16
ST2,0.75_P0.25_D16	25.81	45.20
ST3,0.75_P0.25_D16	39.49	62.00
ST2,1.25_P0.25_D16	44.46	63.15
ST2,1.25_P0.25_D8	37.12	57.49
ST3,0.75_P0_D16 (SFRC)	33.70	53.38
ST3,0.75_P0.25_Per20%_D16	27.94	43.50

Figure 5.36-37 present dynamic flexural strength and toughness values for 7 selected mixtures under impact loading test. Results indicate that the mixture (ST2,1.25_P0.25_D16) with higher content of steel fiber exhibited the highest dynamic flexural strength and toughness of 44.46 MPa and 63.15 Joule respectively. The mixture with the best performance from static bending test (ST3,0.75_P0.25_D16) showed the second highest dynamic flexural strength and toughness of 39.49 MPa and 62 Joule respectively. This decrement is not a lot while comparing with the steel fiber volume fraction increment from 0.75% to1.25%. Therefore, the (ST3,0.75_P0.25_D16) mixture is more economical and adequate to select for real size concrete barriers dynamic test.

Figures 5.36-37 show that for the mixtures with ST2 and ST3, dynamic flexural strength and toughness were higher than those with ST1, due to their longer length and higher aspect ratio. Results also indicate that ST3 dynamic flexural strength and toughness were higher than ST2 due to an extra hook in ST3 type (5D) which was not present in ST2 type (3D).

Similar to static bending test results, dynamic flexural strength and toughness increased when aggregate D_{max} increased from 8mm to 16mm (Figures 5.36-37). The reason can be explained by the fact that larger aggregate size shows more tortuous crack path, providing a rougher fracture surface, and cracks prefer to propagate along the weaker interfacial zone or larger pores in the matrix under loading as the crack reaches an aggregate particle where it is forced to propagate either through the aggregate or travel around the aggregate-mortar interface which increase the mechanical behavior of the matrix (Banyhussan et al. 2016).

Dynamic flexural strength and toughness significantly decreases with replacement of 20% of fine aggregate with expanded perlite. Adding perlite decreased the dynamic flexural strength and toughness by 29.25% and 29.83%, respectively, as compared with same HyFRC mixture without perlite content.

In the case of SFRC (ST3,0.75_P0_D16), dynamic flexural strength and toughness decreased by 14.66% and 13.90%, respectively. In other words, addition of PVA fiber increased dynamic flexural strength and toughness. The typical load-deflection curves under impact loading for a HyFRC, a SFRC, and the HyFRC mixture with 20% perlite content at 28 days age given in Figure 5.38.

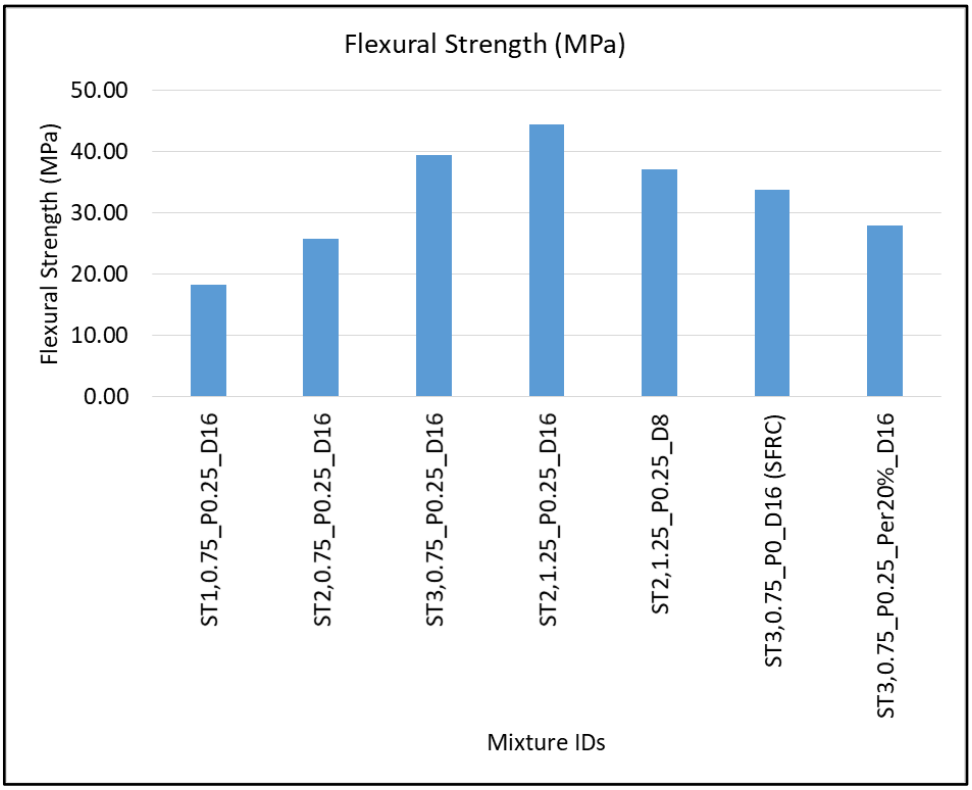

Figure 5.36. Dynamic flexural strength values for selected mixtures at 28 days

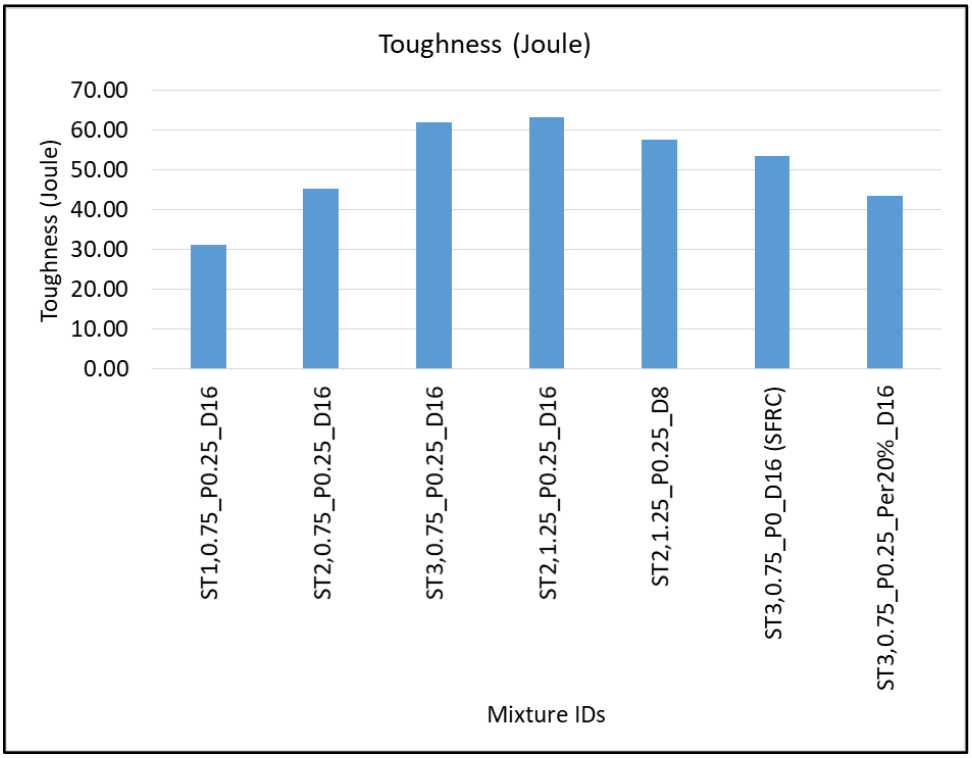

Figure 5.37. Dynamic toughness values for selected mixtures at 28 days

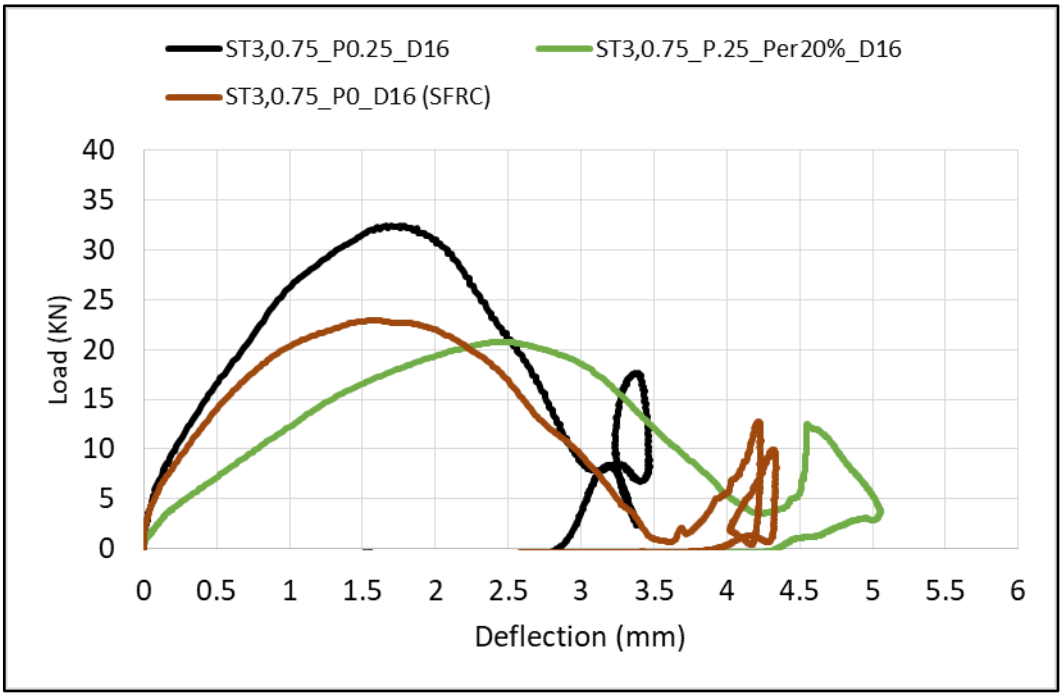

Figure 5.38. Dynamic bending curves for HyFRC, SFRC, and Per20% at 28 days

5.2.5. Comparison of Static and Dynamic Bending Tests Results

At the first stage of the testing program the specimens for static four-point bending test were cast in standard prismatic size of 600 x 150 x 150 mm. However, at the second stage of the testing program, due to the drop-weight test setup size limitation, smaller specimens with 600 x 100 x 100 mm dimensions were tested for the dynamic bending tests. Moreover, dynamic testing specimens were notched specimens with 30 mm notch depth and three-point bending was applied. Therefore, to compare static bending and dynamic bending tests result the 600 x 100 x 100 mm notched specimens with 30 mm notch depth were also cast and tested under static bending test with three-point loading for the seven selected mixtures. The typical load-deflection curves of this size specimens at 28 days are shown in Figures 5.39. Table 5.16 shows flexural strength and toughness values of static bending test and dynamic bending test for five selected HyFRC, a mixture with perlite content, and one steel fiber reinforced concrete (SFRC) mixtures at 28 days.

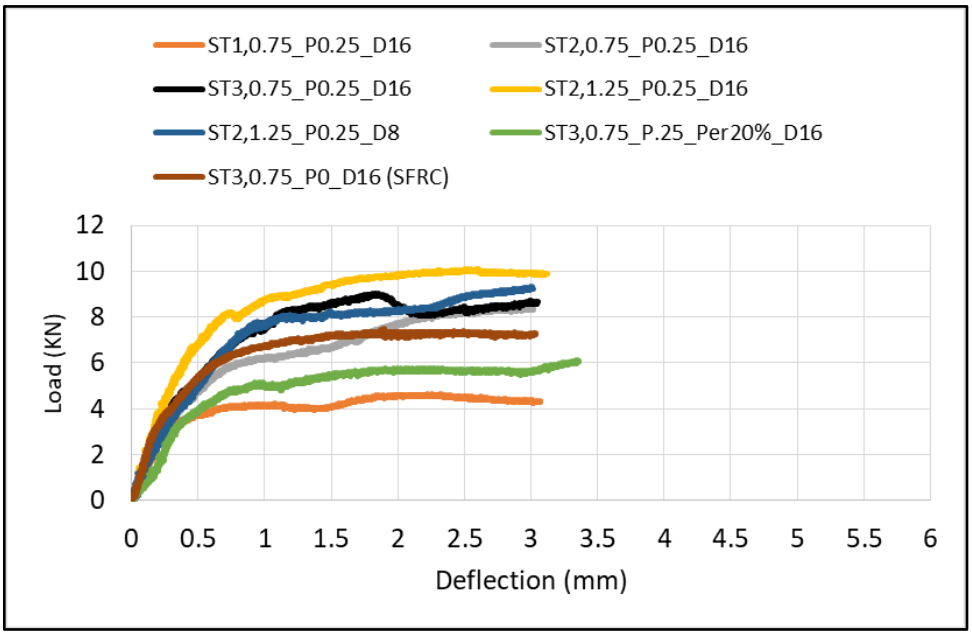

Figure 5.39. Static bending curves for HyFRC, SFRC, and Per20% at 28 days

Table 5.16. Static and dynamic flexure strength and toughness of selected mixtures

Mixture IDs	Flexural strength (MPa)		Toughness (Joule)	
	Static Bending	Dynamic Bending	Static Bending	Dynamic Bending
ST1,0.75_P0.25_D16	6.31	18.30	11.65	31.16
ST2,0.75_P0.25_D16	11.28	25.81	18.93	45.20
ST3,0.75_P0.25_D16	12.14	39.49	21.07	62.00
ST2,1.25_P0.25_D16	13.50	44.46	24.42	63.15
ST2,1.25_P0.25_D8	12.90	37.12	21.45	57.49
ST3,0.75_P0_D16 (SFRC)	10.87	33.70	19.21	53.38
ST3,0.75_P0.25_Per20%_D16	7.90	27.94	13.79	43.50

Table 5.17. Dynamic increase factors of selected mixtures

Mixture IDs	Dynamic Increase Factor	
	Flexural strength	Toughness
ST1,0.75_P0.25_D16	2.90	2.67
ST2,0.75_P0.25_D16	2.29	2.39
ST3,0.75_P0.25_D16	3.25	2.94
ST2,1.25_P0.25_D16	3.29	2.59
ST2,1.25_P0.25_D8	2.88	2.68
ST3,0.75_P0_D16 (SFRC)	3.10	2.78
ST3,0.75_P0.25_Per20%_D16	3.54	3.15

Figure 5.41 and Figure 5.42 compare flexural strength and toughness values of static and dynamic bending tests, respectively. Results confirm that the dynamic increase factor (ratio of dynamic to static test results) for flexural strength ranges between 2.29 and 3.54, and the dynamic increase factor for toughness is between 2.30 and 3.15 as given in Table 5.17. The mixture with perlite (ST3,0.75_P0.25_Per20%_D16) shows the highest dynamic increase factor for both flexural strength (3.54) and toughness (3.15), respectively.

Effects of steel fiber type on flexural strength and toughness values agree with each other in static and impact bending tests. As ST2 and ST3 static and dynamic bending flexural strength and toughness were higher than ST1, due to their longer length and larger aspect ratio. Results also indicate that ST3 static and dynamic bending flexural strength and toughness were higher than ST2 due to an extra hook in ST3 type (5D) which was not present in ST2 type (3D). Results also indicate that flexural strength

and toughness increase as steel fiber content increase for both static bending and dynamic bending tests.

The effects of D_{max} on flexural strength in toughness are same in static and dynamic bending tests. The flexural strength and toughness for both static and dynamic bending tests decrease as the coarse aggregate D_{max} decreases from 16mm to 8mm. The flexural strength decreases about 4.44% and 16.5% for static bending and dynamic bending, respectively. Also the toughness decreases about 13.71% and 9% for static bending and dynamic bending, respectively.

In the case of SFRC, where PVA is not used, the flexural strength and toughness decrease in both static bending and dynamic bending tests. The flexural strength decreases about 10.46% and 14.46% for static bending and dynamic bending, respectively. Toughness decreases about 8.8% and 13.9% for static bending and dynamic bending, respectively.

As explained previously, two different specimen sizes were used in static bending test. In the first stage, specimen size was 600 x 150 x 150 mm, and in the second stage 600 x 100 x 100 mm notched specimens with 30 mm notch depth were used. The only difference of specimen size effect on the selected seven mixtures is that in the first stage with larger specimens the ST3,0.75_P0.25_D16 mixture showed the highest flexural strength and toughness in static bending, on the other hand, in the second stage with smaller notched specimen the ST2,1.25_P0.25_D16 mixture exhibited the highest flexural strength and toughness in static bending which is in agreement with the results of the dynamic bending test.

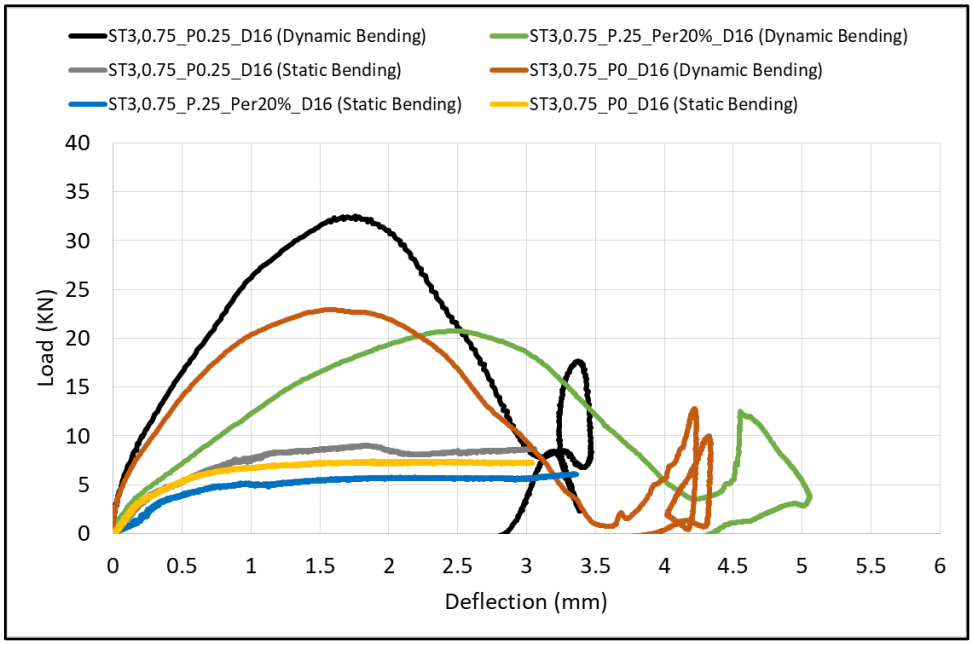

Figure 5.40. Comparing static and dynamic bending tests load-deflection curves

Adding perlite significantly decreased the flexural strength and toughness for both static bending and dynamic bending. The flexural strength decreased about 34.92% and 29.24% for static bending and dynamic bending, respectively. Also toughness decreased about 34.55% and 29.83% for static bending and dynamic bending respectively. In addition, the dynamic increase factor for flexural strength and toughness is the highest for the mixture with perlite. In other words, the perlite usage enhanced the energy absorption of concrete under impact loading relative to static loading. Figure 5.40 compares load-deflection curves of static bending and dynamic bending tests for a HyFRC mixture, a SFRC mixture, and a HyFRC mixture with perlite.

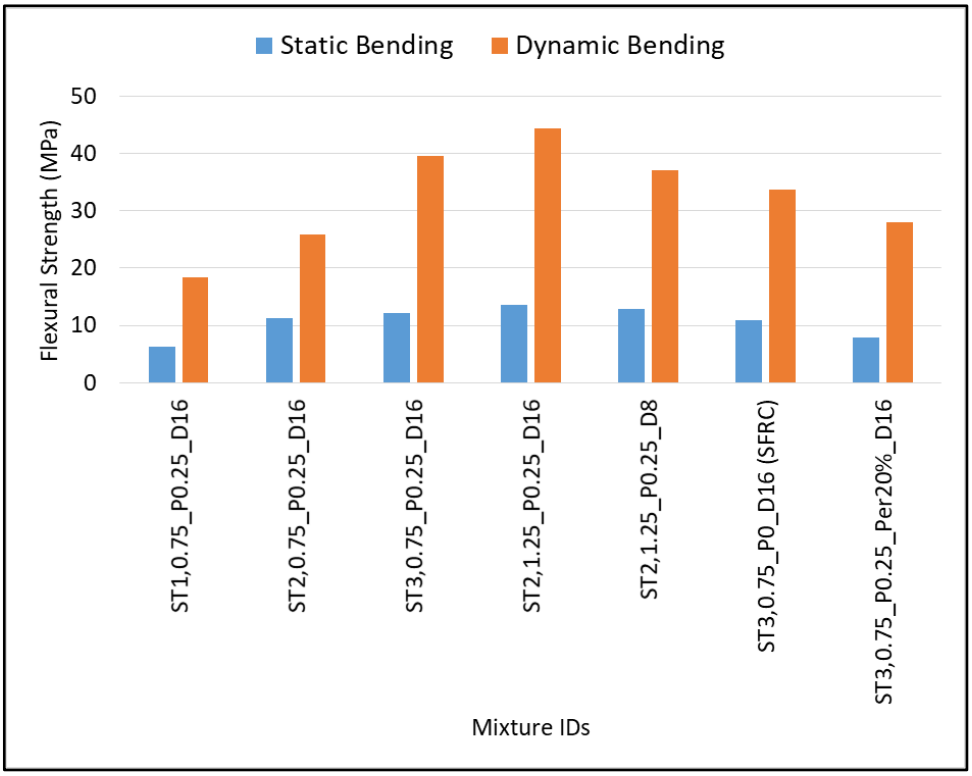

Figure 5.41. Comparison of static and dynamic flexural strengths

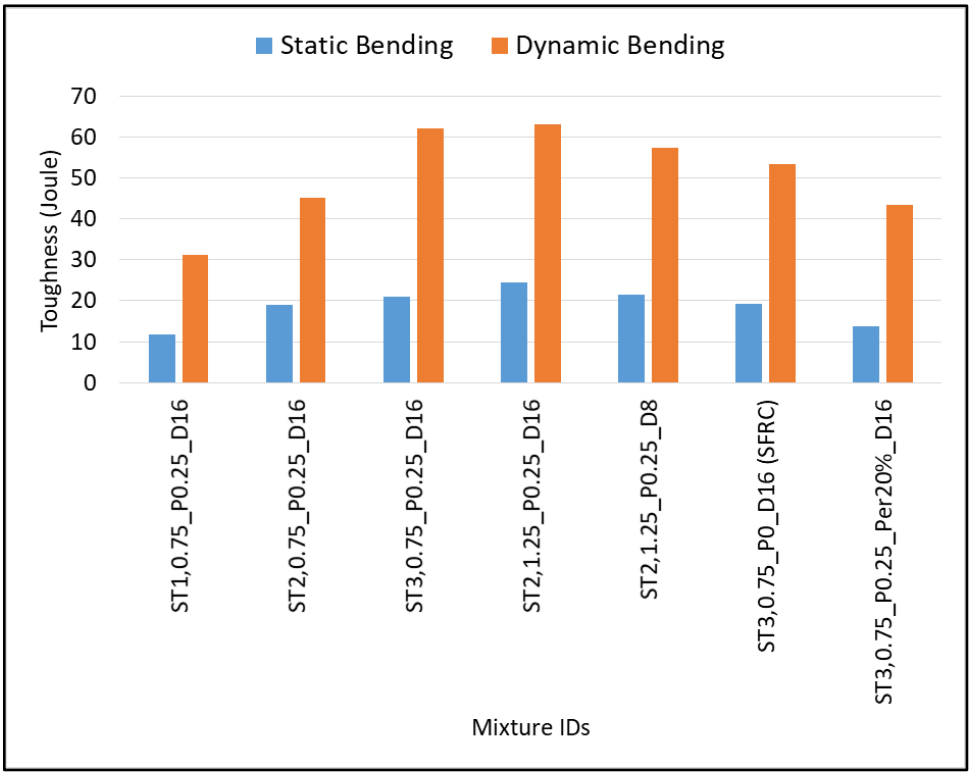

Figure 5.42. Comparison of static and dynamic flexural toughness

5.2.6. Freezing and Thawing (F-T) Test

Table 5.18 shows weight and ultrasonic pulse velocity (UPV) loss after 300 cycles of freezing and thawing for five selected HyFRC without perlite, a normal plain concrete, a HyFRC with perlite, and one SFRC mixture at 28 days.

Table 5.18. Weight and ultrasonic pulse velocity (UPV) loss after 300 cycles

Mixture IDs	Weight Loss After 300 Cycles (%)	UPV Loss After 300 Cycles (%)
Normal Concrete	2.69	28.40
ST1,0.75_P0.25_D16	0.94	6.58
ST2,0.75_P0.25_D16	1.43	8.45
ST3,0.75_P0.25_D16	1.15	9.02
ST2,1.25_P0.25_D16	1.04	11.15
ST2,1.25_P0.25_D8	1.12	10.84
ST3,0.75_P0_D16 (SFRC)	2.34	24.56
ST3,0.75_P0.25_Per20%_D16	–	20.12

Weight loss after 300 cycles are shown in Figure 5.43. Results shows that the normal plain concrete exhibits the highest weight loss after 300 cycles. HyFRC results were close to each other. The ST1,0.75_P0.25_D16 mixture, which contains ST1 type steel fiber, showed the lowest weight loss. As can be recalled, ST1 steel fiber has the shortest length and the lowest aspect ratio. When this mixture is compared with the one having same volume fraction of steel and PVA fibers, this mixture has higher numbers of steel fibers to be distributed to the matrix. This can be the reason for reduced cracking and lower weight loss of the ST1,0.75_P0.25_D16 mixture.

In case of SFRC mixture without PVA, weight loss significantly increased. It means that adding PVA fibers enhanced the freezing and thawing resistance. This improvement in freeze-thaw resistance due to PVA fiber addition is explained as follows: It is known that when water freezes its volume increases by 9%. When the water in small pores of the concrete freezes, the ice expands and cause tensile stress in the concrete. However, randomly distributed PVA fibers in concrete mixture restrains the effects of this expansion and reduces the freeze-thaw damage to concrete.

The weight of the specimens containing perlite aggregate increased during freeze and thawing test. As stated previously, all specimens were stored in isolated plastic bags for 7 days and then at laboratory conditions until 28 days. Therefore, the specimens were partially dried before preparing the specimens to F-T cycles. Before

freeze and thaw cycles all the specimens were put in water for 24 hours to make them saturated. However, the results indicate that the mixture with perlite had not been fully saturated in 24 hours so this mixture absorbed water during the freeze and thaw test, leading to increase in its weight.

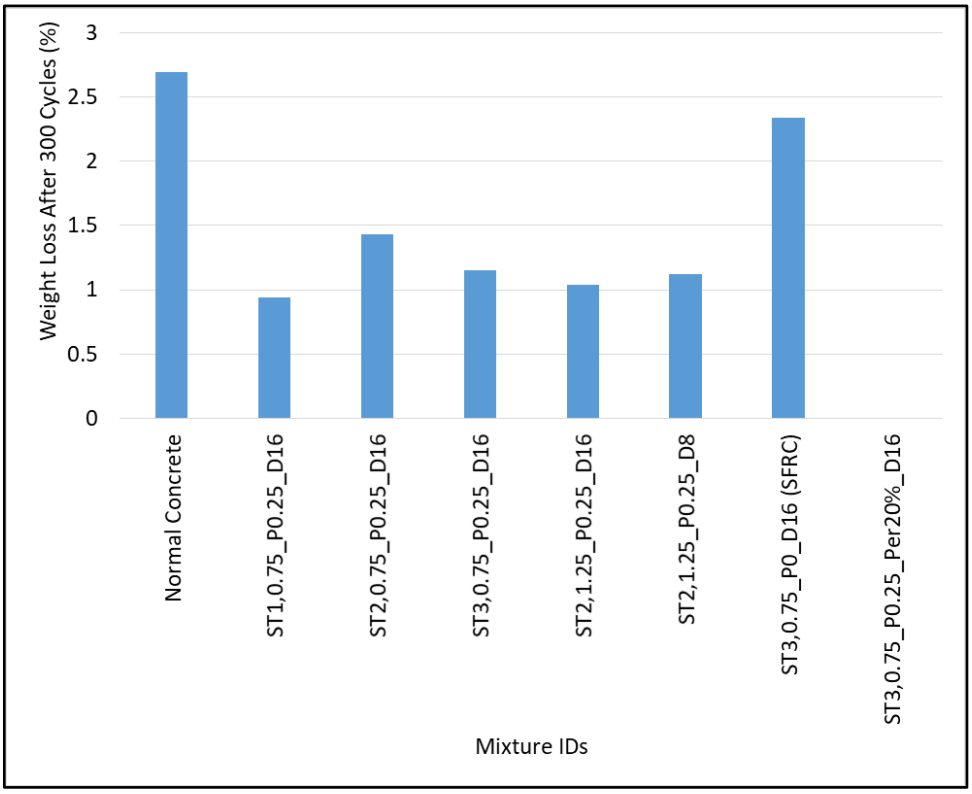

Figure 5.43. F-T test specimens weight loss percentage

The ultrasonic pulse velocity waves are faster when passing through solids. Cracks in the concrete reduce the rate of UPV. For all concrete mixtures, UPV decreased at the end of the F-T cycles. Figure 5.44 shows the UPV loss percentage after 300 cycles. Results indicate that the normal concrete shows the highest UPV loss after 300 cycles. As seen in figure, fibrous concretes performed significantly better performance than fiber-free concrete and SFRC. The weight loss of specimens is related to the surface destroying, and the UPV loss is depended on internal changes of the specimens. Internal degradation in normal plain concrete is much greater than fibrous concrete which causes higher UPV loss. In the case of HyFRC concrete, the UPV loss values are close to each other for all HyFRC mixtures. It is due to the fact that PVA fiber content was the same in all HyFRC mixtures.

Figure 5.44 also shows the results of SFRC without PVA and the mixture with perlite. Results show that the UPV loss increased in SFRC and in mixture with perlite. The UPV loss in SFRC mixture is close to the result of normal plain concrete, indicating that the PVA content reduce internal microcracking of concrete which reduce UPV loss. The perlite replacement significantly increased the UPV loss in HyFRC mixture, it is because of the porous nature of perlite aggregate and the occurring of internal cracks due to freezing of water in weak perlite aggregates. Figure 5.45 shows photos of all tested mixtures after 300 freezing and thawing cycles. Photos indicate that the surface destroying of normal concrete and SFRC mixture is higher, which is due to the absence of PVA content.

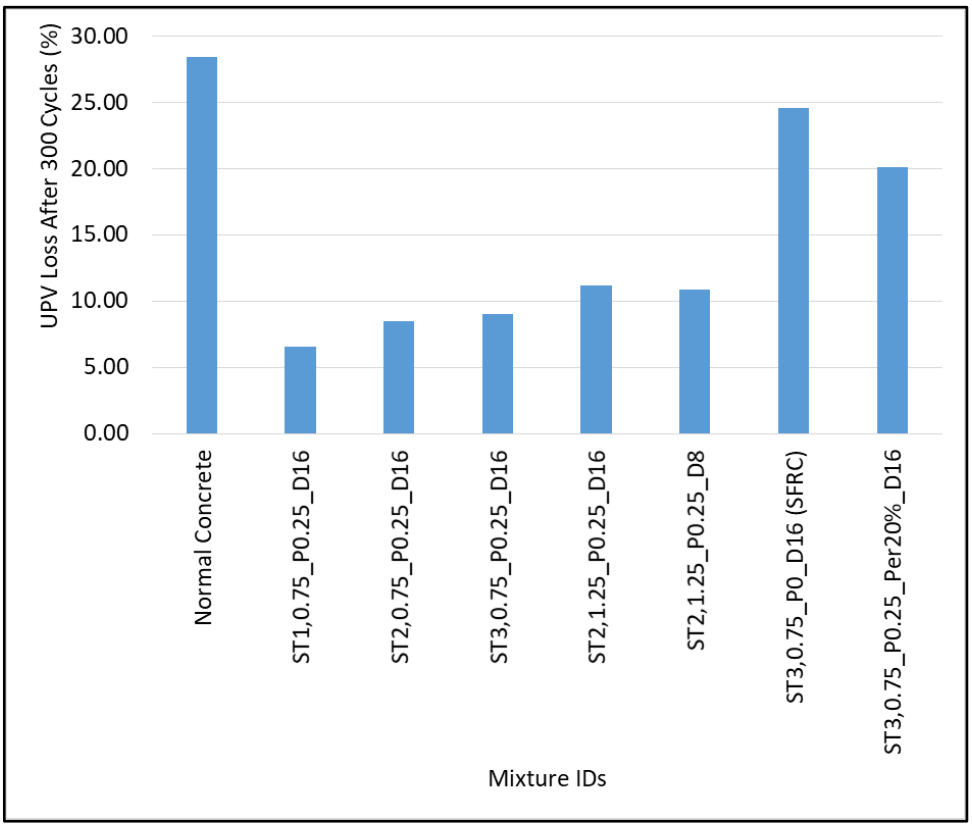

Figure 5.44. F-T test specimens UPV loss percentage

(Normal Concrete)

(ST1,0.75_P0.25_D16)

(ST2,0.75_P0.25_D16)

(ST3,0.75_P0.25_D16)

(ST2,1.25_P0.25_D16)

(ST2,1.25_P0.25_D8)

(ST3,0.75_P0_D16)

(ST3,0.75_P0.25_Per20%_D16)

Figure 5.45. All tested specimens after 300 freeze-thaw cycles

5.2.7. Rapid Chloride Permeability Test (RCPT)

RCPT test evaluate the amount of electrical current passed through of one side to another side of concrete specimens. Passing of charge depends on both the pore structure characteristics and pore solution chemistry of concrete.

Table 5.19 shows charge passing classification according ASTM C 1202 standards. Figure 5.46 and Table 5.20 shows passing charge values after six hours of RCPT for five selected HyFRC, a normal plain concrete, a mixture with perlite, and one SFRC mixture at 28 days.

Table 5.19. ASTM C 1202 Charge Passed Classification

Charge Passed (Coulombs)	Chloride Ion Penetrability
>4,000	High
2,000-4,000	Moderate
1,000-2,000	Low
100-1,000	Very Low
<100	Negligible

Table 5.20. RCPT test results of selected mixtures

Mixture IDs	Charge Passed After 6 Hours (Coulombs)	Chloride Ion Penetrability
Normal Concrete	352	Very Low
ST1,0.75_P0.25_D16	1949	Low
ST2,0.75_P0.25_D16	1988	Low
ST3,0.75_P0.25_D16	1749	Low
ST2,1.25_P0.25_D16	2786	Moderate
ST2,1.25_P0.25_D8	2154	Moderate
ST3,0.75_P0_D16 (SFRC)	3203	Moderate
ST3,0.75_P0.25_Per20%_D16	2582	Moderate

Results indicate that the normal concrete shows the very low charge passed value. There is a big difference between fiber reinforced and plain concrete results. However, this result does not agree with mechanical tests (compressive and bending) and F-T test. The higher current passing of fiber reinforced concrete than normal concrete is due to the presence of metals (steel fibers) which promotes the passing of electrical current.

In the case of HyFRC, the mixtures with higher content of steel fiber show higher chloride ion penetrability due to higher amount of metal in the mixture. Moreover, steel fiber reinforced concrete mixture exhibits the highest charge value. Therefore, RCPT method of durability test was not found suitable for steel fiber reinforced concrete.

The reference mixture (ST3,0.75_P0.25_D16) show the lowest chloride ion penetrability among HyFRC mixtures, indicating better consolidation of this mixture in the casting process because of proper combination of PVA and steel fibers volume fraction. The charge passed through the perlite incorporated mixture was 47.6% higher when compared to the same mixture without perlite. This increase can be explained by the porous structure of perlite, which provides more pores for passing the charges.

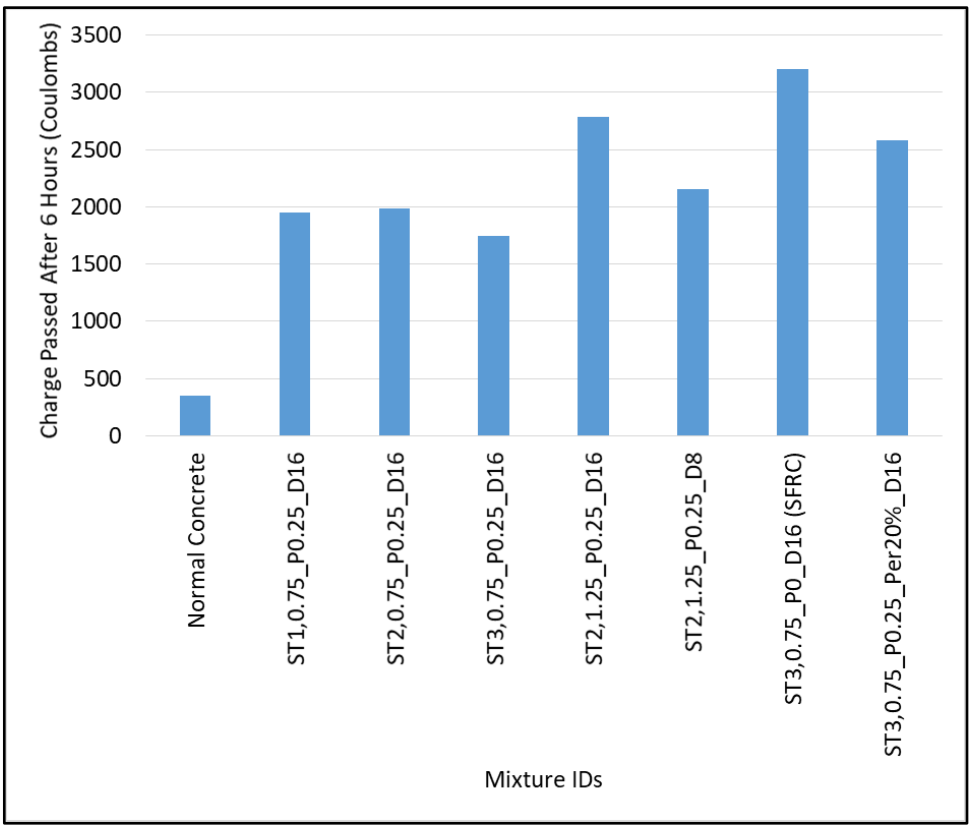

Figure 5.46. RCPT test results for selected mixtures

5.2.8. Sorptivity Test

Figure 5.47 shows capillary water absorption capacity of all selected mixtures during 72 hours and Table 5.21 gives a summary of the values after 72 hours.

Table 5.21. Sorptivity test results of selected mixtures

Mixture IDs	Capillary water absorption after 72 hours(%)
Normal Concrete	0.0374
ST1,0.75_P0.25_D16	0.0403
ST2,0.75_P0.25_D16	0.0384
ST3,0.75_P0.25_D16	0.0363
ST2,1.25_P0.25_D16	0.0534
ST2,1.25_P0.25_D8	0.0431
ST3,0.75_P0_D16 (SFRC)	0.0449
ST3,0.75_P0.25_Per20%_D16	0.0645

Results indicate that the mixture with perlite aggregate shows higher water absorption capacity due to the porous structure of perlite aggregate. In the case of SFRC, the water absorption capacity increased. Capillary water absorption of the HyFRC specimens were close to each other. Among the HyFRC mixtures, the mixture with higher steel fiber content showed slightly higher capillary water absorption capacity probably due to the gaps between the steel fibers in the specimens. Figure 5.48 shows capillary water absorption values after 72 hours for all selected mixtures.

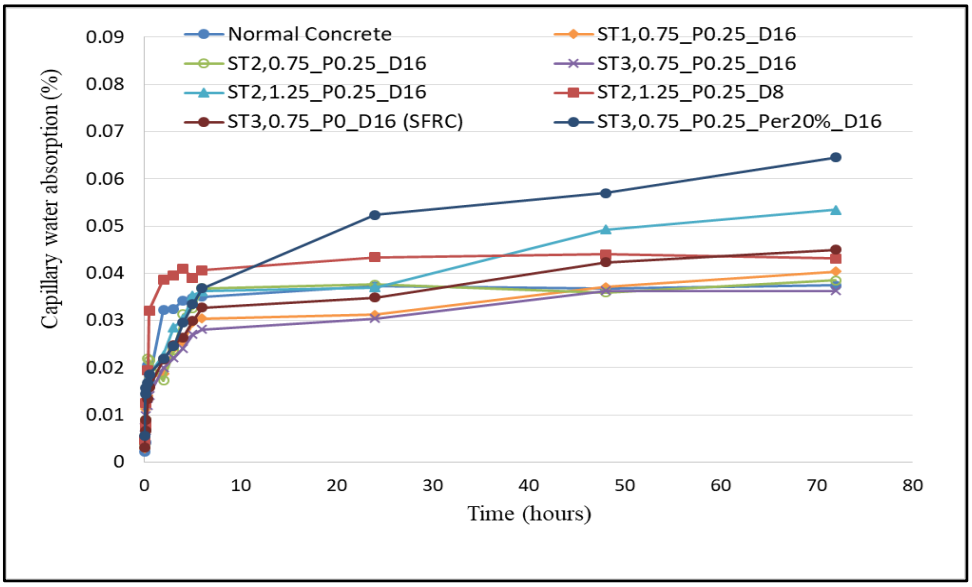

Figure 5.47. Sorptivity test result graphs of selected specimens

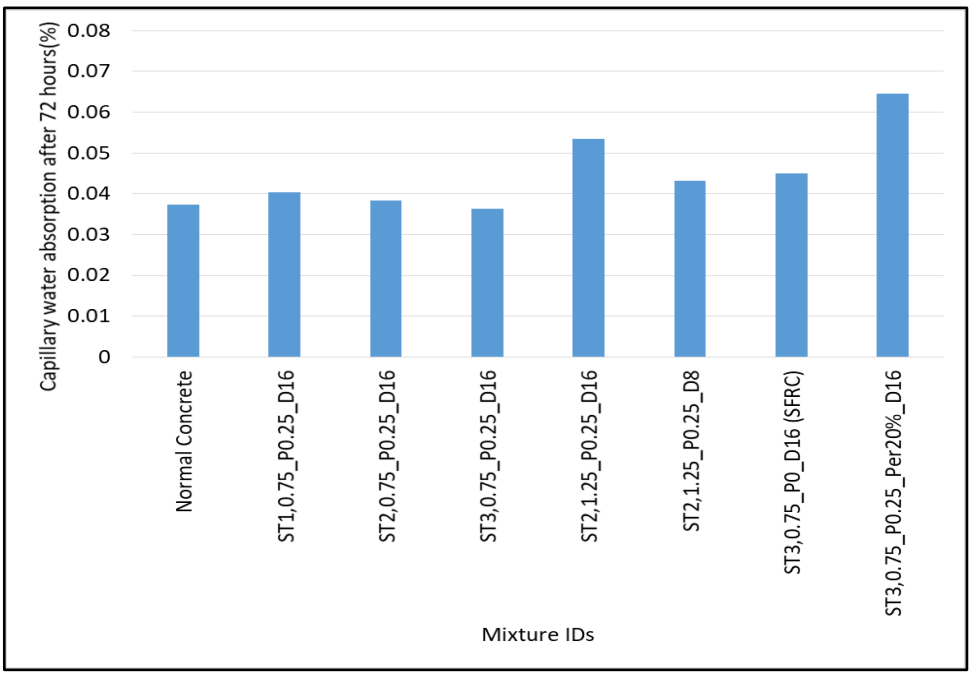

Figure 5.48. Capillary water absorption values after 72 hours

5.2.9. Pendulum Test for Real-Size Barriers

Based on the mechanical behavior and durability test results discussed previously, ST3,0.75_P0.25_D16 mixture was found to have the best performance and accordingly this composite was selected for the real-size barrier pendulum test. The

same mixture without fibers were also tested under pendulum test as control normal concrete since the present road barriers in the market do not employ fibers.

As seen in Figure 5.49, both specimens are damaged at the impact point and moved from initial location after impact loading. In normal concrete, a large part of concrete is broken on the impact face of specimen near to ground and also the specimen moved 49 cm to the back from initial location (Figure 5.49a). HyFRC specimen showed no damage except at the crushing point of impact and the specimen moved about 39 cm to the back from initial location (Figure 5.49b).

(a) (b)

Figure 5.49. Normal concrete and HyFRC barriers after impact test

Figure 5.50 shows the average acceleration values from two accelerometers on the impact mass for both specimens. The acceleration values obtained from the accelerometer on the specimens are shown in Figure 5.51. According to accelerometer data from impact mass, 253 m/s^2 maximum acceleration was recorded for control specimen and 343 m/s^2 maximum acceleration was recorded for HyFRC specimen. These accelerations correspond to maximum load of 253 kN for control specimen and 343 kN for HyFRC specimen. Accelerometer data from specimens illustrate that acceleration increase rate and graph route are similar for both specimens. The maximum acceleration for control and HyFRC are 4.1 m/s^2 and 5.1 m/s^2 respectively. Based on

these results, the impact mass remained in contact for about 1 ms longer on the HyFRC specimen. According the impact point of HyFRC the crushing in impact point is higher and the impact mass penetrated more than control specimen, which verifies the longer contact time of impact mass on the HyFRC specimen.

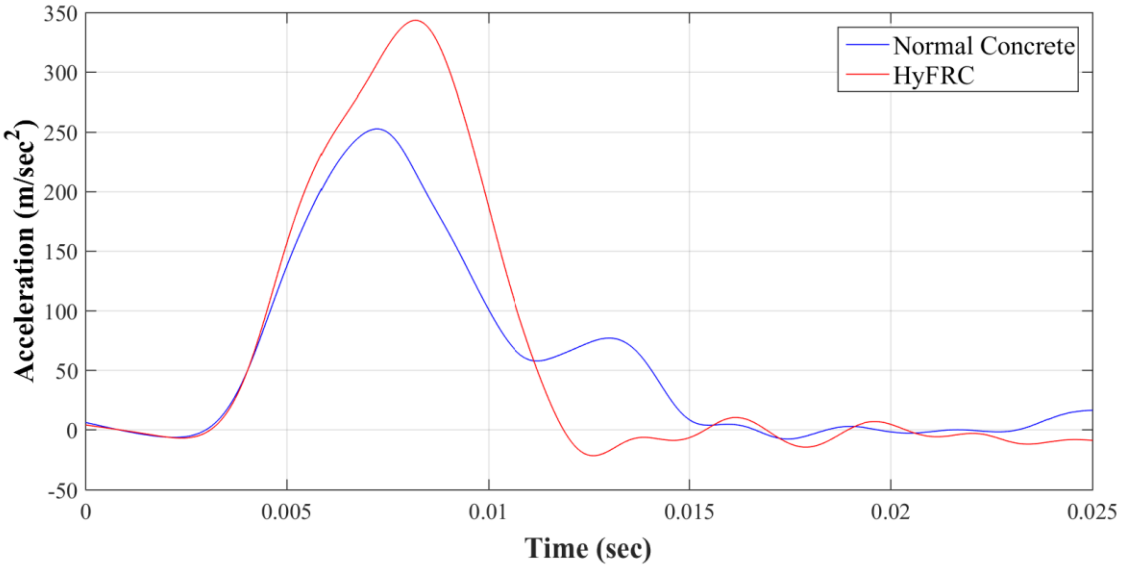

Figure 5.50. Impact mass acceleration change

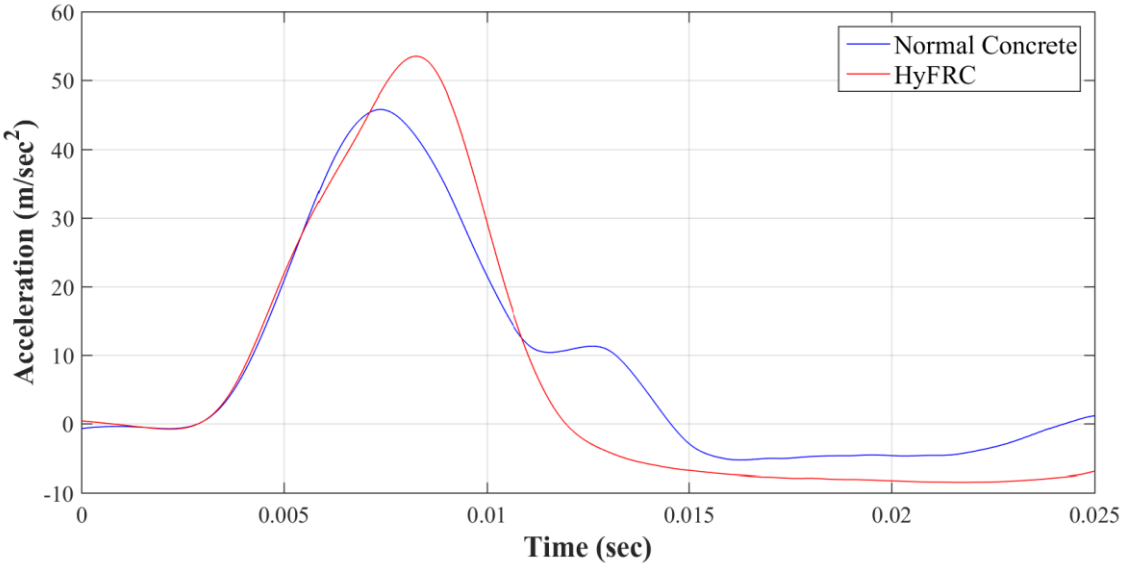

Figure 5.51. Concrete specimens acceleration change

Dynamic balance diagram of concrete barriers during the impact test is shown in Figure 5.52. In this diagram, F_d is the sum-up impact force from accelerometer on impact mass and impact mass weight (1000 kg), F_a is the sum-up inertia force from

accelerometer on the barrier and barrier weight (750 kg) , and F_s is the stability force as the sum-up of friction forces on the ground and the reaction forces from the barriers on the side. Although the direct measurement of F_s is difficult, it can be obtained indirectly as F_d-F_a. Figure 5.52 shows the difference between impact force and specimen inertia force as F_s.

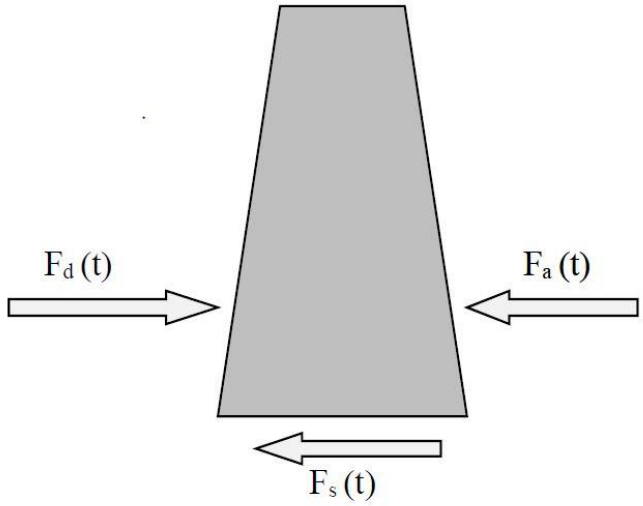

Figure 5.52. Dynamic balance diagram of concrete barriers

As seen in Figure 5.53, the F_s forces of HyFRC specimen are generally higher than those of the control specimen. This difference is due to the interaction of barrier and impact mass. In control specimen testing, the impact energy was partly consumed by cracking and breaking of the specimen, but it was mostly transformed into motion energy and caused the acceleration of the barrier. When the acceleration graphs of control and HyFRC specimens are compared in Figure 5.50, it is seen that the acceleration increase rate (acceleration graph slope) is higher in the control specimen despite the lower maximum value. In HyFRC specimen, the impact mass was entrenched into the sample and caused ground stomping. Therefore, some part of the impact energy was consumed in this way, the remaining part converted into motion energy. More momentum is transferred to the barrier in the control specimen than HyFRC specimen.

Since the difference between the applied force and the inertia force of the sample is also a measure of the absorption energy, it can be considered that the HyFRC

specimen absorbs more energy. Accordingly, the control specimen, despite lower load absorption and shorter time exposure, moved back for 10 cm.

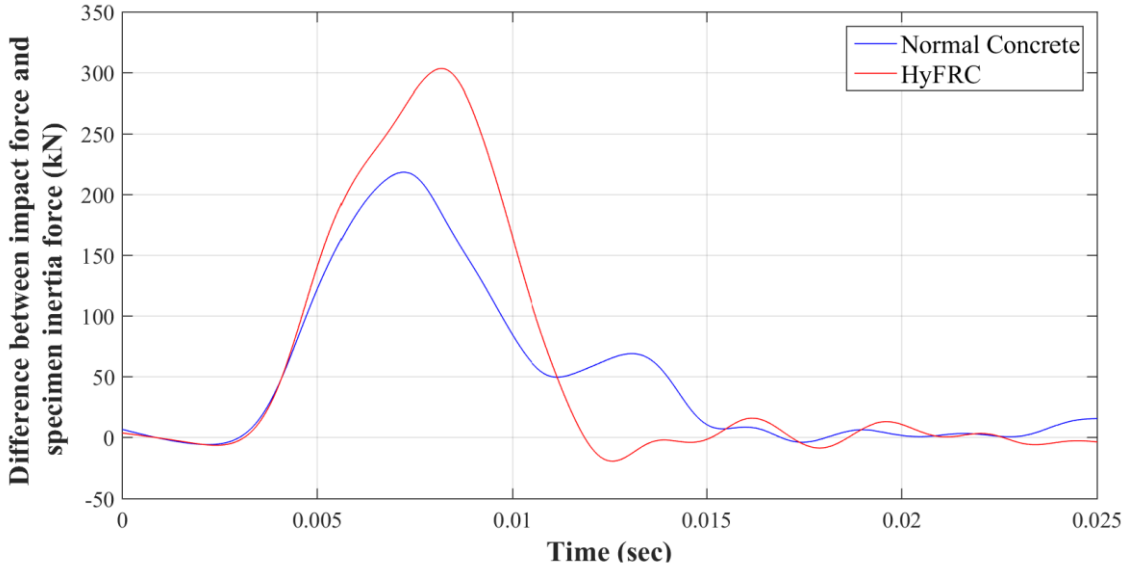

Figure 5.53. Difference between impact force and specimen inertia force

As a result of these experiments, the HyFRC barrier consumes higher impact resistance. Due to ductility against ground stomping of HyFRC barrier, less momentum is transferred to the barrier and less displacement occurred, therefore, the HyFRC barrier has better performance to keeping the barrier on the ground against beating of impact mass.

CHAPTER 6

CONCLUSIONS

6.1. Engineered Cementitious Composite (ECC)

Standard M45 ECC (Li 2007) mixtures with various fly ash ratios (1.2, 1.7, and 2.2) were prepared. Based on the results, the mixture with best performance, which is FA1.2, was reproduced by replacing 10%, 20% or 30% (by weight) of the quartz sand with presoaked expanded perlite. Compressive strength, static bending, impact bending, rapid chloride ions permeability, freeze-thaw cycles, and sorptivity tests were made on all six types of ECC. Following outcomes can be drawn from ECC mixtures.

- ECC results show that generally static bending toughness decrease as the FA/PC increases as well as compressive and flexural strength
- Conversely to the static bending test, ECC results show that dynamic bending toughness increases as the fly ash content increase.
- ECC results point out the significant increasing of dynamic bending toughness when expanded perlite added to FA1.2 mixture. Also dynamic bending toughness is pointedly increasing as perlite content increases.
- RCPT test results show that the charge passed increase as fly ash content increases. Results also specified that passing of charge increases as perlite content increases. FA1.2 mixture which has the lowest fly ash content and no perlite devours the highest permeability resistance
- Generally, concrete weight decreases after freeze and thaw cycles but in this study all ECC mixtures seemed to gained weight. This was probably due to the unsaturated state of the specimens at the beginning of the tests, which may originate from the low permeability and very dense structure of ECC. In addition, visual inspection of the specimens did not imply weight loss since there was not surface scaling for any of the ECC composite.
- Sorptivity test Results show that capillary water absorption capacity increases as fly ash content increases. Results also illustrate that the capillary water absorption capacity increases as expanded perlite content increases. Results also

point out that the mixture (FA1.2) which contains lowest fly ash and no perlite shows the lowest sorptivity.

- According to the ECC results, fly ash/cement =1.2, and perlite 20% replacing sand is selected for HyFRC and SFRC mixtures study.

6.2. Hybrid Fiber Reinforced Concrete (HyFRC)

Total thirty-six mixtures of HyFRC with three types of steel fibers (ST1, ST2, or ST3), and two coarse aggregate types (with 8 mm and 16 mm D_{max}) were tested. Additionally, presoaked expanded perlite was also used in the mixture with best oerformance by replacing 20% (by weight) of the sand, a normal concrete (NC) mixture, and a mixture of steel fiber reinforced concrete (SFRC) were tested. These tests include consistency, compressive strength, static bending, dynamic bending, rapid chloride ion permeability, freeze-thaw, sorptivity, and real-size barriers pendulum tests. Following outcomes can be drawn from HyFRC mixtures:

- Superplasticizer was used to achieve sufficient workability for casting the composites. Superplasticizer contents were not kept constant in the mixtures and special attention was paid to obtain uniform distribution of fibers and sufficient workability. Results show as the Dmax decreases from 16mm to 8mm superplasticizer demand increases. Results illustrate that the superplasticizer demand significantly increased with adding the fibers, demand of superplasticizer for normal concrete is 19 gr/55Lt and it is varying from 72-152 gr/55Lt for HyFRC.
- Generally HyFRC mixtures with Dmax=16mm showed higher mechanical properties (compressive strength, flextural strength, and toughness) when compared to Dmax=8mm.
- Use of fiber hybridization resulted a significant increase of 194 up to 531% in the maximum flexural strength and 2617 up to 6595% in toughness when compares to normal plain concrete.
- HyFRC, toughness decreased as PVA content increases from 0.25% to 0.50%. However, toughness increased when steel fiber content is increased.
- In terms of flexural strength and toughness, ST3 results were higher than ST2, and ST2 results were higher than ST1 results for HyFRC concrete.

- Impact loading results show that the best performance mixture in static loading (ST3,0.75_P0.25_D16) shows the higher flexural strength and toughness as well, however, the flexural strength and toughness increase a little bit when the steel fiber content increases from 0.75% to 1.25%.
- Results shows that the normal plain concrete exhibits the highest weight loss after 300 freeze and thaw cycles. HyFRC results were close to each other. The ST1,0.75_P0.25_D16 mixture, which contains ST1 type steel fiber, showed the lowest weight loss. In case of SFRC mixture without PVA, weight loss significantly increased. It means that adding PVA fibers enhanced the freezing and thawing resistance.
- Results indicate that the normal concrete shows the very low charge passed value. The higher current passing of fiber reinforced concrete than normal concrete is due to the presence of metals (steel fibers) which promotes the passing of electrical current. Therefore, RCPT method of durability test was not found suitable for steel fiber reinforced concrete
- Sorptivity results indicate that the mixture with perlite aggregate shows higher water absorption capacity due to the porous structure of perlite aggregate. In the case of SFRC, the water absorption capacity increased. Capillary water absorption of the HyFRC specimens were close to each other. Among the HyFRC mixtures, the mixture with higher steel fiber content showed slightly higher capillary water absorption capacity probably due to the gaps between the steel fibers in the specimens.
- As a result of these experiments, the HyFRC barrier consumes higher impact resistance. Due to ductility against ground stomping of HyFRC barrier, less momentum is transferred to the barrier and less displacement occurred, therefore, the HyFRC barrier has better performance to keeping the barrier on the ground against beating of impact mass.

6.3. Recommendations

Based on the mechanical behavior and durability test results of HyFRC, ST3,0.75_P0.25_D16 mixture was found to have the best performance, and accordingly, this composite was selected for the real-size barrier pendulum test. The same mixture

without fibers was also tested under pendulum test as control normal concrete. Due to time and budget limitation of this study, the HyFRC mixture with perlite content was not tested under pendulum test. It is recommended that the same HyFRC mixture with 20% perlite content was also tested under pendulum test for further studies.

The HyFRC barrier design should be done not only from materials perspective but also from structural perspective. Material design helps the barrier to keep its integrity, but traffic safety requires additional design. New Jersey type barriers hold the crashing vehicle on road mainly by its weight and geometric design. A ductile material used in this study may allow a lighter and more efficient design, taking advantage of the high deformation capacity.

ECC is a ductile and homogenous material. ECC under various mechanical and environmental conditions is durable and sustainable but it is expensive material and not recommended to use in concrete road barriers. HyFRC is more economical material compared to ECC, therefore, HyFRC is recommended to use in concrete road barriers.

REFERENCES

Afroughsabet, V., & Ozbakkaloglu, T. (2015). Mechanical and durability properties of high-strength concrete containing steel and polypropylene fibers. Construction and building materials, 94, 73-82.

Ahmed, S. F. U., Maalej, M., & Paramasivam, P. (2007). Flexural responses of hybrid steel–polyethylene fiber reinforced cement composites containing high volume fly ash. Construction and building materials, 21(5), 1088-1097.

Ali, M. A. E. M., Soliman, A. M., & Nehdi, M. L. (2017). Hybrid-fiber reinforced engineered cementitious composite under tensile and impact loading. Materials & Design, 117, 139-149.

Al-Masoodi, A. H. H., Kawan, A., Kasmuri, M., Hamid, R., & Khan, M. N. N. (2016). Static and dynamic properties of concrete with different types and shapes of fibrous reinforcement. Construction and Building Materials, 104, 247-262.

Ammasi, A. K. (2018). Strength and durability of high volume fly ash in engineered cementitious composites. Materials today: proceedings, 5(11), 24050-24058.

Banthia, N., Mindess, S., Bentur, A., & Pigeon, M. (1989). Impact testing of concrete using a drop-weight impact machine. Experimental mechanics, 29(1), 63-69.

Banyhussan, Q. S., Yıldırım, G., Bayraktar, E., Demirhan, S., & Şahmaran, M. (2016). Deflection-hardening hybrid fiber reinforced concrete: The effect of aggregate content. Construction and building materials, 125, 41-52.

Barnat-Hunek, D., Góra, J., Andrzejuk, W., & Łagód, G. (2018). The microstructure-mechanical properties of hybrid fibres-reinforced self-compacting lightweight concrete with perlite aggregate. Materials, 11(7), 1093.

Blunt, J. D., & Ostertag, C. P. (2009a). Performance-based approach for the design of a deflection hardened hybrid fiber-reinforced concrete. Journal of engineering mechanics, 135(9), 978-986.

Blunt, J. D., & Ostertag, C. P. (2009b). Deflection hardening and workability of hybrid fiber composites. ACI Materials Journal, 106(3), 265.

Caggiano, A., Pepe, M., Xargay, H., & Martinelli, E. (2020). Analytical Modeling of the Postcracking Response Observed in Hybrid Steel/Polypropylene Fiber-Reinforced Concrete. Polymers, 12(9), 1864.

Choi, Y., & Yuan, R. L. (2005). Experimental relationship between splitting tensile strength and compressive strength of GFRC and PFRC. Cement and Concrete Research, 35(8), 1587-1591.

Dancygier, A. N., Katz, A., Yardimci, M. Y., & Yankelevsky, D. Z. (2012). Behavior of high ductility cement composite beams under low impact. International Journal of Protective Structures, 3(2), 177-191.

Dawod, S. S. E. A. (2006). Damage assessment of impacted hybrid fiber reinforced concrete (Hyfrc). In International Conference on Bridge Management Systems-Monitoring, Assessment and Rehabilitation.

Elfgren, L. (Ed.). (1989). Fracture Mechanics of Concrete Structures: From Theory to Applications: Report of the Technical Committee 90-FMA Fracture Mechanics to Concrete/Applications, RILEM (the International Union of Testing and Research Laboratories for Materials and Structures (Vol. 3). Spon Press.

Emniyet Genel Müdürlüğü. "Genel Kaza İstatistikleri". http://www.trafik.gov.tr/Sayfalar/Istatistikler/Genel-Kaza.aspx. Son erişim tarihi: 03 Mart 2015.

Gözen A. 2008. "Yollarda Kullanılan Beton Bariyerler" TÇMB Hazır Beton Komitesinde sunum metni, İstanbul.

Hay, R., & Ostertag, C. (2015). Development and application of high performance green hybrid fiber-reinforced concrete (HP-G-HyFRC) for sustainable and energy-efficient buildings. In Key Engineering Materials (Vol. 629, pp. 299-305). Trans Tech Publications Ltd.

Jang, S. J., Rokugo, K., Park, W. S., & Yun, H. D. (2014). Influence of rapid freeze-thaw cycling on the mechanical properties of sustainable strain-hardening cement composite (2SHCC). Materials, 7(2), 1422-1440.

Jedidi, M., Benjeddou, O., & Soussi, C. (2015). Effect of expanded perlite aggregate dosage on properties of lightweight concrete. Jordan Journal of Civil Engineering, 9(3).

Jen, G., Trono, W., & Ostertag, C. P. (2016). Self-consolidating hybrid fiber reinforced concrete: Development, properties and composite behavior. Construction and Building Materials, 104, 63-71.

Jirobe, S., Brijbhushan, S., & Maneeth, P. D. (2015). Experimental investigation on strength and durability properties of hybrid fiber reinforced concrete. International Research Journal of Engineering and Technology, 2, 891-896.

Keskin S. B. (2012). Dimensional Stability of Engineered Cementitious Composite. PhD Thesis, Middle East Technical University.

Keskin, S. B., Sulaiman, K., Sahmaran, M., & Yaman, I. O. (2013). Effect of presoaked expanded perlite aggregate on the dimensional stability and mechanical properties of engineered cementitious composites. Journal of materials in civil engineering, 25(6), 763-771.

Kim, D. H., & Park, C. G. (2013). Strength, permeability, and durability of hybrid fiber-reinforced concrete containing styrene butadiene latex. Journal of Applied Polymer Science, 129(3), 1499-1505.

Li, V. C. (1998). Engineered Cementitious Composites – Tailored Composites Through Micromechanical Modelling in Fiber Reinforced Concrete, Present and the Future, Eds. Banthia, N., CSCE, Montreal, 64-97.

Li, V. C. (2003). On engineered cementitious composites (ECC) a review of the material and its applications. Journal of advanced concrete technology, 1(3), 215-230.

Li, V. C., Mishra, D. K., & Wu, H. C. (1995). Matrix design for pseudo-strain-hardening fibre reinforced cementitious composites. Materials and structures, 28(10), 586-595.

Li, V. C., Wu, C., Wang, S., Ogawa, A., & Saito, T. (2002). Interface tailoring for strain-hardening polyvinyl alcohol-engineered cementitious composite (PVA-ECC). Materials Journal, 99(5), 463-472.

Li, V.C., (2007). Engineered Cementitious Composites (ECC): Material, Structure, and Durability Performance, chapter 24 of the book Conncrete Construction Engineering Handbook, Chapter 24 (pp. 1-46).

Li, X., Zhang, Q., & Mao, S. (2021). Investigation of the bond strength and microstructure of the interfacial transition zone between cement paste and aggregate modified by Bayer red mud. Journal of Hazardous Materials, 403, 1-11.

Ma, H., Qian, S., & Li, V. C. (2016). Influence of fly ash type on mechanical properties and self-healing behavior of Engineered Cementitious Composite (ECC). FramCos-9.

Mehta, P. K., & Monteiro P. J. M. (2006). Concrete – structure, properties and materials. 3rd edition. Published by McGraw-Hill Book, New York, ISBAN 0-07-146289-9 USA.

Mindess, S., Young, J. F., & Darwin, D. Concrete. 2nd edition. Published by Prentice Hall Book, ISBAN 0-13-064632-6 USA [2003].

Mohammadi, Y., Carkon-Azad, R., Singh, S. P., & Kaushik, S. K. (2009). Impact resistance of steel fibrous concrete containing fibres of mixed aspect ratio. Construction and Building Materials, 23(1), 183-189.

Monteiro M., V. M., Lima, L. R., & de Andrade Silva, F. (2018). On the mechanical behavior of polypropylene, steel and hybrid fiber reinforced self-consolidating concrete. Construction and Building Materials, 188, 280-291.

Naraganti, S. R., Pannem, R. M. R., & Putta, J. (2019). Impact resistance of hybrid fibre reinforced concrete containing sisal fibres. Ain Shams Engineering Journal, 10(2), 297-305.

Nicolaides, D., Kanellopoulos, A., Savva, P., & Petrou, M. (2015). Experimental field investigation of impact and blast load resistance of Ultra High Performance Fibre Reinforced Cementitious Composites (UHPFRCCs). Construction and Building Materials, 95, 566-574.

Schneider, B. (1992). Development of SIFCON through Applications. In High Performance Fiber Reinforced Cement Composites (pp. 177-194).

Shao, Y., Jiang, L., & He, Z. (2015). Durabılıty performance of straın hardenıng fıber reınforced concrete. Seventh International RILEM Conference on High Performance Fiber Reinforced Cement Composites (HPFRCC7), (pp. 227-234).

Sharma, A., Reddy, G. R., Varshney, L., Bharathkumar, H., Vaze, K. K., Ghosh, A. K., ... & Krishnamoorthy, T. S. (2009). Experimental investigations on mechanical and radiation shielding properties of hybrid lead–steel fiber reinforced concrete. Nuclear Engineering and Design, 239(7), 1180-1185.

Shetty, M. S. (2006). Chapter 7, Concrete technology theory and practice. S. Chand & Company Ltd., New Delhi.

Şahmaran, M., & Yaman, I. O. (2007). Hybrid fiber reinforced self-compacting concrete with a high-volume coarse fly ash. Construction and building materials, 21(1), 150-156.

Şahmaran, M., & Li, V. C. (2009). Durability properties of micro-cracked ECC containing high volumes fly ash. Cement and Concrete Research, 39(11), 1033-1043.

Şahmaran, M., Yurtseven, A., & Yaman, I. O. (2005). Workability of hybrid fiber reinforced self-compacting concrete. Building and Environment, 40(12), 1672-1677.

Şahmaran, M., Özbay, E., Yücel, H. E., Lachemi, M., & Li, V. C. (2012). Frost resistance and microstructure of Engineered Cementitious Composites: Influence of fly ash and micro poly-vinyl-alcohol fiber. Cement and Concrete Composites, 34(2), 156-165.

Şahmaran, M., & Li, V. C. (2009). Influence of microcracking on water absorption and sorptivity of ECC. Materials and structures, 42(5), 593-603.

Tabatabaeian, M., Khaloo, A., Joshaghani, A., & Hajibandeh, E. (2017). Experimental investigation on effects of hybrid fibers on rheological, mechanical, and durability properties of high-strength SCC. Construction and Building Materials, 147, 497-509.

Technical Report No. 63. (2007). Guidelines for the design of steel-fiber reinforced concrete. Published by The Concrete Society, ISBAN 1-904482-32-5 UK.

Thendral, S., & Hemapriya, (2018). Rapid chloride penetration test of hybrid fibre reinforced concrete. International Journal of Pure and Applied Mathematics, 119(12), 9213-9226.

Türkiye Hazır Beton Birliği. https://www.facebook.com/BetonBariyerler. Son erişim tarihi: 03 Mart 2015.

Turk, K., & Nehdi, M. L. (2018). Coupled effects of limestone powder and high-volume fly ash on mechanical properties of ECC. Construction and Building Materials, 164, 185-192.

Vibhuti, R. B., & Aravind, N. (2013). Mechanical properties of hybrid fiber reinforced concrete for pavements. International Journal of Research in Engineering and Technology, pISSN: 2321-7308, 244-247.

Wang, Q., Yi, Y., Ma, G., & Luo, H. (2019). Hybrid effects of steel fibers, basalt fibers and calcium sulfate on mechanical performance of PVA-ECC containing high-volume fly ash. Cement and Concrete Composites, 97, 357-368.

Wang, S., & Li, V. C. (2007). Engineered cementitious composites with high-volume fly ash. ACI Materials journal, 104(3), 233-241.

Wang, S., Le, H. T. N., Poh, L. H., Quek, S. T., & Zhang, M. H. (2017). Effect of high strain rate on compressive behavior of strain-hardening cement composite in comparison to that of ordinary fiber-reinforced concrete. Construction and Building Materials, 136, 31-43.

Yang, E. H., & Li, V. C. (2010). Strain-hardening fiber cement optimization and component tailoring by means of a micromechanical model. Construction and building Materials, 24(2), 130-139.

Yang, E. H., & Li, V. C. (2012). Tailoring engineered cementitious composites for impact resistance. Cement and Concrete Research, 42(8), 1066-1071.

Yang, E. H., & Li, V. C. (2014). Strain-rate effects on the tensile behavior of strain-hardening cementitious composites. Construction and Building materials, 52, 96-104.

Yang, K. H. (2011). Tests on concrete reinforced with hybrid or monolithic steel and polyvinyl alcohol fibers. ACI Materials Journal, 108(6), 664-672.

Yardımcı, M. Y., Aydın, S., & Tuyan, M. (2017). Flexural performance of alkali-activated slag cements under quasi-static and impact loading. Journal of Materials in Civil Engineering, 29(1), 04016192.

Yeğinobalı, A., Atahan, A.O., Gözen, A. (2011). Beton Bariyerler (Otokorkuluklar), TÇMB, 2. Baskı.

Yehia, S., Douba, A., Abdullahi, O., & Farrag, S. (2016). Mechanical and durability evaluation of fiber-reinforced self-compacting concrete. Construction and Building Materials, 121, 120-133.

Zhang, J., Maalej, M., & Quek, S. T. (2007). Performance of hybrid-fiber ECC blast/shelter panels subjected to drop weight impact. Journal of Materials in Civil Engineering, 19(10), 855-863.

Zhang, Z., Qian, S., & Ma, H. (2014). Investigating mechanical properties and self-healing behavior of micro-cracked ECC with different volume of fly ash. Construction and Building Materials, 52, 17-23.

Zhang, Z., Qian, S., & Ma, H. (2014). Investigating mechanical properties and self-healing behavior of micro-cracked ECC with different volume of fly ash. Construction and Building Materials, 52, 17-23.

Zhu Y., Zhang Z., Yang Y., and Yao Y. (2014) “Measurement and Correlation of Ductility and Compressive Strength for Engineered Cementitious Composites (ECC) produced by Binary and Ternary Systems of Binder Materials: Fly ash, slag, silica fume and cement” Construction and building Materials, 68, 192-198.

APPENDIX A

ECC Static Bending Test Load-Deflection Curves at 7, 28, and 90 Days Age

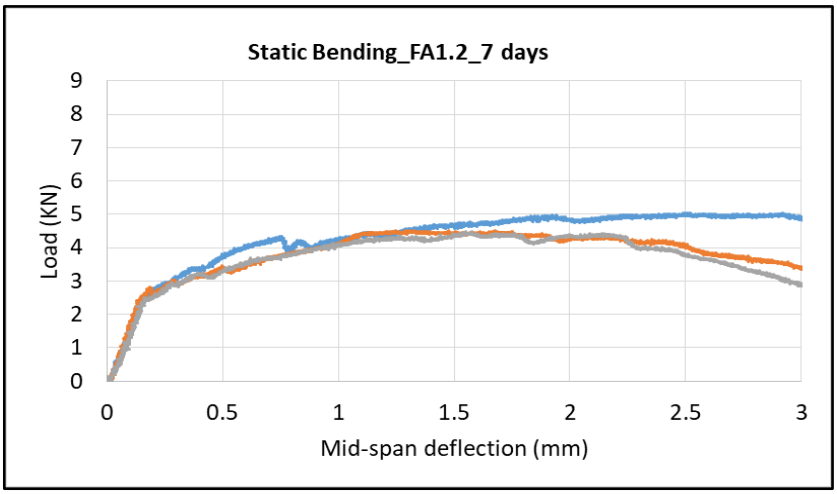

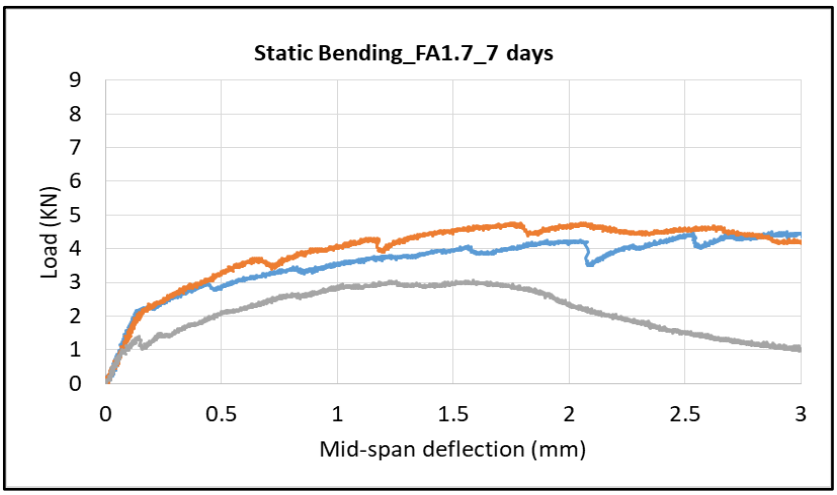

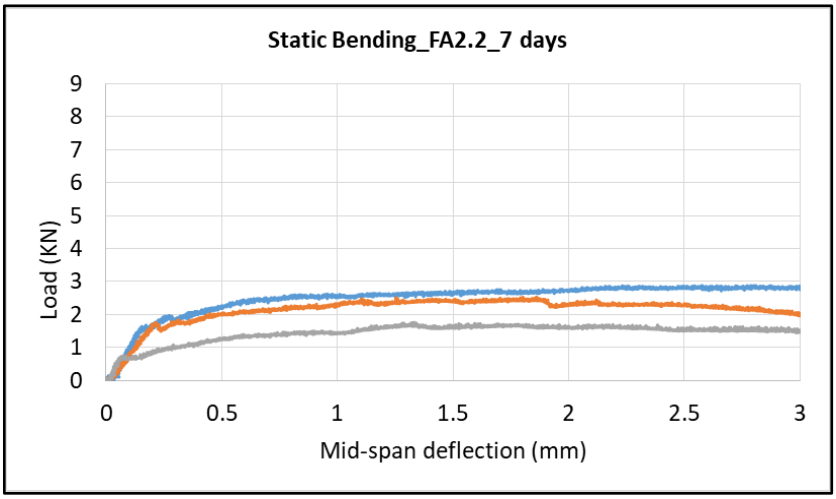
Static Bending_FA2.2_7 days
Load (KN)
Mid-span deflection (mm)
0
1
2
3
4
5
6
7
8
9
0
0.5
1
1.5
2
2.5
3

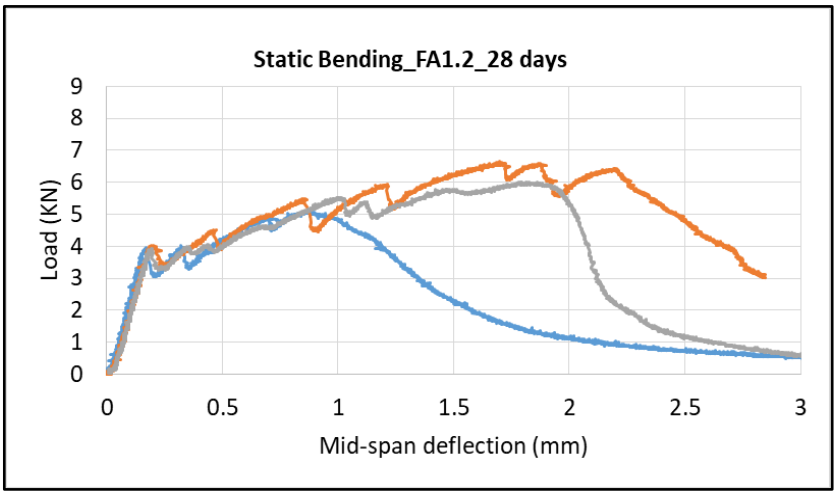
Static Bending_FA1.2_28 days
Load (KN)
Mid-span deflection (mm)
0
1
2
3
4
5
6
7
8
9
0
0.5
1
1.5
2
2.5
3

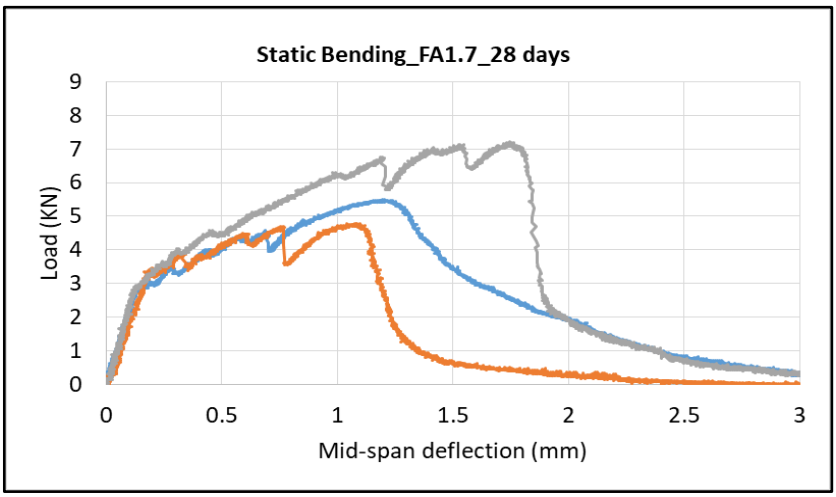
Static Bending_FA1.7_28 days
Load (KN)
Mid-span deflection (mm)
0
1
2
3
4
5
6
7
8
9
0
0.5
1
1.5
2
2.5
3

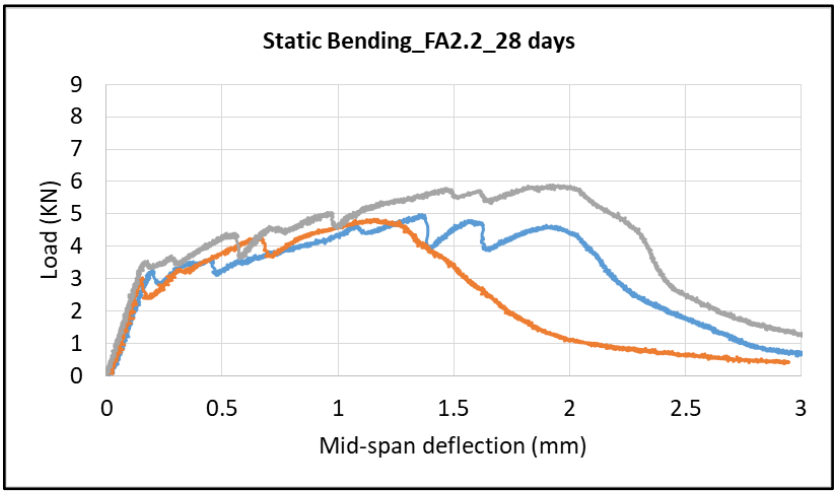
Static Bending_FA2.2_28 days
Load (KN)
Mid-span deflection (mm)
0
1
2
3
4
5
6
7
8
9
0
0.5
1
1.5
2
2.5
3

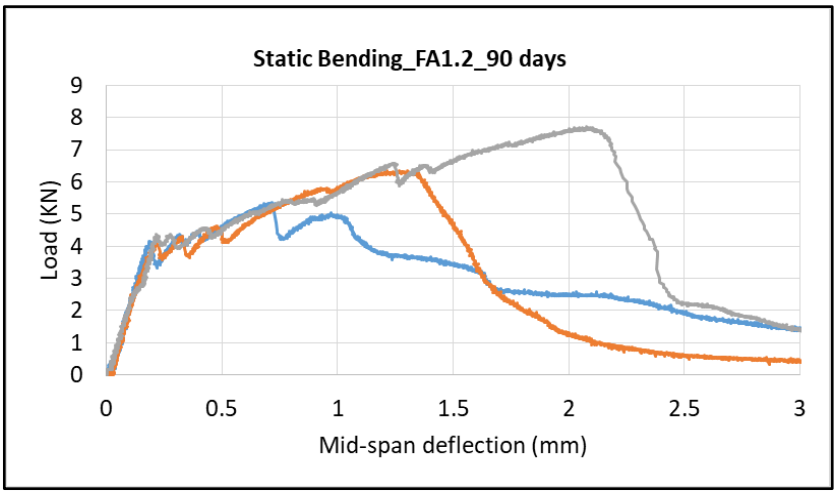
Static Bending_FA1.2_90 days
Load (KN)
Mid-span deflection (mm)
0
1
2
3
4
5
6
7
8
9
0
0.5
1
1.5
2
2.5
3

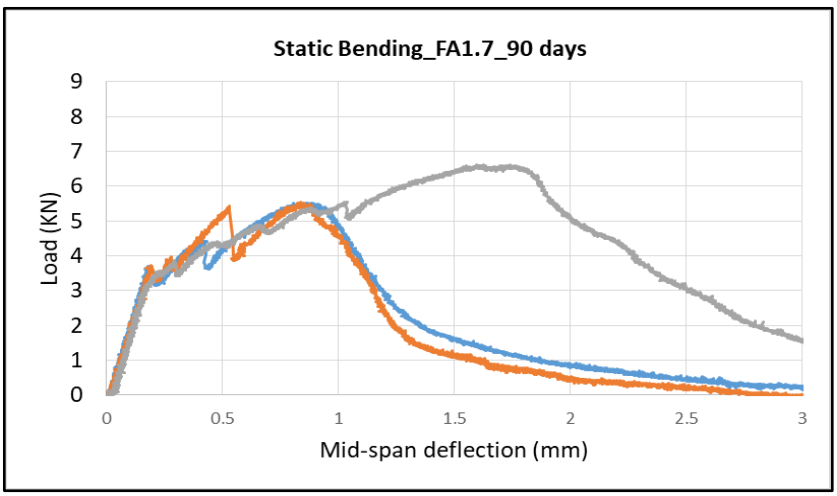
Static Bending_FA1.7_90 days
Load (KN)
Mid-span deflection (mm)
0
1
2
3
4
5
6
7
8
9
0
0.5
1
1.5
2
2.5
3

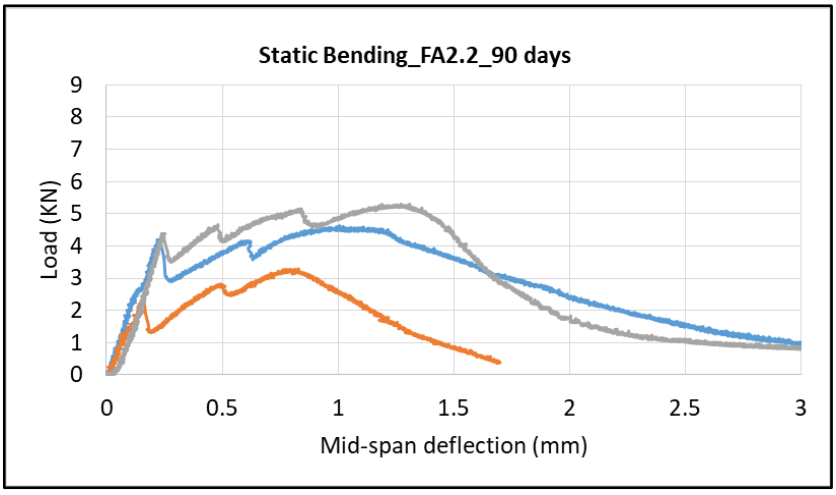
Static Bending_FA2.2_90 days
Load (KN)
Mid-span deflection (mm)
0
1
2
3
4
5
6
7
8
9
0
0.5
1
1.5
2
2.5
3

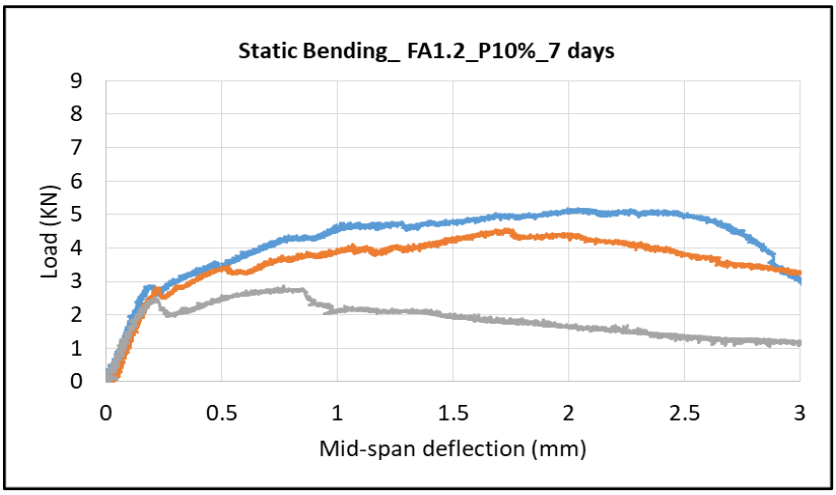
Static Bending_ FA1.2_P10%_7 days
Load (KN)
Mid-span deflection (mm)
0
1
2
3
4
5
6
7
8
9
0
0.5
1
1.5
2
2.5
3

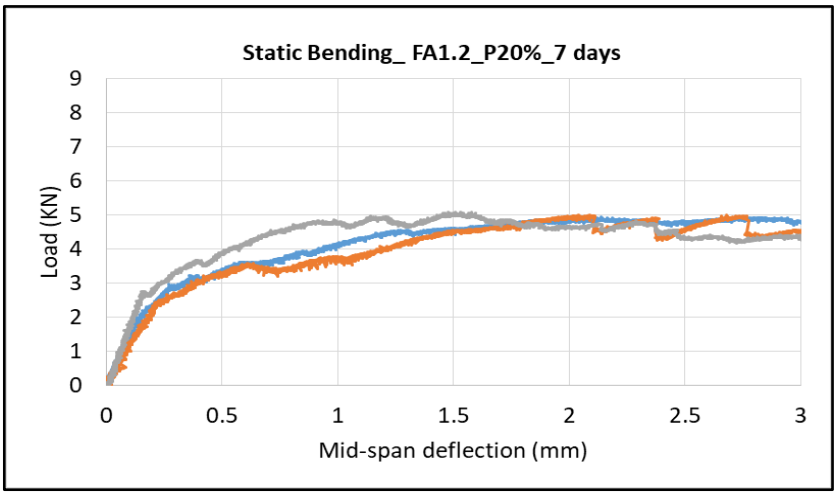
Static Bending_ FA1.2_P20%_7 days
Load (KN)
Mid-span deflection (mm)
0
1
2
3
4
5
6
7
8
9
0
0.5
1
1.5
2
2.5
3

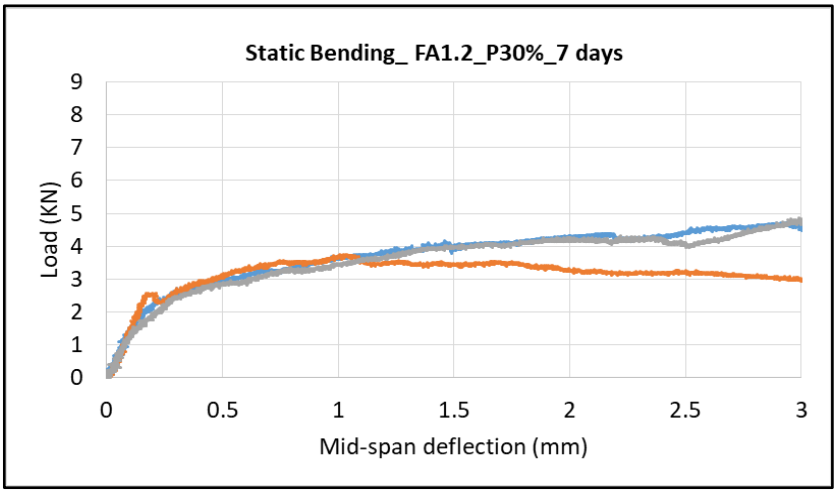
Static Bending_ FA1.2_P30%_7 days
Load (KN)
Mid-span deflection (mm)
0
1
2
3
4
5
6
7
8
9
0
0.5
1
1.5
2
2.5
3

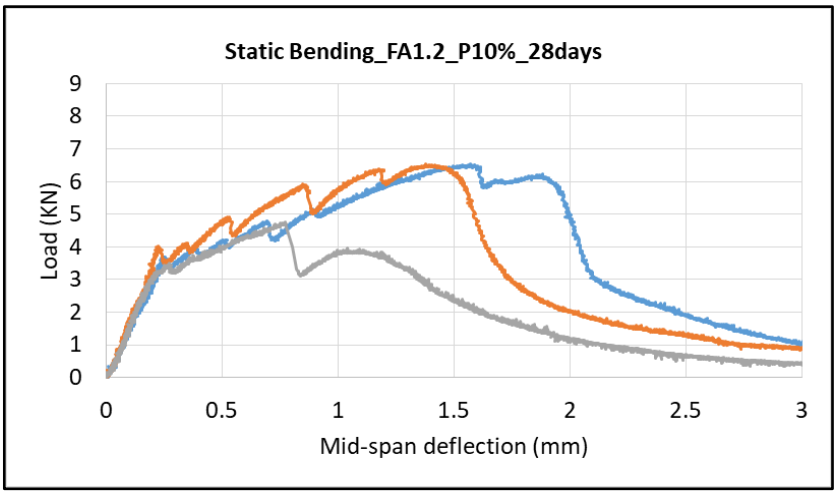
Static Bending_FA1.2_P10%_28days
Load (KN)
Mid-span deflection (mm)
0
1
2
3
4
5
6
7
8
9
0
0.5
1
1.5
2
2.5
3

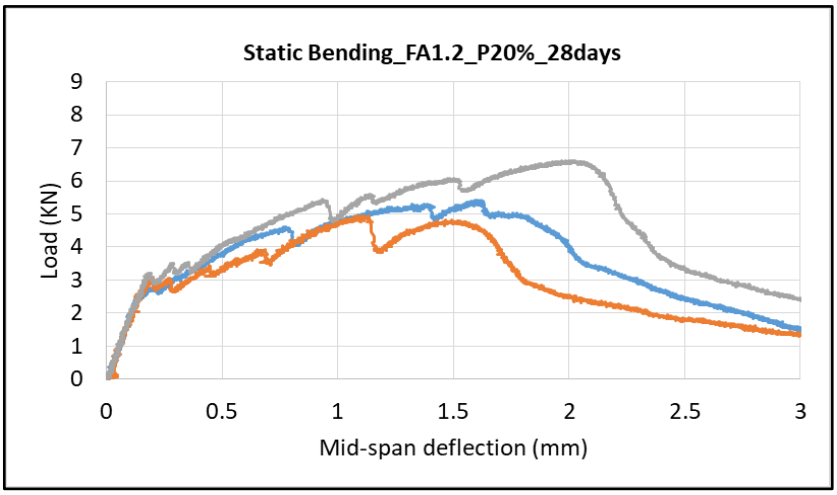
Static Bending_FA1.2_P20%_28days
Load (KN)
Mid-span deflection (mm)
0
1
2
3
4
5
6
7
8
9
0
0.5
1
1.5
2
2.5
3

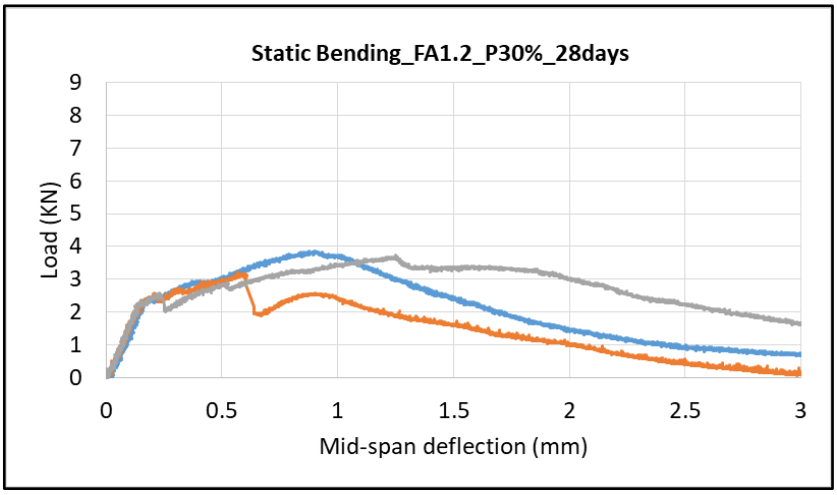
Static Bending_FA1.2_P30%_28days
Load (KN)
Mid-span deflection (mm)
0
1
2
3
4
5
6
7
8
9
0
0.5
1
1.5
2
2.5
3

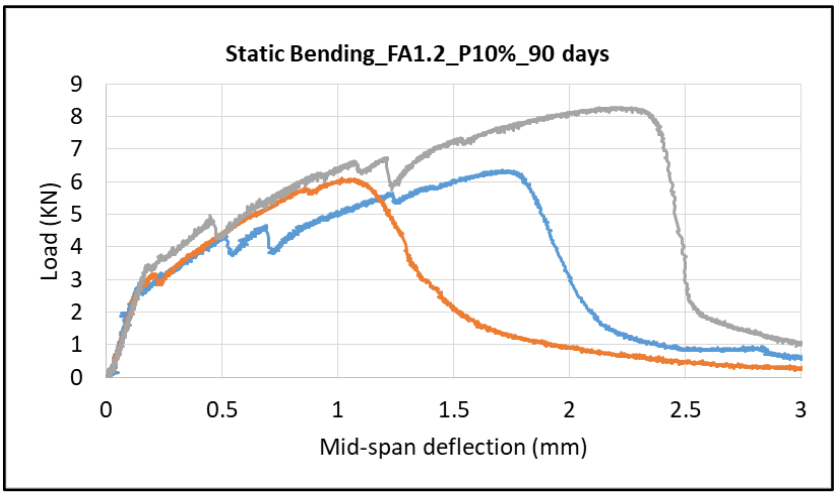
Static Bending_FA1.2_P10%_90 days
Load (KN)
Mid-span deflection (mm)
0
1
2
3
4
5
6
7
8
9
0
0.5
1
1.5
2
2.5
3

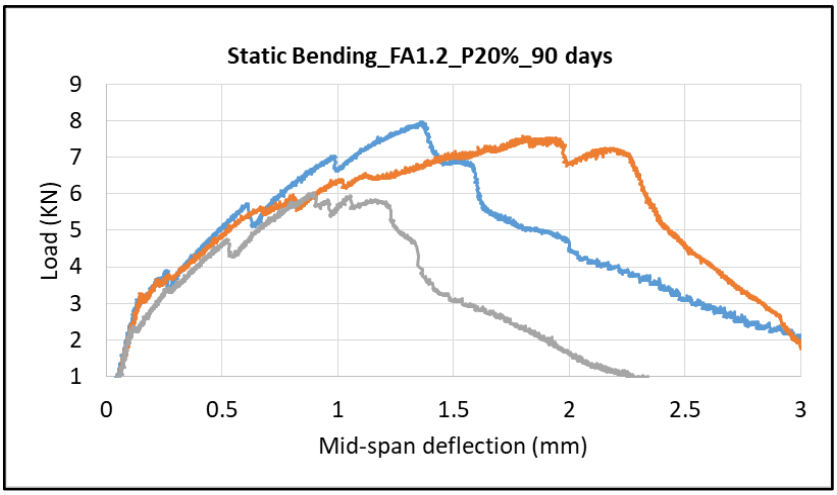
Static Bending_FA1.2_P20%_90 days
Load (KN)
Mid-span deflection (mm)
1
2
3
4
5
6
7
8
9
0
0.5
1
1.5
2
2.5
3

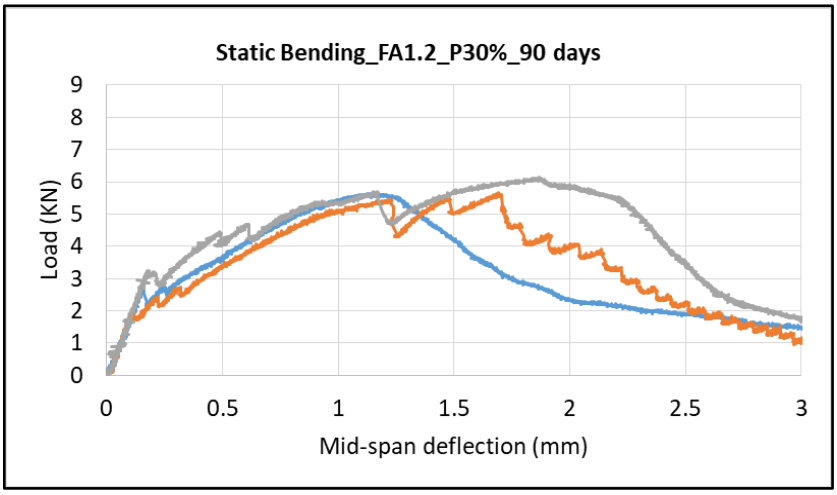
Static Bending_FA1.2_P30%_90 days
Load (KN)
9
8
7
6
5
4
3
2
1
0
0
0.5
1
1.5
2
2.5
3
Mid-span deflection (mm)

APPENDIX B

ECC Dynamic Bending Test Load-Deflection Curves at 90 Days Age

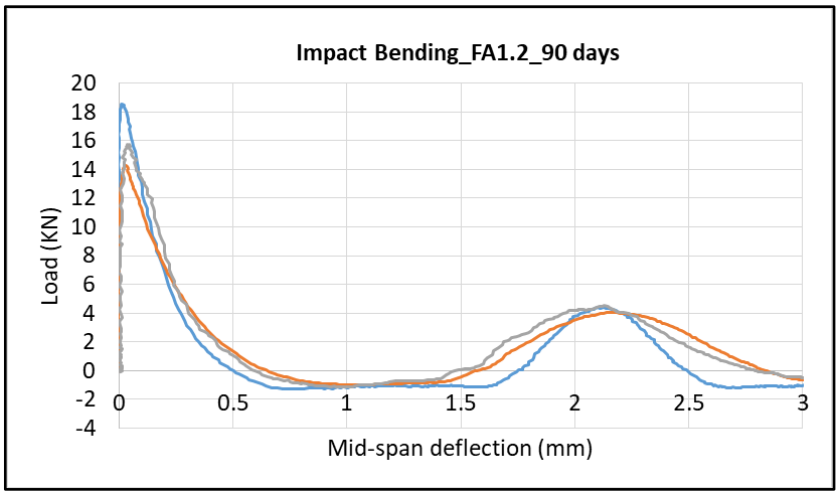

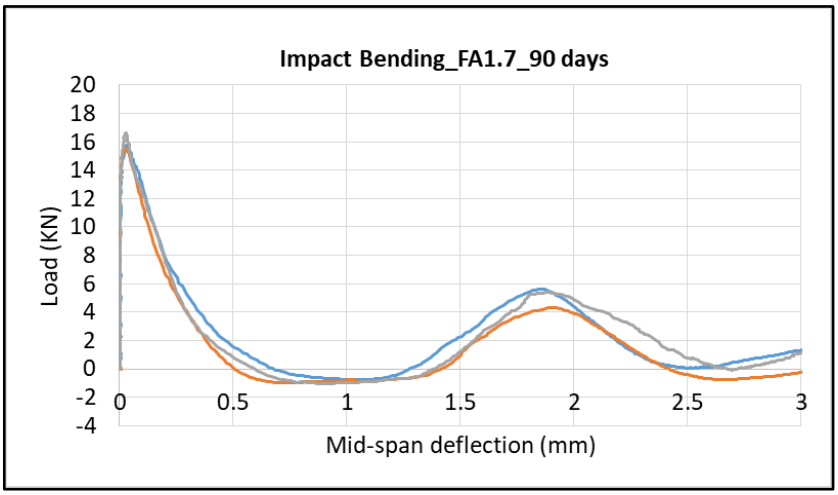

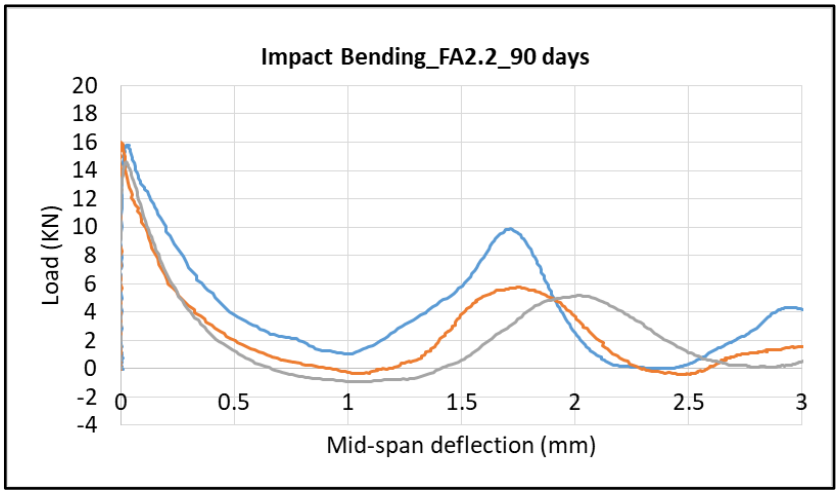
Impact Bending_FA2.2_90 days
Load (KN)
20
18
16
14
12
10
8
6
4
2
0
-2
-4
0
0.5
1
1.5
2
2.5
3
Mid-span deflection (mm)

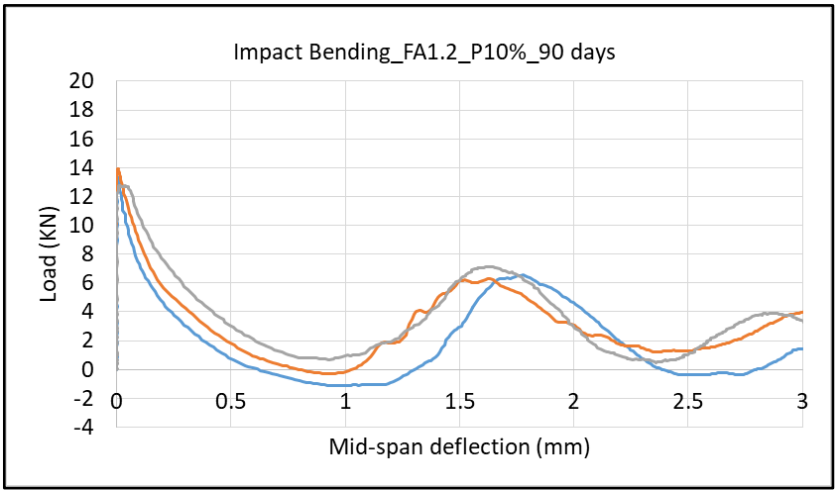
Impact Bending_FA1.2_P10%_90 days
Load (KN)
20
18
16
14
12
10
8
6
4
2
0
-2
-4
0
0.5
1
1.5
2
2.5
3
Mid-span deflection (mm)

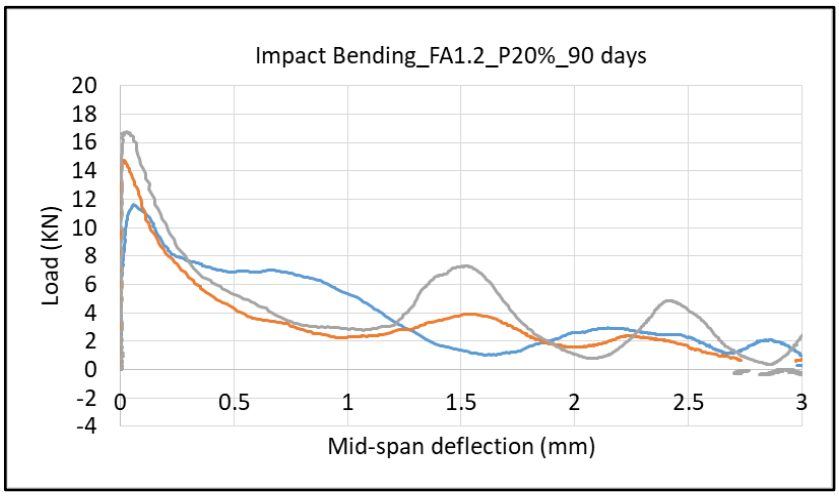
Impact Bending_FA1.2_P20%_90 days
Load (KN)
20
18
16
14
12
10
8
6
4
2
0
-2
-4
0
0.5
1
1.5
2
2.5
3
Mid-span deflection (mm)

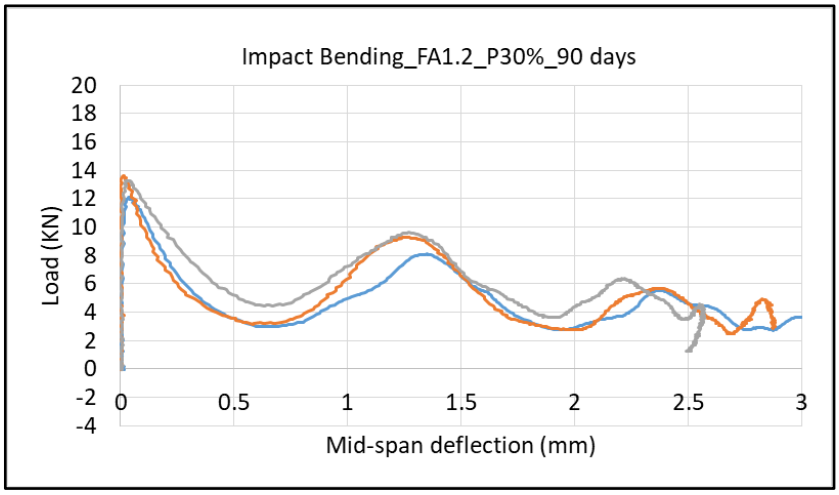
Impact Bending_FA1.2_P30%_90 days
Load (KN)
20
18
16
14
12
10
8
6
4
2
0
-2
-4
0
0.5
1
1.5
2
2.5
3
Mid-span deflection (mm)

APPENDIX C

All HyFRC Static Bending Test Load-Deflection Curves at 28 Days Age

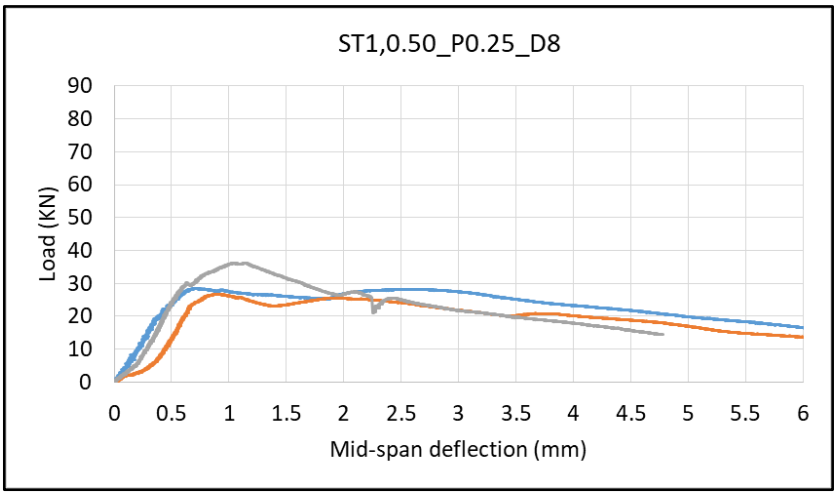

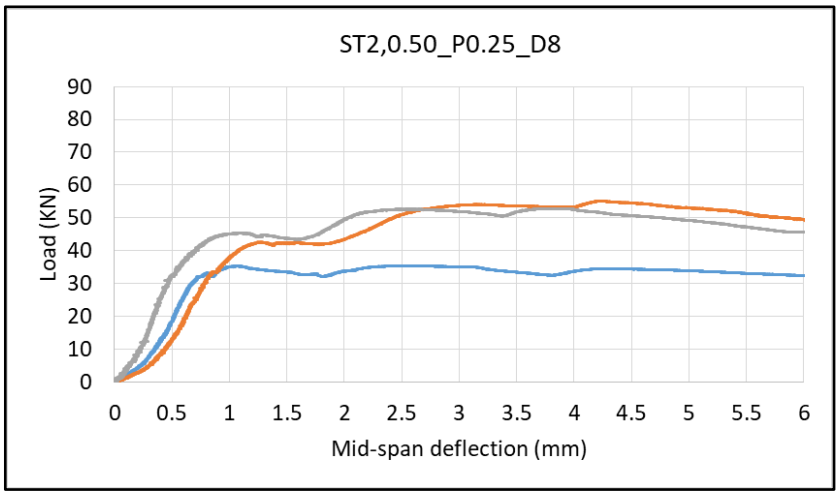

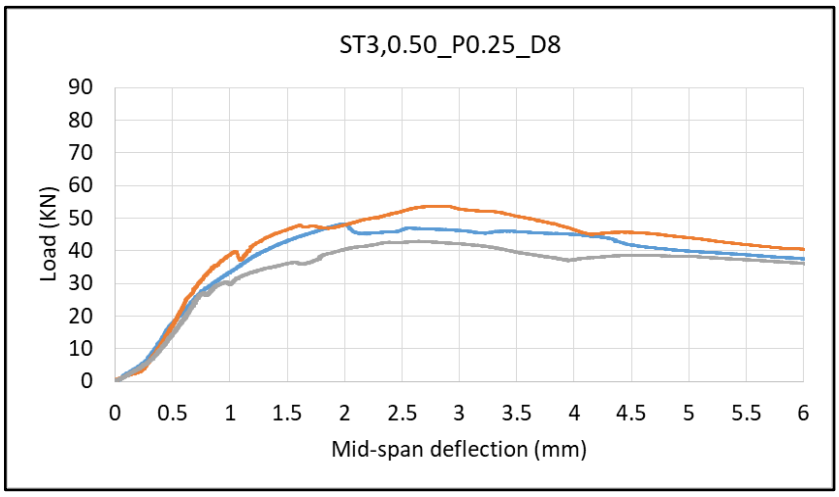

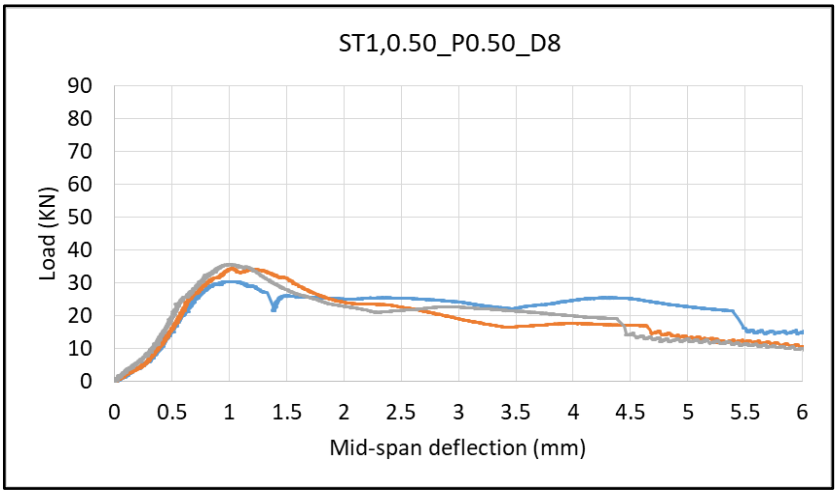
ST1,0.50_P0.50_D8
Load (KN)
90
80
70
60
50
40
30
20
10
0
0 0.5 1 1.5 2 2.5 3 3.5 4 4.5 5 5.5 6
Mid-span deflection (mm)

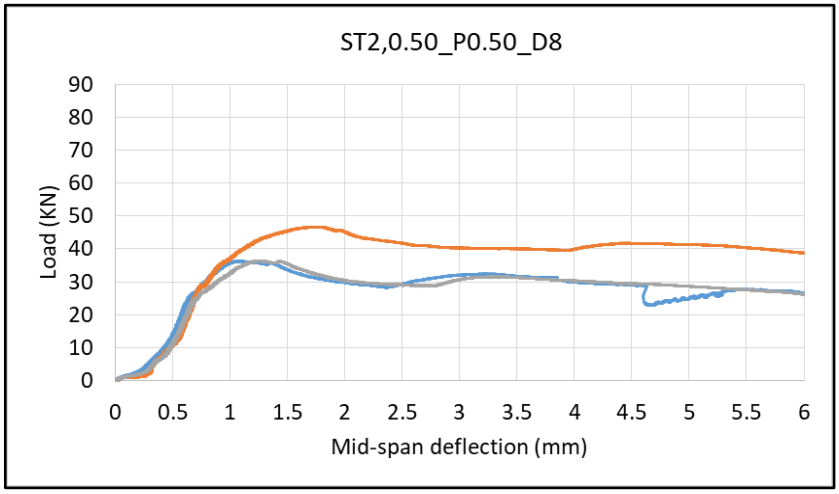
ST2,0.50_P0.50_D8
Load (KN)
90
80
70
60
50
40
30
20
10
0
0 0.5 1 1.5 2 2.5 3 3.5 4 4.5 5 5.5 6
Mid-span deflection (mm)

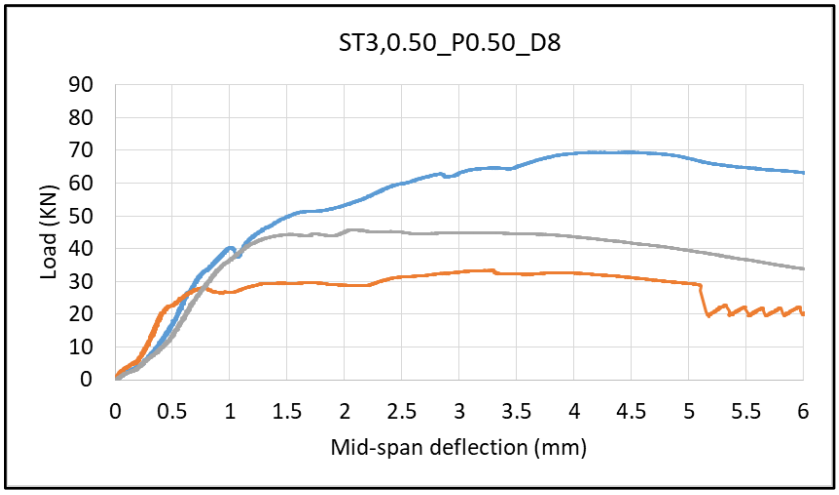
ST3,0.50_P0.50_D8
Load (KN)
90
80
70
60
50
40
30
20
10
0
0 0.5 1 1.5 2 2.5 3 3.5 4 4.5 5 5.5 6
Mid-span deflection (mm)

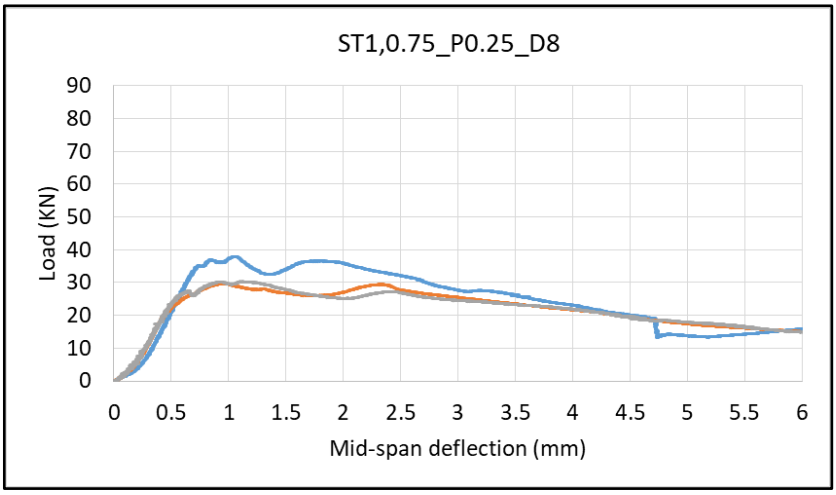
ST1,0.75_P0.25_D8
Load (KN)
90
80
70
60
50
40
30
20
10
0
0 0.5 1 1.5 2 2.5 3 3.5 4 4.5 5 5.5 6
Mid-span deflection (mm)

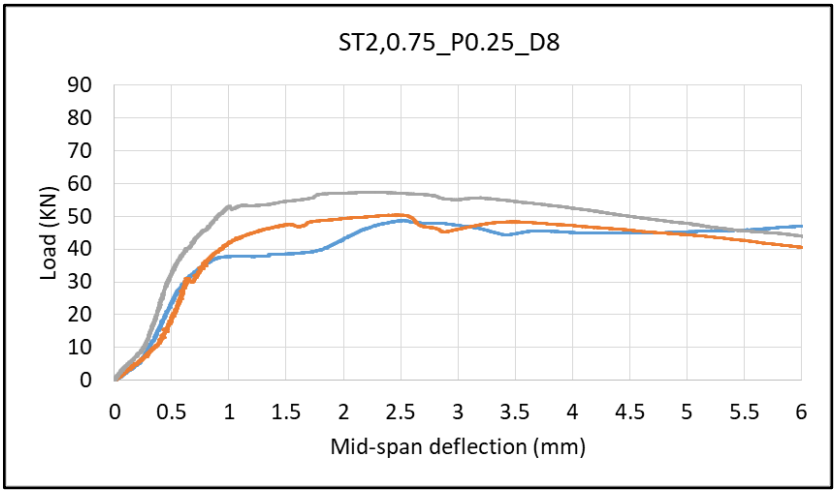
ST2,0.75_P0.25_D8
Load (KN)
90
80
70
60
50
40
30
20
10
0
0 0.5 1 1.5 2 2.5 3 3.5 4 4.5 5 5.5 6
Mid-span deflection (mm)

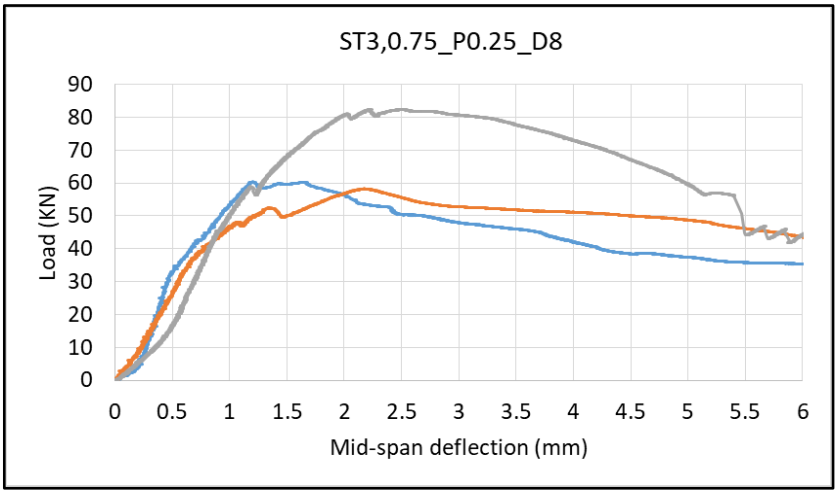
ST3,0.75_P0.25_D8
Load (KN)
90
80
70
60
50
40
30
20
10
0
0 0.5 1 1.5 2 2.5 3 3.5 4 4.5 5 5.5 6
Mid-span deflection (mm)

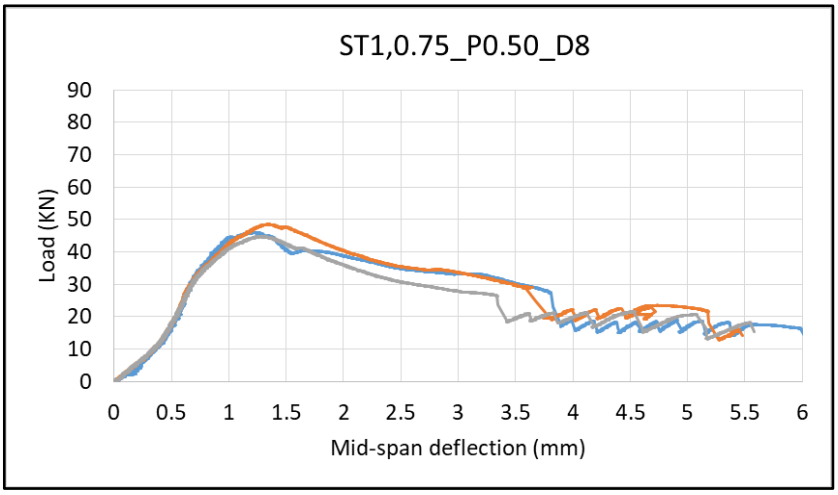
ST1,0.75_P0.50_D8
Load (KN)
90
80
70
60
50
40
30
20
10
0
0 0.5 1 1.5 2 2.5 3 3.5 4 4.5 5 5.5 6
Mid-span deflection (mm)

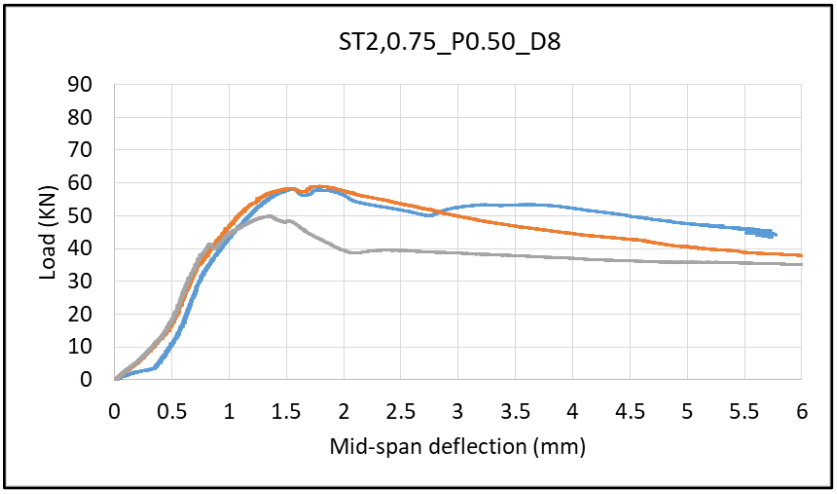
ST2,0.75_P0.50_D8
Load (KN)
90
80
70
60
50
40
30
20
10
0
0 0.5 1 1.5 2 2.5 3 3.5 4 4.5 5 5.5 6
Mid-span deflection (mm)

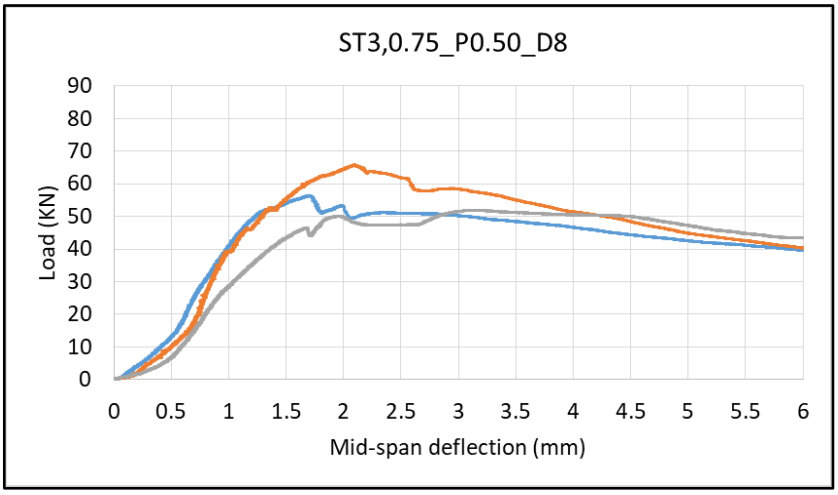
ST3,0.75_P0.50_D8
Load (KN)
90
80
70
60
50
40
30
20
10
0
0 0.5 1 1.5 2 2.5 3 3.5 4 4.5 5 5.5 6
Mid-span deflection (mm)

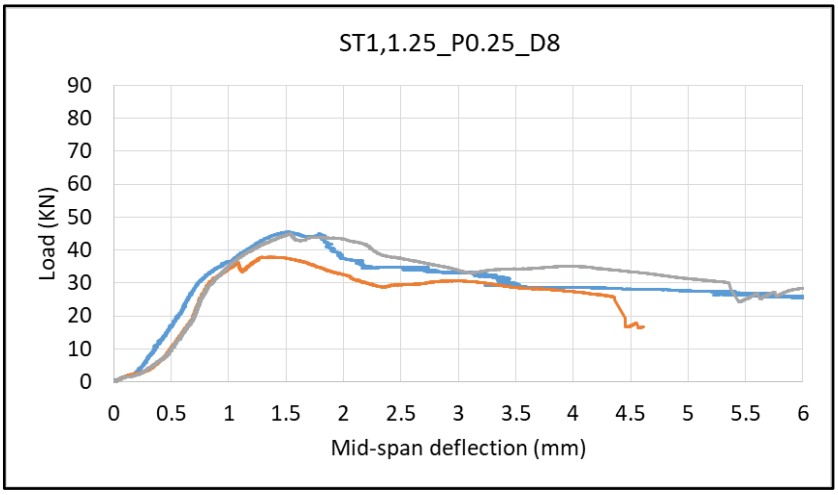
ST1,1.25_P0.25_D8
Load (KN)
90
80
70
60
50
40
30
20
10
0
0 0.5 1 1.5 2 2.5 3 3.5 4 4.5 5 5.5 6
Mid-span deflection (mm)

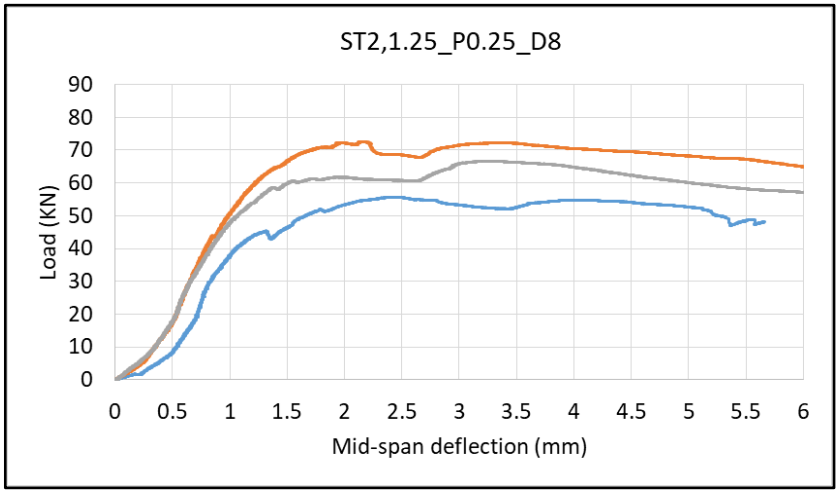
ST2,1.25_P0.25_D8
Load (KN)
90
80
70
60
50
40
30
20
10
0
0 0.5 1 1.5 2 2.5 3 3.5 4 4.5 5 5.5 6
Mid-span deflection (mm)

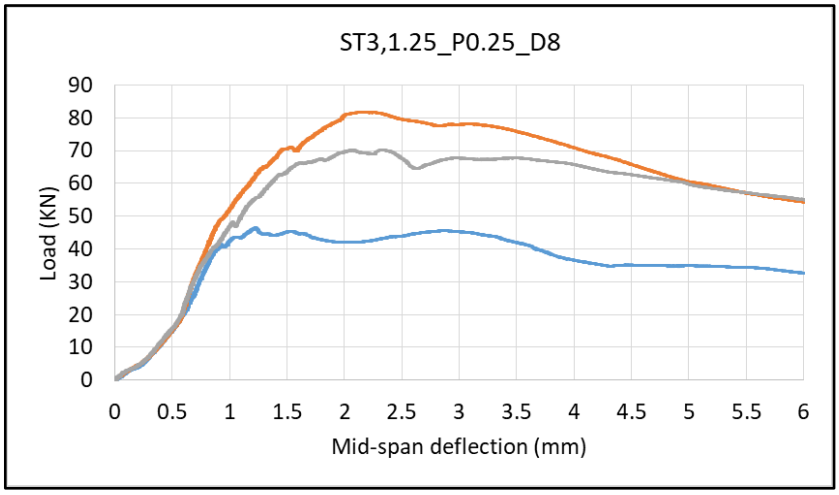
ST3,1.25_P0.25_D8
Load (KN)
90
80
70
60
50
40
30
20
10
0
0 0.5 1 1.5 2 2.5 3 3.5 4 4.5 5 5.5 6
Mid-span deflection (mm)

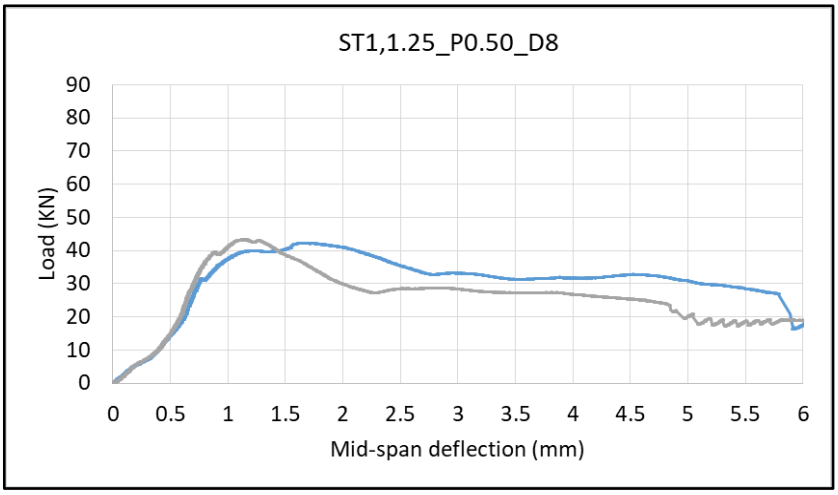
ST1,1.25_P0.50_D8
Load (KN)
90
80
70
60
50
40
30
20
10
0
0 0.5 1 1.5 2 2.5 3 3.5 4 4.5 5 5.5 6
Mid-span deflection (mm)

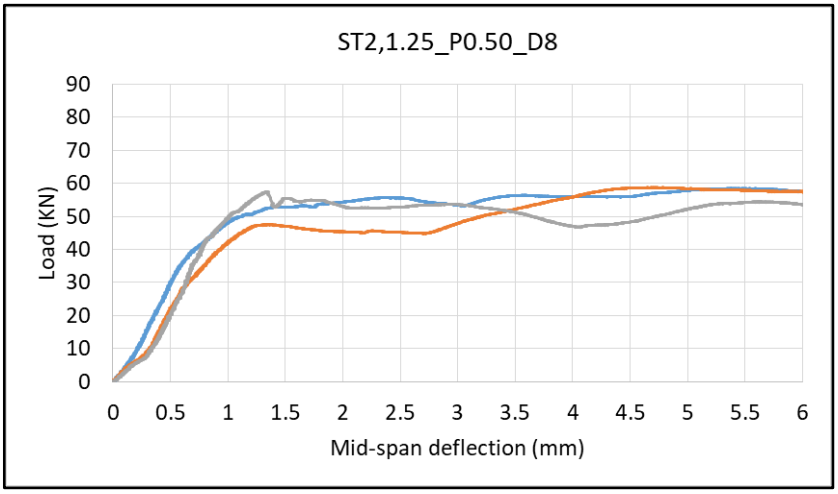
ST2,1.25_P0.50_D8
Load (KN)
90
80
70
60
50
40
30
20
10
0
0 0.5 1 1.5 2 2.5 3 3.5 4 4.5 5 5.5 6
Mid-span deflection (mm)

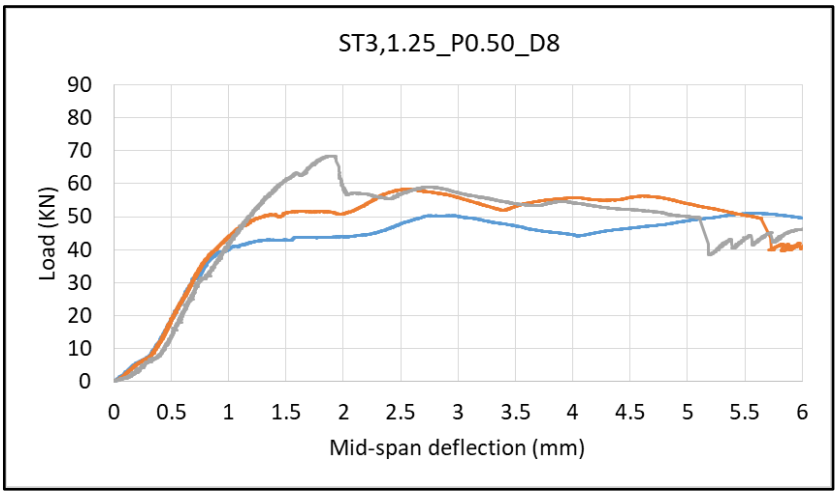
ST3,1.25_P0.50_D8
Load (KN)
90
80
70
60
50
40
30
20
10
0
0 0.5 1 1.5 2 2.5 3 3.5 4 4.5 5 5.5 6
Mid-span deflection (mm)

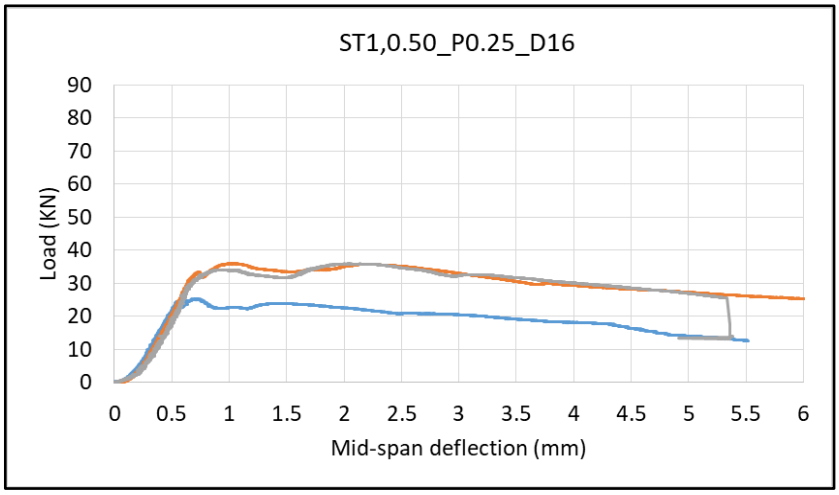
ST1,0.50_P0.25_D16
Load (KN)
Mid-span deflection (mm)
0
10
20
30
40
50
60
70
80
90
0
0.5
1
1.5
2
2.5
3
3.5
4
4.5
5
5.5
6

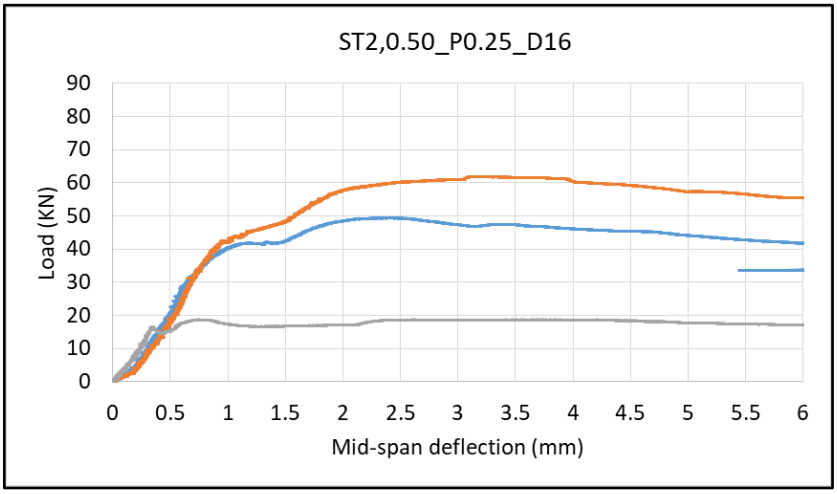
ST2,0.50_P0.25_D16
Load (KN)
Mid-span deflection (mm)
0
10
20
30
40
50
60
70
80
90
0
0.5
1
1.5
2
2.5
3
3.5
4
4.5
5
5.5
6

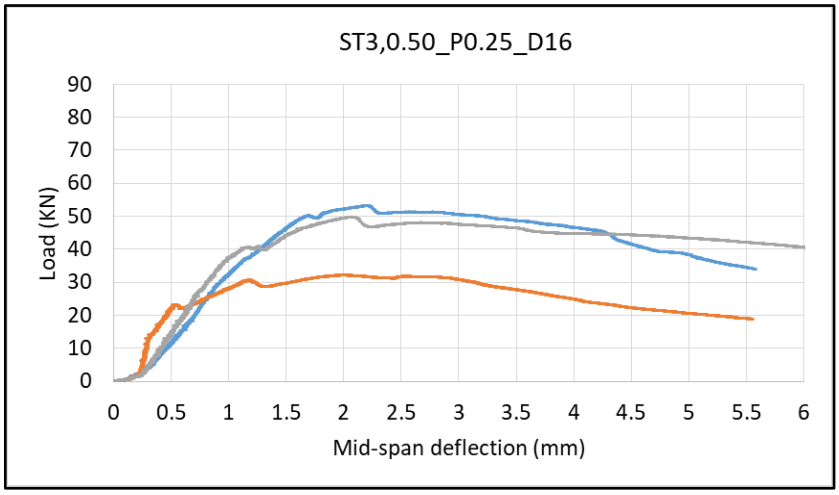
ST3,0.50_P0.25_D16
Load (KN)
Mid-span deflection (mm)
0
10
20
30
40
50
60
70
80
90
0
0.5
1
1.5
2
2.5
3
3.5
4
4.5
5
5.5
6

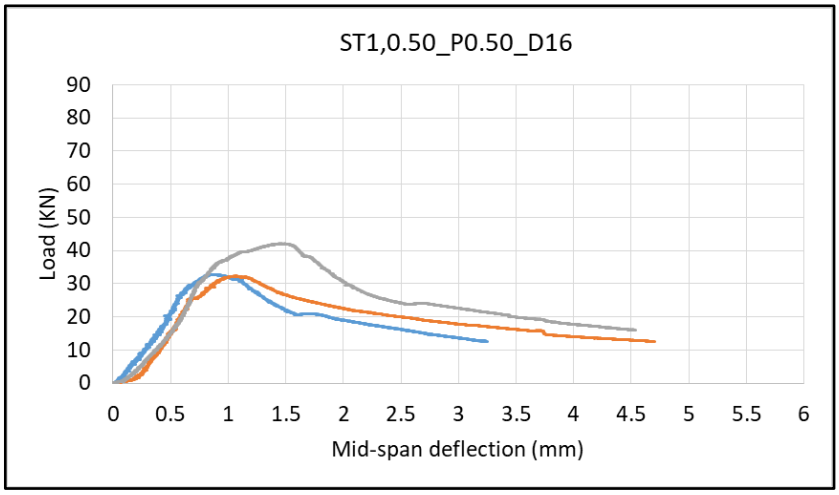
ST1,0.50_P0.50_D16
Load (KN)
90
80
70
60
50
40
30
20
10
0
0 0.5 1 1.5 2 2.5 3 3.5 4 4.5 5 5.5 6
Mid-span deflection (mm)

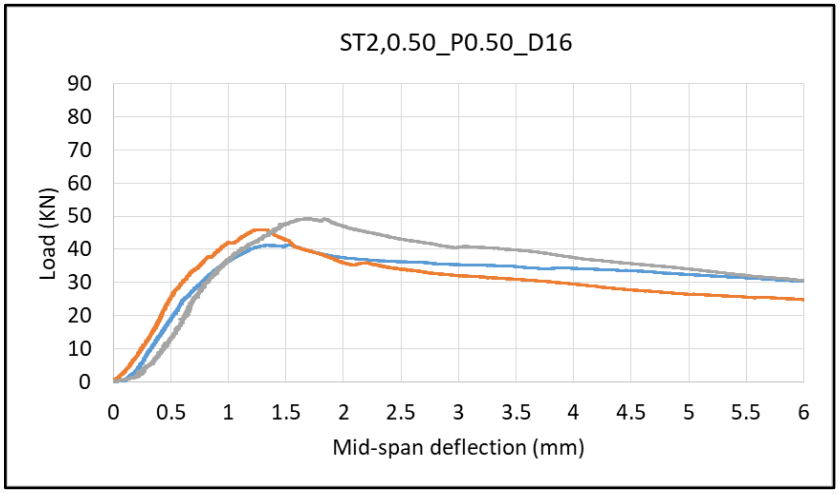
ST2,0.50_P0.50_D16
Load (KN)
90
80
70
60
50
40
30
20
10
0
0 0.5 1 1.5 2 2.5 3 3.5 4 4.5 5 5.5 6
Mid-span deflection (mm)

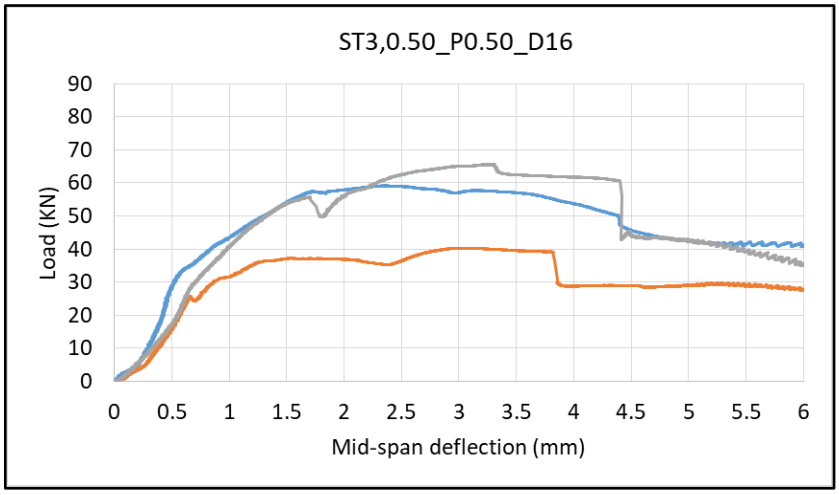
ST3,0.50_P0.50_D16
Load (KN)
90
80
70
60
50
40
30
20
10
0
0 0.5 1 1.5 2 2.5 3 3.5 4 4.5 5 5.5 6
Mid-span deflection (mm)

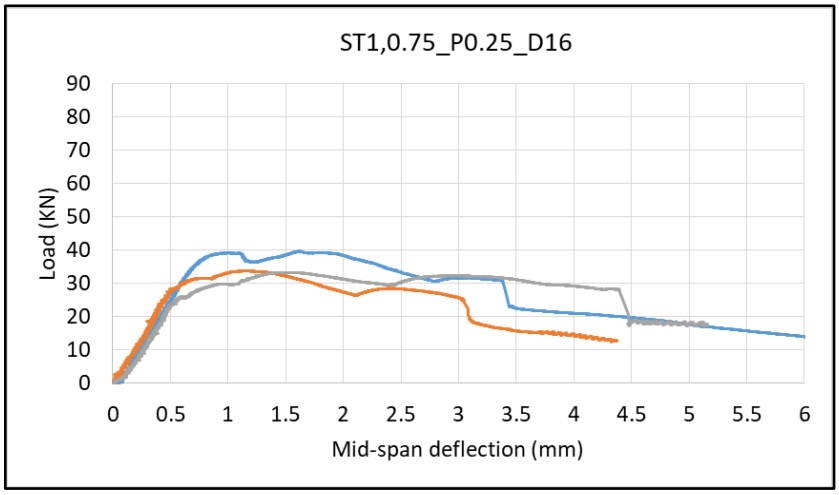
ST1,0.75_P0.25_D16
Load (KN)
90
80
70
60
50
40
30
20
10
0
0 0.5 1 1.5 2 2.5 3 3.5 4 4.5 5 5.5 6
Mid-span deflection (mm)

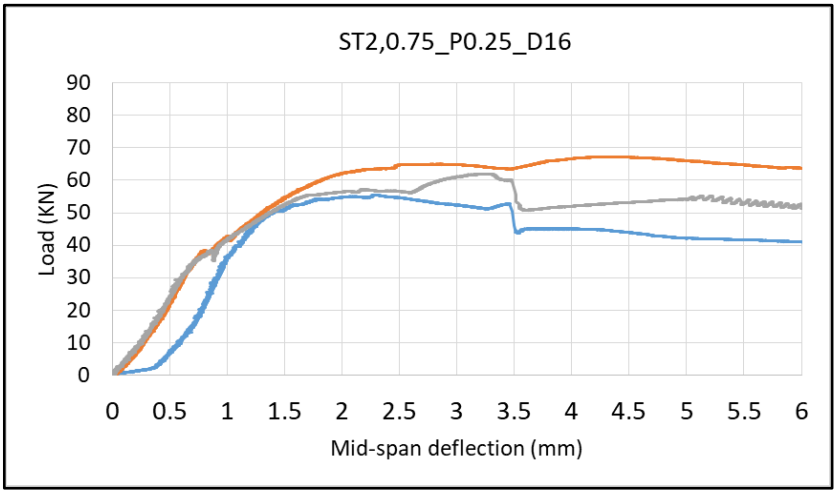
ST2,0.75_P0.25_D16
Load (KN)
90
80
70
60
50
40
30
20
10
0
0 0.5 1 1.5 2 2.5 3 3.5 4 4.5 5 5.5 6
Mid-span deflection (mm)

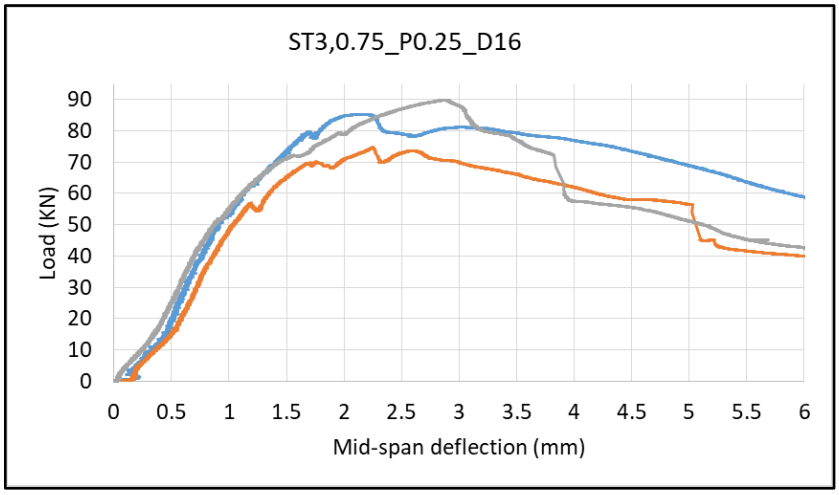
ST3,0.75_P0.25_D16
Load (KN)
90
80
70
60
50
40
30
20
10
0
0 0.5 1 1.5 2 2.5 3 3.5 4 4.5 5 5.5 6
Mid-span deflection (mm)

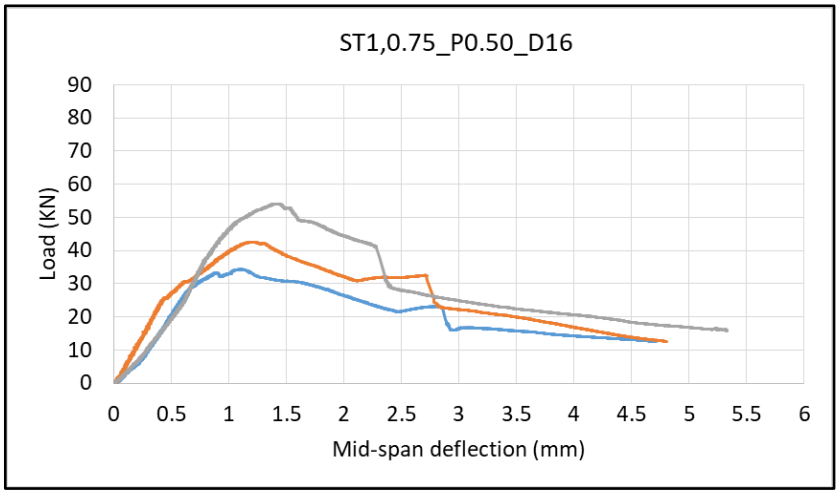
ST1,0.75_P0.50_D16
Load (KN)
Mid-span deflection (mm)
0
10
20
30
40
50
60
70
80
90
0
0.5
1
1.5
2
2.5
3
3.5
4
4.5
5
5.5
6

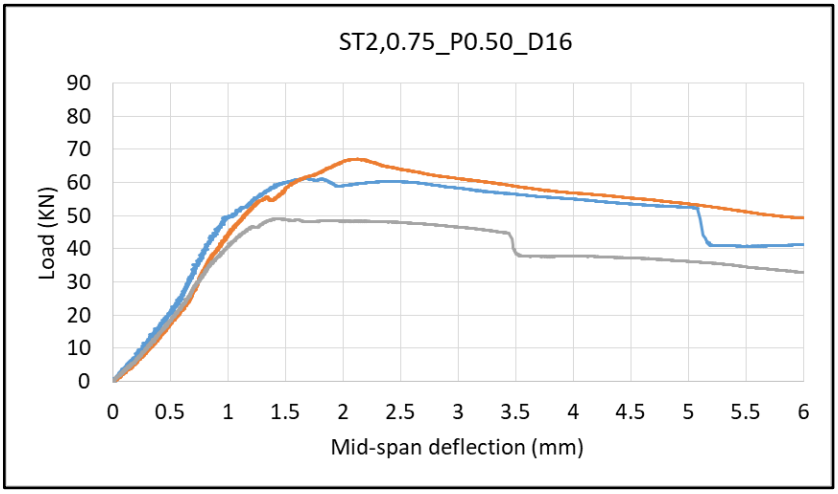
ST2,0.75_P0.50_D16
Load (KN)
Mid-span deflection (mm)
0
10
20
30
40
50
60
70
80
90
0
0.5
1
1.5
2
2.5
3
3.5
4
4.5
5
5.5
6

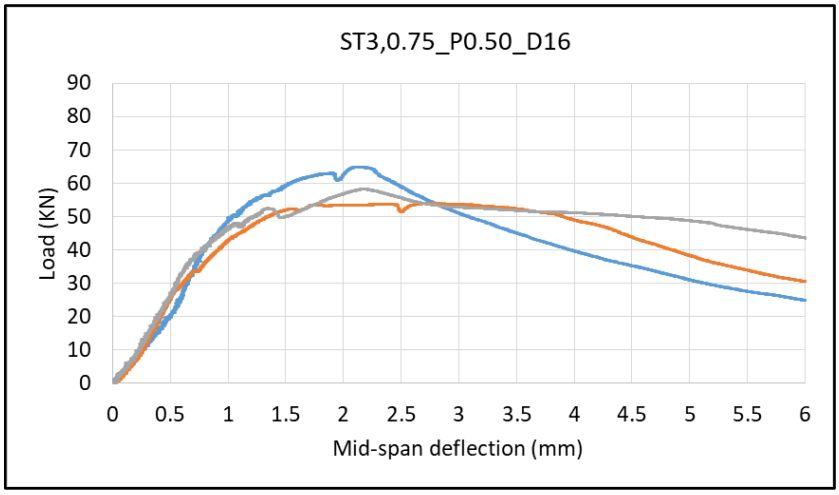
ST3,0.75_P0.50_D16
Load (KN)
Mid-span deflection (mm)
0
10
20
30
40
50
60
70
80
90
0
0.5
1
1.5
2
2.5
3
3.5
4
4.5
5
5.5
6

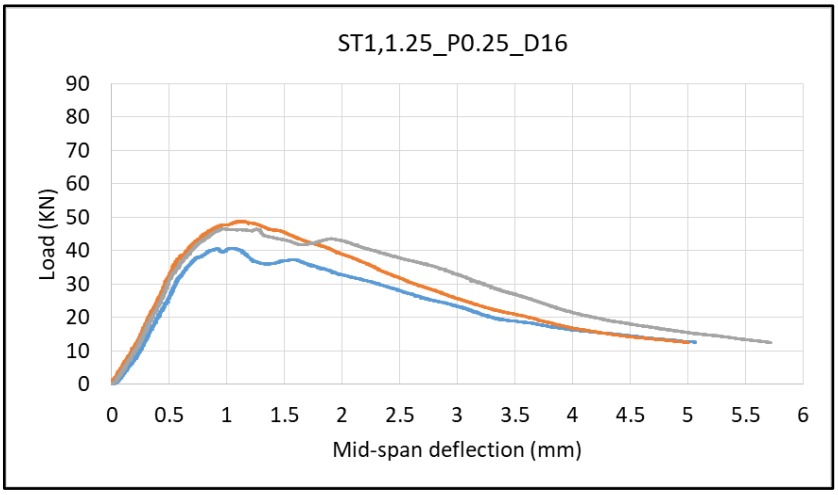
ST1,1.25_P0.25_D16
Load (KN)
90
80
70
60
50
40
30
20
10
0
0 0.5 1 1.5 2 2.5 3 3.5 4 4.5 5 5.5 6
Mid-span deflection (mm)

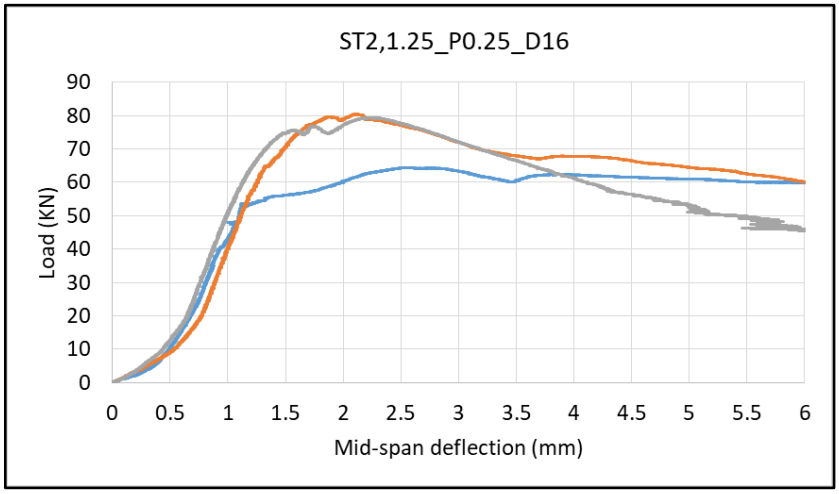
ST2,1.25_P0.25_D16
Load (KN)
90
80
70
60
50
40
30
20
10
0
0 0.5 1 1.5 2 2.5 3 3.5 4 4.5 5 5.5 6
Mid-span deflection (mm)

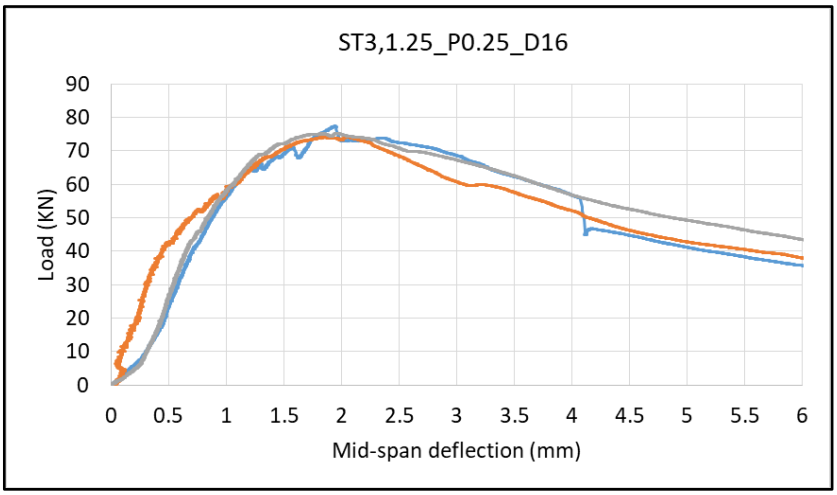
ST3,1.25_P0.25_D16
Load (KN)
90
80
70
60
50
40
30
20
10
0
0 0.5 1 1.5 2 2.5 3 3.5 4 4.5 5 5.5 6
Mid-span deflection (mm)

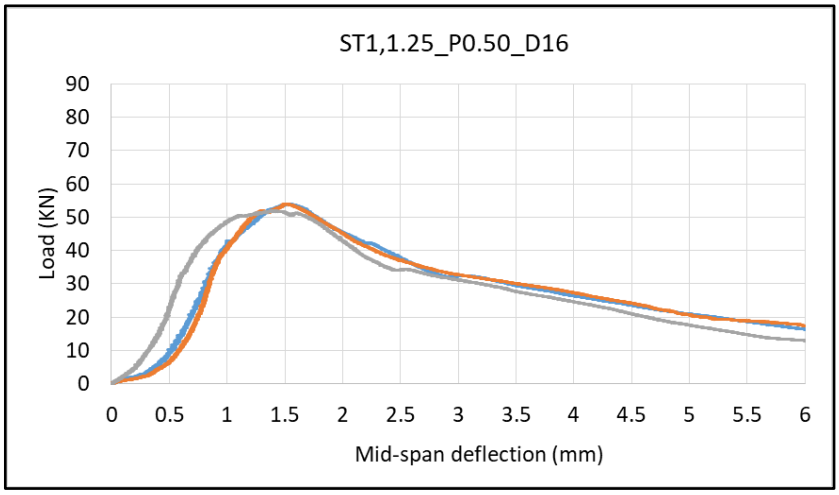
ST1,1.25_P0.50_D16
Load (KN)
Mid-span deflection (mm)
0
10
20
30
40
50
60
70
80
90
0
0.5
1
1.5
2
2.5
3
3.5
4
4.5
5
5.5
6

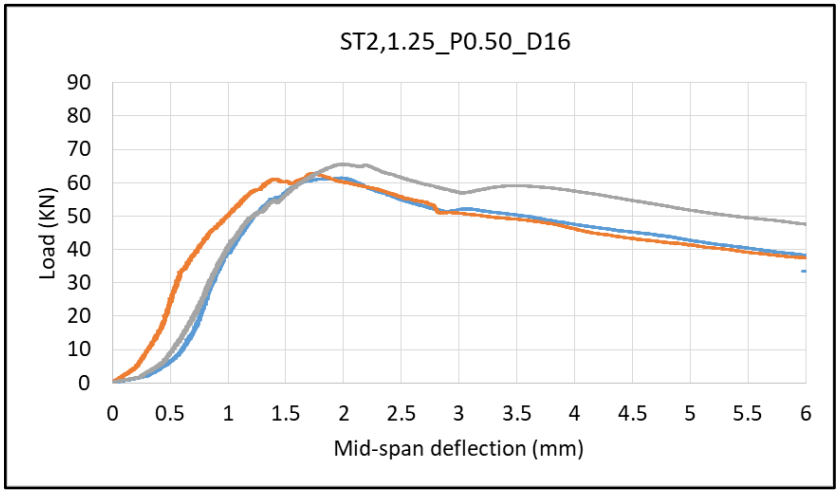
ST2,1.25_P0.50_D16
Load (KN)
Mid-span deflection (mm)
0
10
20
30
40
50
60
70
80
90
0
0.5
1
1.5
2
2.5
3
3.5
4
4.5
5
5.5
6

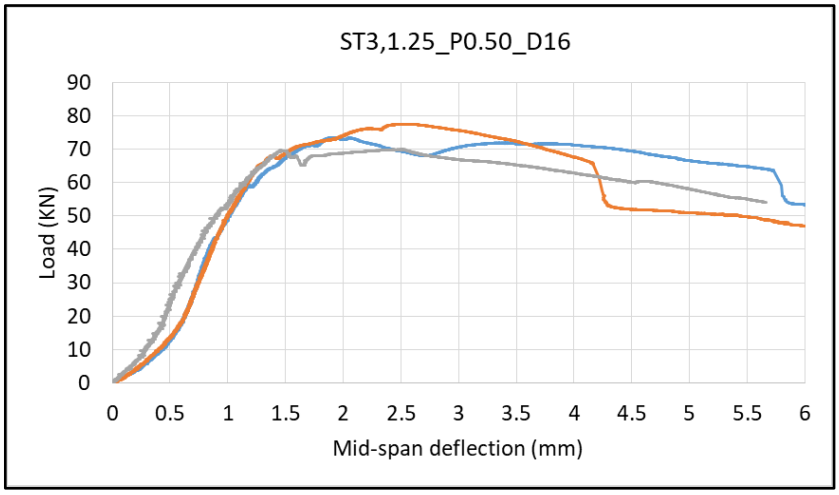
ST3,1.25_P0.50_D16
Load (KN)
Mid-span deflection (mm)
0
10
20
30
40
50
60
70
80
90
0
0.5
1
1.5
2
2.5
3
3.5
4
4.5
5
5.5
6

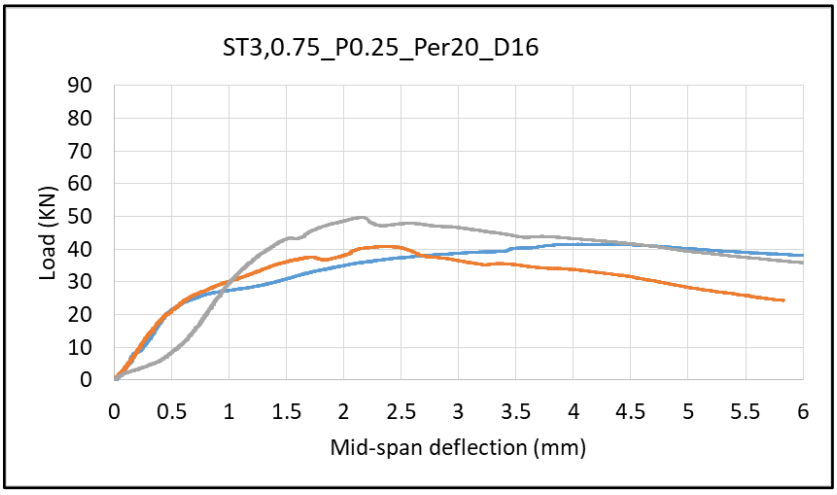
ST3,0.75_P0.25_Per20_D16
Load (KN)
90
80
70
60
50
40
30
20
10
0
0
0.5
1
1.5
2
2.5
3
3.5
4
4.5
5
5.5
6
Mid-span deflection (mm)

APPENDIX E

Five Selected HyFRC Static Bending Test Load-Deflection Curves at 7 Days Age

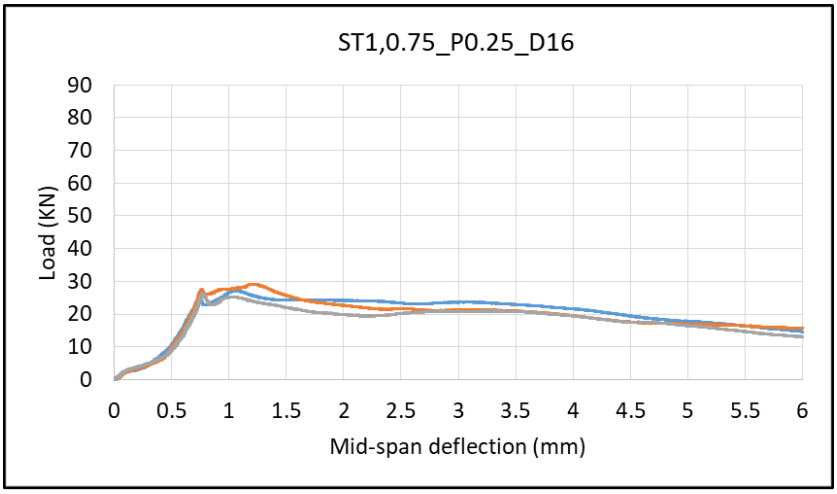

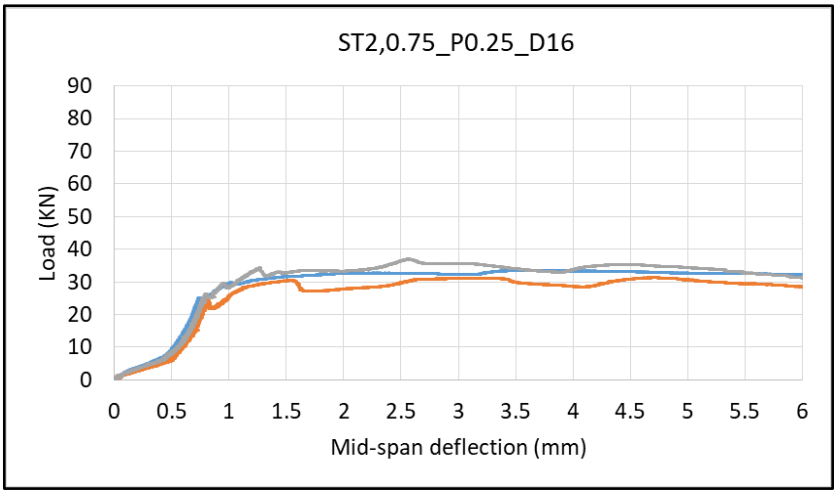

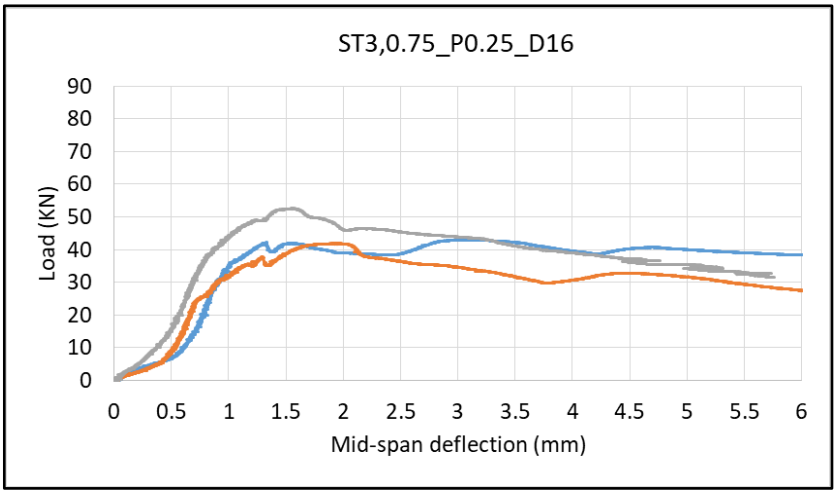
ST3,0.75_P0.25_D16
Load (KN)
Mid-span deflection (mm)
0
10
20
30
40
50
60
70
80
90
0
0.5
1
1.5
2
2.5
3
3.5
4
4.5
5
5.5
6

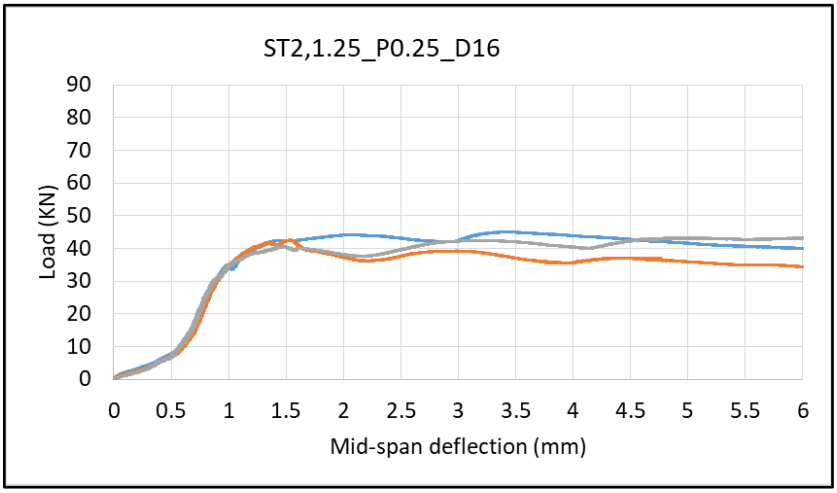
ST2,1.25_P0.25_D16
Load (KN)
Mid-span deflection (mm)
0
10
20
30
40
50
60
70
80
90
0
0.5
1
1.5
2
2.5
3
3.5
4
4.5
5
5.5
6

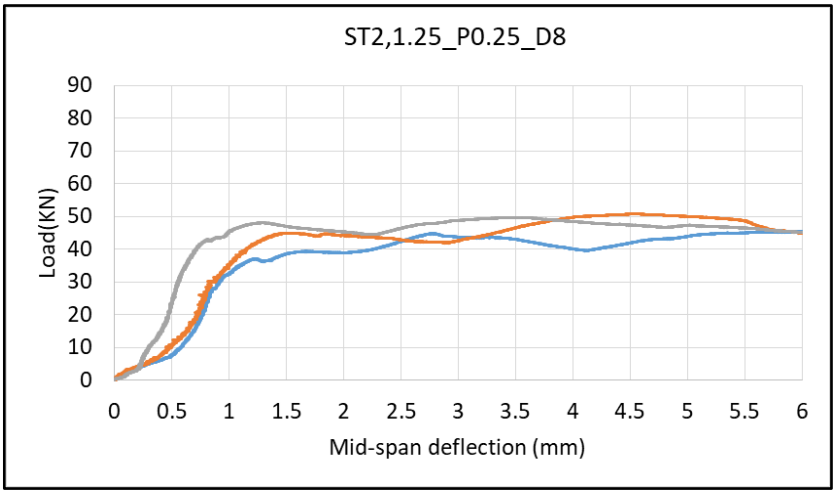
ST2,1.25_P0.25_D8
Load(KN)
Mid-span deflection (mm)
0
10
20
30
40
50
60
70
80
90
0
0.5
1
1.5
2
2.5
3
3.5
4
4.5
5
5.5
6

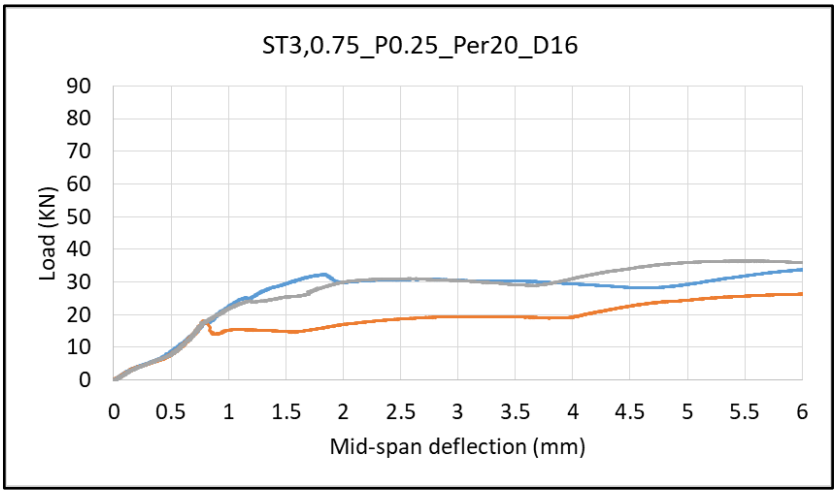
ST3,0.75_P0.25_Per20_D16
Load (KN)
90
80
70
60
50
40
30
20
10
0
0
0.5
1
1.5
2
2.5
3
3.5
4
4.5
5
5.5
6
Mid-span deflection (mm)

APPENDIX F

Five Selected HyFRC Static Bending Test Load-Deflection Curves at 90 Days Age

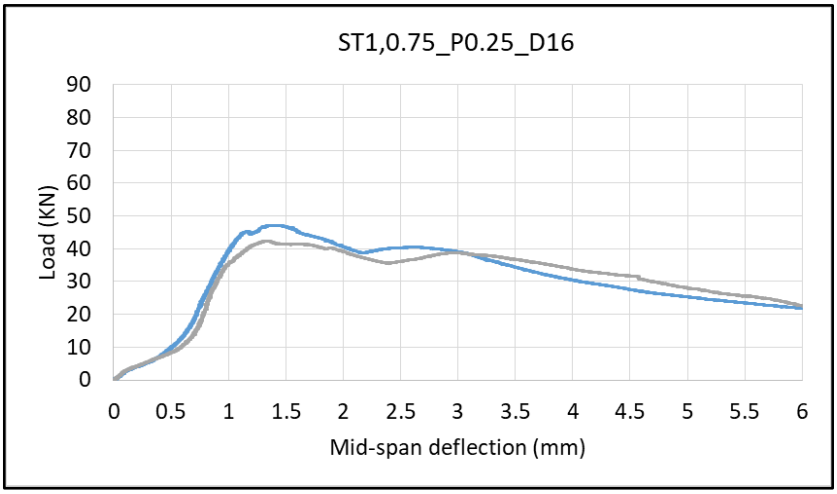

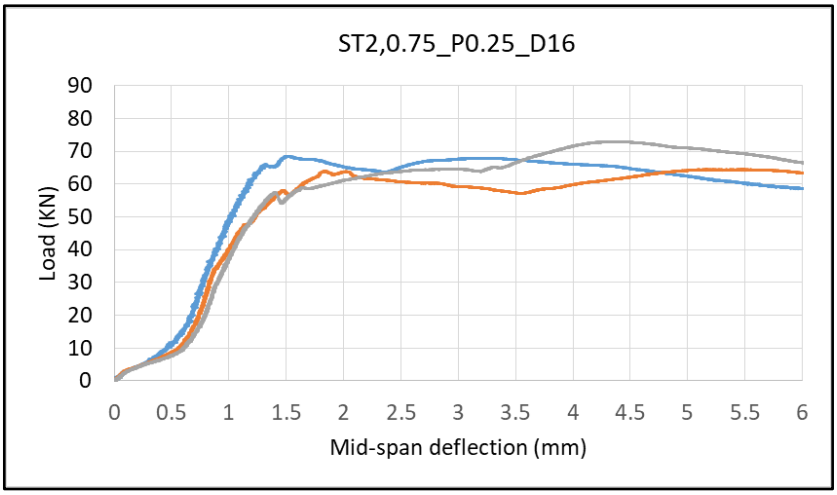

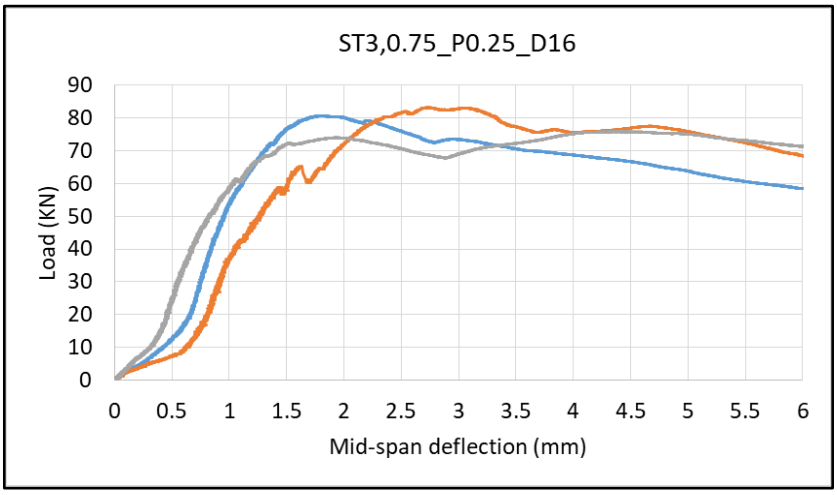

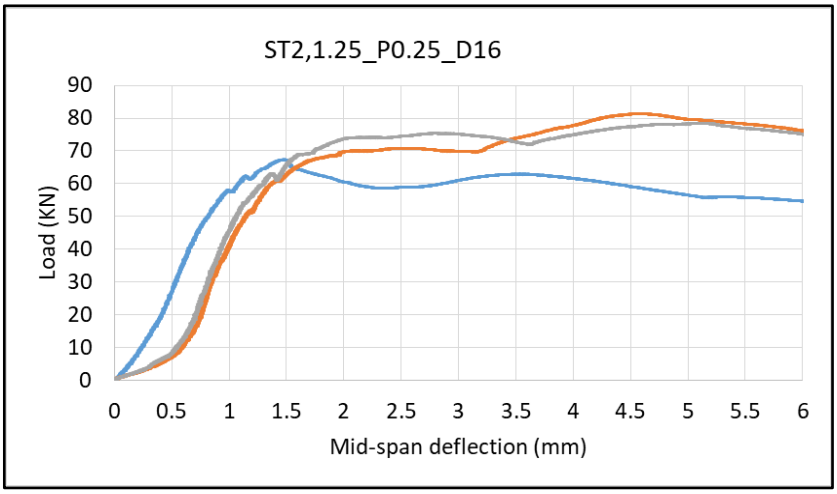
ST2,1.25_P0.25_D16
Load (KN)
90
80
70
60
50
40
30
20
10
0
0 0.5 1 1.5 2 2.5 3 3.5 4 4.5 5 5.5 6
Mid-span deflection (mm)

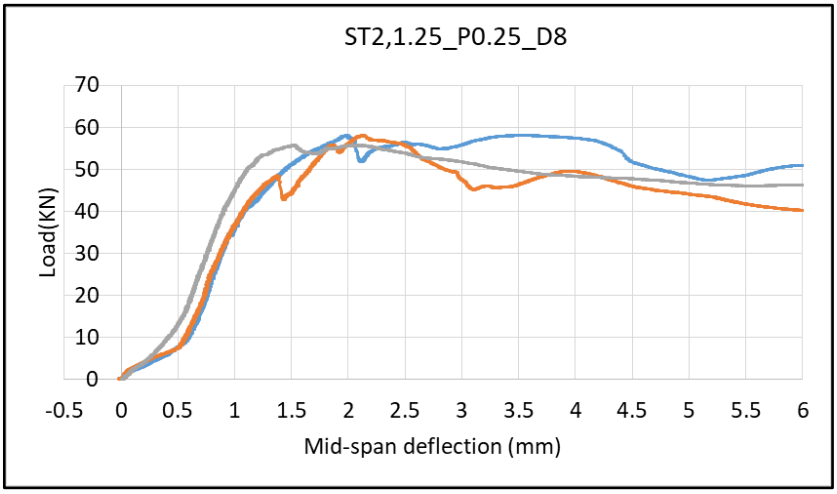
ST2,1.25_P0.25_D8
Load(KN)
70
60
50
40
30
20
10
0
-0.5 0 0.5 1 1.5 2 2.5 3 3.5 4 4.5 5 5.5 6
Mid-span deflection (mm)

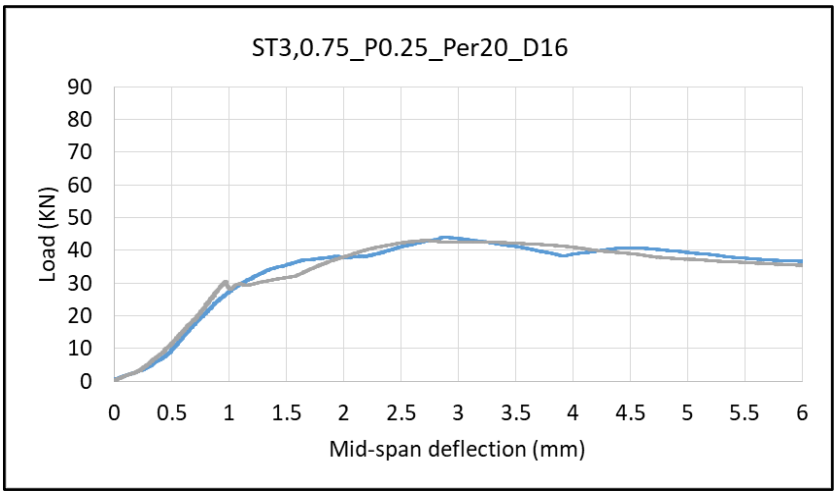
ST3,0.75_P0.25_Per20_D16
Load (KN)
90
80
70
60
50
40
30
20
10
0
0 0.5 1 1.5 2 2.5 3 3.5 4 4.5 5 5.5 6
Mid-span deflection (mm)

APPENDIX G

Normal Concrete 7, 28, and 90 days Static Bending Test Load-Deflection Curves

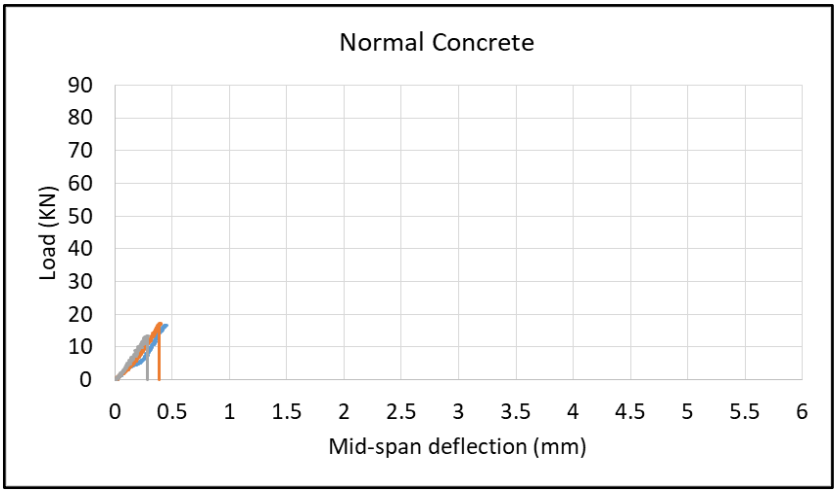

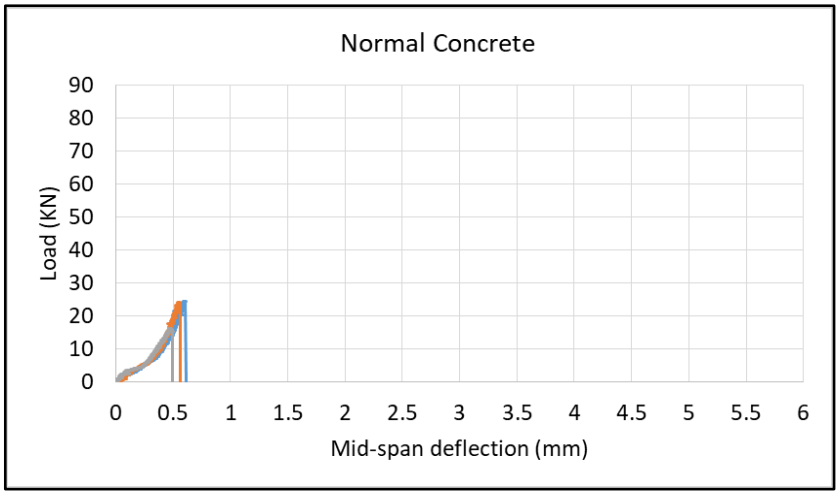

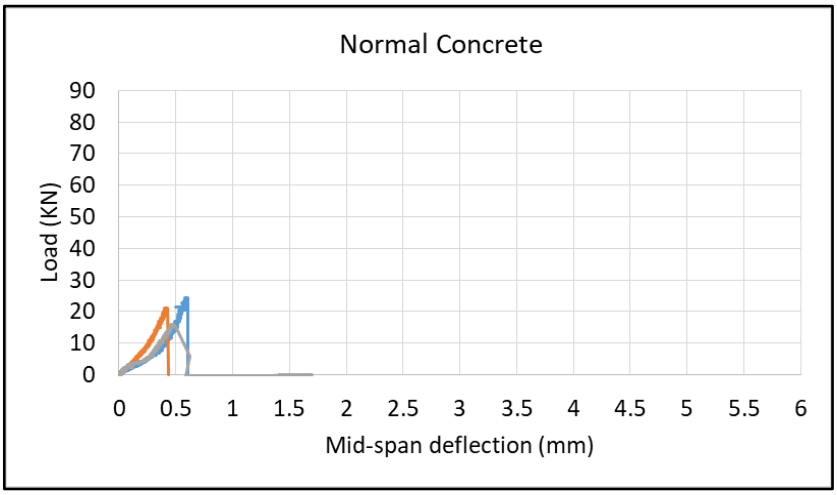

APPENDIX H

SFRC 7, 28, and 90 days Static Bending Test Load-Deflection Curves

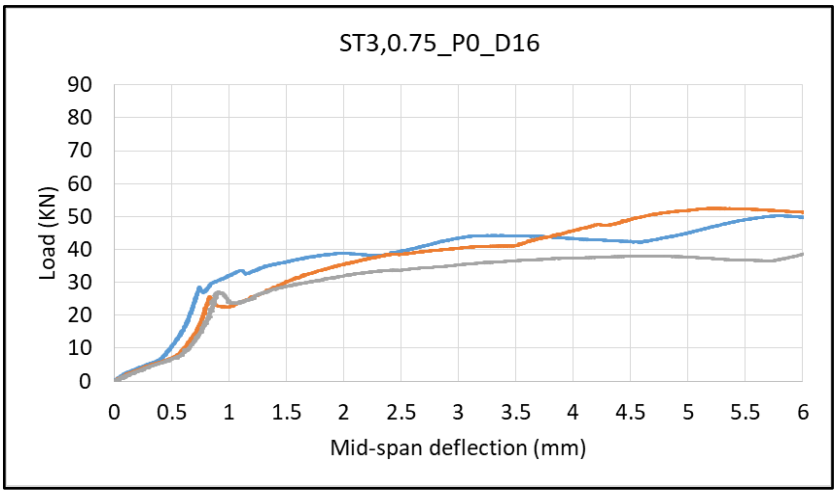

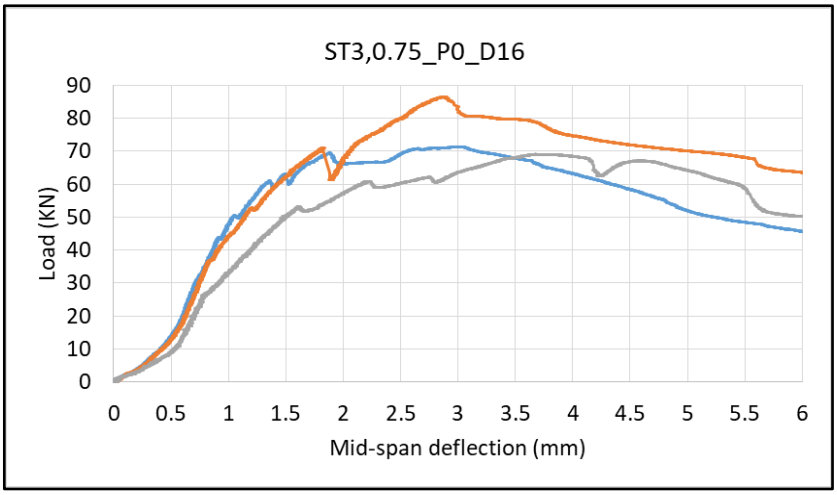

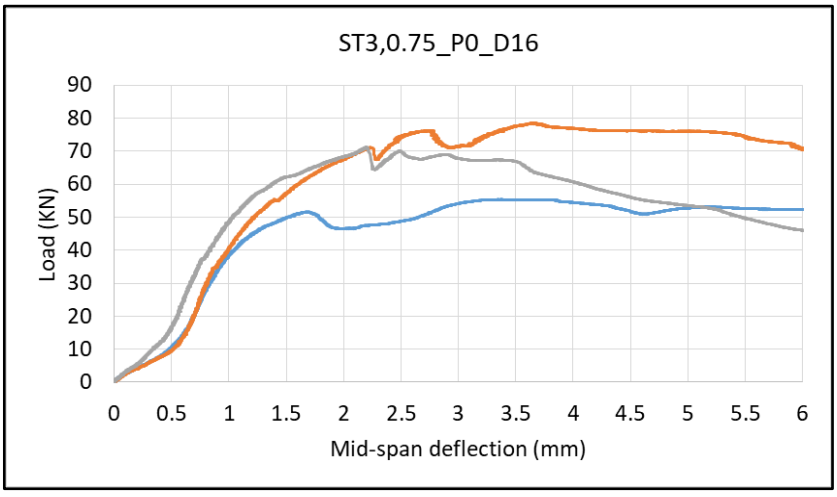

APPENDIX I

Selected Mixtures Dynamic Bending Test Load-Deflection Curves at 28 days

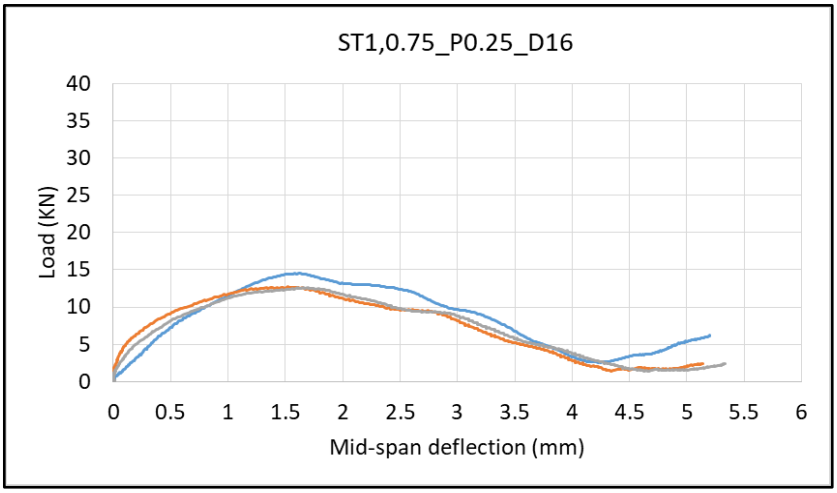

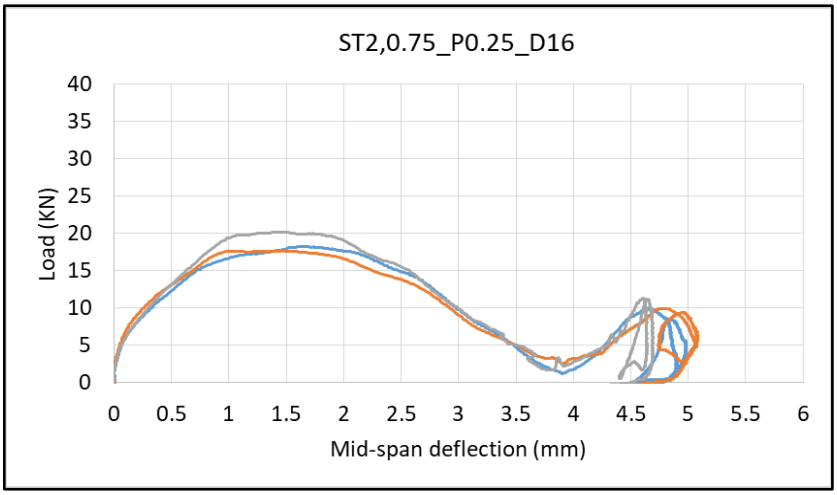

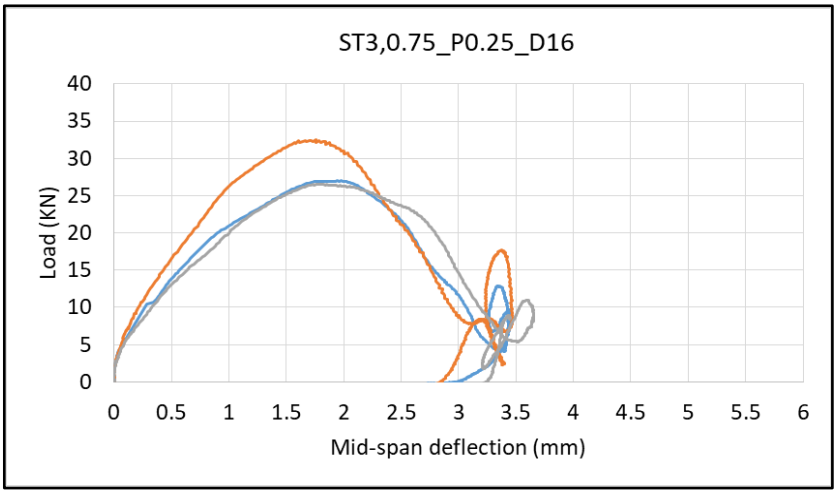
ST3,0.75_P0.25_D16
Load (KN)
Mid-span deflection (mm)
0
5
10
15
20
25
30
35
40
0
0.5
1
1.5
2
2.5
3
3.5
4
4.5
5
5.5
6

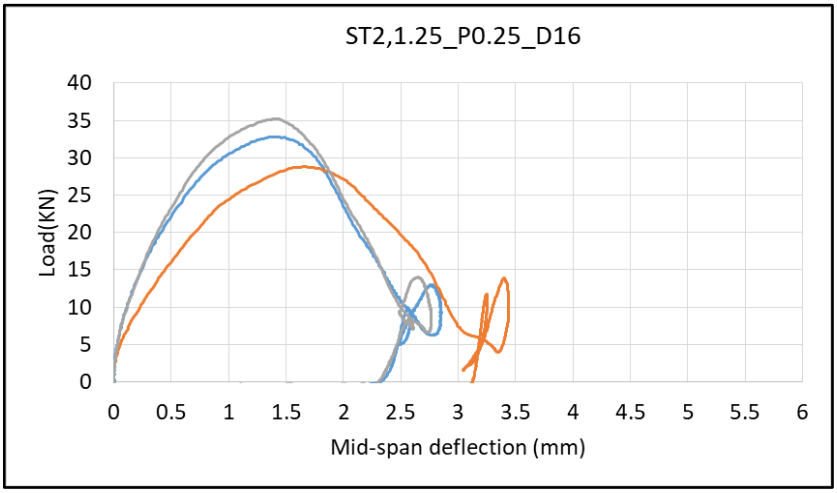
ST2,1.25_P0.25_D16
Load(KN)
Mid-span deflection (mm)
0
5
10
15
20
25
30
35
40
0
0.5
1
1.5
2
2.5
3
3.5
4
4.5
5
5.5
6

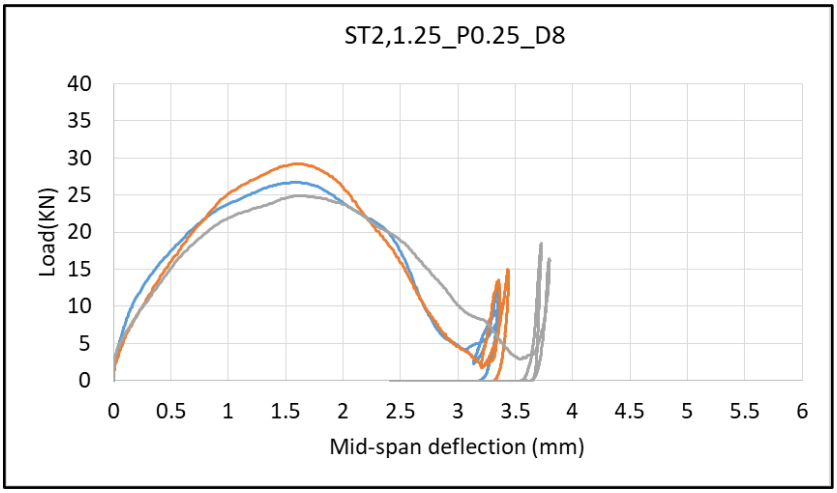
ST2,1.25_P0.25_D8
Load(KN)
Mid-span deflection (mm)
0
5
10
15
20
25
30
35
40
0
0.5
1
1.5
2
2.5
3
3.5
4
4.5
5
5.5
6

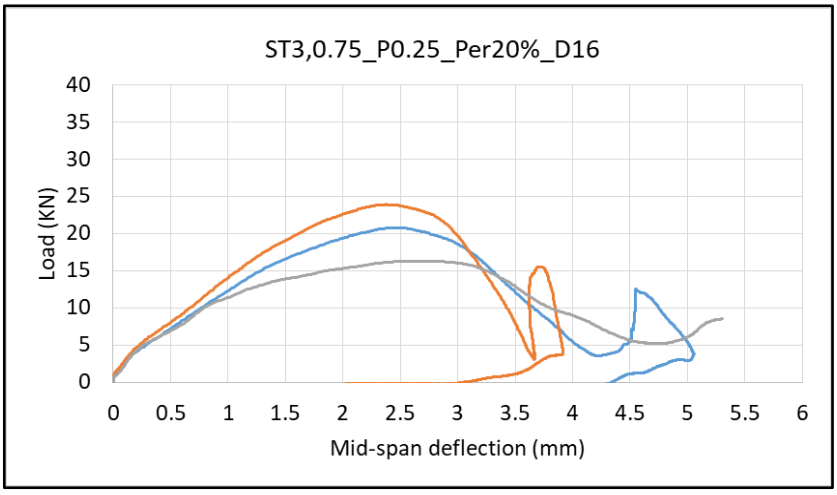
ST3,0.75_P0.25_Per20%_D16
Load (KN)
40
35
30
25
20
15
10
5
0
0 0.5 1 1.5 2 2.5 3 3.5 4 4.5 5 5.5 6
Mid-span deflection (mm)

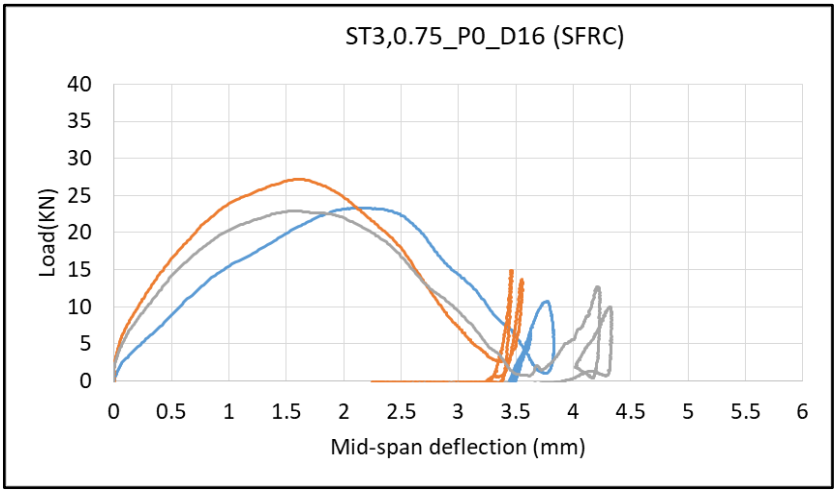
ST3,0.75_P0_D16 (SFRC)
Load(KN)
40
35
30
25
20
15
10
5
0
0 0.5 1 1.5 2 2.5 3 3.5 4 4.5 5 5.5 6
Mid-span deflection (mm)

APPENDIX J

Selected Mixtures Static Bending Test Load-Deflection Curves, specemen size (60 x 10 x 10 cm) at 28 days

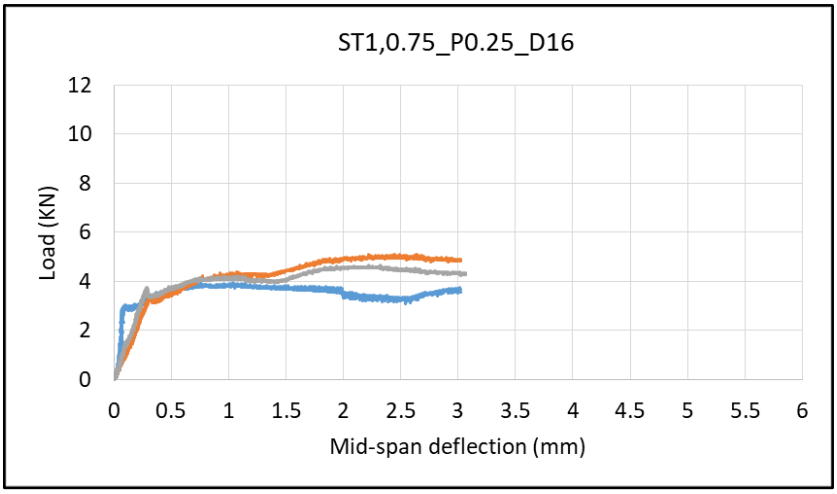

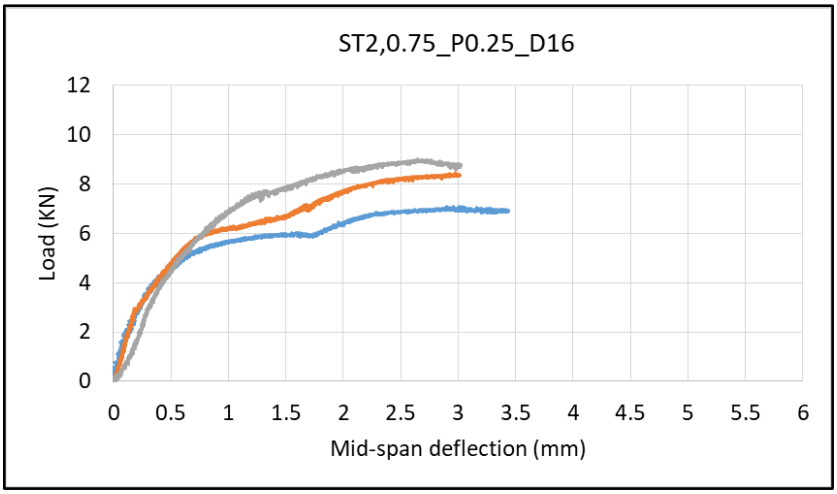

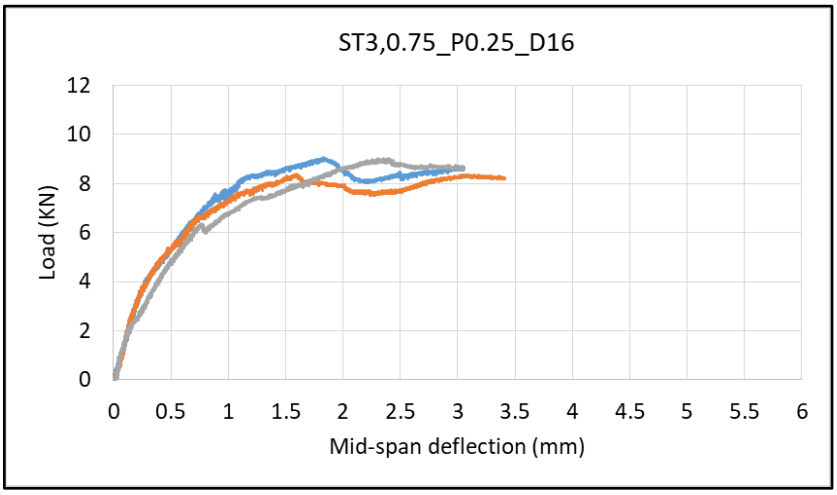

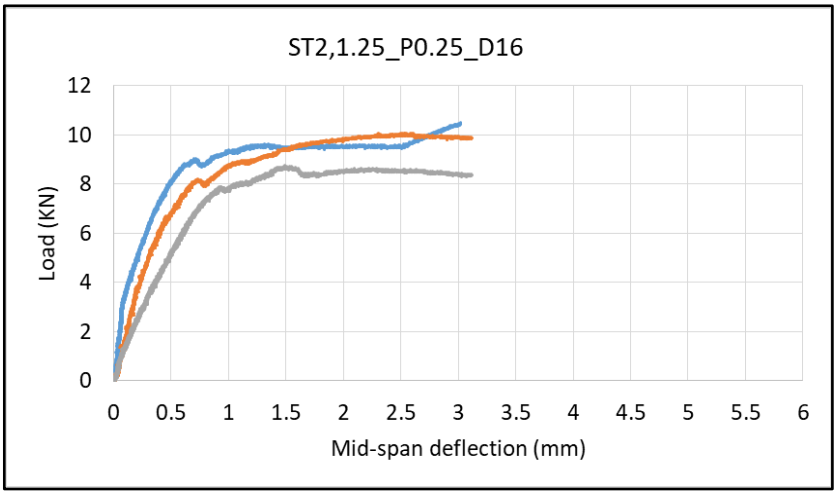
ST2,1.25_P0.25_D16
Load (KN)
Mid-span deflection (mm)
0
2
4
6
8
10
12
0
0.5
1
1.5
2
2.5
3
3.5
4
4.5
5
5.5
6

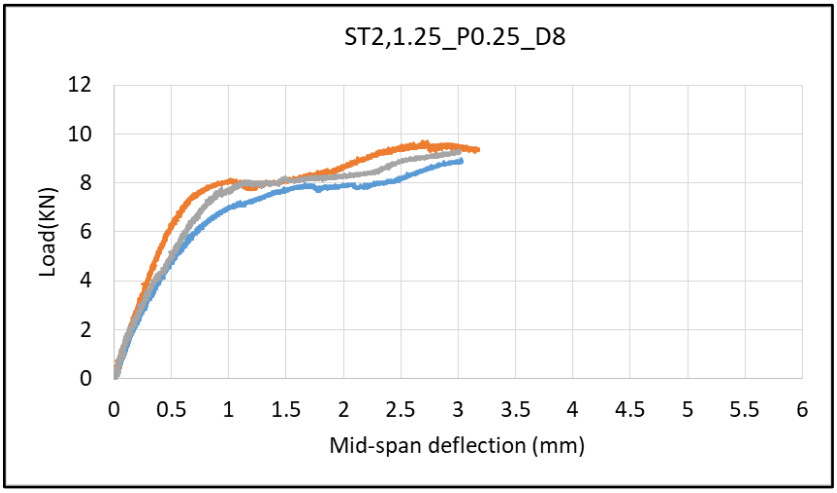
ST2,1.25_P0.25_D8
Load(KN)
Mid-span deflection (mm)
0
2
4
6
8
10
12
0
0.5
1
1.5
2
2.5
3
3.5
4
4.5
5
5.5
6

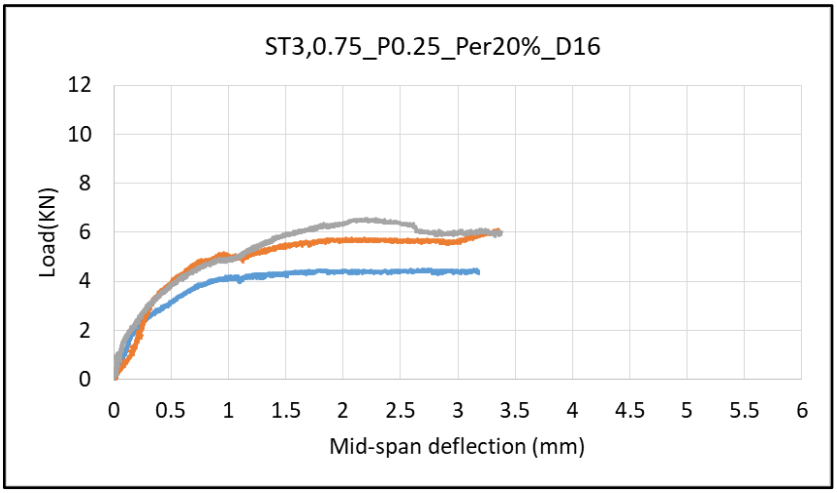
ST3,0.75_P0.25_Per20%_D16
Load(KN)
Mid-span deflection (mm)
0
2
4
6
8
10
12
0
0.5
1
1.5
2
2.5
3
3.5
4
4.5
5
5.5
6

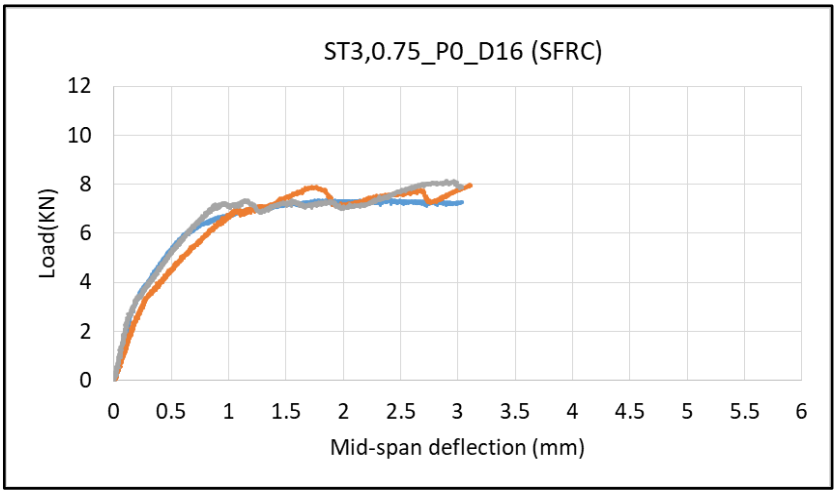
ST3,0.75_P0_D16 (SFRC)
Load(KN)
12
10
8
6
4
2
0
0
0.5
1
1.5
2
2.5
3
3.5
4
4.5
5
5.5
6
Mid-span deflection (mm)

Mohammad Musa ALAMI

Education

Doctorate (Ph.D.) | 12.07.2021 | Civil Engineering | Izmir Institute of Technology | Izmir-Turkey

Master of Science (M.Sc.) | 14.07.2014 | Civil Engineering | Izmir Institute of Technology | Izmir-Turkey

Bachelor of Science (B.Sc.) | 05.06.2008 | Civil Engineering | Kandahar University | Kandahar-Afghanistan

High School | 15.06.2002 | Lashkargah Boys High School | Helmand-Afghanistan

Experience

Director General of Afghanistan National Standards Authority (ANSA)| 22.01.2019 – 15.07.2020 | Kabul-Afghanistan

Dean of Engineering Faculty| Helmand University | 01.08.2017 – 22.01.2019| Helmand-Afghanistan

Research Assistant | Izmir Institute of Technology | 15.10.2015 – 30.06.2017 | Izmir-Turkey

Lecturer | Helmand University | 01.01.2009 – 22.01.2019 | Helmand-Afghanistan

Provincial Director | Creative| 01.02.2010 – 30.11.2011 | Helmand-Afghanistan

Provincial engineer | un-habitat | 01.07.2008 – 31.12.2009 | Helmand-Afghanistan

Director | Sabir Salam Construction Company | 01.01.2008 – 31.12.2011 | Helmand-Afghanistan

Site Engineer | brac-Bangladesh | 01.07.2006 – 31.07.2007 | Helmand-Afghanistan